Mathematical Engineering

Stefan Heinz
Hakima Bessaih *Editors*

Stochastic Equations for Complex Systems

Theoretical and Computational Topics

Springer

Mathematical Engineering

More information about this series at http://www.springer.com/series/8445

Stefan Heinz · Hakima Bessaih
Editors

Stochastic Equations for Complex Systems

Theoretical and Computational Topics

Springer

Editors
Stefan Heinz
University of Wyoming
Laramie, WY
USA

Hakima Bessaih
University of Wyoming
Laramie, WY
USA

ISSN 2192-4732 ISSN 2192-4740 (electronic)
Mathematical Engineering
ISBN 978-3-319-18205-6 ISBN 978-3-319-18206-3 (eBook)
DOI 10.1007/978-3-319-18206-3

Library of Congress Control Number: 2015937209

Springer Cham Heidelberg New York Dordrecht London

Printed on acid-free paper

Springer International Publishing AG Switzerland is part of Springer Science+Business Media (www.springer.com)

Preface

The Rocky Mountain Mathematics Consortium (RMMC) Summer School "Stochastic equations for complex systems: Theory and applications" took place for two weeks in June, 2014 at the University of Wyoming in Laramie. This summer school involved about 80 graduate students and lecturers from all over the United States and Europe. Mathematical analyses and computational predictions of the behavior of complex systems are needed to effectively deal, for example, with weather and climate predictions, and the optimal design of technical processes. Given the random nature of such systems and the recognized relevance of randomness, the equations used to describe such systems usually need to involve stochastics. The basic goal of this summer school was to introduce graduate students to the mathematics and application of stochastic equations to the modeling of complex systems. One of the known problems of research in this field is that mathematicians, engineers, and physicists generally use rather different terminology to present the results of their analyses. Therefore, a particular goal of this summer school was to create bridges between different analysis methods and techniques in order to contribute to a growing cooperation between researchers in different fields.

Following the lectures of our RMMC Summer School, the book presents eight selected chapters. Each of the chapters addresses questions that are relevant to the mathematical analysis and computational prediction of the behavior of complex systems on the basis of stochastic equations. The first three chapters provide introductions to different topics on mathematical analysis. "An Introduction to the Malliavin Calculus and Its Applications" focuses on the Malliavin calculus with applications to stochastic integral representation, density formulas, smoothness of densities, and normal approximations. "Fractional Brownian Motion and An Application to Fluids" describes fractional Brownian motion with application to vortex dynamics in fluids, and "An Introduction to Large Deviations and Equilibrium Statistical Mechanics for Turbulent Flows" deals with large deviations with applications to the equilibrium statistical mechanics of turbulent flows. "Recent Developments on the Micropolar and Magneto-Micropolar Fluid Systems: Deterministic and Stochastic Perspectives" and "Pathwise Sensitivity Analysis in Transient Regimes" focus on the application of mathematical tools to the analysis

of stochastic equations: the analysis of magneto-hydrodynamic equations and the sensitivity analysis of stochastic equations are considered. The development and application of stochastic methods to simulate turbulent flows seen in reality are the concern of "The Langevin Approach: A Simple Stochastic Method for Complex Phenomena," "Monte Carlo Simulations of Turbulent Non-Premixed Combustion Using a Velocity Conditioned Mixing Model," and "Massively Parallel FDF Simulation of Turbulent Reacting Flows." In particular, "The Langevin Approach: A Simple Stochastic Method for Complex Phenomena" explains how observations can be used for the design of stochastic equations. "Monte Carlo Simulations of Turbulent Non-Premixed Combustion Using a Velocity Conditioned Mixing Model" and "Massively Parallel FDF Simulation of Turbulent Reacting Flows" describe the stochastic modeling of turbulent reacting flows using techniques that differ by their predictive capability and computational requirements.

First of all, we would like to thank the Rocky Mountain Mathematics Consortium and University of Wyoming Mathematics Department for providing a frame for organizing this summer school. In particular, we are thankful to the head of the University of Wyoming Mathematics Department Prof. F. Jafari for his constant support of our efforts. We are grateful to V. Staddie, B. Buskirk, L. Roan, R. Johnson, and C. Johnson (University of Wyoming Mathematics Department) for their great help regarding the organization of this event. This summer school would not have been possible without substantial financial support of many organizations: the Rocky Mountain Mathematics Consortium (Prof. T. Sherman), the National Science Foundation (Prof. T. Bartoszynski), the National Center for Atmospheric Research (Dr. J. Tribbia), the Institute for Mathematics and its Applications (Prof. F. Santosa) located at the University of Minnesota, and the University of Wyoming Research Office (Prof. B. Shader and Prof. B. Gern). We are deeply thankful for this support.

Laramie
March 2015

Stefan Heinz
Hakima Bessaih

Contents

An Introduction to the Malliavin Calculus and Its Applications

David Nualart

Abstract The purpose of these notes is to provide an introduction to the Malliavin calculus and its recent application to quantitative results in normal approximations, in combination with Stein's method. The basic differential operators of the Malliavin calculus and their main properties are presented. We explain the connection of these operators with the Wiener chaos expansion and the Ornstein-Uhlenbeck semigroup. We survey several applications of the Malliavin calculus including stochastic integral representation, density formulas, smoothness of densities and normal approximations.

1 Introduction

Paul Malliavin introduced in the 70s a calculus of variations with respect to the trajectories of Brownian motion, in order to provide a probabilistic proof of Hörmander's hypoellipticity theorem (see [18]). This calculus was further developed by Bismut, Kusuoka, Stroock and Watanabe (see [3, 4, 14–16, 34, 37]), among others. The main application of this calculus is to show the existence and smoothness of densities of functionals of Gaussian processes. On the other hand, in combination with Stein's method, the Malliavin calculus has been recently used to establish quantitative results on normal approximations (see Nourdin and Peccati [22]). In this section we introduce some basic elements of Malliavin calculus and we refer the reader to [18, 24–26, 36] for a more complete presentation of these notions.

1.1 Finite Dimensional Case

The Malliavin calculus is a differential calculus on a Gaussian probability space. Consider first the finite dimensional case. That is, the probability space $(\Omega, \mathcal{F}, P)$

D. Nualart (✉)
Department of Mathematics, The University of Kansas, Lawrence, KS 66045, USA
e-mail: nualart@ku.edu

S. Heinz and H. Bessaih (eds.), *Stochastic Equations for Complex Systems*,
Mathematical Engineering, DOI 10.1007/978-3-319-18206-3_1

is such that $\Omega = \mathbb{R}^n$, $\mathcal{F} = \mathcal{B}(\mathbb{R}^n)$ is the Borel σ-field of $\mathbb{R}^n$, and P is the standard Gaussian probability with density $p(x) = (2\pi)^{-n/2} e^{-|x|^2/2}$. In this framework, we consider two basic differential operators. The first one is the *derivative operator*, which is simply the gradient of a differentiable function $F : \mathbb{R}^n \to \mathbb{R}$:

$$\nabla F = \left(\frac{\partial F}{\partial x_1}, \ldots, \frac{\partial F}{\partial x_n} \right).$$

The second basic differential operator is called the *divergence operator* and it is defined on differentiable vector-valued functions $u : \mathbb{R}^n \to \mathbb{R}^n$ as follows

$$\delta(u) = \sum_{i=1}^{n} \left(u_i x_i - \frac{\partial u_i}{\partial x_i} \right) = \langle u, x \rangle - \mathrm{div} u.$$

It turns out that δ is the adjoint of the derivative operator with respect to the Gaussian measure P. This is the contents of the next proposition.

Proposition 1 *The operator δ is the adjoint of ∇, that is,*

$$E(\langle u, \nabla F \rangle) = E(F\delta(u)),$$

if F and u are continuously differentiable and their partial derivatives have at most polynomial growth. Here E denotes the mathematical expectation in the probability space $(\Omega, \mathcal{F}, P)$.

Proof Integrating by parts, and using $\frac{\partial p}{\partial x_i} = -x_i p$, we obtain

$$\begin{aligned} \int_{\mathbb{R}^n} \langle \nabla F, u \rangle p dx &= \sum_{i=1}^{n} \int_{\mathbb{R}^n} \frac{\partial F}{\partial x_i} u_i p dx = \sum_{i=1}^{n} \left(- \int_{\mathbb{R}^n} F \frac{\partial u_i}{\partial x_i} p dx + \int_{\mathbb{R}^n} F u_i x_i p dx \right) \\ &= \int_{\mathbb{R}^n} F\delta(u) p dx. \end{aligned}$$

This completes the proof. □

1.2 Malliavin Calculus on the Wiener Space

Fix $T > 0$, and consider the probability space $(\Omega, \mathcal{F}, P)$, where $\Omega = C([0, T])$, $\mathcal{F}$ is the Borel σ-field of Ω, and P is the *Wiener measure*. This measure is defined on cylindrical sets in the following way. For all $0 \le t_1 < \cdots < t_n \le T$, $a_i < b_i$,

$$P\{\omega : a_i \leq \omega(t_i) \leq b_i, 1 \leq i \leq n\}$$
$$= \int_{a_n}^{b_n} \cdots \int_{a_1}^{b_1} \prod_{i=1}^{n} \frac{1}{\sqrt{2\pi(t_i - t_{i-1})}} e^{-\frac{(x_i - x_{i-1})^2}{2(t_i - t_{i-1})}} dx_1 \cdots dx_n,$$

with the convention $t_0 = 0$ and $x_0 = 0$. This measure can be extended to the Borel σ-field $\mathcal{F}$ and the canonical stochastic process $W = \{W_t(\omega) = \omega(t), t \in [0, T]\}$ is a *Brownian motion*. The process W has independent increments, $W_0 = 0$, and for any $0 \leq s < t$, $W_t - W_s$ has the normal law $N(0, t - s)$.

Set $\mathfrak{H} = L^2([0, T])$ and for any $h \in \mathfrak{H}$, denote by $W(h)$ the Wiener integral $W(h) = \int_0^T h(t)dW(t)$. The Hilbert space $\mathfrak{H}$ plays a basic role in the definition of the derivative operator. In fact, the derivative of a random variable $F : \Omega \to \mathbb{R}$ takes values in $\mathfrak{H} = L^2([0, T])$, and $\{D_t F, T \in [0, T]\}$ is a stochastic process. More precisely, consider the set $\mathcal{S}$ of smooth and cylindrical random variables of the form

$$F = f(W(h_1) \ldots, W(h_n)), \tag{1}$$

where $f \in C_p^\infty(\mathbb{R}^n)$ (f and all ist partial derivatives have polynomial growth) and $h_i \in \mathfrak{H}$.

Definition 1 If $F \in \mathcal{S}$ is a smooth and cylindrical random variable of the form (1), the derivative DF is the $\mathfrak{H}$-valued random variable defined by

$$D_t F = \sum_{i=1}^{n} \frac{\partial f}{\partial x_i}(W(h_1) \ldots, W(h_n))h_i(t).$$

For instance, $D(W(h)) = h$ and $D(W_{t_1}) = \mathbf{1}_{[0,t_1]}$, for any $t_1 \in [0, T]$. The operator D can be interpreted as a directional derivative in the following way. Consider the Cameron-Martin space $H^1 \subset \Omega$ defined as the set of functions of the form $\psi(t) = \int_0^t h(s)ds$, where $h \in \mathfrak{H}$. Then, for ant $h \in \mathfrak{H}$, $\langle DF, h\rangle_{\mathfrak{H}}$ is the derivative of F in the direction of $\int_0^{\cdot} h(s)ds$:

$$\langle DF, h\rangle_{\mathfrak{H}} = \int_0^T h_t D_t F dt = \frac{d}{d\epsilon} F\left(\omega + \epsilon \int_0^{\cdot} h_s ds\right)|_{\epsilon=0}.$$

Let us now introduce the divergence operator on the Wiener space. Denote by $\mathcal{S}_{\mathfrak{H}}$ the class of smooth and cylindrical stochastic process $u = \{u_t, t \in [0, T]\}$ of the form

$$u_t = \sum_{j=1}^{n} F_j h_j(t), \tag{2}$$

where the $F_j \in \mathcal{S}$ and $h_j \in \mathfrak{H}$.

Definition 2 We define the divergence of an element u of the form (2), as the random variable given by

$$\delta(u) = \sum_{j=1}^{n} F_j W(h_j) - \sum_{j=1}^{n} \langle DF_j, h_j \rangle_{\mathfrak{H}}. \tag{3}$$

In particular, for any $h \in \mathfrak{H}$, we have $\delta(h) = W(h)$.

As in the finite dimensional case, the divergence defined by (3) is the adjoint of the derivative operator.

Proposition 2 *Let $F \in \mathcal{S}$ and $u \in \mathcal{S}_{\mathfrak{H}}$. Then,*

$$E(F\delta(u)) = E(\langle DF, u \rangle_{\mathfrak{H}}). \tag{4}$$

Proof We can assume that $F = f(W(h_1) \ldots, W(h_n))$ and

$$u = \sum_{j=1}^{n} g_j(W(h_1) \ldots, W(h_n))h_j,$$

where $h_1, \ldots, h_n$ are orthonormal elements in $\mathfrak{H}$. In this case, the duality relationship reduces to the finite dimensional case. □

We make use of the notation $D_h F = \langle DF, h \rangle_{\mathfrak{H}}$, for any $h \in \mathfrak{H}$ and $F \in \mathcal{S}$. The following proposition states the basic properties of the derivative and divergence operators on smooth and cylindrical random variables.

Proposition 3 *Suppose that $u, v \in \mathcal{S}_{\mathfrak{H}}$, $F \in \mathcal{S}$ and $h \in \mathfrak{H}$. Then, if $\{e_i, i \geq 1\}$ is a complete orthonormal system in $\mathfrak{H}$, we have*

$$E(\delta(u)\delta(v)) = E(\langle u, v \rangle_{\mathfrak{H}}) + E\left(\sum_{i,j=1}^{\infty} D_{e_i} \langle u, e_j \rangle_{\mathfrak{H}} D_{e_j} \langle v, e_i \rangle_{\mathfrak{H}} \right), \tag{5}$$

$$D_h(\delta(u)) = \delta(D_h u) + \langle h, u \rangle_{\mathfrak{H}}, \tag{6}$$

$$\delta(Fu) = F\delta(u) - \langle DF, u \rangle_{\mathfrak{H}}. \tag{7}$$

Property (5) can also be written as

$$E(\delta(u)\delta(v)) = E\left(\int_0^T u_t v_t dt \right) + E\left(\int_0^T \int_0^T D_s u_t D_t v_s ds dt \right).$$

Proof We first show Property (6). Assume $u = \sum_{j=1}^{n} F_j h_j$. Then, using $D_h(W(h_j)) = \langle h, h_j \rangle_{\mathfrak{H}}$, we obtain

$$\begin{aligned} D_h(\delta(u)) &= D_h\left(\sum_{j=1}^{n} F_j W(h_j) - \sum_{j=1}^{n} \langle DF_j, h_j \rangle_{\mathfrak{H}}\right) \\ &= \sum_{j=1}^{n} F_j \left\langle h, h_j \right\rangle_{\mathfrak{H}} + \sum_{j=1}^{n} \left(D_h F_j W(h_j) - \left\langle D_h \left(DF_j \right), h_j \right\rangle_{\mathfrak{H}} \right) \\ &= \langle u, h \rangle_{\mathfrak{H}} + \delta(D_h u). \end{aligned}$$

To show Property (5), using the duality formula (4) and Property (6) yield

$$\begin{aligned} E\left(\delta(u)\delta(v)\right) &= E\left(\langle v, D(\delta(u)) \rangle_{\mathfrak{H}}\right) \\ &= E\left(\sum_{i=1}^{\infty} \langle v, e_i \rangle_{\mathfrak{H}} D_{e_i}(\delta(u))\right) = E\left(\sum_{i=1}^{\infty} \langle v, e_i \rangle_{\mathfrak{H}} \left(\langle u, e_i \rangle_{\mathfrak{H}} + \delta(D_{e_i} u) \right)\right) \\ &= E\left(\langle u, v \rangle_{\mathfrak{H}}\right) + E\left(\sum_{i,j=1}^{\infty} D_{e_i} \left\langle u, e_j \right\rangle_{\mathfrak{H}} D_{e_j} \langle v, e_i \rangle_{\mathfrak{H}}\right). \end{aligned}$$

Finally, to prove Property (7), we choose a smooth random variable $G \in \mathcal{S}$ and we write, using the duality relationship (4)

$$\begin{aligned} E[\delta(u)G] &= E\left(\langle DG, Fu \rangle_{\mathfrak{H}}\right) = E\left(\langle u, D(FG) - GDF \rangle_{\mathfrak{H}}\right) \\ &= E\left(\left(\delta(u)F - \langle u, DF \rangle_{\mathfrak{H}}\right) G\right), \end{aligned}$$

which implies the result because $\mathcal{S}$ is dense in $L^2(\Omega)$. □

As a consequence of the duality relationship, the operator D is closable from $L^p(\Omega)$ to $L^p(\Omega; \mathfrak{H})$ for any $p \geq 1$. This means that if $F_N \in \mathcal{S}$ is a sequence of smooth and cylindrical random variables converging in $L^p(\Omega)$ to 0 and DF_N converges in $L^p(\Omega; \mathfrak{H})$ to some element η, then $\eta = 0$. Indeed, for any $u = \sum_{j=1}^{N} G_j h_j \in \mathcal{S}_{\mathfrak{H}}$ such that G_j and DG_j are bounded, we can write

$$E(\langle \eta, u \rangle_{\mathfrak{H}}) = \lim_{N \to \infty} E(\langle DF_N, u \rangle_{\mathfrak{H}}) = \lim_{N \to \infty} E(F_N \delta(u)) = 0,$$

which implies that $\eta = 0$.

1.3 Sobolev Spaces

For any $p \geq 1$, we denote by $\mathbb{D}^{1,p}$ the closure of $\mathcal{S}$ with respect to the seminorm

$$\|F\|_{1,p} = \left(E[|F|^p] + E\left[\left| \int_0^T (D_t F)^2 dt \right|^{p/2} \right] \right)^{1/p}.$$

For $p = 2$, the space $\mathbb{D}^{1,2}$ is a Hilbert space with the scalar product

$$\langle F, G \rangle_{1,2} = E(FG) + E\left[\int_0^T D_t F D_t G dt \right].$$

In the same way we can introduce the spaces $\mathbb{D}^{1,p}(\mathfrak{H})$ by taking the closure of $\mathcal{S}_{\mathfrak{H}}$.

Definition 3 The domain of the divergence operator Domδ in $L^2(\Omega)$ is the set of processes $u \in L^2(\Omega \times [0,T])$ such that there exists $\delta(u) \in L^2(\Omega)$ satisfying the duality relationship

$$E(\langle DF, u \rangle_{\mathfrak{H}}) = E(\delta(u) F),$$

for any $F \in \mathbb{D}^{1,2}$.

Clearly if $u_n \in \mathcal{S}_{\mathfrak{H}}$ satisfies $u_n \overset{L^2(\Omega;\mathfrak{H})}{\longrightarrow} u$ and $\delta(u_n) \overset{L^2(\Omega)}{\longrightarrow} G$, then u belongs to Domδ and $\delta(u) = G$.

Proposition 3 can be extended to random variables in suitable Sobolev spaces. Property (5) holds for $u, v \in \mathbb{D}^{1,2}(\mathfrak{H}) \subset \text{Dom}\delta$ and in this case, for any $u \in \mathbb{D}^{1,2}(\mathfrak{H})$, we can write

$$E(\delta(u)^2) \leq E\left[\int_0^T (u_t)^2 dt \right] + E\left[\int_0^T \int_0^T (D_s u_t)^2 ds dt \right] = \|u\|^2_{1,2,\mathfrak{H}}.$$

Property (6) holds if $u \in \mathbb{D}^{1,2}(\mathfrak{H})$ and $D_h u$ is in the domain of δ. Finally Property (7) holds if $F \in \mathbb{D}^{1,2}$, $Fu \in L^2(\Omega; \mathfrak{H})$, $u \in \text{Dom}\delta$ and the right-hand side is square integrable.

The next theorem asserts the continuity of the divergence operator in $L^p(\Omega)$ for any $p > 1$. It was first proved by Meyer [20]. An alternative proof based on the boundedness in L^p of the Riesz transform is due to Pisier [32].

Theorem 1 *For any $p > 1$ and $u \in \mathbb{D}^{1,p}(\mathfrak{H})$,*

$$E(|\delta(u)|^p) \leq c_p \left(E(\|Du\|^p_{L^2([0,T]^2)}) + E(\|u\|^p_{\mathfrak{H}}) \right). \tag{8}$$

We can also introduce iterated derivatives and the corresponding Sobolev spaces. The kth derivative $D^k F$ of a random variable $F \in \mathcal{S}$ is a k-parameter process obtained by iteration:

$$D^k_{t_1,\dots t_k} F = \sum_{i_1,\dots,i_k=1}^{n} \frac{\partial^k f}{\partial x_{i_1} \cdots \partial x_{i_k}} (W(h_1), \dots W(h_n)) h_{i_1}(t_1) \cdots h_{i_k}(t_k).$$

For any $p \geq 1$, the operator D^k is closable from $L^p(\Omega)$ into $L^p(\Omega; \mathfrak{H}^{\otimes k})$ and we denote by $\mathbb{D}^{k,p}$ the closure of $\mathcal{S}$ with respect to the norm

$$\|F\|_{k,p} = \left(E[|F|^p] + E\left[\sum_{j=1}^{k} \left| \int_{[0,T]^j} (D^j_{t_1,\dots,t_j} F)^2 dt_1 \cdots dt_j \right|^{p/2} \right] \right)^{1/p}.$$

1.4 The Divergence as a Stochastic Integral

For each $t \in [0, T]$, we denote by $\mathcal{F}_t$ the σ-field generated by the random variables $\{W_s, 0 \leq s \leq t\}$. A stochastic process $u = \{u_t, t \in [0, T]\}$ is *adapted* if for each $t \in [0, T]$, u_t is $\mathcal{F}_t$-measurable. We denote by L^2_a the subspace of $L^2(\Omega \times [0, T])$ formed by adapted processes. The following result says that the divergence operator is an extension of the Itô integral [10].

Theorem 2 *$L^2_a \subset \mathrm{Dom}\delta$ and for any $u \in L^2_a$, $\delta(u)$ coincides with the Itô's stochastic integral:*

$$\delta(u) = \int_0^T u_t dW_t.$$

Proof Let $u = \sum_{j=1}^{n} F_j \mathbf{1}_{[a_j,b_j]}$, where the random variables $F_j \in \mathcal{S}$ are $\mathcal{F}_{a_j}$-measurable. Then, $\delta(u)$ coincides with the Itô integral of u because

$$\delta(u) = \sum_{j=1}^{n} F_j (W(b_j) - W(a_j)) - \sum_{j=1}^{n} \int_{a_j}^{b_j} D_t F dt = \sum_{j=1}^{n} F_j (W(b_j) - W(a_j)),$$

taking into account that $D_t F = 0$ if $t > a_j$. Then, the result follows by approximating any square integrable adapted process by cylindrical adapted smooth processes. □

If u not adapted, $\delta(u)$ coincides with an anticipating stochastic integral introduced by Skorohod in [33]. Using techniques of Malliavin calculus, Nualart and Pardoux developed in [28] a stochastic calculus for the Skorohod integral.

If u and v are adapted, then for $s < t$, $D_t v_s = 0$ and for $s > t$, $D_s u_t = 0$. As a consequence, Property (5) leads to the isometry property of the Itô integral

$$E[\delta(u)\delta(v)] = E\left[\int_0^T u_t v_t dt\right].$$

If u is an adapted process in $\mathbb{D}^{1,2}(\mathfrak{H})$, then from Property (6) we obtain

$$D_t\left(\int_0^T u_s dW_s\right) = u_t + \int_t^T D_t u_s dW_s,$$

because $D_t u_s = 0$ if $t > s$.

2 Wiener Chaos and the Ornstein-Uhlenbeck Semigroup

In this section we introduce the Wiener chaos expansion for square integrable random variables and we show how the operators defined in Sect. 1 act on the Wiener chaos. We recall the $W = \{W_t, t \in [0, T]\}$ is a Brownian motion defined in the canonical probability space $(\Omega, \mathcal{F}, P)$.

2.1 Multiple Stochastic Integrals

Let $L^2_s([0, T]^n)$ be the space of symmetric square integrable functions $f : [0, T]^n \to \mathbb{R}$. The multiple stochastic integral of $f \in L^2_s([0, T]^n)$ is defined as an iterated Itô integral:

$$I_n(f) = n! \int_0^T \int_0^{t_n} \cdots \int_0^{t_2} f(t_1, \ldots, t_n) dW_{t_1} \cdots dW_{t_n}.$$

We have the following property $E[I_n(f)I_m(g)] = 0$ if $n \neq m$ and

$$E[I_n(f)I_n(g)] = n!\langle f, g\rangle_{L^2([0,T]^n)} \tag{9}$$

for all $n \geq 1$. If $f \in L^2([0, T]^n)$ is not necessarily symmetric we define $I_n(f) = I_n(\widetilde{f})$, where the $\widetilde{f}$ is the symmetrization of f defined by

$$\widetilde{f}(t_1, \ldots, t_n) = \frac{1}{n!} \sum_{\sigma} f(t_{\sigma(1)}, \ldots, t_{\sigma(n)}),$$

where the sum runs over all permutations σ of $\{1, 2, \ldots, n\}$.

There is a basic relation between multiple stochastic integrals and Hermite polynomials. Denote by h_n the nth Hermite polynomial given by

$$h_n(x) = (-1)^n e^{x^2/2} \frac{d^n}{dx^n}(e^{-x^2/2}).$$

The first Hermite polynomials are $h_0(x) = 1$, $h_1(x) = x$, $h_2(x) = x^2 - 1$, $h_3(x) = x^3 - 3x$, ... Then, for any $g \in L^2([0, T])$ of norm one we have

$$I_n(g^{\otimes n}) = h_n\left(\int_0^T g_t dW_t\right), \tag{10}$$

where $g^{\otimes n}(t_1, \ldots, t_n) = g(t_1) \cdots g(t_n)$.

Let $f \in L^2_s([0, T]^n)$ and $g \in L^2_s([0, T]^m)$. For any $r = 0, \ldots, n \wedge m$, we define the *contraction* of f and g of order r to be the element of $L^2([0, T]^{n+m-2r})$ defined by

$$\begin{aligned}&(f \otimes_r g)(t_1, \ldots, t_{n-r}, s_1, \ldots, s_{m-r}) \\ &= \int_{[0,T]^r} f(t_1, \ldots, t_{n-r}, x_1, \ldots, x_r) g(s_1, \ldots, s_{m-r}, x_1, \ldots, x_r) dx_1 \cdots dx_r.\end{aligned}$$

Notice that $f \otimes_r g$ is not necessarily symmetric, and we denote by $f \widetilde{\otimes}_r g$ its symmetrization. The next equation is the product of two multiple stochastic integrals

$$I_n(f) I_m(g) = \sum_{r=0}^{n \wedge m} r! \binom{n}{r} \binom{m}{r} I_{n+m-2r}(f \otimes_r g). \tag{11}$$

The following result is the *Wiener chaos expansion.*

Theorem 3 *A random variable $F \in L^2(\Omega)$ can be uniquely expanded into a sum of multiple stochastic integrals:*

$$F = E[F] + \sum_{n=1}^{\infty} I_n(f_n).$$

For any $n \geq 1$ we denote by $\mathcal{H}_n$ the closed subspace of $L^2(\Omega)$ formed by all multiple stochastic integrals of order n. For $n = 0$, $\mathcal{H}_0$ is the space of constants. Then, Theorem 3 can be reformulated by saying that we have the orthogonal decomposition $L^2(\Omega) = \oplus_{n=0}^{\infty} \mathcal{H}_n$.

Theorem 3 follows from the fact that if a random variable $G \in L^2(\Omega)$ is orthogonal to $\oplus_{n=0}^{\infty} \mathcal{H}_n$, then it is orthogonal to all random variables of the form $\left(\int_0^T g_t dW_t\right)^k$, where $g \in L^2([0, T])$, $k \geq 0$. This implies that G is orthogonal to all the exponentials $\exp\left(\int_0^T g_t dW_t\right)$, which form a total set in $L^2(\Omega)$. So $G = 0$.

Let us compute the derivative of a multiple stochastic integral. Suppose that $f \in L^2_s([0,T]^n)$. Then $I_n(f) \in \mathbb{D}^{1,2}$, and

$$D_t I_n(f) = n I_{n-1}(f(\cdot, t)). \tag{12}$$

Formula (12) can be proved as follows. Assume $f = g^{\otimes n}$, with $\|g\|_{\mathfrak{H}} = 1$. Let $\theta = \int_0^T g_t dW_t$. Then, using (10) and the properties of Hermite polynomials yields

$$\begin{aligned} D_t I_n(f) &= D_t(h_n(\theta)) = h_n'(\theta) D_t\theta = n h_{n-1}(\theta) g_t \\ &= n g_t I_{n-1}(g^{\otimes(n-1)}) = n I_{n-1}(f(\cdot, t)). \end{aligned}$$

Moreover, applying (9), we obtain

$$\begin{aligned} E\int_0^T [D_t I_n(f)]^2 dt &= n^2 \int_0^T E[I_{n-1}(f(\cdot, t))^2] dt \\ &= n^2 (n-1)! \int_0^T \|f(\cdot, t)\|^2_{L^2([0,T]^{n-1})} dt \\ &= n n! \|f\|^2_{L^2([0,T]^n)} = n E[I_n(f)^2]. \end{aligned} \tag{13}$$

As a consequence of (12) and (13) we deduce the following result.

Proposition 4 *Let $F \in L^2(\Omega)$ with the Wiener chaos expansion $F = \sum_{n=0}^{\infty} I_n(f_n)$. Then $F \in \mathbb{D}^{1,2}$ if and only if*

$$E(\|DF\|^2_{\mathfrak{H}}) = \sum_{n=1}^{\infty} n n! \|f_n\|^2_{L^2([0,T]^n)} < \infty,$$

and in this case

$$D_t F = \sum_{n=1}^{\infty} n I_{n-1}(f_n(\cdot, t)).$$

Similarly, if $F \in \mathbb{D}^{k,2}$, then

$$D^k_{t_1,\ldots,t_k} F = \sum_{n=k}^{\infty} n(n-1)\cdots(n-k+1) I_{n-k}(f_n(\cdot, t_1, \ldots, t_k)),$$

provided this series converges in $L^2(\Omega \times T^k)$. As a consequence, if $F \in \mathbb{D}^{\infty,2} := \cap_k \mathbb{D}^{k,2}$, then the following *Stroock's formula* (see [35]) allows us to compute explicitly the kernels in the Wiener chaos expansion of F:

$$f_n = \frac{1}{n!} E(D^n F).$$

Example 1 Let $F = W_1^3$, assuming $1 \leq T$. Then,

$$f_1(t_1) = E(D_{t_1} W_1^3) = 3E(W_1^2)\mathbf{1}_{[0,1]}(t_1) = 3\mathbf{1}_{[0,1]}(t_1),$$
$$f_2(t_1, t_2) = \frac{1}{2} E(D^2_{t_1,t_2} W_1^3) = 3E(W_1)\mathbf{1}_{[0,1]}(t_1 \vee t_2) = 0,$$
$$f_3(t_1, t_2, t_3) = \frac{1}{6} E(D^3_{t_1,t_2,t_3} W_1^3) = \mathbf{1}_{[0,1]}(t_1 \vee t_2 \vee t_3),$$

and we obtain the Wiener chaos expansion

$$W_1^3 = 3W_1 + 6 \int_0^1 \int_0^{t_1} \int_0^{t_2} dW_{t_1} dW_{t_2} dW_{t_3}.$$

Let us now compute the divergence operator on the Wiener chaos expansion. A square integrable stochastic process $u = \{u_t, t \in [0, T]\} \in L^2(\Omega \times [0, T])$ has an orthogonal expansion of the form

$$u_t = \sum_{n=0}^{\infty} I_n(f_n(\cdot, t)),$$

where $f_0(t) = E[u_t]$ and for each $n \geq 1$, $f_n \in L^2([0, T]^{n+1})$ is a symmetric function in the first n variables.

Proposition 5 *The process u belongs to the domain of δ if and only if the series*

$$\delta(u) = \sum_{n=0}^{\infty} I_{n+1}(\widetilde{f}_n) \tag{14}$$

converges in $L^2(\Omega)$.

Proof Suppose that $G = I_n(g)$ is a multiple stochastic integral of order $n \geq 1$, where g is symmetric. Then,

$$\begin{aligned} E(\langle u, DG\rangle_{\mathfrak{H}}) &= \int_0^T E(I_{n-1}(f_{n-1}(\cdot, t)) n I_{n-1}(g(\cdot, t)))dt \\ &= n(n-1)! \int_0^T \langle f_{n-1}(\cdot, t), g(\cdot, t)\rangle_{L^2([0,T]^{n-1})} dt \\ &= n! \langle f_{n-1}, g\rangle_{L^2([0,T]^n)} = n! \left\langle \widetilde{f}_{n-1}, g \right\rangle_{L^2([0,T]^n)} \\ &= E\left(I_n\left(\widetilde{f}_{n-1}\right) I_n(g)\right) = E\left(I_n\left(\widetilde{f}_{n-1}\right) G\right). \end{aligned}$$

If $u \in \mathrm{Dom}\delta$, we deduce that

$$E(\delta(u)G) = E\left(I_n\left(\widetilde{f}_{n-1}\right) G\right)$$

for every $G \in \mathcal{H}_n$. This implies that $I_n\left(\widetilde{f}_{n-1}\right)$ coincides with the projection of $\delta(u)$ on the nth Wiener chaos. Consequently, the series in (14) converges in $L^2(\Omega)$ and its sum is equal to $\delta(u)$. The converse can be proved by similar arguments. □

2.2 The Ornstein-Uhlenbeck Semigroup

Consider the one-parameter semigroup $\{T_t, t \geq 0\}$ of contraction operators on $L^2(\Omega)$ defined by

$$T_t(F) = \sum_{n=0}^{\infty} e^{-nt} I_n(f_n),$$

where $F = \sum_{n=0}^{\infty} I_n(f_n)$. An alternative and useful formula for the Ornstein-Uhlenbeck semigroup is the following Mehler's formula.

Proposition 6 *Let $W' = \{W'_t, t \in [0, T]\}$ be an independent copy of W. Then, for any $t \geq 0$ and $F \in L^2(\Omega)$ we have*

$$T_t(F) = E'(F(e^{-t}W + \sqrt{1 - e^{-2t}}W')), \tag{15}$$

where E' denotes the mathematical expectation with respect to W'.

Proof Both T_t and the right-hand side of (15) give rise to linear contraction operators on $L^2(\Omega)$. Thus, it suffices to show (15) when $F = \exp\left(\lambda W(h) - \frac{1}{2}\lambda^2\right)$, where $W(h) = \int_0^T h_t dW_t$, $h \in \mathfrak{H}$ is an element of norm one, and $\lambda \in \mathbb{R}$. We have,

$$\begin{aligned} &E'\left(\exp\left(e^{-t}\lambda W(h) + \sqrt{1 - e^{-2t}}\lambda W'(h) - \frac{1}{2}\lambda^2\right)\right) \\ &= \exp\left(e^{-t}\lambda W(h) - \frac{1}{2}e^{-2t}\lambda^2\right) = \sum_{n=0}^{\infty} e^{-nt}\frac{\lambda^n}{n!}h_n\left(W(h)\right) = T_t F, \end{aligned}$$

because

$$F = \sum_{n=0}^{\infty} \frac{\lambda^n}{n!} h_n\left(W(h)\right)$$

and for any $a, z \in \mathbb{R}$ the Hermite polynomials satisfy

$$e^{az - \frac{1}{2}a^2} = \sum_{n=0}^{\infty} \frac{a^n}{n!} h_n(z).$$

This completes the proof. □

Mehler's formula implies that the operator T_t is nonnegative. On the other hand, the operator T_t is symmetric:

$$E(GT_t(F)) = E(FT_t(G)) = \sum_{n=0}^{\infty} e^{-nt} E(I_n(f_n) I_n(g_n)),$$

where $F = \sum_{n=0}^{\infty} I_n(f_n)$ and $G = \sum_{n=0}^{\infty} I_n(g_n)$. It turns out that $\{T_t, t \geq 0\}$ is the semigroup of transition probabilities of a Markov process with values in $C([0, T])$, whose invariant measure in the Wiener measure. This process can be expressed in terms of a Wiener sheet W as follows:

$$X_{t,\tau} = \sqrt{2} \int_{-\infty}^{t} \int_{0}^{\tau} e^{-(t-s)} W(d\sigma, ds),$$

$\tau \in [0, T]$, $t \geq 0$.

The Ornstein-Uhlenbeck semigroup has the following *hypercontractivity property*: If $F \in L^p(\Omega)$, $p > 1$ and $q(t) = e^{2t}(p-1) + 1 > p$, $t > 0$, then

$$\|T_t F\|_{q(t)} \leq \|F\|_p. \tag{16}$$

As a consequence, for any $1 < p < q < \infty$ the norms $\|\cdot\|_p$ and $\|\cdot\|_q$ are equivalent on any Wiener chaos $\mathcal{H}_n$, and for each $n \geq 1$ and $1 < p < \infty$, the projection on the nth Wiener chaos is bounded in $L^p(\Omega)$.

The generator of the Ornstein-Uhlenbeck semigroup in $L^2(\Omega)$ is the operator given by

$$LF = \lim_{t \downarrow 0} \frac{T_t F - F}{t} = \sum_{n=1}^{\infty} -n I_n(f_n),$$

if $F = \sum_{n=0}^{\infty} I_n(f_n)$. The domain of L in $L^2(\Omega)$ coincides with the space $\mathbb{D}^{2,2}$. The next proposition provides a useful relationship between the operators D, δ, and L.

Proposition 7 *Let $F \in L^2(\Omega)$. Then $F \in \operatorname{Dom} L$ if and only if $F \in \mathbb{D}^{1,2}$ and $DF \in \operatorname{Dom} \delta$, and in this case, we have*

$$\delta DF = -LF.$$

Proof Let $F = I_n(f)$. Then, using (12) and (14) we obtain

$$\delta DF = \delta(D_t I_n(f)) = n\delta(I_{n-1}(f(\cdot, t)) = n I_n(f) = -LF,$$

and the result follows easily. □

The operator L behaves as a second-order differential operator on smooth random variables.

Proposition 8 *Suppose that $F = (F^1, \dots, F^m)$ is a random vector whose components belong to $\mathbb{D}^{2,4}$. Let φ be a function in $C^2(\mathbb{R}^m)$ with bounded first and second partial derivatives. Then $\varphi(F) \in \operatorname{Dom} L$ and*

$$L(\varphi(F)) = \sum_{i,j=1}^{m} \frac{\partial^2 \varphi}{\partial x_i \partial x_j}(F)\langle DF^i, DF^j\rangle_{\mathfrak{H}} + \sum_{i=1}^{m} \frac{\partial \varphi}{\partial x_i}(F) L F^i.$$

Proof Suppose first that $F \in \mathcal{S}$ is of the form

$$F = f(W(h_1), \dots, W(h_n)),$$

$f \in C_p^\infty(\mathbb{R}^n)$ and $h_i \in \mathfrak{H}$. Then

$$D_t F = \sum_{i=1}^{n} \frac{\partial f}{\partial x_i}(W(h_1), \dots, W(h_n)) h_i(t).$$

Consequently, $DF \in \mathcal{S}_{\mathfrak{H}} \subset \operatorname{Dom} \delta$ and we obtain

$$\begin{aligned} \delta DF = &\sum_{i=1}^{n} \frac{\partial f}{\partial x_i}(W(h_1), \dots, W(h_n)) W(h_i) \\ &- \sum_{i,j=1}^{n} \frac{\partial^2 f}{\partial x_i \partial x_j}(W(h_1), \dots, W(h_n))\langle h_i, h_j\rangle_{\mathfrak{H}}, \end{aligned}$$

which yields the desired result because $L = -\delta D$. In the general case, it suffices to approximate F by smooth random variables in the norm $\|\cdot\|_{2,4}$, and φ by functions in $C_p^\infty(\mathbb{R}^m)$, and use the continuity of the operator L in the norm $\|\cdot\|_{2,2}$. □

In the finite-dimensional case ($\Omega = \mathbb{R}^n$ equipped with the standard Gaussian law), $L = \Delta - x \cdot \nabla$ coincides with the generator of the Ornstein-Uhlenbeck process $\{X_t, t \geq 0\}$ in $\mathbb{R}^n$, which is the solution to the stochastic differential equation

$$dX_t = \sqrt{2} dW_t - X_t dt,$$

where $\{W_t, t \geq 0\}$ is a standard n-dimensional Brownian motion.

The following integration-by-parts formula will play an important role in the applications of Malliavin calculus to normal approximations.

Proposition 9 *Let $F \in \mathbb{D}^{1,2}$ with $E(F) = 0$. Let f be a continuously differentiable function with bounded derivative. Then,*

$$E[f(F)F] = E[f'(F)\langle DF, -DL^{-1}F\rangle_{\mathfrak{H}}]. \tag{17}$$

Proof Using that

$$F = LL^{-1}F = -\delta(DL^{-1}F)$$

yields

$$\begin{aligned} E[f(F)F] &= -E[f(F)\delta(DL^{-1}F)] \\ &= -E[\langle D(f(F)), DL^{-1}F\rangle_{\mathfrak{H}}] \\ &= E[f'(F)\langle DF, -DL^{-1}F\rangle_{\mathfrak{H}}]. \end{aligned}$$

This completes the proof. □

If we define, for almost all x in the support of F, the function g_F by

$$g_F(x) = E[\langle DF, -DL^{-1}F\rangle_{\mathfrak{H}}|F = x],$$

then, for any $f \in C_b^1(\mathbb{R})$ we have $E[f(F)F] = E[f'(F)g_F(F)]$. Moreover, $g_F(F) \geq 0$ almost surely. Indeed, taking $f(x) = \int_0^x \varphi(y)dy$, where φ is smooth and non-negative we obtain

$$E[E[\langle DF, -DL^{-1}F\rangle_{\mathfrak{H}}|F]\varphi(F)] \geq 0,$$

because $xf(x) \geq 0$.

3 Clark Ocone's Formula

Let $W = \{W_t, 0 \leq t \leq T\}$ be a Brownian motion defined on the canonical probability space $(\Omega, \mathcal{F}, P)$. Recall that L_a^2 denotes the space of adapted process $u = \{u_t, t \in [0, T\}$ such that $E\left(\int_0^T u_t^2 dt\right) < \infty$. The following result is the Itô's stochastic integral representation theorem.

Theorem 4 *Let $F \in L^2(\Omega)$. Then, there exists a unique process $u \in L_a^2$ such that*

$$F = E(F) + \int_0^T u_t dW_t.$$

Then, Clark Ocone's formula (see [30]) provides an explicit expression for the process u in terms of the Malliavin derivative of the random variable F. More precisely, u coincides with the predictable projection of the derivative of F. That is, if $F \in \mathbb{D}^{1,2}$, then, $u_t = E(D_t F|\mathcal{F}_t)$, and we can write

$$F = E(F) + \int_0^T E(D_t F|\mathcal{F}_t)dW_t. \tag{18}$$

Proof For any $v \in L_a^2$ we can write, using the duality relationship (4), we obtain

$$E\left(F\int_0^T v_t dW_t\right) = E(F\delta(v)) = E\left(\int_0^T D_t F v_t dt\right)$$
$$= \int_0^T E[E(D_t F|\mathcal{F}_t)v_t]dt.$$

If we assume that $F = E(F) + \int_0^T u_t dW_t$, then by the Itô isometry

$$E\left(F\int_0^T v_t dW_t\right) = \int_0^T E(u_t v_t)dt.$$

Comparing these two expressions we deduce that

$$u_t = E(D_t F|\mathcal{F}_t)$$

almost everywhere in $\Omega \times [0, T]$. □

Example 2 Suppose that $F = W_t^3$. Then $D_s F = 3W_t^2 \mathbf{1}_{[0,t]}(s)$ and

$$E(D_s F|\mathcal{F}_s) = 3E[(W_t - W_s + W_s)^2|\mathcal{F}_s] = 3[t - s + W_s^2].$$

Therefore,

$$W_t^3 = 3\int_0^t [t - s + W_s^2]dW_s. \tag{19}$$

This formula should be compared with Itô's formula

$$W_t^3 = 3\int_0^t W_s^2 dW_s + 3\int_0^t W_s ds. \tag{20}$$

Notice that Eq. (19) contains only a stochastic integral, but it is not a martingale, because the integrand depends on t, whereas (20) contains two terms and one is a martingale. Moreover, the integrand in (19) is unique.

Example 3 The local time of the Brownian motion $\{L_t^x, t \in [0, T], x \in \mathbb{R}\}$ is defined as the density of the occupation measure:

$$\int_0^t \mathbf{1}_{\{W_s \in C\}} ds = \int_C L_t^x dx,$$

for any Borel set $C \in \mathcal{B}(\mathbb{R})$. Formally, $L_t^x = \int_0^t \delta_x(W_s)ds$. Then, if for any $\varepsilon > 0$, we set $p_\varepsilon(x) = (2\pi\varepsilon)^{-\frac{1}{2}} e^{-x^2/2\varepsilon}$, it holds that

$$F_\varepsilon = \int_0^t p_\varepsilon(W_s - x)ds \overset{L^2(\Omega)}{\longrightarrow} L_t^x.$$

Applying the derivative operator yields

$$D_r F_\varepsilon = \int_0^t p'_\varepsilon(W_s - x) D_r W_s ds = \int_r^t p'_\varepsilon(W_s - x)ds,$$

and

$$\begin{aligned} E(D_r F_\varepsilon | \mathcal{F}_r) &= \int_r^t E\left(p'_\varepsilon(W_s - W_r + W_r - x)|\mathcal{F}_r\right) ds \\ &= \int_r^t p'_{\varepsilon+s-r}\left(W_r - x\right) ds. \end{aligned}$$

As a consequence, taking the limit as ε tends to zero, we obtain the following integral representation for the Brownian local time

$$L_t^x = E(L_t^x) + \int_0^t \left(\int_r^t p'_{s-r}(W_r - x)ds \right) dW_r.$$

4 Application of Malliavin Calculus to Regularity and Estimations of Densities

In this section we establish two different formulas for the density of a Brownian functional using Malliavin calculus. Recall that $W = \{W_t, t \in [0, T]\}$ is a Brownian motion on the canonical probability space $(\Omega, \mathcal{F}, P)$ and D and δ are the fundamental operators in the Malliavin calculus.

4.1 First Density Formula

Proposition 10 *Let F be a random variable in the space $\mathbb{D}^{1,2}$. Suppose that $\frac{DF}{\|DF\|^2_{\mathfrak{H}}}$ belongs to the domain of the operator δ in $L^2(\Omega)$. Then the law of F has a continuous and bounded density given by*

$$p(x) = E\left[\mathbf{1}_{\{F>x\}} \delta\left(\frac{DF}{\|DF\|^2_{\mathfrak{H}}} \right) \right]. \tag{21}$$

Proof Let ψ be a nonnegative smooth function with compact support, and set $\varphi(y) = \int_{-\infty}^{y} \psi(z)dz$. Then $\varphi(F)$ belongs to $\mathbb{D}^{1,2}$, and we can write

$$\langle D(\varphi(F)), DF\rangle_{\mathfrak{H}} = \psi(F)\|DF\|_{\mathfrak{H}}^2.$$

Using the duality formula (4), we obtain

$$E[\psi(F)] = E\left[\left\langle D(\varphi(F)), \frac{DF}{\|DF\|_{\mathfrak{H}}^2}\right\rangle_{\mathfrak{H}}\right] = E\left[\varphi(F)\delta\left(\frac{DF}{\|DF\|_{\mathfrak{H}}^2}\right)\right]. \tag{22}$$

By an approximation argument, Eq. (22) holds for $\psi(y) = \mathbf{1}_{[a,b]}(y)$, where $a < b$. As a consequence, we apply Fubini's theorem to get

$$\begin{aligned} P(a \le F \le b) &= E\left[\left(\int_{-\infty}^{F} \psi(x)dx\right)\delta\left(\frac{DF}{\|DF\|_{\mathfrak{H}}^2}\right)\right] \\ &= \int_a^b E\left[\mathbf{1}_{\{F>x\}}\delta\left(\frac{DF}{\|DF\|_{\mathfrak{H}}^2}\right)\right]dx \end{aligned}$$

which implies the desired result. □

Remark 1 Equation (21) still holds under the hypotheses $F \in \mathbb{D}^{1,p}$ and $\frac{DF}{\|DF\|_{\mathfrak{H}}^2} \in \mathbb{D}^{1,p'}(\mathfrak{H})$ for some p, $p' > 1$. Sufficient conditions for these hypotheses are $F \in \mathbb{D}^{2,\alpha}$ and $E(\|DF\|^{-2\beta}) < \infty$ with $\frac{1}{\alpha} + \frac{1}{\beta} < 1$.

Example 4 Let $F = W(h)$. Then, $DF = h$ and

$$\delta\left(\frac{DF}{\|DF\|_{\mathfrak{H}}^2}\right) = W(h)\|h\|_{\mathfrak{H}}^{-2}.$$

As a consequence, formula (21) yields

$$p(x) = \|h\|_{\mathfrak{H}}^{-2} E\left[\mathbf{1}_{\{F>x\}}F\right],$$

which is true because $p(x)$ is the density of $N(0, \|h\|_{\mathfrak{H}}^2)$.

Applying Eq. (21) we can derive density estimates. Notice first that (21) holds if $\mathbf{1}_{\{F>x\}}$ is replaced by $\mathbf{1}_{\{F<x\}}$, because the divergence has zero expectation. Fix p and q such that $p^{-1} + q^{-1} = 1$. Then, by Hölder's inequality, we obtain

$$p(x) \le (P(|F| > |x|))^{1/q} \left\|\delta\left(\frac{DF}{\|DF\|_{\mathfrak{H}}^2}\right)\right\|_p, \tag{23}$$

for all $x \in \mathbb{R}$. Then, applying Meyer's inequalities we dan deduce the following result (see [25, Propsition 2.1.3]).

Proposition 11 *Let q, α, β be three positive real numbers such that $q^{-1} + \alpha^{-1} + \beta^{-1} = 1$. Let F be a random variable in the space $\mathbb{D}^{2,\alpha}$, such that $\mathbb{E}(\|DF\|_{\mathfrak{H}}^{-2\beta}) < \infty$. Then the density $p(x)$ of F can be estimated as follows*

$$p(x) \leq c_{q,\alpha,\beta} \left(P(|F| > |x|)\right)^{1/q} \times \left(E(\|DF\|_{\mathfrak{H}}^{-1}) + \left\| D^2 F \right\|_{L^{\alpha}(\Omega;\mathfrak{H}\otimes\mathfrak{H})} \left\| \|DF\|_{\mathfrak{H}}^{-2} \right\|_{\beta} \right). \tag{24}$$

Example 5 Set $M_t = \int_0^t u(s) dW_s$, where $u = \{u(t), t \in [0,T]\}$ is an adapted process such that $|u(t)| \geq \rho > 0$ for some constant ρ, $E\left(\int_0^T u(t)^2 dt\right) < \infty$, $u(t) \in \mathbb{D}^{2,2}$ for each $t \in [0,T]$, and

$$\lambda := \sup_{s,t\in[0,T]} \mathbb{E}(|D_s u_t|^p) + \sup_{r,s\in[0,T]} \mathbb{E}\left[\left(\int_0^T |D^2_{r,s} u_t|^p dt \right)^{p/2} \right] < \infty,$$

for some $p > 3$. Then, applying Proposition 11 one can show that the density of M_t, denoted by $p_t(x)$ satisfies

$$p_t(x) \leq \frac{c}{\sqrt{t}} P(|M_t| > |x|)^{\frac{1}{q}},$$

for all $t > 0$, where $q > \frac{p}{p-3}$ and the constant c depends on λ, ρ and p.

Example 6 Consider the process $\xi = \{\xi_{r,t}, 0 \leq r \leq t \leq T\}$ solution of the stochastic differential equation

$$\xi_{r,t} = x + W_t - W_r + \int_r^t \int_{\mathbb{R}} h\left(y - \xi_{r,u}\right) Z\left(du, dy\right),$$

where $x \in \mathbb{R}$, W is a standard Brownian motion, Z is a Brownian sheet independent of W and $h \in H_2^2(\mathbb{R})$. The process ξ represents the position of a particle in a random environment. A measure valued process obtained as the limit of critical branching particles moving with the dynamics of ξ was studied by Dawson, Li and Wang in [9]. For $r \leq t$ we define the conditional transition density given Z by

$$p(r, x; t, y) = P\left(\xi_t \in dy | \xi_r = x, Z\right).$$

Then, Proposition 10 leads to the following expression for this conditional density

$$p(r, x; t, y) = E^W \left[\mathbf{1}_{\{\xi_{r,t} > y\}} \delta(u_{r,t}) \right],$$

where E^W denotes the mathematical expectation with respect to W. From this formula, one can derive the following result (see [11]):

Lemma 1 *Let $c = 1 \vee \|h\|_2^2$. For any $0 \leq r < t \leq T$, $y \in \mathbb{R}$ and $p \geq 1$,*

$$\| p\,(r, x; t, y)\,\|_{2p} \leq 2K_p \exp\left(-\frac{(x-y)^2}{64pc\,(t-r)}\right)(t-r)^{-\frac{1}{2}},$$

where K_p is a constant depending on p.

This lemma has been used by Hu et al. [11] to establish the Hölder continuity in space and time of the solution of the stochastic partial differential equation satisfied by the density of the associated limiting branching particles, improving previous results by Li et al. [17].

4.2 Second Density Formula

Let $F \in \mathbb{D}^{1,2}$ be such that $E[F] = 0$. Recall that $g_F(x) = E[\langle DF, -DL^{-1}F\rangle_{\mathfrak{H}}|F = x] \geq 0$. The following density formula was proved by Nourdin and Viens in [23].

Theorem 5 *Let $F \in \mathbb{D}^{1,2}$ be such that $E[F] = 0$. Then, the law of F has a density p if and only if $g_F(F) > 0$ a.s. In this case the support of p is a closed interval containing zero and for all x in the support of p*

$$p(x) = \frac{E[|F|]}{2g_F(x)} \exp\left(-\int_0^x \frac{ydy}{g_F(y)}\right).$$

Proof Suppose that F has a density p. We consider only the case where the support of p is $\mathbb{R}$. Let ϕ be a smooth function with compact support and consider a function Φ such that $\Phi' = \phi$. Then

$$E[\phi(F)g_F(F)] = E[\Phi(F)F] = \int_{\mathbb{R}} \Phi(x)xp(x)dx = \int_{\mathbb{R}} \phi(x)\varphi(x)dx,$$

where $\varphi(x) = \int_x^\infty yp(y)dy$. This implies $\varphi(x) = p(x)g_F(x)$. Taking into account that $\varphi'(x) = -xp(x)$ we obtain

$$\frac{\varphi'(x)}{\varphi(x)} = -\frac{x}{g_F(x)}.$$

Using that $\varphi(0) = \frac{1}{2}E[|F|]$, we get $\varphi(x) = \frac{1}{2}E[|F|]\exp\left(-\int_0^x \frac{ydy}{g_F(y)}\right)$, which completes the proof. □

Corollary 1 *If there exist constants* $\sigma^2_{\min}, \sigma^2_{\max} > 0$ *such that*

$$\sigma^2_{\min} \leq g_F(F) \leq \sigma^2_{\max}$$

a.s., then F *has a density* p *satisfying*

$$\frac{E[|F|]}{2\sigma^2_{\max}} \exp\left(-\frac{x^2}{2\sigma^2_{\min}}\right) \leq p(x) \leq \frac{E[|F|]}{2\sigma^2_{\min}} \exp\left(-\frac{x^2}{2\sigma^2_{\max}}\right).$$

The random variable $g_F(F)$ can be computed using Mehler's formula (15) and the fact that $-DL^{-1}F = \int_0^\infty e^{-t} T_t(DF)dt$. In this way we obtain

$$g_F(F) = \int_0^\infty e^{-t} E\left[\langle DF, E'[DF(e^{-t}W + \sqrt{1-e^{-2t}}W')]\rangle_{\mathfrak{H}} | F\right] dt.$$

Then, the above corollary can be applied in particular case where we have uniform upper and lower bounds for $\langle DF, E'[DF(e^{-t}W + \sqrt{1-e^{-2t}}W')]\rangle_{\mathfrak{H}}$, as it is illustrated by Example 7.

We would like to point out here that the Malliavin calculus can be developed replacing $\mathfrak{H}$ by a general separable Hilbert space and assuming that $\{W(h), h \in \mathfrak{H}\}$ is an *isonormal Gaussian process*, that is, a centered Gaussian family satisfying $E[W(h)W(g) = \langle h, g\rangle_{\mathfrak{H}}$ for any $h, g \in \mathfrak{H}$.

Example 7 Suppose that $B^H = \{B^H_t, t \in [0, T]\}$ is a fractional Brownian motion with Hurst parameter $H \in (0, 1)$. That is, B^H is a zero mean Gaussian process with covariance

$$E[B^H_t B^H_s] = \frac{1}{2}\left(t^{2H} + s^{2H} - |t-s|^{2H}\right).$$

We define $\mathfrak{H}$ as the closed span of the indicator functions on $[0, T]$ under the inner product $\langle \mathbf{1}_{[0,t]}, \mathbf{1}_{[0,t]}\rangle_{\mathfrak{H}} = E[B^H_t B^H_s]$. Then, the mapping $\mathbf{1}_{[0,t]} \mapsto B^H_t$ can be extended to a linear isometry between $\mathfrak{H}$ and the Gaussian space spanned by B^H. In this way, B^H defines an isonormal Gaussian process associated with $\mathfrak{H}$. Consider the random variable

$$F = \max_{t\in[a,b]} B^H_t - E\left(\max_{t\in[a,b]} B^H_t\right),$$

where $0 < a < b \leq T$. Then, $F \in \mathbb{D}^{1,2}$ and $D_r F = \mathbf{1}_{[0,\tau]}(r)$, where τ is the random point in $[0, T]$ where B^H attains its maximum. As a consequence, if $H > 1/2$, the previous corollary holds with $\sigma_{\min} = a^H$ and $\sigma_{\max} = b^H$, because $a^{2H} \leq E[B^H_t B^H_s] \leq b^{2H}$.

4.3 Existence and Smoothness of Densities

Let $F = (F^1, \ldots, F^m)$ be such that $F^i \in \mathbb{D}^{1,2}$ for $i = 1, \ldots, m$. We define the *Malliavin matrix* of F as the random symmetric nonnegative definite matrix

$$\gamma_F = (\langle DF^i, DF^j \rangle_{\mathfrak{H}})_{1 \le i,j \le m}.$$

Theorem 6 *If* $\det \gamma_F > 0$ *a.s., then the law of* F *is absolutely continuous with respect to the Lebesgue measure on* $\mathbb{R}^m$.

This theorem was proved by Bouleau and Hirsch in [5] using the coarea formula and techniques of geometric measure theory. The measure $(\det \gamma_F \times P) \circ F^{-1}$ is always absolutely continuous, that is, $P(F \in B, \det \gamma_F > 0) = 0$ for any $B \in \mathcal{B}(\mathbb{R}^m)$ of zero Lebesgue measure. In the one-dimensional case, $\gamma_F = \|DF\|^2_{\mathfrak{H}}$.

Definition 4 Let $F = (F^1, \ldots, F^m)$ be a random vector such that $F^i \in \mathbb{D}^{1,2}$ for $i = 1, \ldots, m$. We say that F is *nondegenerate* if $E[(\det \gamma_F)^{-p}] < \infty$ for all $p \ge 2$.

Set $\partial_i = \partial/\partial x_i$, and for any multiindex $\alpha \in \{1, \ldots, m\}^k$, $k \ge 1$, we denote by ∂_α the partial derivative $\partial^k/(\partial x_{\alpha_1} \cdots \partial x_{\alpha_k})$.

Lemma 2 *Let* γ *be an* $m \times m$ *random matrix such that* $\gamma^{ij} \in \mathbb{D}^{1,\infty}$ *for all* i, j *and* $E[(\det \gamma)^{-p}] < \infty$ *for all* $p \ge 2$. *Then* $\left(\gamma^{-1}\right)^{ij}$ *belongs to* $\mathbb{D}^{1,\infty}$ *for all* i, j, *and*

$$D\left(\gamma^{-1}\right)^{ij} = -\sum_{k,l=1}^{m} \left(\gamma^{-1}\right)^{ik} \left(\gamma^{-1}\right)^{lj} D\gamma^{kl}.$$

Proof Approximate γ^{-1} by $\gamma_\epsilon^{-1} = (\det \gamma + \epsilon)^{-1} A(\gamma)$, where $A(\gamma)$ is the adjoint matrix of γ. □

The following result can be regarded as an integration by parts formula and plays a fundamental role in the proof of the regularity of densities.

Proposition 12 *Let* $F = (F^1, \ldots, F^m)$ *be a nondegenerate random vector. Fix* $k \ge 1$ *and suppose that* $F^i \in \mathbb{D}^{k+1,\infty}$ *for* $i = 1, \ldots, m$. *Let* $G \in \mathbb{D}^\infty$ *and let* $\varphi \in C_p^\infty(\mathbb{R}^m)$. *Then for any multiindex* $\alpha \in \{1, \ldots, m\}^k$, *there exists an element* $H_\alpha(F, G) \in \mathbb{D}^\infty$ *such that*

$$E\left[\partial_\alpha \varphi(F) G\right] = E\left[\varphi(F) H_\alpha(F, G)\right],$$

where the elements $H_\alpha(F, G)$ *are recursively given by*

$$H_{(i)}(F, G) = \sum_{j=1}^{m} \delta\left(G\left(\gamma_F^{-1}\right)^{ij} DF^j\right), \tag{25}$$

$$H_\alpha(F, G) = H_{\alpha_k}(F, H_{(\alpha_1, \ldots, \alpha_{k-1})}(F, G)). \tag{26}$$

Proof By the chain rule we have

$$\langle D(\varphi(F)), DF^j\rangle_{\mathfrak{H}} = \sum_{i=1}^m \partial_i\varphi(F)\langle DF^i, DF^j\rangle_{\mathfrak{H}} = \sum_{i=1}^m \partial_i\varphi(F)\gamma_F^{ij},$$

and, consequently,

$$\partial_i\varphi(F) = \sum_{j=1}^m \langle D(\varphi(F)), DF^j\rangle_{\mathfrak{H}}(\gamma_F^{-1})^{ji}.$$

Taking expectations and using the duality relationship (4), yields

$$E\left[\partial_i\varphi(F)G\right] = E\left[\varphi(F)H_{(i)}(F,G)\right],$$

where $H_{(i)} = \sum_{j=1}^m \delta\left(G\left(\gamma_F^{-1}\right)^{ij} DF^j\right)$. Notice that. Meyer's inequality (8) and Lemma 2 imply that $H_{(i)}$ belongs to L^p for any $p \geq 2$. We can finish the proof by a recurrence argument. □

One can show that for any $p > 1$ there exist constants β, $\gamma > 1$ and integers n, m such that

$$\|H_\alpha(F,G)\|_p \leq c_{p,q}\left\|\det\gamma_F^{-1}\right\|_\beta^m \|DF\|_{k,\gamma}^n \|G\|_{k,q}.$$

The following result is a multidimensional version of the density formula (21).

Proposition 13 *Let $F = (F^1, \ldots, F^m)$ be a nondegenerate random vector such that $F^i \in \mathbb{D}^{m+1,\infty}$ for $i = 1, \ldots, m$. Then, F has a continuous and bounded density given by*

$$p(x) = E\left[\mathbf{1}_{\{F>x\}}H_\alpha(F,1)\right]. \tag{27}$$

where $\alpha = (1, 2, \ldots, m)$.

Recall that

$$H_\alpha(F,1) = \sum_{j_1,\ldots,j_m=1}^m \delta\left((\gamma_F^{-1})^{1j_1}DF^{j_1}\delta\left((\gamma_F^{-1})^{2j_2}DF^{j_2}\ldots\delta\left((\gamma_F^{-1})^{mj_m}DF^{j_m}\right)\ldots\right)\right).$$

Proof Equality (26) applied to the multiindex $\alpha = (1, 2, \ldots, m)$ yields

$$E\left[\partial_\alpha\varphi(F)\right] = E[\varphi(F)H_\alpha(F,1)].$$

Notice that

$$\varphi(F) = \int_{-\infty}^{F^1}\cdots\int_{-\infty}^{F^m}\partial_\alpha\varphi(x)dx.$$

Hence, by Fubini's theorem we can write

$$E\left[\partial_\alpha \varphi(F)\right] = \int_{\mathbb{R}^m} \partial_\alpha \varphi(x) E\left[\mathbf{1}_{\{F>x\}} H_\alpha(F,1)\right] dx. \tag{28}$$

We can take as $\partial_\alpha \varphi$ any function in $C_0^\infty(\mathbb{R}^m)$ and the result follows. □

The following theorem is the basic criterion for smoothness of densities.

Theorem 7 *Let $F = (F^1, \ldots, F^m)$ be a nondegenerate random vector such that $F^i \in \mathbb{D}^\infty$ for all $i = 1, \ldots, m$. Then the law of F possesses an infinitely differentiable density.*

Proof For any multiindex β we have (with $\alpha = (1, 2, \ldots, m)$)

$$\begin{aligned} E\left[\partial_\beta \partial_\alpha \varphi(F)\right] &= E[\varphi(F) H_\beta(F, H_\alpha(F,1)))] \\ &= \int_{\mathbb{R}^m} \partial_\alpha \varphi(x) E\left[\mathbf{1}_{\{F>x\}} H_\beta(F, H_\alpha(F,1))\right] dx. \end{aligned}$$

Hence, for any $\xi \in C_0^\infty(\mathbb{R}^m)$

$$\int_{\mathbb{R}^m} \partial_\beta \xi(x) p(x) dx = \int_{\mathbb{R}^m} \xi(x) E\left[\mathbf{1}_{\{F>x\}} H_\beta(F, H_\alpha(F,1))\right] dx.$$

Therefore $p(x)$ is infinitely differentiable, and for any multiindex β we have

$$\partial_\beta p(x) = (-1)^{|\beta|} E\left[\mathbf{1}_{\{F>x\}} H_\beta(F, (H_\alpha(F,1))\right].$$

This completes the proof. □

We finish this section with a density formula obtained using the Riesz transform, following the methodology introduced by Bally and Caramellino [1, 2]. In comparison with (27), here we only need two derivatives, instead of $m+1$.

Let Q_m be the fundamental solution to the Laplace equation $\Delta Q_m = \delta_0$ on $\mathbb{R}^m$, $m \geq 2$. That is,

$$Q_2(x) = a_2^{-1} \ln \frac{1}{|x|}, \quad Q_m(x) = a_m^{-1} |x|^{2-m}, \quad m > 2,$$

where a_m is the area of the unit sphere in $\mathbb{R}^m$. We know that $\partial_i Q_m(x) = -c_m \frac{x_i}{|x|^m}$, where $c_m = 2(m-2)/a_m$ if $m > 2$ and $c_2 = 2/a_2$. Notice that any function φ in $C_0^1(\mathbb{R}^m)$ can be written as

$$\varphi(x) = \nabla \varphi * \nabla Q_m(x). \tag{29}$$

Indeed,

$$\nabla \varphi * \nabla Q_m(x) = \varphi * \Delta Q_m(x) = \varphi(x).$$

Theorem 8 *Let F be an m-dimensional nondegenerate random vector whose components are in $\mathbb{D}^{2,\infty}$. Then the law of F admits a continuous and bounded density p given by*

$$p(x) = \sum_{i=1}^{m} E\left(\partial_i Q_m(F-x) H_{(i)}(F,1)\right),$$

where

$$H_{(i)}(F,1) = \sum_{j=1}^{m} \delta\left((\gamma_F^{-1})^{ij} DF^j\right).$$

Proof Let $\varphi \in C_0^1(\mathbb{R}^m)$. Applying (29), Fubini's theorem, Proposition 12, and integrating by parts, we get

$$\begin{aligned} E\left(\varphi(F)\right) &= \sum_{i=1}^{m} \int_{\mathbb{R}^m} \partial_i Q_m(y) E\left(\partial_i \varphi(F-y)\right) dy \\ &= \sum_{i=1}^{m} \int_{\mathbb{R}^m} \partial_i Q_m(y) E\left(\varphi(F-y) H_{(i)}(F,1)\right) dy \\ &= \sum_{i=1}^{m} \int_{\mathbb{R}^m} \varphi(y) E\left(\partial_i Q_m(F-y) H_{(i)}(F,1)\right) dy. \end{aligned}$$

The use of Fubini's theorem needs to be justified by showing that all the functions are integrable. Assume that the support of φ is included in the ball $B_R(0)$ for some $R > 1$. Then,

$$\begin{aligned} E \int_{\mathbb{R}^m} |\partial_i Q_m(y) \partial_i \varphi(F-y)|\, dy &\le |\partial_i \varphi|_\infty E \int_{\{y:|F|-R\le|y|\le|F|+R\}} |\partial_i Q_m(y)| dy \\ &\le C_m |\partial_i \varphi|_\infty E \int_{|F|-R}^{|F|+R} \frac{r}{r^m} r^{m-1} dr \\ &= 2C_m R |\partial_i \varphi|_\infty < \infty. \end{aligned}$$

This completes the proof. □

The approach based on the Riesz transform can also be used to obtain the following uniform estimate for densities due to Stroock.

Lemma 3 *Under the assumptions of Theorem 8, for any $p > m$ there exists a constant c depending only on m and p such that*

$$\|p\|_\infty \le c \left(\max_{1\le i\le m} \|H_{(i)}(F,1)\|_p\right)^m.$$

Proof Suppose $m \geq 3$. From

$$p(x) = \sum_{i=1}^{m} E\left(\partial_i Q_m(F-x) H_{(i)}(F,1)\right),$$

applying Hölder's inequality with $\frac{1}{p} + \frac{1}{q} = 1$ and the estimate

$$|\partial_i Q_m(F-x)| \leq c_m |F-x|^{1-m}$$

yields

$$p(x) \leq m c_m A \left(E[|F-x|^{(1-m)q}]\right)^{1/q},$$

where $A = \max_{1\leq i\leq m} \|H_{(i)}(F,1)\|_p$.

Suppose first that p is bounded by a constant M. We can write for any $\epsilon > 0$,

$$\begin{aligned} E[|F-x|^{(1-m)q}] &\leq \epsilon^{(1-N)q} + \int_{|z-x|\leq\epsilon} |z-x|^{(1-N)q} p(x)dx \\ &\leq \epsilon^{(1-N)q} + C_N \epsilon^{\frac{p-N}{p-1}} M. \end{aligned}$$

Therefore,

$$M \leq ANk_N \left(\epsilon^{1-N} + C_N^{\frac{1}{q}} \epsilon^{\frac{p-N}{p}} M^{\frac{1}{q}}\right).$$

Now we minimize with respect to ϵ and we obtain $M \leq AC_{N,p} M^{1-\frac{1}{N}}$, for some constant $c_{N,p}$, which implies $M \leq c_{N,p}^N A^N$. If p is not bounded, we apply the procedure to $p * \psi_\delta$, where ψ_δ is an approximation of the identity and let δ tend to zero at the end. □

5 Malliavin Calculus and Normal Approximation

In this section we present the application of Malliavin calculus combined with Stein's method (see [8]) to normal approximations. We refer the reads to the reference book by Nourdin and Peccati [22] for a detailed account of this topic.

5.1 Stein's Method for Normal Approximation

A random variable Z has the standard normal distribution $N(0,1)$ if and only if for any function $f \in C_b^1(\mathbb{R})$, we have $E(f(Z)Z) = E(f'(Z))$. Then, if the expectation

$E(f(Z)Z - f'(Z))$ is small for functions f in some large set, we might conclude that the distribution of Z is close to the normal distribution. The purpose of Stein's method is to quantify this assertion in a proper way. To do this, consider a random variable Z with the $N(0, 1)$ distribution and fix a continuous function $h : \mathbb{R} \to [0, 1]$. The Stein's equation associated with h is the linear differential equation

$$f_h'(x) - x f_h(x) = h(x) - E(h(Z)). \tag{30}$$

One can show that this equation has a unique solution satisfying $\lim_{x\to\pm\infty} e^{-x^2/2} f_h(x) = 0$, given by

$$\begin{aligned} f_h(x) &= e^{x^2/2} \int_{-\infty}^{x} (h(y) - E[h(Z)]) e^{-y^2/2} dy \\ &= -e^{x^2/2} \int_{x}^{\infty} (h(y) - E[h(Z)]) e^{-y^2/2} dy. \end{aligned} \tag{31}$$

Moreover, $f_h \in C^1(\mathbb{R})$ and $|x f_h(x)| \le 1$, $|f_h'(x)| \le 2$.

Recall that the *total variation distance* between the laws of two random variables Y and Z is

$$d_{TV}(Y, Z) = \sup_{B\in\mathcal{B}(\mathbb{R})} |P(Y \in B) - P(Z \in B)|.$$

Proposition 14 *Let F and Z be such that $E[F] = 0$ and Z has the $N(0, 1)$ distribution. Then,*

$$d_{TV}(F, Z) \le \sup_{f\in\mathcal{F}_0} |E[f'(F)] - E[Ff(F)]|,$$

where $\mathcal{F}_0$ is the class of C^1-functions, such that $|xf(x)| \le 1$ and $|f'(x)| \le 2$.

Proof Let $B \subset [-K, K]$ be a bounded Borel set. There is a sequence of continuous functions $h_n : \mathbb{R} \to [0, 1]$ such that $h_n(x) \to \mathbf{1}_B(x)$ for $(\lambda + P_F)$-almost all x, where λ and P_F denote, respectively, the Lebesgue measure and the law of F. Substituting x by F in Stein's equation (30) yields

$$\begin{aligned} |E[h_n(F)] - E[h_n(Z)]| &= |E[f_{h_n}'(F)] - E(F f_{h_n}(F))| \\ &\le \sup_{f\in\mathcal{F}_0} |E[f'(F)] - E[Ff(F)]. \end{aligned}$$

Letting n go to infinity and applying the dominated convergence theorem, we obtain the desired result. □

Suppose now that our probability space $(\Omega, \mathcal{F}, P)$ is the canonical space associated to the standard Brownian motion $W = \{W_t, t \in [0, T]\}$. Combining Stein's method with Malliavin calculus leads to the following result due to Nourdin and Peccati.

Theorem 9 *Suppose that $F \in \mathbb{D}^{1,2}$ satisfies $E[F] = 0$. Let Z be a $N(0,1)$ random variable. Then,*

$$d_{TV}(F, Z) \leq 2E[|1 - \langle DF, -DL^{-1}F\rangle_{\mathfrak{H}}|].$$

Proof Using (17) we obtain for any $f \in \mathcal{F}_0$,

$$\begin{aligned} |E[f'(F)] - E[Ff(F)]| &= |E[f'(F)(1 - \langle DF, -DL^{-1}F\rangle_{\mathfrak{H}}| \\ &\leq 2E\left[|1 - \langle DF, -DL^{-1}F\rangle_{\mathfrak{H}}|\right], \end{aligned}$$

which competes the proof. □

If $E[F^2] = \sigma^2 > 0$ and we take Z to have the law $N(0, \sigma^2)$, we can derive the following inequality using similar arguments

$$d_{TV}(F, Z) \leq \frac{2}{\sigma^2} E[|\sigma^2 - \langle DF, -DL^{-1}F\rangle_{\mathfrak{H}}|]. \tag{32}$$

5.2 Normal Approximation on a Fixed Wiener Chaos

Suppose that $F \in \mathcal{H}_q$ for some $q \geq 2$ and $E(F^2) = \sigma^2$. Then $L^{-1}F = -\frac{1}{q}F$. Taking into account that $E[\|DF\|^2_{\mathfrak{H}}] = q\sigma^2$ we obtain form (32) that

$$d_{TV}(F, Z) \leq \frac{2}{q\sigma^2}\sqrt{\text{Var}\left(\|DF\|^2_{\mathfrak{H}}\right)}.$$

Indeed,

$$E[|\sigma^2 - \langle DF, -DL^{-1}F\rangle_{\mathfrak{H}}|] = E\left[\left|\sigma^2 - \frac{1}{q}\|DF\|^2_{\mathfrak{H}}\right|\right] \leq \frac{1}{q}\sqrt{\text{Var}\left(\|DF\|^2_{\mathfrak{H}}\right)}.$$

The next proposition shows that the variance of $\|DF\|^2_{\mathfrak{H}}$ is equivalent to $E(F^4) - 3\sigma^4$.

Proposition 15 *Suppose that $F = I_q(f) \in \mathcal{H}_q$, $q \geq 2$. Then,*

$$\text{Var}\left(\|DF\|^2_{\mathfrak{H}}\right) \leq \frac{(q-1)q}{3}(E(F^4) - 3\sigma^4) \leq (q-1)\text{Var}\left(\|DF\|^2_{\mathfrak{H}}\right).$$

Proof This proposition is a consequence of the following two formulas for the variance of $\|DF\|^2_{\mathfrak{H}}$ and for $E(F^4) - 3\sigma^4$.

Formula 1:

$$\text{Var}\left(\|DF\|_{\mathfrak{H}}^2\right) = \sum_{r=1}^{q-1} r^2 (r!)^2 \binom{q}{r}^4 (2q-2r)! \|f \widetilde{\otimes}_r f\|_{\mathfrak{H}^{\otimes(2q-2r)}}^2. \tag{33}$$

To establish (33), we start with $D_t F = q I_{q-1}(f(\cdot, t))$, and using the product formula for multiple stochastic integrals (see (11)) we obtain

$$\begin{aligned}
\|DF\|_{\mathfrak{H}}^2 &= q^2 \int_0^T I_{q-1}(f(\cdot,t))^2 dt \\
&= q^2 \sum_{r=0}^{q-1} r! \binom{q-1}{r}^2 I_{2q-2r-2}(f \widetilde{\otimes}_{r+1} f) \\
&= q^2 \sum_{r=1}^{q} (r-1)! \binom{q-1}{r-1}^2 I_{2q-2r}(f \widetilde{\otimes}_r f) \\
&= q q! \|f\|_{\mathfrak{H}^{\otimes q}}^2 + q^2 \sum_{r=1}^{q-1} (r-1)! \binom{q-1}{r-1}^2 I_{2q-2r}(f \widetilde{\otimes}_r f).
\end{aligned} \tag{34}$$

Then Formula (33) follows from the isometry property of multiple integrals.
Formula 2: We claim that

$$E[F^4] - 3\sigma^4 = \frac{3}{q} \sum_{r=1}^{q-1} r (r!)^2 \binom{q}{r}^4 (2q-2r)! \|f \widetilde{\otimes}_r f\|_{\mathfrak{H}^{\otimes(2q-2r)}}^2. \tag{35}$$

To show this formula, using that $-L^{-1}F = \frac{1}{q}F$ and $L = -\delta D$ we first write

$$\begin{aligned}
E[F^4] &= E[F \times F^3] = E[(-\delta D L^{-1} F) F^3] = E[\langle -DL^{-1}F, D(F^3)\rangle_{\mathfrak{H}}] \\
&= \frac{1}{q} E[\langle DF, D(F^3)\rangle_{\mathfrak{H}}] = \frac{3}{q} E[F^2 \|DF\|_{\mathfrak{H}}^2].
\end{aligned} \tag{36}$$

By the product formula of multiple integrals,

$$F^2 = I_q(f)^2 = q! \|f\|_{\mathfrak{H}^{\otimes q}}^2 + \sum_{r=1}^{q} r! \binom{q}{r}^2 I_{2q-2r}(f \tilde{\otimes}_r f). \tag{37}$$

Then, Formula (35) follows from (36), (37), (34) and the isometry property of multiple integrals (see (11)). □

These results can be applied to derive the so-called *Fourth Moment theorem*, proved by Nualart and Peccati in [29] (see also [27]), which represents a drastic simplification of the method of moments.

Theorem 10 *Fix $q \geq 2$. Consider a sequence of multiple stochastic integrals of order q, $F_n = I_q(f_n) \in \mathcal{H}_q$, $n \geq 1$, such that*

$$\lim_{n\to\infty} E(F_n^2) = \sigma^2.$$

The following conditions are equivalent:

(i) $F_n \Rightarrow N(0, \sigma^2)$, *as* $n \to \infty$.
(ii) $E(F_n^4) \to 3\sigma^4$, *as* $n \to \infty$.
(iii) $\|DF_n\|_{\mathfrak{H}}^2 \to q\sigma^2$ *in* $L^2(\Omega)$, *as* $n \to \infty$.
(iv) *For all* $1 \leq r \leq q-1$, $f_n \otimes_r f_n \to 0$, *as* $n \to \infty$.

Proof First notice that (i) implies (ii) because for any $p > 2$, the hypercontractivity property of the Ornstein-Uhlenbeck semigroup (16) implies

$$\sup_n \|F_n\|_p \leq (p-1)^{\frac{n}{2}} \sup_n \|F_n\|_2 < \infty.$$

The equivalence of (ii) and (iii)) follows from Proposition 15, and these conditions imply (i), with convergence in total variation. Moreover (iv) implies (ii) and (iii) because $\|f_n \tilde{\otimes}_r f_n\|_{\mathfrak{H}^{\otimes(2q-2r)}} \leq \|f_n \otimes_r f_n\|_{\mathfrak{H}^{\otimes(2q-2r)}}$. Finally, the fact that (ii) implies (iv) follows form the expression

$$E[F_n^4] = \sum_{r=0}^{q} (r!)^2 \binom{q}{r}^2 (2q-2r)! \|f_n \tilde{\otimes}_r f_n\|_{\mathfrak{H}^{\otimes(2q-r)}}^2,$$

and the fact that $(2q)!\|f_n \tilde{\otimes} f_n\|_{\mathfrak{H}^{\otimes 2q}}^2$ equals to $2(q!)^2\|f\|_{\mathfrak{H}}^4$ plus a linear combination of the terms $\|f_n \otimes_r f_n\|_{\mathfrak{H}^{\otimes(2q-2r)}}^2$, with $1 \leq r \leq q-1$. □

As an application we include a simple proof of the classical Breuer-Major Theorem (see [6]). A function $f \in L^2(\mathbb{R}, \gamma)$, where $\gamma = N(0,1)$, has *Hermite rank* $d \geq 1$ if

$$f(x) = \sum_{q=d}^{\infty} a_q h_q(x),$$

and $a_d \neq 0$. For instance, $f(x) = |x|^p - \int_{\mathbb{R}} |x|^p d\gamma(x)$ has Hermite rank 1. Let $X = \{X_k, k \in \mathbb{Z}\}$ be a centered stationary sequence with unit variance. Set $\rho(v) = E[X_0 X_v]$ for $v \in \mathbb{Z}$.

Theorem 11 *Let $f \in L^2(\mathbb{R}, \gamma)$ with Hermite rank d and assume $\sum_{v\in\mathbb{Z}} |\rho(v)|^d < \infty$. Then,*

$$V_n := \frac{1}{\sqrt{n}} \sum_{k=1}^{n} f(X_k) \Rightarrow N(0, \sigma^2),$$

as $n \to \infty$, where $\sigma^2 = \sum_{q=d}^{\infty} q! a_q^2 \sum_{v\in\mathbb{Z}} \rho(v)^q$.

Proof It suffices to consider the case $f = a_q h_q$, $q \geq d$. The result for the sum would follow from a multidimensional version of the Fourth Moment Theorem due to Peccati and Tudor [31]. There exists a sequence $\{e_k, k \geq 1\}$ in $\mathfrak{H} = L^2([0,T])$ such that

$$\langle e_k, e_j \rangle_{\mathfrak{H}} = \rho(k-j).$$

The sequence $\{W(e_k)\}$ has the same law as $\{X_k\}$, and we may replace V_n by

$$F_n = \frac{a_q}{\sqrt{n}} \sum_{k=1}^{n} h_q(W(e_k)) = I_q(f_{n,q}),$$

where $f_{n,q} = \frac{a_q}{\sqrt{n}} \sum_{k=1}^{n} e_k^{\otimes q}$. We can write

$$q! \| f_{n,q} \|^2_{H^{\otimes q}} = \frac{q! a_q^2}{n} \sum_{i,j=1}^{n} \rho(i-j)^q = q! a_q^2 \sum_{v \in \mathbb{Z}} \rho(v)^q \left(1 - \frac{|v|}{n}\right) \mathbf{1}_{\{|v|<n\}},$$

and by the dominated convergence theorem

$$E[F_n^2] = q! \| f_{n,q} \|^2_{H^{\otimes q}} \to q! a_q^2 \sum_{v \in \mathbb{Z}} \rho(v)^q = \sigma^2,$$

as n tends to infinity. It suffices to show that $\|DF_n\|^2_{\mathfrak{H}}$ converges in $L^2(\Omega)$ to $qq! a_q^2 \sum_{v \in \mathbb{Z}} \rho(v)^q$. We have

$$\|DF_n\|^2_{\mathfrak{H}} = \frac{a_q^2}{n} \sum_{i,j=1}^{n} h_q'(X_i) h_q'(X_j) \rho(i-j),$$

which has the same limit in L^2 as the sequence

$$B_n := \frac{a_q^2}{n} \sum_{j=1}^{n} h_q'(X_j) \left(\sum_{m=-\infty}^{\infty} h_q'(X_{j+m}) \rho(m) \right).$$

The sequence

$$\left\{ h_q'(X_j) \left(\sum_{m=-\infty}^{\infty} h_q'(X_{j+m}) \rho(m) \right), j \geq 1 \right\}$$

is strictly stationary and ergodic. By the *Ergodic Theorem*, converges in $L^2(\Omega)$ to its expectation which is equal to $qq! a_q^2 \sum_{v \in \mathbb{Z}} \rho(v)^q$. This concludes the proof. □

5.3 Convergence of Densities

The total variation distance is equivalent to L^1 norm of the densities:

$$d_{TV}(F,G) = \int_{\mathbb{R}} |p_F(x) - p_G(x)| dx,$$

where p_F and p_G are the densities of the random variables F and G, respectively. Uniform convergence, however, requires stronger hypotheses. The following result was proved by Hu et al. in [12].

Theorem 12 *Let $F \in \mathcal{H}_q$, $q \geq 2$, be such that $E(F^2) = 1$ and $E(\|DF\|_{\mathfrak{H}}^{-6}) \leq M$. Then,*

$$\sup_{s \in \mathbb{R}} |p_F(x) - \phi(x)| \leq C_{M,q} \sqrt{E(F^4) - 3},$$

where ϕ is the density of the law $N(0,1)$.

Using the notion of *Fisher information*, Nourdin and Nualart [21], provided alternative proof of this theorem under the weaker assumption $E(\|DF\|_{\mathfrak{H}}^{-4-\epsilon}) \leq M$ for some $\epsilon > 0$.

Proof Using the density formula (21), Property (7) and $\delta DF = qF$, we can write

$$\begin{aligned} p_F(x) &= E\left[\mathbf{1}_{\{F>x\}} \delta\left(\frac{DF}{\|DF\|_{\mathfrak{H}}^2}\right)\right] \\ &= E\left[\mathbf{1}_{\{F>x\}} \frac{qF}{\|DF\|_{\mathfrak{H}}^2}\right] - E[\mathbf{1}_{\{F>x\}} \langle DF, D(\|DF\|_{\mathfrak{H}}^{-2})\rangle_{\mathfrak{H}}] \\ &= E[\mathbf{1}_{\{F>x\}} F] + E[q\|DF\|_{\mathfrak{H}}^{-2} - 1] - E[\mathbf{1}_{\{F>x\}} \langle DF, D(\|DF\|_{\mathfrak{H}}^{-2})\rangle_{\mathfrak{H}}]. \end{aligned}$$

The terms $E[|q\|DF\|_{\mathfrak{H}}^{-2} - 1|]$ and $E[|\langle DF, D(\|DF\|_{\mathfrak{H}}^{-2})\rangle_{\mathfrak{H}}|]$ can be estimated by a constant times $\sqrt{E(F^4) - 3}$. Taking into account that

$$\phi(x) = E[\mathbf{1}_{\{Z>x\}} Z],$$

where Z has the $N(0,1)$ distribution, it suffices to estimate the difference

$$E[\mathbf{1}_{\{F>x\}} F] - E[\mathbf{1}_{\{Z>x\}} Z],$$

which can be done by Stein's method and Malliavin calculus. □

Example 8 Let $q = 2$ and $F = \sum_{i=1}^{\infty} \lambda_i (X(e_i)^2 - 1)$, where $\{e_i, i \geq 1\}$ is a complete orthonormal system in $\mathfrak{H}$ and λ_i is a decreasing sequence of positive numbers such

that $\sum_{i=1}^{\infty} \lambda_i^2 < \infty$. Suppose $E[F^2] = 1$. Then, if $\lambda_N \neq 0$ for some $N > 4$, we obtain

$$\sup_{x \in \mathbb{R}} |p_F(x) - \phi(x)| \leq C_{N,\lambda_N} \sqrt{\sum_{i=1}^{\infty} \lambda_i^4}.$$

We can also establish the uniform convergence of densities in the framework of the Breuer-Major theorem. Fix $q \geq 2$ and consider the sequence

$$V_n = \frac{1}{\sqrt{n}} \sum_{k=1}^{n} \sum_{j=d}^{q} a_j h_j(X_k), \quad a_d \neq 0,$$

where $X = \{X_k, k \in \mathbb{Z}\}$ is a centered Gaussian stationary sequence with unit variance and covariance $\rho(v)$. The following result have been proved by Hu et al. in [13].

Theorem 13 *Suppose the spectral density of X, f_ρ, satisfies* $\log(f_\rho) \in L^1([-\pi, \pi])$. *Assume* $\sum_{v \in \mathbb{Z}} |\rho(v)|^d < \infty$. *Set* $\sigma^2 := q! a_q^2 \sum_{v \in \mathbb{Z}} \rho(v)^q \in (0, \infty)$. *Then for any* $p \geq 1$, *there exists* n_0 *such that*

$$\sup_{n \geq n_0} E[\|DV_n\|_{\mathfrak{H}}^{-p}] < \infty. \tag{38}$$

Therefore, if $q = d$ and $F_n = V_n / \sqrt{E[V_n^2]}$, we have

$$\sup_{x \in \mathbb{R}} |p_{F_n}(x) - \phi(x)| \leq c \sqrt{E[F_n^4] - 3}.$$

Proof Here is a sketch of the proof of this result. From the non-causal representation $X_k = \sum_{j=0}^{\infty} \psi_j w_{k-j}$, where $w = \{w_k, k \in \mathbb{Z}\}$ is a discrete Gaussian white noise, and using the Malliavin calculus for the discrete white noise w, it follows that

$$\|DV_n\|_{\mathfrak{H}}^2 \geq \frac{1}{n} \sum_{m=1}^{n} \left(\sum_{k=m}^{n} \sum_{j=d}^{q} a_j h_j'(X_k) \psi_{k-m} \right)^2 := B_n.$$

Fix N and consider a block decomposition $B_n = \sum_{i=1}^{N} B_n^i$, where B_n^i is the sum of $\frac{n}{N}$ squares. We use the estimate

$$B_n^{-\frac{p}{2}} \leq \prod_{i=1}^{N} (B_n^i)^{-\frac{p}{2N}}$$

and we apply the Carbery-Wright inequality (see [7]) to control the expectation of $(B_n^i)^{-\frac{p}{2N}}$ if $\frac{p}{2N}$ is small enough. This inequality says that there is a universal constant

$c > 0$ such that, for any polynomial $Q : \mathbb{R}^n \to \mathbb{R}$ of degree at most d and any $\alpha > 0$, we have

$$E[Q(X_1, \ldots, X_n)^2]^{\frac{1}{2d}} P(|Q(X_1, \ldots, X_n)| \leq \alpha) \leq cd\alpha^{\frac{1}{d}},$$

where $X_1, \ldots, X_n$ are independent random variables with law $N(0, 1)$. □

This theorem can be applied to the increments of a fractional Brownian motion with Hurst parameter $H \in (0, 1)$, that is, $\{X_k = B_k^H - B_{k-1}^H, k \geq 1\}$. In this case, the spectral density satisfies the required conditions. As a consequence, we obtain the uniform convergence of densities to ϕ for the sequence of Hermite variations $F_n = V_n / E[V_n^2]$, where

$$V_n = \frac{1}{\sqrt{n}} \sum_{k=1}^{n} h_q(n^H \Delta_k B^H), \quad q \geq 2,$$

for $0 < H < 1 - \frac{1}{2q}$, where $\Delta_k B^H = B_{k/n}^H - B_{(k-1)/n}^H$. In the particular case $q = 2$ we need $H \in (0, \frac{3}{4})$ and we have

$$\sup_{x \in \mathbb{R}} |p_{F_n}(x) - \phi(x)| \leq c\sqrt{E(F_n^4) - 3} \leq c_H \begin{cases} n^{-\frac{1}{2}} & \text{if } H \in (0, \frac{5}{8}) \\ n^{-\frac{1}{2}} (\log n)^{\frac{3}{2}} & \text{if } H = \frac{5}{8} \\ n^{4H-3} & \text{if } H \in (\frac{5}{8}, \frac{3}{4}) \end{cases}$$

The following further results on uniform convergence of densities have been also proved in [12].

(i) One can show the uniform approximation of the mth derivative of p_F by the corresponding mth derivative of the Gaussian density $\phi^{(m)}$ under the stronger assumption $E(\|DF\|_{\mathfrak{H}}^{-\beta}) < \infty$ for some $\beta > 6m + 6\left(\lfloor \frac{m}{2} \rfloor \vee 1\right)$.

(ii) Consider a d-dimensional vector F, whose components are in a fixed chaos, and such that $E[(\det \gamma_F)^{-p}] < \infty$ for all p, where γ_F denotes the Malliavin matrix of F. In this case for any multi-index $\beta = (\beta_1, \ldots, \beta_k)$, $1 \leq \beta_i \leq d$, one can show

$$\sup_{x \in \mathbb{R}^d} \left|\partial_\beta f_F(x) - \partial_\beta \phi_d(x)\right| \leq c\left(|C - I|^{\frac{1}{2}} + \sum_{j=1}^{d} \sqrt{E[F_j^4] - 3(E[F_j^2])^2}\right)$$

where C is the covariance matrix of F, ϕ_d is the standard d-dimensional normal density, and $\partial_\beta = \frac{\partial^k}{\partial x_{\beta_1} \cdots \partial x_{\beta_k}}$.

References

1. Bally V, Caramellino L (2011) Riesz transform and integration by parts formulas for random variables. Stoch Process Appl 121:1332–1355
2. Bally V, Caramellino L (2013) Positivity and lower bounds for the density of Wiener functionals. Potential Anal 39:141–168
3. Bismut JM (1981) Martingales, the Malliavin calculus and hypoellipticity under general Hörmander's conditions. Z Wahrsch Verw Gebiete 56:469–505
4. Bismut JM (1984) Large deviations and the Malliavin calculus. Progress in mathematics, vol 45. Birkhäuser, Boston
5. Bouleau N, Hirsch F (1991) Dirichlet forms and analysis on Wiener space. Walter de Gruyter & Co., Berlin
6. Breuer P, Major P (1983) Central limit theorems for nonlinear functionals of Gaussian fields. J Multivar Anal 13:425–441
7. Carbery A, Wright J (2001) Distributional and L^q norm inequalities for polynomials over convex bodies in $\mathbb{R}^n$. Math Res Lett 8:233–248
8. Chen L, Goldstein L, Shao QM (2011) Normal approximation by Stein's method. Springer, Berlin
9. Dawson DA, Li Z, Wang H (2001) Superprocesses with dependent spatial motion and general branching densities. Electron J Probab 6:1–33
10. Gaveau B, Trauber P (1982) L'intégrale stochastique comme opérateur de divergence dans l'espace fonctionnel. J Funct Anal 46:230–238
11. Hu Y, Lu F, Nualart D (2013) Hölder continuity of the solutions for a class of nonlinear SPDE's arising from one dimensional superprocesses. Probab Theory Relat Fields 156:27–49
12. Hu Y, Lu F, Nualart D (2014) Convergence of densities for some functionals of Gaussian processes. J Funct Anal 266:814–875
13. Hu Y, Nualart D, Tindel S, Xu F, Density convergence in the Breuer-major theorem for Gaussian stationary sequences. Bernoulli (to appear)
14. Kusuoka S, Stroock D (1984) Applications of the Malliavin calculus. I. Stochastic analysis (Katata/Kyoto, 1982). North-Holland, Amsterdam
15. Kusuoka S, Stroock D (1985) Applications of the Malliavin calculus. II. J Fac Sci Univ Tokyo Sect IA Math 32:1–76
16. Kusuoka S, Stroock D (1987) Applications of the Malliavin calculus. III. J Fac Sci Univ Tokyo Sect IA Math 34:391–442
17. Li Z, Wang H, Xiong J, Zhou X (2011) Joint continuity for the solutions to a class of nonlinear SPDE. Probab Theory Relat Fields 153(3–4):441–469
18. Malliavin P (1978) Stochastic calculus of variation and hypoelliptic operators. In: Proceedings of the international symposium on stochastic differential equations, Kyoto, 1976. Wiley, New York-Chichester-Brisbane, pp 195-263
19. Malliavin P (1997) Stochastic analysis. Grundlehren der Mathematischen Wissenschaften, vol 313. Springer, Berlin
20. Meyer PA (1984) Transformations de Riesz pour les lois gaussiennes. Seminaire de Probabilités XVIII. Lecture notes in mathematics, vol 1059. Springer, Berlin, pp 179–193
21. Nourdin I, Nualart D, Fisher information and the fourth moment problem. Annals Inst Henri Poincaré (to appear)
22. Nourdin I, Peccati G (2012) Normal approximations with Malliavin calculus. From Stein's method to universality. Cambridge University Press, Cambridge
23. Nourdin I, Viens F (2009) Density formula and concentration inequalities with Malliavin calculus. Electron J Probab 14:2287–2309
24. Nualart D (1998) Analysis on Wiener space and anticipating stochastic calculus. Lectures on probability theory and statistics (Saint-Flour, 1995). Lecture notes in mathematics, vol 1690. Springer, Berlin, pp 123–227
25. Nualart D (2006) The Malliavin calculus and related topics, 2nd edn. Springer, New York

26. Nualart D (2009) Malliavin calculus and its applications. CBMS regional conference series in mathematics, vol 110. AMS & NSF
27. Nualart D, Ortiz-Latorre S (2007) Central limit theorems for multiple stochastic integrals. Stoch Process Appl 118:614–628
28. Nualart D, Pardoux E (1988) Stochastic calculus with anticipating integrands. Probab Theory Relat Fields 78:535–581
29. Nualart D, Peccati G (2005) Central limit theorems for sequences of multiple stochastic integrals. Ann Probab 33:177–193
30. Ocone D (1984) Malliavin calculus and stochastic integral representation of diffusion processes. Stochastics 12:161–185
31. Peccati G, Tudor C (2005) Gaussian limits for vector-valued multiple stochastic integrals. Séminaire de Probabilités XXXVIII. Lecture notes in mathematics, vol 1857. Springer, Berlin, pp 247–262
32. Pisier G (1988) Riesz transforms. A simple analytic proof of P.A. Meyer's inequality. Seminaire de Probabilités XXIII. Lecture notes in mathematics, vol 1321. Springer, Berlin, pp 485–501
33. Skorohod AV (1975) On a generalization of a stochastic integral. Theory Probab Appl 20:219–233
34. Stroock DW (1983) Some applications of stochastic calculus to partial differential equations. In: Eleventh Saint Flour probability summer school 1981 (Saint Flour, 1981). Lecture notes in mathematics, vol 976. Springer, Berlin, pp 267–382
35. Stroock DW (1987) Homogeneous chaos revisited. Seminaire de Probabilités XXI. Lecture notes in mathematics, vol 1247, Springer, Berlin, pp 1–8
36. Üstünel AS (1995) An introduction to analysis on Wiener space. Lecture notes in mathematics, vol 1610. Springer, Berlin
37. Watanabe S (1984) Lectures on stochastic differential equations and Malliavin calculus. Tata Institute of Fundamental Research. Springer, Berlin

Fractional Brownian Motion and an Application to Fluids

Chandana Wijeratne and Hakima Bessaih

Abstract In this chapter, we review the fractional Brownian motion (fBm) and some of its properties. It is a Gaussian process that is characterized by its covariance function and its hurst parameter $H \in (0, 1)$. When $H > 1/2$, we introduce the stochastic integral with respect to a fBm by using fractional integrals. This is a pathwise approach based on the Riemann Stieltjes construction using the Hölder continuity of the process. An application related to fluids is provided. This is an integrodifferential equation representing the dynamic of a vortex filament associated to an inviscid, incompressible, homogeneous fluid in $\mathbb{R}^3$. We prove existence and uniqueness of solutions in a functional space of Sobolev type.

1 Introduction

This chapter begins with a short introduction to fractional Brownian motion (fBm) and a description on the vortex filament associated to a 3D turbulent fluid flow. In Sect. 2, assumptions and the functional setting of our problem have been introduced. We recall the notions of fractional integrals and some related a priori estimates in Sect. 3. In Sect. 4, we introduce the notion of integration with respect to a fBm. Section 5 contains our main results about the existence and uniqueness of a global solution for the Eq. (5) with most of their proofs.

C. Wijeratne (✉)
Faculty of Engineering, Sri Lanka Institute of Information Technology,
New Kandy Road, Malabe 10115, Sri Lanka
e-mail: chandana.w@sliit.lk

H. Bessaih
Department of Mathematics, University of Wyoming, Ross Hall 210,
Laramie, WY 82071-3036, USA
e-mail: bessaih@uwyo.edu

S. Heinz and H. Bessaih (eds.), *Stochastic Equations for Complex Systems*,
Mathematical Engineering, DOI 10.1007/978-3-319-18206-3_2

1.1 Fractional Brownian Motion

Fractional Brownian motion (fBm) was first introduced by Kolmogorov in 1940 by the name "Wiener spiral" [26] within a Hilbert space setting. The name "fractional Brownian motion" is due to Mandelbrot and Van Ness as they gave a representation to the fractional Brownian motion through a fractional integral with respect to the standard Brownian motion in 1968 [31].

Definition 1 Let $B^H = \{B^H_\eta, \eta \geq 0\}$ be a stochastic process, and $H \in (0, 1)$. B^H is called a fractional Brownian motion (fBm) with Hurst parameter H, if it is a centered Gaussian process with the covariance function

$$R_H(\gamma, \eta) = E[B^H_\gamma B^H_\eta] = \frac{1}{2}(\eta^{2H} + \gamma^{2H} - |\eta - \gamma|^{2H}), \quad \gamma, \eta \geq 0. \tag{1}$$

Fractional Brownian motion is parameterized by a parameter H, known as the 'Hurst parameter', and it is also due to Mandelbrot. Mandelbrot named the parameter after the hydrologist Hurst who did a statistical study of the yearly water run-offs of the Nile river [23]. The parameter $H \in (0, 1)$ and when $H = \frac{1}{2}$, we recover the well known standard Brownian motion. Hence fractional Brownian motion is a generalization of the standard Brownian motion. Many authors treat the fBm in three different families corresponding respectively to $0 < H < \frac{1}{2}, H = \frac{1}{2}$ and $\frac{1}{2} < H < 1$.

Fractional Brownian motion finds applications in diverse fields such as finance, economics, biology, physics and engineering. Whenever we are interested in processes with self similarity, long memory, stationary increments fBm is a natural candidate. Applications of fBm have been studied by many authors. For instance in mathematical finance, Cheridito [10] constructed arbitrage strategies using fBm, Comte and Renault [12] presents continuous time models with long memory with fBm, and Rogers [38] discussed use of fBm in modeling long range dependence of share returns. In engineering applications for instance, in [19] a queue with an infinite buffer space and fBm as a long-range dependent input have been studied. In [34] Norros presented a model for connectionless traffic using fBm. In [28] the self similarity of fBm has been studied in capturing fractal behavior in Ethernet local area network traffic.

1.2 Properties of Fractional Brownian Motion

Many authors have studied fBm in different approaches. For instance, [20] describes fBm together with a detailed presentation on self similarity which is an interesting property of fBm. Theory and applications of the long range dependence, another widely used property of fBm can be found in [17]. For a comprehensive treatment of fBm, see for instance [8, 33, 35]. The Hurst parameter H relates with the sign

of the correlation of the increments, regularity of the sample paths, and many other properties of fBm as described below.

• *Self-similarity*: Fractional Brownian motion with Hurst parameter H is H self similar. For any constant $a > 0$, the two processes $\{B^H(at),\ t \geq 0\}$ and $\{a^H B^H(t),\ t \geq 0\}$ are equal in their probability distributions. This is a fractal property of fBm and results from its covariance function (1).

• *Stationary increments*: Fractional Brownian motion has stationary increments. Using the covariance function (1), one could verify that $\{B^H(t+h) - B^H(h)\}$ and $\{B^H(t)\}$ have the same probability distribution for $h > 0$.

• *Independent increments*: Fractional Brownian motion has independent increments if and only if $H = \frac{1}{2}$. When $H = \frac{1}{2}$ it can be seen that $\mathbb{E}[B^H(t)B^H(s)] = \min\{s,t\}$ and we recover the ordinary Brownian motion. For $H \neq \frac{1}{2}$ increments of fBm are not independent. When $H > \frac{1}{2}$, the increments are positively correlated, and for $H < \frac{1}{2}$, they are negatively correlated.

• *Long range dependence*: Let $\{X(t), t \geq 0\}$ be an $H-$self similar process with stationary increments, and non-degenerate for all t, with $\mathbb{E}[X(1)^2] < \infty$. Suppose $\xi(n) = X(n+1) - X(n)$ and $r(n) = \mathbb{E}[\xi(0)\xi(n)]$, for $n = 0, 1, 2 \ldots$. Then, for $\frac{1}{2} < H < 1$ we have $\sum_n |r(n)| = \infty$ and this property is known as long range dependence. Fractional Brownian motion exhibits long range dependence or long memory when $H > \frac{1}{2}$. The coupling between values at distinct points of time decreases quite slowly as the time difference increases. This is in contrast with the short range dependence of some processes where the coupling between values at distinct points of time decreases quite rapidly (exponentially) as the time difference increases.

• *Markovian property*: Recall that a Gaussian process with covariance R is Markovian if and only if $R(s,u) = \frac{R(s,t)R(s,u)}{R(t,t)}$ for all $s \leq t \leq u$. Applying the covariance function in (1) one can see that fBm is Markovian if and only if $H = \frac{1}{2}$.

• *β Hölder continuity*: For the sample path properties of fBm, it has continuous trajectories. In particular, fBm admits a modification which is Hölder continuous of order β if and only if $\beta \in (0, H)$. This can be seen ny applying Kolmogorov's continuity criterion, for instance see [20]. Thus, value of the Hurst parameter H decides the regularity of sample paths.

• *Differentiability*: Fractional Brownian motion is almost surely nowhere differentiable. As fBm has stationary increments, consider the point $t = 0$. If the derivative $(B^H)'(0)$ exists, then we have $B^H(s) \leq (\epsilon + (B^H)'(0))s$, for some positive $s \leq s_\epsilon$ and B^H is 1-Hölder continuous at $t = 0$, contradicting the Hölder continuity of fBm.

• *p-variation*: Let f be a real valued function on $[0, T]$, $\Pi := \{t_k \mid 0 = t_0 < t_1 < \cdots < t_n = T\}$, be a partition of $[0, T]$, and $p \in [1, \infty)$. Then the p-variation of f along the partition Π is $V_p(f : \Pi) := \sum_{t_k \in \Pi} |f(t_k) - f(t_{k-1})|^p$. If $V_p(f) := \sup_\Pi V_p(f : \Pi)$ is finite, then f has bounded p-variation. Fractional Brownian motion has zero bounded p-variation when $p > \frac{1}{H}$ a.s. and unbounded p-variation when $p < \frac{1}{H}$.

• *Semimartingale*: A semimartingale can be written as the sum of a bounded variation process and a local martingale which has finite quadratic variation. If $H < \frac{1}{2}$ the quadratic variation is infinite, and if $H > \frac{1}{2}$ the 1-variation is infinite. Thus, most importantly the fBm with $H \neq \frac{1}{2}$ is not a semimartingale. As a consequence, the well developed Itô calculus which is applicable to semi martingales can't be used to define the stochastic integral with respect to the fBm. As a result, different approaches have been introduced when working with fBm.

The definition of stochastic integrals with respect to the fractional Brownian motion $\int_0^t u_s dB_s^H$ where u is a stochastic process has been investigated intensively by several authors. One approach is deterministic pathwise approach that is based on the Riemann-Stieltjes construction using the Hölder continuity and is due to Young [40]. This is applicable only for Hurst parameters $H > \frac{1}{2}$. This idea has been extended, see [14, 15, 22, 29, 30] and a rough path theory which is valid for Hurst parameters $H > \frac{1}{4}$ has been introduced and studied. As fBm is a Gaussian process another approach is to use Malliavin calculus or stochastic calculus of variation with the use of divergence operator and for more details refer [27, 35, 36]. For a comprehensive treatment of stochastic integrals with respect to the fractional Brownian motion refer [1, 2, 9, 13, 16, 18, 25, 37].

1.3 An Application of fBm to Fluids

In the present work, we are using the pathwise argument to solve an integral equation which is an approximation of the line vortex equation. In particular, we will assume that the vorticity field associated to an ideal inviscid incompressible homogeneous fluid in $\mathbb{R}^3$ is described by a fractional Brownian motion with Hurst parameter $H > \frac{1}{2}$ and we will study its evolution through a pathline equation. Let us denote by ω this vorticity field then

$$\boldsymbol{\omega} := \nabla \times \mathbf{u},$$

where $\mathbf{u}$ is the velocity field in $\mathbb{R}^3$. If we denote by $\mathbf{X}_t(\mathbf{x})$ the position at time t of the fluid particle that at time 0 was at $\mathbf{x} \in \mathbb{R}^3$. We have the following path-lines equation

$$\frac{d\mathbf{X}_t(\mathbf{x})}{dt} = \mathbf{u}(t, \mathbf{X}_t(\mathbf{x})). \tag{2}$$

Now, let us assume that the vorticity field is concentrated on a fractional Brownian curve $\mathbf{B}^H$ as follows

$$\boldsymbol{\omega}(t, \mathbf{x}) = \Gamma \int_0^1 \delta(\mathbf{x} - \mathbf{B}_\xi^H(t))\, d\mathbf{B}_\xi^H(t), \tag{3}$$

where δ is the usual "Dirac delta function", $\Gamma > 0$ is the intensity of vorticity, $\xi \in [0, 1]$ is the arc-length, while the parameter t represents the time. Using the Biot-Savart formula, the Eq. (2) becomes

$$\frac{d\mathbf{X}_\xi(t)}{dt} = \int_0^1 Q(\mathbf{X}_\xi(t) - \mathbf{B}_\eta^H(t))\, d\mathbf{B}_\eta^H(t), \tag{4}$$

with

$$\mathbf{X}_\xi(0) = \boldsymbol{\phi}_\xi.$$

Here $\boldsymbol{\phi}$ is the initial condition and the matrix valued function Q is the singular matrix

$$\frac{-\Gamma}{4\pi|\mathbf{y}|^3} \begin{pmatrix} 0 & y_3 & -y_2 \\ -y_3 & 0 & y_1 \\ y_2 & -y_1 & 0 \end{pmatrix}.$$

For an introduction to this topic we refer to [5, 11, 32, 39] and for a more probabilistic approach to [21]. When $\mathbf{B}^H$ is replaced by $\mathbf{X}$, the Eq. (4) has been studied by [3] for a smooth closed curve $\mathbf{X}$ in the Sobolev space $W^{1,2}$ and an existence and uniqueness theorem has been proved for local solutions in time. Later, local solutions in some spaces of Hölder continuous functions have been investigated in [6] that have been extended to global solutions in [4].

In this work, we will be dealing with an approximation of Eq. (4), the approximation will be on the matrix Q, while the study of Eq. (4) is left for a subsequent paper. Furthermore, in order to make the exposition of our results easier to understand, we will make the assumption that the function $\mathbf{X}$ is a real valued function, however, our results will still be true for a vector valued function $\mathbf{X}$. More precisely, we are interested in the following integrodifferential equation

$$Y_\xi(t) = \phi_\xi + \int_0^t \int_0^\xi A(Y_\eta(s))\, dB_\eta^H(s) ds, \tag{5}$$

where for all $t \in [0, T]$, $B^H(t) = \left\{ B_\xi^H(t),\ \xi \in [0, 1] \right\}$ is a real valued fractional Brownian motion of Hurst parameter $H > \frac{1}{2}$, A is a bounded and differentiable real valued function with a Lipschitz continuity property, ξ is a parameter in [0,1].

2 Some Preliminaries

2.1 The Integrodifferential Equation

Here we study the following equation.

$$\frac{\partial Y_\xi(t)}{\partial t} = \int_0^\xi A(Y_\eta(t))\, dB_\eta^H(t),\ \xi \in [0,1] \text{ and } t \in [0,T] \tag{6}$$

with

$$Y_\xi(0) = \phi_\xi$$

or alternatively, we can consider the integral form

$$Y_\xi(t) = \phi_\xi + \int_0^t \int_0^\xi A(Y_\eta(s))\, dB_\eta^H(s)ds, \tag{7}$$

where B^H is a fractional Brownian motion defined on a complete probability space $(\Omega, \mathcal{F}, P)$. Here the stochasticity is with respect to ξ and this is deterministic with respect to time. The initial condition is ϕ_ξ and $A : \mathbb{R} \to \mathbb{R}$ is a measurable function that satisfies the assumptions given below.

2.2 Assumptions

Let us assume that:
A1. A is differentiable.
A2. There exists $M_1 > 0$ such that $|A(x) - A(y)| \le M_1|x - y|$ for all $x, y \in \mathbb{R}$.
A3. There exists $M_2 > 0$ such that $|A(x)| \le M_2$ for all $x \in \mathbb{R}$.
A4. For every N there exists $M_N > 0$, such that
$|A'(x) - A'(y)| \le M_N|x - y|$ for all $|x|, |y| \le N$.

2.3 Functional Setting

Let $\frac{1}{2} < H < 1, 1 - H < \alpha < \frac{1}{2}$. We will introduce the following functional spaces.

Let $C([0,T], W^{\alpha,\infty}[0,1])$ be the space of measurable functions $f : [0,T] \times [0,1] \to \mathbb{R}$ such that

$$\| f \|_{\alpha,\infty} := \sup_{t\in[0,T]} \sup_{\xi\in[0,1]} \left(|f(t,\xi)| + \int_0^\xi \frac{|f(t,\xi) - f(t,\eta)|}{(\xi - \eta)^{\alpha+1}} d\eta \right) < \infty. \tag{8}$$

Let $C([0,T], W_0^{1-\alpha,\infty}[0,1])$ be the space of measurable functions $f : [0,T] \times [0,1] \to \mathbb{R}$ such that

$$\| f \|_{1-\alpha,\infty,0} := \sup_{t\in[0,T]} \sup_{0<\eta<\xi<1} \left(\frac{|f(t,\xi) - f(t,\eta)|}{(\xi-\eta)^{1-\alpha}} + \int_\eta^\xi \frac{|f(t,\gamma) - f(t,\eta)|}{(\gamma-\eta)^{2-\alpha}} d\gamma \right) < \infty. \tag{9}$$

Let $W^{\alpha,1}([0,1])$ be the space of measurable functions $f : [0,1] \to \mathbb{R}$ such that

$$\| f \|_{\alpha,1} := \int_0^1 \frac{|f(\eta)|}{\eta^\alpha} d\eta + \int_0^1 \int_0^\eta \frac{|f(\eta) - f(\delta)|}{(\eta-\delta)^{\alpha+1}} d\delta d\eta < \infty. \tag{10}$$

3 Some a Priori Estimates

Since fBm with Hurst parameters $H > \frac{1}{2}$ have sample paths that are λ-Hölder continuous for all $\lambda \in (0, H)$, the construction of the integral with respect to a fBm will be performed using a pathwise argument by means of fractional derivatives and integrals. We refer to [24, 37] for more details.

3.1 Fractional Integrals and Derivatives

As usual we denote by $L^p(a,b)$ the space of all Lebesgue measurable functions $f : (a,b) \to \mathbb{R}$ such that

$$\| f \|_{L^p(a,b)} := \left(\int_a^b |f(x)|^p dx \right)^{\frac{1}{p}} < \infty \tag{11}$$

for $a < b$ and $1 \le p < \infty$. Let us recall some definitions on Riemann-Liouville fractional integrals and Weyl derivative.

Definition 2 Let $f \in L^1(a,b)$ and $\alpha > 0$. The left-sided and right-sided Riemann-Liouville fractional integrals of f of order α are defined for almost all $x \in (a,b)$ by

$$I_{a+}^\alpha f(x) = \frac{1}{\Gamma(\alpha)} \int_a^x \frac{f(y)}{(x-y)^{1-\alpha}} dy \tag{12}$$

and

$$I_{b-}^\alpha f(x) = \frac{(-1)^{-\alpha}}{\Gamma(\alpha)} \int_x^b \frac{f(y)}{(y-x)^{1-\alpha}} dy \tag{13}$$

respectively, where $(-1)^{-\alpha} = e^{-i\pi\alpha}$ and $\Gamma(\alpha) = \int_0^\infty r^{(\alpha-1)}e^{-r}dr$ is the Gamma function or the Euler integral of the second kind.

Definition 3 Suppose $I^{\alpha}_{a+}(L^p)$ is the image of $L^p(a,b)$ under the operator I^{α}_{a+} and $I^{\alpha}_{b-}(L^p)$ is the image of $L^p(a,b)$ under the operator I^{α}_{b-}. Let $0 < \alpha < 1$, then we define the Weyl derivative for almost all $x \in (a,b)$ as

$$D^{\alpha}_{a+}f(x) = \frac{1}{\Gamma(1-\alpha)}\left(\frac{f(x)}{(x-a)^{\alpha}} + \alpha\int_a^x \frac{f(x)-f(y)}{(x-y)^{\alpha+1}}dy\right)1_{(a,b)}(x) \tag{14}$$

when $f \in I^{\alpha}_{a+}(L^p)$, and

$$D^{\alpha}_{b-}f(x) = \frac{(-1)^{\alpha}}{\Gamma(1-\alpha)}\left(\frac{f(x)}{(b-x)^{\alpha}} + \alpha\int_x^b \frac{f(x)-f(y)}{(y-x)^{\alpha+1}}dy\right)1_{(a,b)}(x) \tag{15}$$

when $f \in I^{\alpha}_{b-}(L^p)$.

The convergence of the integrals at the singularity $y = x$ holds pointwise for almost all $x \in (a,b)$ when $p = 1$, and in L^p sense when $1 < p < \infty$.

We now introduce the following notations in order to define the generalized Stieltjes integrals. Assuming the limits exist and are finite, let

$f(a+) = \lim_{\epsilon\searrow 0} f(a+\epsilon)$,
$g(b-) = \lim_{\epsilon\searrow 0} g(b-\epsilon)$,
$f_{a+}(x) = [f(x) - f(a+)]1_{(a,b)}(x)$,
$g_{b-}(x) = [g(x) - g(b-)]1_{(a,b)}(x)$.

Definition 4 Suppose that f and g are functions such that $f(a+)$, $g(a+)$ and $g(b-)$ exist, $f_{a+} \in I^{\alpha}_{a+}(L^p)$ and $g_{b-} \in I^{1-\alpha}_{b-}(L^q)$ for some $p, q \geq 1$, $\frac{1}{p} + \frac{1}{q} \leq 1$ and $0 < \alpha < 1$. Then the generalized Stieltjes integral of f with respect to g is defined as follows, (using (14) and (15)),

$$\int_a^b f dg = (-1)^{\alpha}\int_a^b D^{\alpha}_{a+}f_{a+}(x)D^{1-\alpha}_{b-}g_{b-}(x)\,dx + f(a+)[g(b-) - g(a+)]. \tag{16}$$

Remark that if $\alpha p < 1$, under the assumptions of the above definition, we have $f \in I^{\alpha}_{a+}(L^p)$, and (16) can be written as

$$\int_a^b f dg = (-1)^{\alpha}\int_a^b D^{\alpha}_{a+}f_{a+}(x)D^{1-\alpha}_{b-}g_{b-}(x)\,dx. \tag{17}$$

For $a \leq c < d \leq b$, the restriction of $f \in I^{\alpha}_{a+}(L^p(a,b))$ to (c,d) belongs to $I^{\alpha}_{c+}(L^p(c,d))$ and the continuation of $f \in I^{\alpha}_{c+}(L^p(c,d))$ by zero beyond (c,d)

belongs to $I^{\alpha}_{a+}(L^p(a,b))$. Thus, if $f \in I^{\alpha}_{a+}(L^p)$ and $g_{b-} \in I^{1-\alpha}_{b-}(L^q)$, then the integral $\int_a^b 1_{(c,d)} f\, dg$ in the sense of (17) exists for any $a \le c < d \le b$, and whenever the left-hand side is defined in the sense of (17), we have

$$\int_c^d f\, dg = \int_a^b 1_{(c,d)} f\, dg. \tag{18}$$

3.2 A Priori Estimates

We have the following basic estimates. Let

$$\Lambda_{\alpha}(g) := \frac{1}{\Gamma(1-\alpha)} \sup_{0<\eta<\xi<1} |(D^{1-\alpha}_{\xi-} g_{\xi-})(\eta)|. \tag{19}$$

Then

$$\Lambda_{\alpha}(g) \le \frac{1}{\Gamma(1-\alpha)\Gamma(\alpha)} \parallel g \parallel_{1-\alpha,\infty,0} < \infty. \tag{20}$$

If $f \in W^{\alpha,1}(0,1)$, and $g \in W_0^{1-\alpha,\infty}(0,1)$ then the integral $\int_0^{\xi} f\, dg$ exists for all $\xi \in [0,1]$.

Also, by (18) we have

$$\int_0^{\xi} f\, dg = \int_0^1 f 1_{(0,\xi)}\, dg.$$

Using (17) we get

$$\int_0^{\xi} f\, dg = (-1)^{\alpha} \int_0^{\xi} D^{\alpha}_{0+} f(\eta) D^{1-\alpha}_{\xi-} g_{\xi-}(\eta)\, d\eta.$$

Then

$$\left| \int_0^{\xi} f\, dg \right| \le \sup_{0<\eta<\xi} |D^{1-\alpha}_{\xi-} g_{\xi-}(\eta)| \int_0^{\xi} |D^{\alpha}_{0+} f(\eta)|\, d\eta.$$

Hence

$$\left| \int_0^{\xi} f\, dg \right| \le \Lambda_{\alpha}(g) \parallel f \parallel_{\alpha,1}. \tag{21}$$

4 Stochastic Integrals with Respect to a fBm

Let us recall the following result, for details and proofs see [37].

Lemma 1 *Let* $\{B_\eta^H : \eta \geq 0\}$ *be a real-valued fBm of Hurst parameter* $H \in (\frac{1}{2}, 1)$. *If* $1 - H < \alpha < \frac{1}{2}$, *then*

$$\mathbb{E} \sup_{0 \leq \gamma \leq \eta \leq 1} |D_{\eta-}^{1-\alpha} B_{\eta-}^H(\gamma)|^p < \infty, \tag{22}$$

for all $p \in [1, \infty)$.

Let $\{B_\eta^H : \eta \in [0, 1]\}$ be a real-valued fBm, with the Hurst parameter $\frac{1}{2} < H < 1$, defined on a complete probability space $(\Omega, \mathcal{F}, P)$. By (1), we have

$$\mathbb{E}(|B_\eta^H - B_\gamma^H|^2) = |\eta - \gamma|^{2H},$$

and for any $p \geq 1$ we have

$$\| B_\eta^H - B_\gamma^H \|_p = [\mathbb{E}(|B_\eta^H - B_\gamma^H|^p)]^{\frac{1}{p}} = c_p |\eta - \gamma|^H. \tag{23}$$

By Lemma (1) we know that the random variable

$$G = \frac{1}{\Gamma(1-\alpha)} \sup_{0 < \gamma < \eta < 1} |D_{\eta-}^{1-\alpha} B_{\eta-}^H(\gamma)| \tag{24}$$

has moments of all orders.

As a consequence for $1 - H < \alpha < \frac{1}{2}$, the pathwise integral $\int_0^\eta u_\gamma dB_\gamma^H$ exists when $u = \{u_\eta, \eta \in [0, 1]\}$ is a stochastic process whose trajectories belong to the space $W^{\alpha,1}$ and B_γ^H is a fBm with $H > \frac{1}{2}$. Moreover, we have the estimate

$$\left| \int_0^1 u_\gamma \, dB_\gamma^H \right| \leq G \|u\|_{\alpha,1}. \tag{25}$$

5 Main Results with Proofs

5.1 Main Result

We state the main result of the present work:

Theorem 1 *Let* $\alpha \in (1 - H, \frac{1}{2})$. *Assume that* $\phi \in W^{\alpha,\infty}[0, 1]$ *and the function A satisfies the assumptions A1, A2, A3, and A4. Then for every* $T > 0$, *there exists*

a unique stochastic process $Y \in L^0((\Omega, \mathcal{F}, P), C([0,T], W^{\alpha,\infty}[0,1]))$ *solution of the Eq.* (6).

As we already defined in Sect. 4, the stochastic integral with respect to the fBm is well defined pathwise. The above theorem will be proved using a contraction principle that will give us the existence and uniqueness of local solutions. In order to get the global solution, we will need to have an a priori estimate of the solution in some functional spaces. The proof will follow after several steps and will be stated in Sect. 5.3.

5.2 Fixed Point Argument

Consider the operator

$$F : C([0,T], W^{\alpha,\infty}[0,1]) \longrightarrow C([0,T], W^{\alpha,\infty}[0,1])$$

defined by

$$F(Y_\xi(t)) := \phi_\xi + \int_0^t \int_0^\xi A(Y_\gamma(s))\, dg_\gamma ds, \tag{26}$$

where $g \in C([0,T], W_0^{1-\alpha,\infty}[0,1])$, $\phi \in W^{\alpha,\infty}[0,1]$ and A satisfies the assumptions A1, A2, A3, and A4.

Remark 1 Let us remark that the function g in the Eq. (26) is a function of time t and γ and the fractional integration is with respect to the parameter $\gamma \in (0,1)$.

For a given $R > 0$, let us define the ball $B_{R,T}$ in $C([0,T], W^{\alpha,\infty}[0,1])$ as

$$B_{R,T} = \{Y \in C([0,T], W^{\alpha,\infty}[0,1]) : ||Y||_{\alpha,\infty} \leq R\}.$$

We state the following lemmas and propositions without proof. Detailed proofs for this particular equation can be found in [7].

Lemma 2 *Given a positive constant* $R_1 > \|\phi\|_{\alpha,\infty}$, *there exists* $T_1 > 0$ *such that* $F(B_{R_1,T_1}) \subseteq B_{R_1,T_1}$. *The time* T_1 *depends on* R_1, α *and the initial condition* $\|\phi\|_{\alpha,\infty}$.

Now in order to prove that the operator F is a contraction, we will need the following two propositions.

Proposition 1 *Let* $f \in C([0,T], W_0^{\alpha,\infty}[0,1])$ *and* $g \in C([0,T], W_0^{1-\alpha,\infty}[0,1])$. *Then, for all* $\xi \in [0,1]$ *and* $t \in [0,T]$

$$\begin{aligned}
&\left|\int_0^t \int_0^\xi f_\gamma(s)\, dg_\gamma ds\right| \\
&+ \int_0^\xi (\xi-\eta)^{-\alpha-1} \left|\int_0^t \int_0^\xi f_\gamma(s)\, dg_\gamma ds - \int_0^t \int_0^\eta f_\gamma(s)\, dg_\gamma ds\right| d\eta \\
&\leq \sup_{0\leq t\leq T} \Lambda_\alpha(g) b_\alpha^{(3)} \int_0^t \int_0^\xi [(\xi-\gamma)^{-2\alpha} + \gamma^{-\alpha}]\Bigg(|f_\gamma(s)| \\
&+ \int_0^\gamma \frac{|f_\gamma(s) - f_\delta(s)|}{(\gamma-\delta)^{\alpha+1}}\, d\delta\Bigg) d\gamma ds. \qquad (27)
\end{aligned}$$

where $b_\alpha^{(3)}$ is a constant which depends on α, its explicit expression is given below.

Proposition 2 *Let $h : \mathbb{R} \to \mathbb{R}$ be a function satisfying the assumptions A3 and A4. Then for all $N > 0$ and $|X_1|, |X_2|, |X_3|, |X_4| \leq N$ for all $X_1, X_2, X_3, X_4 \in \mathbb{R}$,*

$$\begin{aligned}
&|h(X_1) - h(X_2) - h(X_3) + h(X_4)| \\
&\leq M_1 |X_1 - X_2 - X_3 + X_4| + M_N |X_1 - X_3|(|X_1 - X_2| + |X_3 - X_4|). \qquad (28)
\end{aligned}$$

Lemma 3 *Given a positive constant $R_2 > \|\phi\|_{\alpha,\infty}$, there exists $T_2 > 0$ and a constant $0 < C < 1$ such that,*

$$||F(Y_1) - F(Y_2)||_{\alpha,\infty} \leq C||Y_1 - Y_2||_{\alpha,\infty}$$

for all $Y_1, Y_2 \in B_{R_2,T_2}$.

Now, we are able to state the following theorem:

Theorem 2 *Let $0 < \alpha < \frac{1}{2}$, $g \in C([0,T], W_0^{1-\alpha,\infty}[0,1])$. Consider the integrodifferential equation*

$$Y_\xi(t) = \phi_\xi + \int_0^t \int_0^\xi A(Y_\eta(s))\, dg_\eta(s) ds \qquad (29)$$

where $t \in [0,T]$, $\xi \in [0,1]$. Assume that A satisfies assumptions A1, A2, A3, and A4 and that $\phi \in W^{\alpha,\infty}([0,1])$. Then, there exists $T_0 > 0$ such that the above equation has a unique solution

$$Y \in C([0,T], W^{\alpha,\infty}[0,1]),$$

for all $T \leq T_0$.

Proof Choose $T_0 = \min\{T_1, T_2\}$, and $R = \min\{R_1, R_2\}$. Then, using Lemma 2 and Lemma 3 the operator F is a contraction on $B_{R,T}$ for all $T \leq T_0$ and this completes the proof. □

Now, we can show that the solution of (29) is global in time.

Theorem 3 *Let* $1 - H < \alpha < \frac{1}{2}$, $g \in C([0,T], W^{1-\alpha,\infty,0}[0,1])$. *Assume that A satisfies assumptions A1, A2, A3, and A4 and that* $\phi \in W^{\alpha,\infty}([0,1])$. *Then for all* $T > 0$, *there exists a unique* $Y \in C([0,T], W^{\alpha,\infty}[0,1])$ *solution of* (29).

Proof It is enough to get an estimate in $C([0,T], W^{\alpha,\infty}[0,1])$. We can write

$$||Y(t)||_{\alpha,\infty} = \sup_{\xi\in[0,1]} \left(Y_\xi(t) + \int_0^\xi \frac{|Y_\xi(t) - Y_\eta(t)|}{(\xi-\eta)^{\alpha+1}}\, d\eta \right). \tag{30}$$

Consider the first term on the right side of the above equality,

$$|Y_\xi(t)| \le |\phi(\xi)| + \int_0^t \left| \int_0^\xi A(Y_\eta(s))\, dg(s,\eta) \right| ds.$$

From Lemma (2) we can obtain

$$|Y_\xi(t)| \le |\phi_\xi| + \int_0^t \Lambda_\alpha(g) t \left(\frac{M_2}{1-\alpha} + M_1 ||Y(s)||_{\alpha,\infty} ds \right). \tag{31}$$

Consider the second term. We have

$$\begin{aligned}
&\left| \int_0^\xi \frac{|Y_\xi(t) - Y_\eta(t)|}{(\xi-\eta)^{\alpha+1}}\, d\eta \right| \\
&= \int_0^\xi \frac{1}{(\xi-\eta)^{\alpha+1}} \\
&\left| \phi(\xi) + \int_0^t \int_0^\xi A(Y_\gamma(s))\, dg_\gamma ds - \left(\phi(\eta) + \int_0^t \int_0^\eta A(Y_\gamma(s))\, dg_\gamma ds \right) \right| \\
&\le \int_0^\xi \frac{1}{(\xi-\eta)^{\alpha+1}} \left(|\phi_\xi - \phi_\eta| + \int_0^t \left| \int_\eta^\xi A(Y_\gamma(s))\, dg_\gamma \right| ds d\eta \right) \\
&\le \int_0^\xi \frac{|\phi_\xi - \phi_\eta|}{(\xi-\eta)^{\alpha+1}}\, d\eta + \int_0^t \int_0^\xi \frac{1}{(\xi-\eta)^{\alpha+1}} \left| \int_\eta^\xi A(Y_\gamma(s))\, dg_\gamma \right| d\eta ds.
\end{aligned}$$

From Lemma (2) we can obtain

$$\begin{aligned}
&\left| \int_0^\xi \frac{|Y_\xi(t) - Y_\eta(t)|}{(\xi-\eta)^{\alpha+1}}\, d\eta \right| \\
&\le \int_0^\xi \frac{|\phi_\xi - \phi_\eta|}{(\xi-\eta)^{\alpha+1}}\, d\eta \\
&+ \Lambda_\alpha(g) \int_0^t \left(\frac{M_2 b_\alpha^{(1)}}{1-2\alpha} \xi^{1-2\alpha} + \frac{M_1}{\alpha(1-\alpha)} ||Y(s)||_{\alpha,\infty} \xi^{1-\alpha} \right) ds.
\end{aligned} \tag{32}$$

By (31) and (32) we get,

$$
\begin{aligned}
&||Y(t)||_{\alpha,\infty} \\
&\leq ||\phi||_{\alpha,\infty} \\
&+ \Lambda_\alpha(g) \int_0^t \left(M_2 \left(\frac{1}{1-\alpha} + \frac{b_\alpha^{(1)}}{1-2\alpha} \right) + M_1 \left(1 + \frac{1}{\alpha(1-\alpha)} \right) ||Y(s)||_{\alpha,\infty} \right) ds.
\end{aligned}
$$

By Gronwall's inequality we obtain,

$$||Y||_{\alpha,\infty} \leq ||\phi||_{\alpha,\infty} \exp(KT),$$

where $K = \sup_{0\leq t\leq T} \Lambda_\alpha(g) \left[M_2 \left(\frac{1}{1-\alpha} + \frac{b_\alpha^{(1)}}{1-2\alpha} \right) + M_1 \left(1 + \frac{1}{\alpha(1-\alpha)} \right) \right].$

Hence, the local solution is global in time. □

5.3 *Proof of Theorem 1*

For every $t \in [0, T]$, the random variable

$$G = \frac{1}{\Gamma(1-\alpha)} \sup_{0<\eta<\xi<1} |(D_{\xi-}^{1-\alpha} B_{\xi-})_\eta(t)|$$

has moments of all orders by Proposition 1. Hence, the pathwise integral

$$\int_0^1 A(Y_\eta(t)) dB_\eta(t)$$

exists for $1 - H < \alpha < \frac{1}{2}$ and the existence and uniqueness of solutions follows from Theorem 3 which completes the proof.

Acknowledgments The authors gratefully acknowledge support and facilities from RMMC and University of Wyoming. This work was partially supported by NSF grant No. DMS 0608494.

References

1. Alòs E, Mazet O, Nualart D (2001) Stochastic calculus with respect to Gaussian processes. Ann Probab 29(2):766–801
2. Alós E, Nualart D (2003) Stochastic integration with respect to the fractional Brownian motion. Stoch Stoch Rep 75(3):129–152

3. Berselli LC, Bessaih H (2002) Some results for the line vortex equation. Nonlinearity 15:1729–1746
4. Berselli LC, Gubinelli M (2007) On the global evolution of vortex filaments, blobs, and small loops in 3d ideal flows. Commun Math Phys 269(3):693–713
5. Bertozzi AL, Majda AJ (2002) Vorticity and incompressible flow. Cambridge University Press, Cambridge
6. Bessaih H, Gubinelli M, Russo F (2005) The evolution of a random vortex filament. Ann Probab 33(5):1825–1855
7. Bessaih H, Wijeratne C (2011) An integrodifferential equation driven by fractional Brownian motion. arXiv:1103.3489
8. Biagini F, Hu Y, Øksendal B, Zhang T (2008) Stochastic calculus for fractional Brownian motion and applications. Springer, Berlin
9. Carmona P, Coutin L, Montseny G (2003) Stochastic integration with respect to fractional Brownian motion. Ann Inst H Poincaré Probab Stat 39(1):27–68
10. Cheridito P (2003) Arbitrage in fractional Brownian motion models. Financ Stoch 7(4):533–553
11. Chorin AJ (1994) Vorticity and turbulence. Springer, New York
12. Comte F, Renault E (1996) Long memory continuous time models. J Econom 73(1):101–149
13. Coutin L (2007) An introduction to (stochastic) calculus with respect to fractional Brownian motion. Séminaire de Probabilités XL. Lectures Notes in Math 1899:3–65
14. Coutin L, Lejay A (2005) Semi-martingales and rough paths theory. Electron J Probab 10(23):761–785
15. Coutin L, Qian Z (2002) Stochastic analysis, rough path analysis and fractional Brownian motions. Probab Theory Relat Fields 122(1):108–140
16. Decreusefond L, Üstünel AS (1998) Stochastic analysis of the fractional Brownian motion. Potential Anal 10(2):177–214
17. Doukhan P, Oppenheim G, Taqqu MS (eds) (2003) Theory and applications of long-range dependence. Birkhäuser, Boston
18. Duncan TE, Hu Y, Pasik-Duncan B (2000) Stochastic calculus for fractional Brownian motion i. Theory. SIAM J Control Optim 38(2):582–612
19. Duncan TE, Yan Y, Yan P (2001) Exact asymptotics for a queue with fractional Brownian input and applications in ATM networks. J Appl Probab 36(4):932–945
20. Embrechts P, Maejima M (2002) Selfsimilar processes. Princeton University Press, Princeton
21. Flandoli F (2002) On a probabilistic description of small scale structures in 3D fluids. Ann Inst H Poincaré Probab Stat. 38(2):207–228
22. Gubinelli M, Lejay A, Tindel S (2006) Young integrals and SPDEs. Potential Anal 25(4):307–326
23. Hurst HE (1951) Long-term storage capacity of reservoirs. Trans Am Soc Civ Eng 116:770–799
24. Kilbas AA, Marichev OI, Samko SG (1993) Fractional integrals and derivatives: theory and applications. Princeton University Press, Princeton
25. Klingenhöfer F, Zähle M (1999) Ordinary differential equations with fractal noise. Proc Am Math Soc 127(4):1021–1028
26. Kolmogorov AN (1940) Wienersche Spiralen und einige andere interessante kurven im Hilbertschen Raum. Comptes Rendus (Doklady) Acad Sci USSR (NS) 30:299–303
27. Kruka I, Russoa F, Tudorb CA (2007) Wiener integrals, Malliavin calculus and covariance measure structure. J Funct Anal 249(1):92–142
28. Leland WE, Taqqu MS, Willinger W, Wilson DV (1993) On the self-similar nature of ethernet traffic. ACM SIGCOMM Comput Commun Rev 23(4):183–193
29. Lyons T (1994) Differential equations driven by rough signals. I. An extension of an inequality of LC young. Math Res Lett 1(4):451–464
30. Lyons TJ (1998) Differential equations driven by rough signals. Rev Mat Iberoamericana 14(2):215–310
31. Mandelbrot B, Van Ness J (1968) Fractional Brownian motions, fractional noises and applications. SIAM Rev 10:422–437

32. Marchioro C, Pulvirenti M (1994) Mathematical theory of incompressible nonviscous fluids. Springer, New York
33. Mishura YS (2008) Stochastic calculus for fractional Brownian motion and related processes. Springer, Berlin
34. Norros I (1995) On the use of fractional Brownian motion in the theory of connectionless networks. IEEE J Sel Areas Commun 13(6):953–962
35. Nualart D (2003) Stochastic integration with respect to fractional Brownian motion and applications. Stoch Stoch Rep 336:3–40
36. Nualart D (2006) The Malliavin calculus and related topics. Springer, Berlin
37. Nualart D, Răscanu A (2001) Differential equations driven by fractional Brownian motion. Collectanea Mathematica 53(1):55–81
38. Rogers LCG (1997) Arbitrage with fractional Brownian motion. Math Financ 7:95–105
39. Saffman PG (1992) Vortex dynamics. Cambridge University Press, New York
40. Young LC (1936) An inequality of the Hölder type connected with Stieltjes intergration. Acta Math 67(1):251–282

An Introduction to Large Deviations and Equilibrium Statistical Mechanics for Turbulent Flows

Corentin Herbert

Abstract Two-dimensional turbulent flows, and to some extent, geophysical flows, are systems with a large number of degrees of freedom, which, albeit fluctuating, exhibit some degree of organization: coherent structures emerge spontaneously at large scales. In this short course, we show how the principles of equilibrium statistical mechanics apply to this problem and predict the condensation of energy at large scales and allow for computing the resulting coherent structures. We focus on the structure of the theory using the language of large deviation theory.

1 Introduction

Various characterizations of turbulent flows can be encountered; the components they usually entail are a chaotic dynamics on a strange attractor [81], a large range of scales (i.e. a large number of degrees of freedom), and strong nonlinear effects due to the prevalence of inertia over molecular dissipation [29]. Such flows can be found in industrial problems, but also in nature, for instance in geophysical flows and astrophysical flows. The above mentioned properties typically mean that not much can be said about the system in a deterministic framework, and that one should try instead to predict statistical properties.

This is exactly the purpose of the field of statistical mechanics: given a dynamical system (or set of ordinary or partial differential equations) in a large phase space (the microscopic state), can we predict typical values for specific functions on phase space (the macroscopic observables) without knowing the exact trajectory in phase space? For a large class of systems, said to be *in equilibrium*, such typical values can be obtained by assuming that the microscopic variables are random and distributed according to probability measures built upon a few macroscopic quantities, the invariants of the dynamical system. A classical example is that of the ideal gas: the exact position and velocity of the molecules matters little to us, but knowing the

C. Herbert (✉)
National Center for Atmospheric Research, Boulder, CO 80307, USA
e-mail: cherbert@ucar.edu

S. Heinz and H. Bessaih (eds.), *Stochastic Equations for Complex Systems*,
Mathematical Engineering, DOI 10.1007/978-3-319-18206-3_3

relations between macroscopic quantities such as temperature, pressure, energy and entropy is fundamental.

The ideas of statistical mechanics have been applied successfully to a large number of models of physical phenomena. An example of achievement of this approach is the theory of phase transitions, in which systems such as the Ising model, a toy-model of ferromagnetism, have been instrumental. However, turbulent flows present a number of difficulties: (i) they are directly formulated as continuous fields (infinite number of degrees of freedom) and can have an infinity of conserved quantities, (ii) the interactions between constituents have a long range, (iii) in many practical applications, the system is driven out of equilibrium by external forces.

Although we shall not tackle issue (iii) at all in this chapter, we will try to show how (i) and (ii) are actually useful ingredients to make probabilistic predictions for the system. They are the cornerstones of a mean-field theory: interacting degrees of freedom can be treated as statistically independent random variables in the limit of a large number of degrees of freedom. A natural language to express these properties is that of *large deviations theory* [25, 46, 80]: the probability of the outcome of a given observable concentrates exponentially around a set of values when the size of the system goes to infinity. The focus of the chapter is on the presentation of the large deviation principles for carefully chosen observables for a discretized form of 2D turbulence. To show that the principles at work are very general, we shall underline the connection with simpler models such as variants of the Ising model of ferromagnetism. Although it is shown that the theory allows us to compute the equilibrium states of the system, we shall not dwell on the description of such equilibrium states; the reader is referred to the review articles [13, 53] on this topic. We shall also refrain from discussing the connections with earlier applications of statistical mechanics, like the point vortex approach of Onsager, reviewed in [28], or the Kraichnan approach to Galerkin truncated flows [44], only mentioned briefly in Sect. 3.6.1.

These notes are based on lectures given at the *Stochastic Equations for Complex Systems: Theory and Applications* summer school organized at the University of Wyoming in June 2014. They mostly serve a pedagogical purpose, and we shall not give proofs of the results with the required mathematical rigor. However, we have tried as much as possible to provide the original references for the interested readers. The presentation adopted here owes much to the references [10, 69, 89]. Note that the ideas discussed here are applicable to many other systems with long range interactions [14, 23] and in particular gravitational systems [17, 66], plasmas, cold atoms or toy models of statistical physics.

2 Models of Turbulent Flows

2.1 3D and 2D Hydrodynamics

We are mainly interested here in the behavior of incompressible fluid flows, which is governed by the Navier-Stokes equations:

$$\partial_t \mathbf{u} + \mathbf{u} \cdot \nabla \mathbf{u} = -\nabla P + \nu \Delta \mathbf{u}, \tag{1}$$

$$\nabla \cdot \mathbf{u} = 0, \tag{2}$$

where $\mathbf{u}$ is the velocity field, P the pressure and ν the viscosity. The equations can be recast into non-dimensional form by introducing a velocity scale U, a length scale L, the corresponding time scale or *eddy turnover time* $T = L/U$, and the Reynolds number $Re = UL/\nu$. In other words, the Reynolds number measures the ratio of the nonlinear term and the dissipative term, or equivalently, of inertia and viscosity [29, 45]. Since viscosity acts at small scales, it is also a measure of the range of scales characteristic of the flow: the smallest scale is the Kolmogorov scale $\ell_\eta = (\nu^3/\epsilon)^{1/4}$, where ϵ is the energy dissipation rate. Now, with $\epsilon = U^3/L$, we obtain $L/\ell_\eta = Re^{3/4}$. Hence, the effective number of degrees of freedom in 3D flows grows as $Re^{9/4}$: flows with Reynolds number on the order of 10^9 are not uncommon in nature (the atmosphere and the ocean for instance), leading to a very large typical number of degrees of freedom.

The Navier-Stokes equations can be recast in terms of the vorticity field $\boldsymbol{\omega} = \nabla \times \mathbf{u}$:

$$\partial_t \boldsymbol{\omega} + \mathbf{u} \cdot \nabla \boldsymbol{\omega} = \boldsymbol{\omega} \cdot \nabla \mathbf{u} + \nu \Delta \boldsymbol{\omega}. \tag{3}$$

The first term on the right hand side corresponds to stretching of vorticity tubes. When we consider a flow on a two-dimensional surface rather than the three-dimensional space, this vorticity stretching term vanishes (the only non-vanishing component of vorticity ω is normal to the surface), yielding conservation of vorticity along streamlines in the inviscid ($\nu = 0$) case:

$$\partial_t \omega + \mathbf{u} \cdot \nabla \omega = 0. \tag{4}$$

This difference between 2D and 3D flows have important consequences on their respective behavior. While 3D flows tend to transfer energy from the large scales to the small scales, where it is dissipated by viscosity, in a process referred to as a direct energy cascade [31, 41] (big vortices break up into smaller and smaller vortices), 2D flows, on the contrary, transfer energy from the small scales to the large scales, and this is called an inverse energy cascade [6, 44, 86, 87]. In this inverse cascade process, vortices merge to form larger and larger vortices [55]. Unless sufficient large scale dissipation (e.g. bottom friction) is present, the energy piles up at the largest available scales, forming a *condensate* which dominates the flow [6, 21, 85].

The physical problem we are interested in here is the inverse energy cascade and the emergence of large scale coherent structures.

2.2 Global Invariants

The equations of motion for 3D and 2D hydrodynamics have a Hamiltonian structure, although non-canonical: there exists a Poisson structure, but it is degenerate [64]. This degeneracy leads to the existence of invariants, described in this section.

Inviscid 3D flows have two global invariants, the energy and the helicity [84]:

$$E = \frac{1}{2}\int \mathbf{u}^2, \tag{5}$$

$$H = \int \mathbf{u}\cdot\boldsymbol{\omega}. \tag{6}$$

Helicity being sign indefinite, it does not in general constrain the nonlinear transfers sufficiently to hamper the direct energy cascade process [43] (see however, [5, 34] for particular cases). On the contrary, in 2D, vorticity conservation along streamlines leads to a family of invariants in addition to the energy (ψ being the stream function, defined by $\omega = -\Delta\psi$)

$$\mathcal{H} = \int_{\mathcal{D}} \omega(\mathbf{x})\psi(\mathbf{x})d\mathbf{x}, \tag{7}$$

the Casimir invariants:

$$I_g = \int_{\mathcal{D}} g(\omega(\mathbf{x}))d\mathbf{x}, \tag{8}$$

where g is an arbitrary function. As a particular case, all the moments (or L^p norms) of the vorticity field are conserved:

$$\Gamma_p = \frac{1}{|\mathcal{D}|}\int_{\mathcal{D}} \omega(\mathbf{x})^p d\mathbf{x}, \tag{9}$$

including the L^2 norm of the vorticity field, referred to as the *enstrophy*. It was anticipated early on [2, 42, 48] that the existence of a second, positive-definite, quadratic invariant, in addition to the energy, is sufficient to reverse the direction of the energy cascade. The basic idea is that enstrophy is stronger in the presence of small-scale activity: transferring energy towards the small-scales while keeping the total energy constant cannot be done if we also need to conserve enstrophy. This loose statement was made more precise by a number of analytic arguments [2, 30, 42, 48, 56, 63], and verified in experiments [67, 82] and high-resolution numerical

simulations [6]. Statistical mechanics provides one of these analytical arguments (see Sect. 3.6.1).

Conservation of the Casimir invariants can be formulated equivalently in terms of the moments of the vorticity field, as above, or in terms of the vorticity distribution. Indeed, the fraction of the domain area $|\mathcal{D}|$, occupied by the vorticity level σ, which can be written as

$$\gamma(\sigma) = \frac{1}{|\mathcal{D}|} \int_{\mathcal{D}} \delta(\omega(\mathbf{x}) - \sigma) d\mathbf{x}, \tag{10}$$

is conserved. We shall see that this form is particularly convenient in Sect. 3, but note that the two formulations are connected by the formula

$$\Gamma_p = \frac{1}{|\mathcal{D}|} \int_{\mathcal{D}} d\mathbf{x} \int_{\mathbb{R}} d\sigma \sigma^p \delta(\omega(\mathbf{x}) - \sigma) = \int_{\mathbb{R}} d\sigma \sigma^p \gamma(\sigma), \tag{11}$$

and, conversely, using an integral representation of the Dirac distribution,

$$\gamma(\sigma) = \frac{1}{2\pi} \sum_{p=0}^{+\infty} \frac{(-1)^p \Gamma_p}{p!} \delta^{(p)}(\sigma). \tag{12}$$

Finally, note that the vorticity distribution is normalized:

$$\int_{\mathbb{R}} \gamma(\sigma) d\sigma = 1. \tag{13}$$

2.3 Geophysical Flows

Although 2D flows are interesting in themselves, part of the motivation for studying them comes from their common features with geophysical flows. Indeed, in addition to the small aspect ratio of the atmosphere and the ocean, their dynamics is subjected to the effect of strong rotation and density stratification. These properties allow for an asymptotic regime which describes well the large-scale dynamics, the *quasi-geostrophic* regime [93]. This regime is very similar to 2D flows, because it reduces to a quantity, called *potential vorticity*, being advected by the flow, similarly to the vorticity (see (4)). In particular, the velocity field is purely horizontal. The only difference is that the fields also depend on the vertical, and whereas the vorticity is the laplacian of the stream function: $\omega = -\Delta\psi$ in 2D, here the potential vorticity is related to the stream function by a slightly more complicated linear differential operator. The existence of Casimir invariants similar to those of 2D flows leads again to an inverse cascade of energy and the formation of coherent structures at large scales [15, 72, 83]. Therefore, the considerations presented here may apply to such flows as well, and attempts to extend the theory in this context have flourished over the

past few years. For the sake of simplicity, we shall restrict ourselves here to the case of 2D flows; the interested reader may consult the literature on extensions to quasi-geostrophic flows in the barotropic case [12, 36, 61, 95], the baroclinic case [24, 33, 94, 96], shallow-water equations [18, 20], as well as the general references [13, 53, 54], for instance.

The quasi-geostrophic regime breaks down at smaller scales, and we enter an intermediate regime, often referred to as stratified turbulence [50]. In this regime, even though we can still define a potential vorticity which is a Lagrangian invariant, it does not put as strong a constraint on the system as in the 2D case. Indeed, the fields (velocity, density) can be decomposed into a *balanced* part which contributes to potential vorticity, and *inertia-gravity waves*, which do not. As a result, the organization of the system in terms of inertial ranges and energy cascades is not so simple. High-resolution numerical simulations have indicated the existence of two inertial ranges with a constant and opposite flux of energy [70]. A possible interpretation is that the vortical modes are responsible for the inverse cascade of energy while the inertia-gravity waves have to do with the direct energy cascade. This interpretation is supported by a statistical mechanics argument [37], which is an adaptation of the Kraichnan argument (see Sect. 3.6.1) in the context of the restricted canonical ensemble [68].

Independently of the constraining effect of rotation and stratification (which can be seen as forces breaking isotropy), another direction of generalization which has been considered is that of 3D flows with symmetries, and especially axisymmetric flows [49, 62, 88]. This configuration is relevant for setups used in laboratory experiments, such as the von Karman experiment. It has been shown in particular that one could define a microcanonical measure using an approach analogous to that of Sect. 3.1, with, however, some considerable complications to treat the fluctuations of the poloidal field [88].

2.4 Discretized Form for 2D Euler Flows and Analogies with Toy Models of Magnetic Systems

Instead of the continuous vorticity field ω and the infinite dimensional phase space it belongs to, it may be more convenient to introduce finite dimensional models. Here we shall mostly consider a discretization on a square lattice with N sites equally spaced in the domain $\mathcal{D}$ (see Fig. 1), and the variables of interest are the values taken by vorticity at each site. In this form, the system can be related to some classical models of statistical physics.

2.4.1 Two-Vorticity Level System and Long-Range Ising Model

The Ising model is one of the most famous models in statistical physics. It can be seen as a toy model of ferromagnetism, but it has served as a testbed for a very large

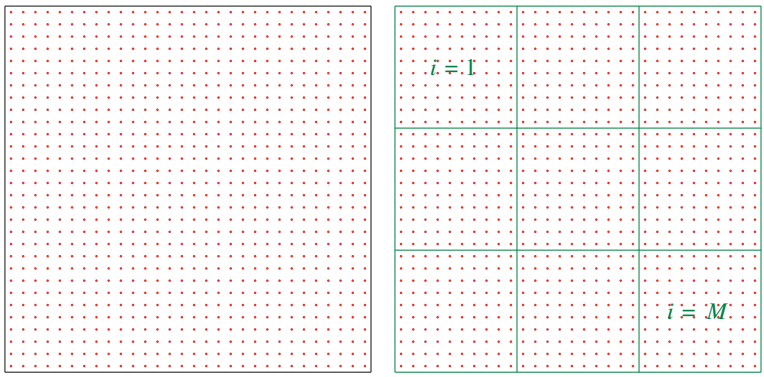

Fig. 1 Discretization and coarse-graining. *Left* We replace the 2D domain by a finite lattice and the continuous vorticity field by a N-dimensional vector whose components are the values of the vorticity at each site. *Right* We decompose the lattice in M cells, each containing $n = N/M$ sites. The coarse-grained vorticity is a M dimensional vector whose components are the average value of the vorticity in each cell

number of ideas going far beyond this particular problem [22]. It consists of a finite number N of spins $s_i \in \{-1, 1\}$ located on a lattice of arbitrary shape and dimension (although a square lattice is often considered) and interacting through a hamiltonian (per degree of freedom) of the form:

$$\mathcal{H}_I[\hat{s}] = -\frac{1}{N}\sum_{i,j=1}^{N} J_{ij} s_i s_j. \tag{14}$$

In this form, the hamiltonian is just any quadratic function. A standard choice of interaction is the nearest-neighbor model: $J_{ij} = J$ if the sites i and j are connected in the lattice, and $J_{ij} = 0$ if they are not. That way, aligned neighboring spins will contribute a term $-J$ to the hamiltonian, while anti-aligned neighboring spins will contribute J. If J is positive the system is called *ferromagnetic* and if it is negative the system is called *antiferromagnetic*. An observable of interest is the *magnetization* (per spin):

$$\mathcal{M}[\hat{s}] = \frac{1}{N}\sum_{i=1}^{N} s_i. \tag{15}$$

When one finds about the same proportion of positive and negative spins, the magnetization should vanish. Applying an external magnetic field, represented by a term of the form $-h\sum_i s_i$ in the hamiltonian, leads to alignment of spins, and therefore a non-vanishing magnetization. This is the standard behavior of so-called *paramagnetic* materials. By contrast, in *ferromagnetic* materials, spins may align spontaneously and yield unit magnetization (in absolute value) without imposing an external magnetic field (or, in experiments, the system retains its magnetization

when the applied magnetic field is switched off). The Ising model can be seen as a toy model of the paramagnetic-ferromagnetic transition.

In the above case, the system has short-range interactions, since only neighboring spins interact. Versions with long-range interactions can be built by allowing non-vanishing J_{ij} for distant sites i and j. For instance, one may assume that all the spins interact with all the other spins with the same coupling constant: $J_{ij} = 1/N$, where the $1/N$ ensures that the energy per degree of freedom is an intensive quantity. In this case, the Hamiltonian becomes a function of magnetization only:

$$\mathcal{H}_{IMF}[\hat{s}] = -\frac{1}{N^2} \sum_{i,j=1}^{N} s_i s_j = -\mathcal{M}[\hat{s}]^2. \tag{16}$$

This version of the Ising model is referred to as *mean-field*, because it is tantamount to saying that each spin feels the effect of a magnetic field created by all the other spins rather than the individual effect of each of his neighbors. Indeed, let us consider a given spin s_i; it provides a contribution $-1/N s_i \sum_j J_{ij} s_j$, which is the same as a non-interacting spin under external magnetic field $1/N \sum_j J_{ij} s_j$ would. If we replace this magnetic field by the magnetization, we obtain the mean-field Hamiltonian. Note that the geometric shape (square, triangle, etc.) and the dimension of the lattice do not matter here since all the spins interact with the same intensity.

An advantage of the mean-field Ising model is that it has an exact solution in any dimension [3]. On the contrary, exact solutions for the standard, short-range Ising model are only know for dimension one [38] and two [65].

The discretized version of 2D flows described above is related to the Ising model in the following way: rather than allowing the vorticity to take any real value, we can restrict it to a two-level set $\{\sigma, -\sigma\}$. Then the system becomes analogous to the Ising model, with an interaction matrix given by the Green function of the Laplacian on the lattice. On a plane, this amounts to interactions proportional to the logarithm of the distance between sites: $J_{ij} \propto \ln|i - j|$ for $i \neq j$. This is a kind of long-range interaction. The difference with the Ising model is the presence of the vorticity distribution conservation constraint. This would amount to fixing the number of $+$ spins and the number of $-$ spins in the Ising model.

2.4.2 Energy-Enstrophy Ensemble and the Long-Range Spherical Model

Another variant of the Ising model consists in letting the spins s_i take any real value, while satisfying the global constraint $\sum_{i=1}^{N} s_i^2 = N$. Clearly, this constraint is satisfied in the standard Ising model with spins in $\{1, -1\}$. The name *spherical model* was coined for this variant because of the form of the global constraint, which means that the set of all spin values lies on the surface of a sphere in $\mathbb{R}^N$. It was introduced by Berlin and Kac [4] as an attempt to patch the divergence arising from assuming that the spins are distributed according to a normal distribution (the *Gaussian model*) while remaining exactly solvable in any dimension [3]. The observables of interest

(Hamiltonian, magnetization) are the same as for the Ising model. Versions with short-range [4] or long-range [39] interactions can again be considered by choosing different quadratic forms J_{ij}.

In their discretized version, 2D flows resemble a long-range spherical model if we only retain one Casimir invariant: the enstrophy. Indeed, enstrophy conservation implies $\sum_i \omega_i^2 = N\Gamma_2$. Again, the interaction matrix is given by the Green function of the Laplacian on the lattice. This connection is further investigated in Sect. 3.6. It has also been pointed out in a series of papers by Lim [51, 52].

3 Mean-Field Theory for 2D Flows

We provide here a heuristic presentation of the mean-field theory introduced independently by Miller [59, 60], Robert and Sommeria [75, 77], and further developed by many others. The presentation is inspired by the original work by Miller and the more recent references [10, 13, 69]. More rigorous mathematical proofs can be found in the original papers by Robert and coworkers [57, 58, 73–77] and Ellis, Turkington and coworkers [7, 8, 26, 27, 91].

3.1 Microcanonical Measure and Large Deviations for the Energy and Vorticity Distribution

The general idea is to consider the vorticity field ω, referred to as the *microstate*, as a random variable distributed according to the *microcanonical distribution*. In other words, we introduce a probability measure on the phase space $\Lambda = L^\infty(\mathcal{D})$, where $\mathcal{D}$ is a 2D domain (we shall mostly consider the case of a rectangular domain here). We are going to give a sketch of the construction of this measure as a limit of measures on finite-dimensional phase spaces corresponding to approximations of the continuous vorticity field. Then, we will be able to make predictions on the value of *macrostates*, i.e. observables $\mathcal{A} : \Lambda \longrightarrow \mathbb{R}$ (or more generally $\mathcal{A} : \Lambda \longrightarrow M$ where the space M is *macroscopic* in some sense, e.g. has a dimension much lower than Λ) on phase space, which, as we shall see, satisfy large deviation properties: they concentrate in probability around some specific values, the equilibrium states.

To keep things simple, we shall consider a finite number of vorticity levels $\mathfrak{S} = \{\sigma_1, \dots, \sigma_K\}$. This amounts to saying that the vorticity distribution has the form $\gamma(\sigma) = \sum_{k=1}^K \gamma_k \delta(\sigma - \sigma_k)$. We consider the discretized system with N sites on the square lattice introduced in Sect. 2.4 (see Fig. 1), and define a *microstate* as being simply the value of the vorticity field at all the points of the lattice. Therefore the phase space is simply $\Lambda_N = \mathfrak{S}^N$.

Considering the conservation laws mentioned above, there are two observables of primary interest: the energy observable, i.e. the Hamiltonian, given by

$$\mathcal{H}_N : \hat{\omega} \in \Lambda_N \longmapsto \frac{1}{2N^2} \sum_{1 \leq i \neq j \leq N} G_{ij}^N \omega_i \omega_j, \tag{17}$$

with G_{ij}^N the Green function of the Laplacian on the lattice, and the vorticity distribution observables

$$\mathcal{G}_N^{(k)} : \hat{\omega} \in \Lambda_N \longmapsto \frac{1}{N} \sum_{i=1}^{N} \delta_{\omega_i, \sigma_k}. \tag{18}$$

Note that the set of accessible energies (i.e. the values taken by the observable $\mathcal{H}_N$) is finite and depends both on the vorticity levels σ_k and on the number of sites N. Ultimately, in the limit $N \to \infty$, we shall be interested in a continuum of energy levels. One approach to circumvent this difficulty is to consider in a first step energy shells with finite width ΔE, large enough so that each shell is attained by the energy observable for some microstates [69]. In the limit $N \to +\infty$, the results will not depend on the value of ΔE. To keep notations as simple as possible, we shall refrain from doing so here, but in all rigor one should understand $\mathcal{H}_N[\hat{\omega}] \in [E, E + \Delta E]$ whenever we write $\mathcal{H}_N[\hat{\omega}] = E$. In this framework, the set of microstates with vorticity distribution γ and energy E is

$$\Lambda_N(\gamma, E) = \{\hat{\omega} \in \Lambda_N \mid \mathcal{H}_N[\hat{\omega}] = E, \forall k \in [\![1, K]\!], \mathcal{G}_N^{(k)}[\hat{\omega}] = \gamma_k\}, \tag{19}$$

$$= \mathcal{H}_N^{-1}(\{E\}) \cap \bigcap_{k=1}^{K} {\mathcal{G}_N^{(k)}}^{-1}(\{\gamma_k\}). \tag{20}$$

This is a finite set whose cardinality we denote by $\Omega_N(\gamma, E) = \text{Card}\, \Lambda_N(\gamma, E)$.

We are going to introduce two probability measures on phase space: first, let us consider a *prior measure* $\mu^{(N)}$, which here is just the normalized counting measure: if $M \subset \Lambda_N$, $\mu^{(N)}(M) = \frac{\text{Card}\, M}{K^N}$. This amounts to saying that all the microstates are equiprobable: for any observable $\mathcal{A}_N : \Lambda_N \longrightarrow \mathbb{R}$, the probability of the outcome x is just the fraction of microstates for which $\mathcal{A}_N[\hat{\omega}] = x$. Now, we want to restrict that statement to all the microstates with a fixed energy and vorticity distribution, while assigning vanishing probability to all the other microstates. Hence, we introduce the (finite-N) microcanonical measure $\mu_{\gamma,E}^{(N)}$: if $M \subset \Lambda_N$, $\mu_{\gamma,E}^{(N)}(M) = \text{Card}(M \cap \Lambda_N(\gamma, E))/\Omega_N(\gamma, E)$. Hence, for an observable $\mathcal{A}_N$, the probability law of the random variable $\mathcal{A}_N[\hat{\omega}]$ is $\mu_{\gamma,E}^{(N)}(\mathcal{A}_N[\hat{\omega}] = x) = \mu_{\gamma,E}^{(N)}(\mathcal{A}_N^{-1}(\{x\}))$. Note that we have introduced indices γ and E to distinguish from probabilities computed with respect to the prior measure. Probabilities in the microcanonical ensemble are thus just conditional probabilities:

$$\mu^{(N)}_{\gamma,E}(\mathcal{A}_N[\hat{\omega}] = x) = \mu^{(N)}(\mathcal{A}_N[\hat{\omega}] = x | \mathcal{H}_N[\hat{\omega}] = E, \mathcal{G}^{(k)}_N[\hat{\omega}] = \gamma_k), \tag{21}$$

$$= \begin{cases} \frac{\mu^{(N)}(\mathcal{A}_N[\hat{\omega}]=x, \mathcal{H}_N[\hat{\omega}]=E, \mathcal{G}^{(k)}_N[\hat{\omega}]=\gamma_k)}{\mu^{(N)}(\mathcal{H}_N[\hat{\omega}]=E, \mathcal{G}^{(k)}_N[\hat{\omega}]=\gamma_k))} & \text{if } \mathcal{H}_N[\hat{\omega}]=E, \text{ and} \\ & \forall k \in [\![1, K]\!], \mathcal{G}^{(k)}_N[\hat{\omega}]=\gamma_k \\ 0 & \text{otherwise.} \end{cases} \tag{22}$$

As mentioned above, observables of particular interest are the hamiltonian $\mathcal{H}_N$ and the vorticity distribution observables $\mathcal{G}^{(k)}_N$. The joint probability to observe an energy E and a vorticity distribution γ, with respect to the prior measure, satisfies a large-deviation property, and the large deviation rate function is (up to an unimportant constant term) the opposite of the entropy $S(E, \gamma)$:

$$\mu^{(N)}(\mathcal{H}_N[\hat{\omega}] = E, \mathcal{G}^{(k)}_N[\hat{\omega}] = \gamma_k) = \frac{\Omega_N(\gamma, E)}{K^N} = e^{NS(E,\gamma) - N \ln K + o(N)}, \tag{23}$$

with

$$S(E, \gamma) = \lim_{N \to \infty} \frac{1}{N} \ln \Omega_N(\gamma, E). \tag{24}$$

3.2 Large Deviations for the Macrostates

We now introduce a new class of observables associated with the coarse-graining of the vorticity field. We decompose the lattice into M cells, each containing $n = N/M$ sites. For a microstate $\hat{\omega} \in \mathfrak{S}^N$, we shall denote the components as $\omega_{i\alpha}$ where $1 \leq i \leq M$ is the index of the cell and $1 \leq \alpha \leq n$ is the index of the site within the cell (see Fig. 1). The coarse-graining observable is given by

$$\mathfrak{C} : \hat{\omega} \in \mathfrak{S}^N \longmapsto \bar{\omega} \in \mathbb{R}^M, \text{ with } \bar{\omega}_i = \frac{1}{n} \sum_{\alpha=1}^{n} \omega_{i\alpha}, \, 1 \leq i \leq M. \tag{25}$$

More generally, we can define an observable which corresponds to the distribution of vorticity levels in each cell. It is just the empirical vector

$$\mathfrak{P} : \hat{\omega} \in \mathfrak{S}^N \longmapsto P = (p_{ik})_{\substack{1 \leq i \leq M \\ 1 \leq k \leq K}} \in \mathcal{M}_{M,K}(\mathbb{R}), \text{ with } p_{ik} = \frac{1}{n} \sum_{\alpha=1}^{n} \delta_{\omega_{i\alpha}, \sigma_k}. \tag{26}$$

Note that $\sum_{k=1}^{K} p_{ik} = 1$. Besides, the observable $\mathfrak{C}$ can be deduced from $\mathfrak{P}$ since $\bar{\omega}_i = \sum_{k=1}^{K} \sigma_k p_{ik}$ for $1 \leq i \leq M$. Let us refer to the elements of the image of $\mathfrak{P}$ as the *macrostates*. The set of microstates corresponding to a given macrostate

P is simply its pre-image $\mathfrak{P}^{-1}(P)$. The number of microstates realizing a given macrostate P will be denoted $W(P) = \text{Card}\,\mathfrak{P}^{-1}(P)$. It is easily computed that:

$$W(P) = \prod_{i=1}^{M} \binom{n}{np_{i1}} \binom{n - np_{i1}}{np_{i2}} \cdots \binom{n - np_{i1} - \cdots - np_{in-1}}{np_{in}}, \tag{27}$$

$$= \prod_{i=1}^{M} \frac{n!}{\prod_{k=1}^{K} (np_{ik})!}. \tag{28}$$

The vorticity distribution observables $\mathcal{G}_N^{(k)}$ take a constant value over an equivalence class $\mathfrak{P}^{-1}(P)$:

$$\mathcal{G}_N^{(k)}[\hat{\omega}] = \frac{1}{M} \sum_{i=1}^{M} p_{ik}, \tag{29}$$

so that if $\hat{\omega}_1, \hat{\omega}_2 \in \mathfrak{S}^N$ are such that $\mathfrak{P}[\hat{\omega}_1] = \mathfrak{P}[\hat{\omega}_2]$, then for $1 \leq k \leq K$, $\mathcal{G}_N^{(k)}[\hat{\omega}_1] = \mathcal{G}_N^{(k)}[\hat{\omega}_2]$. In other words, the equivalence kernel of the observable $\mathfrak{P}$ is finer than that of any of the observables $\mathcal{G}_N^{(k)}$. In practice, this means that we need not worry about enforcing the vorticity distribution constraint when counting the number of microstates realizing a given macrostate. For the energy observable, the situation is slightly more subtle: denoting $G^{M,n}_{i\alpha,j\beta}$ the Green function of the Laplacian on the lattice with the new indexing of the sites, the energy observable is given by:

$$\mathcal{H}_{N,M}[\hat{\omega}] = \frac{1}{2N^2} \sum_{\substack{1 \leq i,j \leq M \\ 1 \leq \alpha,\beta \leq n \\ (i,\alpha) \neq (j,\beta)}} G^{M,n}_{i\alpha,j\beta} \omega_{i\alpha} \omega_{j\beta}, \tag{30}$$

which is not necessarily constant over equivalence classes. However, it can be shown that the dominant contribution is the *mean-field* energy, i.e. the energy of the coarse-grained vorticity field:

$$\mathcal{H}_{N,M}[\hat{\omega}] = \frac{1}{2M^2} \sum_{1 \leq i \neq j \leq M} G^{M}_{ij} \bar{\omega}_i \bar{\omega}_j + o\left(\frac{1}{N}\right), \tag{31}$$

$$= \mathcal{H}_M[\mathfrak{C}[\hat{\omega}]] + o\left(\frac{1}{N}\right). \tag{32}$$

The above results are sometimes restated by saying that we have an *energy* (and here, also vorticity distribution) *representation function* [89] (see Fig. 2). It allows us to obtain the most probable states with respect to the microcanonical measure by obtaining a large deviation property with respect to the prior (unconstrained) measure.

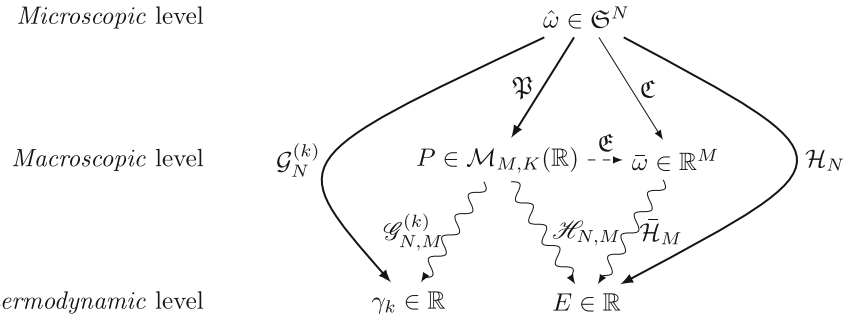

Fig. 2 The different levels of description of the system, and the observables/representation function relating them. Observables are represented with *straight arrows*, representation functions with *wiggly arrows* and contraction principles with *dashed arrows*. Observables for which a large deviation principle has been obtained directly are represented with *thick arrows*

Indeed, the unconstrained probability of observing a macrostate P is

$$\mu^{(N)}(\mathfrak{P}[\hat{\omega}] = P) = \mu^{(N)}(\mathfrak{P}^{-1}(P)), \tag{33}$$

$$= \frac{W(P)}{K^N}. \tag{34}$$

Using the Stirling approximation, it is easily shown that when $N \to \infty$, this probability satisfies a large deviation property:

$$\mu^{(N)}(\mathfrak{P}[\hat{\omega}] = P) = e^{N\mathscr{S}_{M,K}[P]+o(N)}, \tag{35}$$

where we have introduced the mean-field entropy

$$\mathscr{S}_{M,K}[P] = \lim_{N\to+\infty} \frac{1}{N} \ln \mu^{(N)}(\mathfrak{P}[\hat{\omega}] = P), \tag{36}$$

$$= -\frac{1}{M} \sum_{i=1}^{M} \sum_{k=1}^{K} p_{ik} \ln p_{ik}, \tag{37}$$

which again appears as a large deviation rate function (up to an additive constant and a minus sign), although this time it is a large deviation of an empirical vector (observable $\mathfrak{P}$) rather than a sample mean (energy observable $\mathcal{H}$). Hence, the above result should in all rigor be seen as a consequence of the Sanov theorem.

Now, in the microcanonical ensemble, the probability $\mu_{\gamma,E}^{(N)}(\mathfrak{P}[\hat{\omega}] = P)$ involves the joint (unconstrained) probability $\mu^{(N)}(\mathfrak{P}[\hat{\omega}] = P, \mathcal{H}_N[\hat{\omega}] = E, \mathcal{G}_N^{(k)}[\hat{\omega}] = \gamma_k)$. But due to the existence of the energy and vorticity distribution representation

functions, we have:

$$\begin{aligned}\mu^{(N)}(\mathfrak{P}[\hat{\omega}] = P, &\mathcal{H}_N[\hat{\omega}] = E, \mathcal{G}_N^{(k)}[\hat{\omega}] = \gamma_k) \\ &= \mu^{(N)}(\mathfrak{P}[\hat{\omega}] = P, \mathscr{H}_{N,M}[P] = E, \mathscr{G}_{N,M}^{(k)}[P] = \gamma_k),\end{aligned} \tag{38}$$

therefore,

$$\mu_{\gamma,E}^{(N)}(\mathfrak{P}[\hat{\omega}] = P) = \begin{cases} \frac{\mu^{(N)}(\mathfrak{P}[\hat{\omega}]=P)}{\mu^{(N)}(\mathcal{H}_N[\hat{\omega}]=E, \mathcal{G}_N^{(k)}[\hat{\omega}]=\gamma_k))} & \text{if } \mathscr{H}_{N,M}[P]=E, \text{ and} \\ & \forall k \in [\![1,K]\!], \mathscr{G}_{N,M}^{(k)}[P]=\gamma_k \\ 0 & \text{otherwise.} \end{cases} \tag{39}$$

It follows that the probability of a given macrostate also satisfies a large deviation result with respect to the microcanonical measure:

$$\mu_{\gamma,E}^{(N)}(\mathfrak{P}[\hat{\omega}] = P) = e^{-NI[P]+o(N)}, \tag{40}$$

with the large deviation rate function

$$I[P] = \begin{cases} S(E,\gamma) - \mathscr{S}_{M,K}[P] & \text{if } \mathscr{H}_{N,M}[P] = E, \text{ and } \forall k \in [\![1,K]\!], \mathscr{G}_{N,M}^{(k)}[P] = \gamma_k \\ +\infty & \text{otherwise.} \end{cases} \tag{41}$$

Hence, the most probable macrostates with respect to the microcanonical measure are those which minimize the large deviation rate function, i.e. those which maximize the entropy $\mathscr{S}_{M,K}$ while satisfying the constraints on energy and vorticity distribution: they are solutions of a constrained variational problem. It is worthy of note that the Boltzmann-Gibbs entropy $\mathscr{S}_{M,K}$, defined in (37), evaluated at a solution P^* of the variational problem, agrees with the entropy $S(E,\gamma)$ defined from the Boltzman formula (24). This is not a coincidence, but a cornerstone of the mean-field approach. It can be understood in the language of large deviation theory as a *contraction principle* [89]. Roughly speaking, due to the existence of representation functions, the probability of observing an energy E and a vorticity distribution γ can be computed as the integral over all the macrostates (rather than the microstates) with these constraints: denoting

$$\tilde{\Lambda}_{N,M}(\gamma, E) = \{P \in \mathcal{M}_{M,K}(\mathbb{R}) \mid \mathscr{H}_{N,M}[P] = E, \forall k \in [\![1,K]\!], \mathscr{G}_{N,M}^{(k)}[P] = \gamma_k\}, \tag{42}$$

we have

$$\mu^{(N)}(\mathcal{H}_N[\hat{\omega}] = E, \mathcal{G}_N^{(k)}[\hat{\omega}] = \gamma_k) = \int_{\Lambda_N(\gamma,E)} \mu^{(N)}(d\hat{\omega}), \tag{43}$$

$$= \int_{\tilde{\Lambda}_{N,M}(\gamma,E)} \mu^{(N)}(\mathfrak{P}^{-1}(P)), \tag{44}$$

$$= \int_{\tilde{\Lambda}_{N,M}(\gamma,E)} e^{N\mathcal{S}_{M,K}[P]+o(N)}, \tag{45}$$

Using Laplace's approximation, the integral evaluates to

$$= \exp\left(N \max_{P\in\tilde{\Lambda}_{N,M}(\gamma,E)} \mathcal{S}_{M,K}[P] + o(N)\right). \tag{46}$$

As a conclusion, the most probables macrostates P^* with respect to the microcanonical measure satisfy $I[P^*] = 0$: they are solutions of the constrained variational problem:

$$S(E,\gamma) = \max_P\{\mathcal{S}_{M,K}[P] \mid \mathscr{H}_{N,M}[P] = E, \forall k \in [\![1,K]\!], \mathscr{G}_{N,M}^{(k)}[P] = \gamma_k\}. \tag{47}$$

3.3 Thermodynamic Limit and Mean-Field Equation

We are now interested in the macrostates obtained in the limit $M \to +\infty$. Letting also $K \to +\infty$, they are the probability distributions for fine-grained vorticity $\rho(\mathbf{r},\sigma)$: $\rho(\mathbf{r},\sigma)d\sigma$ is the probability that the vorticity at point $\mathbf{r}$ lies in the interval $[\sigma, \sigma + d\sigma]$. The local normalization condition $\int_{\mathbb{R}} \rho(\mathbf{r},\sigma)d\sigma = 1$ must still be satisfied for each point $\mathbf{r} \in \mathcal{D}$. The coarse-grained vorticity field is now $\bar{\omega}(\mathbf{r}) = \int_{\mathbb{R}} \sigma\rho(\mathbf{r},\sigma)d\sigma$. As explained above, the energy and vorticity distribution depend only on the macrostate ρ:

$$\mathscr{H}[\rho] = \frac{1}{2}\int_{\mathcal{D}^2} d\mathbf{r}d\mathbf{r}' \int_{\mathbb{R}^2} d\sigma d\sigma' G(\mathbf{r},\mathbf{r}')\sigma\sigma'\rho(\mathbf{r},\sigma)\rho(\mathbf{r}',\sigma'), \tag{48}$$

$$\mathscr{D}_\sigma[\rho] = \int_{\mathcal{D}} \rho(\sigma,\mathbf{r})d\mathbf{r}. \tag{49}$$

Similarly, the mean field entropy becomes

$$\mathcal{S}[\rho] = -\int_{\mathcal{D}} d\mathbf{r} \int_{\mathbb{R}} d\sigma\rho(\sigma,\mathbf{r}) \ln \rho(\sigma,\mathbf{r}). \tag{50}$$

The most probable macrostates are now those maximizing (50) while satisfying the energy and vorticity distribution constraints. They are solutions of the microcanonical variational problem:

$$S(E,\gamma) = \max_{\rho}\{\mathscr{S}[\rho] \mid \mathscr{H}[\rho] = E, \forall \sigma \in \mathbb{R}, \mathscr{D}_\sigma[\rho] = \gamma(\sigma)\}. \tag{51}$$

The critical points of the variational problem are readily found: there exist Lagrange multipliers β and $\alpha(\sigma)$ such that the first variations vanish:

$$0 = \delta\mathscr{S} - \int_{\mathcal{D}} d\mathbf{r}\zeta(\mathbf{r}) \int_{\mathbb{R}} d\sigma\delta\rho(\sigma,\mathbf{r}) - \beta\delta\mathscr{H} - \int_{\mathbb{R}} d\sigma\alpha(\sigma) \int_{\mathcal{D}} d\mathbf{r}\delta\rho(\sigma,\mathbf{r}), \tag{52}$$

which leads to the Gibbs states

$$\rho^*(\sigma,\mathbf{r}) = \frac{e^{-\beta\sigma\overline{\psi}(\mathbf{r})-\alpha(\sigma)}}{\mathcal{Z}_\alpha(\beta\overline{\psi}(\mathbf{r}))}, \tag{53}$$

where the coarse grained stream function $\bar{\psi}$ and the partition function $\mathcal{Z}_\alpha$ are given by

$$\overline{\psi} = -\Delta^{-1}\overline{\omega}, \qquad \mathcal{Z}_\alpha(u) = \int_{\mathbb{R}} e^{-\sigma u-\alpha(\sigma)} d\sigma. \tag{54}$$

It follows that the coarse-grained vorticity field satisfies

$$\overline{\omega}(\mathbf{r}) = F_\alpha(\beta\overline{\psi}(\mathbf{r})), \qquad \text{with } F_\alpha(u) = -\frac{d\ln\mathcal{Z}_\alpha(u)}{du}. \tag{55}$$

This is a (elliptic) partial differential equation, referred to as the *mean-field equation*, characterizing the most probable coarse-grained vorticity fields. Note that the equation is of the same form as the equation defining steady-states of the Euler equation: equilibrium states form a subclass of steady-states for which the function relating vorticity and stream function is fixed by the invariants of the system.

The equilibrium states of the system can thus be obtained by solving (55). In general, this is a difficult task. Analytical solutions have been obtained in the limit of a linear function F_α (the mean-field equation then reduces to a Helmholtz equation), using the method introduced by Chavanis and Sommeria [19], which consists in decomposing the vorticity field and stream function on a basis of Laplacian eigenfunctions. Numerical methods are also available: Turkington and Whitaker have proposed an algorithm to iteratively solve the variational problem described above [92], while Robert and Sommeria [78] have proposed relaxation equations where the dynamics maximize the entropy production rate, thereby reaching a maximum entropy state. We shall not describe in details these methods here, nor the solutions they yield. Note, however, that in general, they correspond to large scale coherent structures, like vortices or unidirectional (e.g. zonal) flows, depending on the

geometry of the domain: for instance dipole/monopole in a rectangular domain [19], dipole/unidirectional flow in a doubly periodic domain [11], Fofonoff flows on a beta-plane [61], and solid-body rotation/dipole/quadrupole/unidirectional flow on a sphere [32, 35, 36, 71].

3.4 Non-equivalence of Ensembles

3.4.1 Statistical Ensembles and Variational Problems

So far we have been using exclusively the microcanonical measure

$$\mu_{\gamma,E}^{(N)}(d\hat{\omega}) = \delta(\mathcal{H}_N[\hat{\omega}] - E) \prod_{k=1}^{K} \delta\left(\mathcal{G}_N^{(k)}[\hat{\omega}] - \gamma_k\right) \mu^{(N)}(d\hat{\omega}), \tag{56}$$

which assigns uniform probability to microstates with a given energy and vorticity distribution, and zero probability to other microstates. We could make different choices and consider the canonical measure

$$\mu_{\gamma,\beta}^{(N)}(d\hat{\omega}) = \frac{e^{-\beta\mathcal{H}_N[\hat{\omega}]}}{\mathcal{Z}} \prod_{k=1}^{K} \delta\left(\mathcal{G}_N^{(k)}[\hat{\omega}] - \gamma_k\right) \mu^{(N)}(d\hat{\omega}), \tag{57}$$

or the grand-canonical measure

$$\mu_{\alpha,\beta}^{(N)}(d\hat{\omega}) = \frac{e^{-\beta\mathcal{H}_N[\hat{\omega}] - \sum_{k=1}^{K} \alpha_k \mathcal{G}_N^{(k)}[\hat{\omega}]}}{\Xi} \mu^{(N)}(d\hat{\omega}), \tag{58}$$

and similarly in the thermodynamic limit $N \to +\infty$. If we replace the microcanonical measure in Sect. 3.2 by any of these two measures, we obtain *mutas mutandi* a large deviation principle for the macrostates. In the thermodynamic limit, the most probable macrostates (i.e. the equilibrium states) are therefore solutions of the following variational problems:

$$S(E,\gamma) = \max_{\rho}\{\mathscr{S}[\rho] \mid \mathscr{H}[\rho] = E, \forall\sigma \in \mathbb{R}, \mathscr{D}_\sigma[\rho] = \gamma(\sigma)\}, \tag{59}$$

$$F(\beta,\gamma) = \max_{\rho}\{\mathscr{S}[\rho] - \beta\mathscr{H}[\rho] \mid \forall\sigma \in \mathbb{R}, \mathscr{D}_\sigma[\rho] = \gamma(\sigma)\}, \tag{60}$$

$$J(\beta,\alpha) = \max_{\rho}\{\mathscr{S}[\rho] - \beta\mathscr{H}[\rho] - \int_{\mathbb{R}} d\sigma\alpha(\sigma)\mathscr{D}_\sigma[\rho]\}, \tag{61}$$

respectively for the microcanonical measure, the canonical measure and the grand-canonical measure. The maximized functions arise as large deviation rate functions, and the constraints stem from the definition of the ensembles as conditional probabilities and from the existence of representation functions. The entropy $S(E,\gamma)$, the

free energy $F(\beta, \gamma)$ and the *grand potential* $J(\beta, \alpha)$ are referred to generically as *thermodynamic potentials*.

The existence of a large deviation principle for the macrostates does not depend on the particular choice of ensemble, but the most probable macrostates may depend on this choice. The task that we set out to investigate in this section is therefore how the different ensembles are related. The discussion closely follows the Refs. [26, 90].

3.4.2 Ensemble Equivalence at the Macrostate Level

First of all, it is clear from the structure of the variational problems and the Lagrange multiplier rule that they all have the same critical points. However, the critical points may be of different nature: a maximizer of one variational problem may be a saddle point of another variational problem for instance. Nevertheless, it is easily seen that a solution of a variational problem with a constraint relaxed (e.g. the canonical variational problem) is always a solution of the original constrained variational problem (e.g. the microcanonical problem). We can formalize this remark by introducing the sets of equilibrium states (i.e. solutions of the variational problems):

$$\mathscr{MC}(E, \gamma) = \{\rho \mid \mathscr{S}[\rho] = S(E, \gamma), \mathscr{H}[\rho] = E, \forall \sigma \in \mathbb{R}, \mathscr{D}_\sigma[\rho] = \gamma(\sigma)\}, \tag{62}$$

$$\mathscr{C}(\beta, \gamma) = \{\rho \mid \mathscr{S}[\rho] - \beta\mathscr{H}[\rho] = F(\beta, \gamma), \forall \sigma \in \mathbb{R}, \mathscr{D}_\sigma[\rho] = \gamma(\sigma)\}, \tag{63}$$

$$\mathscr{GC}(\beta, \alpha) = \{\rho \mid \mathscr{S}[\rho] - \beta\mathscr{H}[\rho] - \int_{\mathbb{R}} d\sigma\alpha(\sigma)\mathscr{D}_\sigma[\rho] = J(\beta, \alpha)\}. \tag{64}$$

As per the above remark, we always have,

$$\forall \beta, \alpha, \forall \rho \in \mathscr{GC}(\beta, \alpha), \rho \in \mathscr{C}(\beta, \mathscr{D}_\sigma[\rho]) \text{ and } \rho \in \mathscr{MC}(\mathscr{H}[\rho], \mathscr{D}_\sigma[\rho]), \tag{65}$$

$$\forall \beta, \gamma, \forall \rho \in \mathscr{C}(\beta, \gamma), \rho \in \mathscr{MC}(\mathscr{H}[\rho], \gamma). \tag{66}$$

In particular,

$$\bigcup_{\beta,\alpha} \mathscr{GC}(\beta, \alpha) \subset \bigcup_{\beta,\gamma} \mathscr{C}(\beta, \gamma) \subset \bigcup_{E,\gamma} \mathscr{MC}(E, \gamma). \tag{67}$$

If the converse statements hold, i.e.

$$\forall E, \gamma, \forall \rho \in \mathscr{MC}(E, \gamma), \exists \beta \in \mathbb{R} : \rho \in \mathscr{C}(\beta, \gamma), \tag{68}$$

or

$$\forall \beta, \gamma, \forall \rho \in \mathscr{C}(\beta, \gamma), \exists \alpha : \rho \in \mathscr{GC}(\beta, \alpha), \tag{69}$$

we say, respectively, that the microcanonical and canonical ensembles are *equivalent at the macrostate level* or that the canonical and grand canonical ensembles are *equivalent at the macrostate level*. It is straightforward to see that it is a transitive relation, in the sense that if the microcanonical ensemble is equivalent to the canonical ensemble at the macrostate level, and if the canonical ensemble and the grand-canonical ensemble are equivalent at the macrostate level, then the microcanonical and the grand-canonical ensembles are equivalent a the macrostate level. Besides, if the grand-canonical ensemble is equivalent to the microcanonical ensemble at the macrostate level, then the canonical ensemble is equivalent to both the microcanonical and the grand-canonical ensembles at the macrostate level.

If the three ensembles are equivalent at the macrostate level, we have the equalities:

$$\bigcup_{\beta,\alpha} \mathscr{GC}(\beta,\alpha) = \bigcup_{\beta,\gamma} \mathscr{C}(\beta,\gamma) = \bigcup_{E,\gamma} \mathscr{MC}(E,\gamma). \tag{70}$$

3.4.3 Ensemble Equivalence at the Thermodynamic Level

Due to the definition of the thermodynamic potentials through the variational problems, connections exist between them as well. For the free energy for instance, we have

$$\begin{aligned} F(\beta,\gamma) &= \max_{\rho,\mathscr{N}[\rho](\mathbf{x})=1} \{\mathscr{S}[\rho] - \beta\mathscr{H}[\rho] \mid \forall\sigma \in \mathbb{R}, \mathscr{D}_\sigma[\rho] = \gamma(\sigma)\}, \\ &= \max_{E\geq 0} \left(\max_{\rho,\mathscr{N}[\rho](\mathbf{x})=1,\mathscr{H}[\rho]=E} \{\mathscr{S}[\rho] - \beta E \mid \forall\sigma \in \mathbb{R}, \mathscr{D}_\sigma[\rho] = \gamma(\sigma)\} \right), \\ &= \max_{E\geq 0} \left(S(E,\gamma) - \beta E\right). \end{aligned}$$

This exactly means that the free energy is the *Legendre-Fenchel* transform of the entropy. The Legendre-Fenchel transform is a generalization of the Legendre transform to functions which need not be differentiable and convex [79]. Denoting the Legendre-Fenchel of an arbitrary function with a star (the variable with respect to which the transform is taken should be clear from the arguments of the function), we have the compact form:

$$F(\beta,\gamma) = S^\star(E,\gamma).$$

Similarly,

$$J(\beta,\alpha) = F^\star(\beta,\gamma).$$

We know that the Legendre transform is an involution [1]. This is not necessarily the case for the Legendre-Fenchel transform, because the Legendre-Fenchel transform of an arbitrary function is always a concave function, but it is true when the original function is concave. In general, when applying the Legendre-Fenchel

transform twice, we only obtain the concave hull of the original function [79]. Hence, the free energy F is always a concave function of β and the grand-potential J is always a concave function of its arguments, while $F^\star = S^{\star\star}$ is always a concave function of E, and is the smallest concave function satisfying $S(E,\gamma) \leq S^{\star\star}(E,\gamma)$. The equality holds if S is a concave function. Therefore, we say that the microcanonical and canonical ensemble are *equivalent at the thermodynamic level* if $S = F^\star = S^{\star\star}$, or equivalently, if S is a concave function of E. Similarly, the grand canonical and the canonical ensembles are equivalent at the thermodynamic level if $F = J^\star = F^{\star\star}$, i.e. if F is a concave function of γ.

Again, we have a transitivity property: equivalence of the grand canonical and canonical ensembles on the one hand, and of the canonical and microcanonical ensembles on the other hand implies equivalence of the grand canonical and microcanonical ensembles. Besides, if the grand canonical and the microcanonical ensembles are equivalent, then the canonical ensemble is equivalent to both the grand canonical and the microcanonical ensembles. In both these cases, the entropy S is a concave function of all its arguments.

3.4.4 Equivalence and Non-equivalence of Statistical Ensembles

The notions of ensemble equivalence at the macrostate level (Sect. 3.4.2) and at the thermodynamic level (Sect. 3.4.3) are connected. Indeed, the local concavity properties of the thermodynamic potential determine the possibility to invert the relation with the Lagrange multiplier, or in other words, the possibility that the macrostates can be obtained by solving a relaxed variational problem. Following [26], let us examine the three possibilities in the context of the microcanonical and canonical ensembles. Let us fix E, γ, then one of the three following assertions holds:

(i) **Total Ensemble Equivalence:** If $S = S^{\star\star}$ and S is not locally flat, then $\mathscr{MC}(E,\gamma) = \mathscr{C}(\beta,\gamma)$ for $\beta = \partial S/\partial E$.
(ii) **Marginal Ensemble Equivalence:** If $S = S^{\star\star}$ and S is locally flat, then $\mathscr{MC}(E,\gamma) \subsetneq \mathscr{C}(\beta,\gamma)$ for $\beta = \partial S/\partial E$.
(iii) **Ensemble Inequivalence:** If $S \neq S^{\star\star}$, then $\forall \beta \in \mathbb{R}$, $\mathscr{MC}(E,\gamma) \cap \mathscr{C}(\beta,\gamma) = \emptyset$.

3.5 Large Deviations for the Coarse-Grained Vorticity Field

In Sect. 3.2, we have considered how the probability of the outcome of a given observable (the distribution of fine-grained vorticity) behaves when the size of the system goes to infinity. We have found that it satisfies a large deviation property, which allows us to compute the most probable outcomes (see Sect. 3.3). From there, we are able to deduce what the most probable coarse-grained vorticity fields are. But can we apply the same methods directly to the coarse-graining observable to compute the most probable coarse-grained vorticity fields? In other words, can we obtain a large deviation principle directly for the observable $\mathfrak{C}$?

In general this is not straightforward, because we do not have a representation function for the vorticity distribution in terms of the coarse-grained vorticity field. Let us give an exemple in the simple case where we have only three levels of vorticity: $\mathfrak{S} = \{-1, 0, 1\}$. We have represented on Fig. 3 two microstates which lead to the same coarse-grained vorticity field, with different vorticity distributions. As a consequence, we cannot deduce a large deviation principle with respect to the microcanonical measure (or any of the other ensembles) from a large deviation principle with respect to the prior measure. In principle it remains possible to evaluate directly the probability of a coarse-grained vorticity field in the microcanonical ensemble, but this is a much more complicated combinatorial problem. However, in the special case of a two-level vorticity system, we do have a representation function for the vorticity distribution. We illustrate this in the following sections by making use of the analogy with the mean-field Ising model pointed out above.

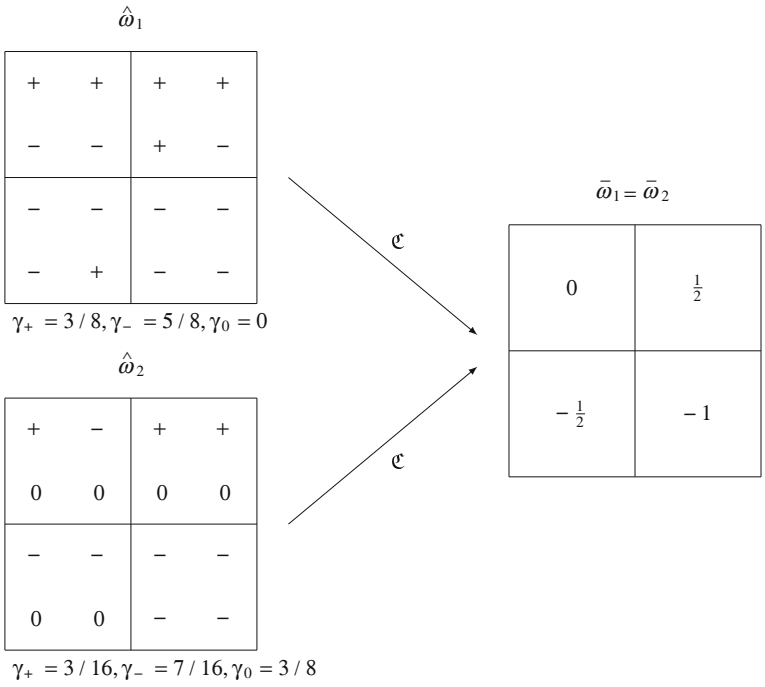

Fig. 3 Exemples of two microstates with different vorticity distribution, which are mapped to the same coarse-grained vorticity field by the operator $\mathfrak{C}$, in the three-level case: $\mathfrak{S} = \{-1, 0, 1\}$

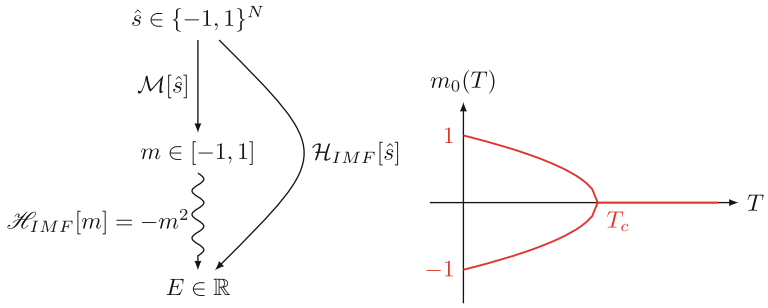

Fig. 4 Mean-field Ising model: observables (hamiltonian and magnetization) and representation function for the energy (*left*) and most probable magnetization as a function of temperature in the canonical ensemble (*right*)

3.5.1 Mean-Field Ising Model

Remember the mean-field Ising model described in Sect. 2.4.1. We have mentioned above that there is a representation function for the energy in terms of the magnetization (Fig. 4). Therefore it is sufficient to obtain a large deviation principle for the magnetization with respect to the unconstrained measure. If N_+ (resp. N_-) is the number of $+$ (resp. $-$) spins, the magnetization is given by $\mathcal{M}[\hat{s}] = (N_+ - N_-)/N$, and we have $N_+ + N_- = N$. In other words, $N_\pm/N = (1 \pm \mathcal{M}[\hat{s}])/2$. Hence, the unconstrained probability to observe a given magnetization is

$$\mu^{(N)}(\mathcal{M}[\hat{s}] = m) = \frac{N!}{2^N N_+! N_-!} \tag{71}$$

$$= e^{N\mathscr{S}[m]+o(N)}, \tag{72}$$

where the mean-field entropy is given by (up to an unimportant constant $\ln 2$)

$$\mathscr{S}[m] = -\frac{1+m}{2}\ln\left(\frac{1+m}{2}\right) - \frac{1-m}{2}\ln\left(\frac{1-m}{2}\right), \tag{73}$$

which proves that the magnetization observable satisfies a large deviation principle. It is customary to work in the canonical ensemble (see Sect. 3.4), and the most probable states are therefore solutions of the variational problem:

$$F(\beta) = \min_{m\in[-1,1]} \left(\beta\mathscr{H}_{IMF}[m] - \mathscr{S}[m]\right), \tag{74}$$

where F is the free energy (per spin). Using $\mathscr{H}_{IMF}[m] = -m^2$ and (73), it is easily shown that for $\beta = 1/(kT)$ smaller than a critical value $\beta_c = 1/(kT_c)$ (high temperature T), there is a unique solution $m = 0$, while for β larger than the critical value

(low temperature), there are two non-zero solutions $\pm m_0(T)$. The most probable magnetization as a function of the temperature is represented on Fig. 4.

3.5.2 Two-Level System

We have noted above that when the vorticity level set is made of two opposite values, $\mathfrak{S} = \{\sigma_0, -\sigma_0\}$ (with $\sigma_0 > 0$), the system becomes analogous to the mean-field Ising model studied above. The only difference is the vorticity distribution conservation constraint (and the interaction coefficients). This amounts to keeping fixed the number of $+$ and $-$ spins in the Ising model, or equivalently, to fixing the magnetization. But the magnetization here is nothing but the circulation Γ_1. Therefore, conservation of the Casimir invariants in the discretized two-level model reduces to conservation of the circulation.

Another way to see this is to show explicitly that there exists a representation function for the vorticity distribution in this case. The coarse-graining operator $\mathfrak{C}$ takes value in a discrete subset of $\mathbb{R}^M$: denoting $\tilde{\mathfrak{S}}_n = \{\left(\frac{2k}{n} - 1\right)\sigma_0, 0 \leq k \leq n\}$, the image of the operator is $\tilde{\mathfrak{S}}_n^M$. Here, k corresponds to the number of sites with value σ_0 in each coarse-graining cell. The relation between k and $\bar{\omega}_i$ can be inverted: $k = n(1 + \bar{\omega}_i/\sigma_0)/2$, and we obtain

$$\gamma_+ = \frac{1}{N}\sum_{i=1}^{M} \frac{n}{2}\left(1 + \frac{\bar{\omega}_i}{\sigma_0}\right), \tag{75}$$

$$= \frac{1}{2} + \frac{\Gamma_1}{2\sigma_0}, \tag{76}$$

and similarly,

$$\gamma_- = \frac{1}{2} - \frac{\Gamma_1}{2\sigma_0}. \tag{77}$$

Note that, as expected, $\gamma_+ + \gamma_- = 1$ (Eq. (13)) and $(\gamma_+ - \gamma_-)\sigma_0 = \Gamma_1$ (Eq. (11)). Now, it is an easy task to evaluate the unconstrained probability of a given coarse-grained vorticity field:

$$\mu^{(N)}(\mathfrak{C}[\hat{\omega}] = \bar{\omega}) = \frac{\text{Card}\,\mathfrak{C}^{-1}[\bar{\omega}]}{2^N} = 2^{-N}\prod_{i=1}^{M} \frac{n!}{(n/2(1 + \bar{\omega}_i/\sigma_0))!(n/2(1 - \bar{\omega}_i/\sigma_0))!}, \tag{78}$$

$$= e^{N\bar{\mathscr{S}}_{M,2}[\bar{\omega}] + o(N)}, \tag{79}$$

with the entropy of the coarse-graining observable (up to an unimportant constant $\ln 2$)

$$\bar{\mathscr{S}}_{M,2}[\bar{\omega}] = -\frac{1}{2M}\sum_{i=1}^{M}\left[\left(1+\frac{\bar{\omega}_i}{\sigma_0}\right)\ln\left(1+\frac{\bar{\omega}_i}{\sigma_0}\right)+\left(1-\frac{\bar{\omega}_i}{\sigma_0}\right)\ln\left(1-\frac{\bar{\omega}_i}{\sigma_0}\right)\right]. \tag{80}$$

The contraction principle ensures that, as can be checked explicitly,

$$\bar{\mathscr{S}}_{M,2}[\bar{\omega}] = \max_{P\in\mathcal{M}_{M,2}(\mathbb{R})}\{\mathscr{S}_{M,2}[P] \mid \mathfrak{E}[P]=\bar{\omega}\}. \tag{81}$$

By the same token as in Sect. 3.2, it follows that the most probable coarse-grained vorticity fields are solutions of the constrained variational problem:

$$S(E,\gamma) = \max_{\bar{\omega}\in\bar{\mathfrak{S}}_n^M}\{\bar{\mathscr{S}}_{M,2}[\bar{\omega}] \mid \bar{\mathcal{H}}_M[\bar{\omega}]=E, \bar{\mathcal{G}}_M^{(+)}[\bar{\omega}]=\gamma_+, \bar{\mathcal{G}}_M^{(-)}[\bar{\omega}]=\gamma_-\}, \tag{82}$$

or equivalently,

$$S(E,\Gamma_1) = \max_{\bar{\omega}\in\bar{\mathfrak{S}}_n^M}\{\bar{\mathscr{S}}_{M,2}[\bar{\omega}] \mid \bar{\mathcal{H}}_M[\bar{\omega}]=E, \bar{\mathcal{M}}_M[\bar{\omega}]=\Gamma_1\}. \tag{83}$$

Straightforward computations show that the critical points of the variational problem are solutions of the equation:

$$\bar{\omega} = \sigma_0\tanh\left(\frac{(\beta\bar{\psi}+\alpha_1)\sigma_0}{2}\right). \tag{84}$$

3.5.3 Fragile Constraints and Constrained Casimir Variational Problem

It has been observed by several authors that none of the Casimir invariants Γ_p (moments of the vorticity field) except the first (circulation) can be obtained from the coarse-grained vorticity field $\bar{\omega}$. For this reason they are often referred to as *fragile invariants*, in the sense that they do not survive coarse-graining. This is exactly the same as saying that there is no representation function for the Casimir invariants (or, equivalently, for the vorticity distribution $\gamma(\sigma)$) in terms of the coarse-grained vorticity field $\bar{\omega}$, except in the particular case mentioned above. However, with an arbitrary vorticity distribution, a large deviation principle can still be obtained by contraction, as illustrated above in the two-layer case. This provides a variational problem for the most probable coarse-grained vorticity field, even though it still relies on an auxiliary maximization on the distribution P for the vorticity levels.

Because of their fragile nature, and because an infinite number of invariants is difficult to handle in practice, it was suggested [16, 27] to treat these invariants in a

canonical ensemble, and to consider the Lagrange parameter $\alpha(\sigma)$ as a prior vorticity distribution chosen based on physical intuition of the problem at hand. This provides a subset of solutions of the microcanonical variational problem, but not necessarily the full set (see Sect. 3.4). However, this variational problem, expressed in terms of the distribution P for the vorticity levels, is equivalent to minimizing, with respect to the coarse-grained vorticity field $\bar{\omega}$, the so-called *Casimir functionals* $\int_{\mathcal{D}} s(\omega)$ with fixed energy, where s is a convex function, choosing for s the Legendre-Fenchel transform of $\ln \mathcal{Z}_\alpha$ [9].

3.6 The Energy-Enstrophy Measure

3.6.1 Gibbs Measure for Galerkin Truncated Flows

In this section we investigate the statistical mechanics of the 2D Euler equations resulting from simplifying the conservation constraints: we retain only the energy and the enstrophy invariants. This was actually one of the starting points for statistical mechanics of turbulent flows: Lee in 3D [47] and Kraichnan in 2D [42] considered Fourier series of the dynamical fields truncated at a given order N. In 3D, the only invariants are the energy and the helicity, while in 2D, Kraichnan considered the energy:

$$\mathcal{H}_N[\hat{\omega}] = \frac{1}{2}\sum_{i=1}^{N} \frac{|\hat{\omega}_i|^2}{\lambda_i}, \tag{85}$$

and the enstrophy

$$\mathcal{G}_N[\hat{\omega}] = \frac{1}{2}\sum_{i=1}^{N} |\hat{\omega}_i|^2, \tag{86}$$

where the truncated vorticity field is given by

$$\hat{\omega}(x) = \sum_{i=1}^{N} \hat{\omega}_i \phi_i(x), \quad \Delta\phi_i = -\lambda_i \phi_i, 0 \leq \lambda_i \leq \lambda_{i+1}. \tag{87}$$

It is assumed that the truncated vorticity field $\hat{\omega}$ is a random variable distributed according to the canonical (Gibbs) measure:

$$\mu_{\beta,\alpha}^{(N)}(d\hat{\omega}) = \frac{1}{\mathcal{Z}} e^{-\beta\mathcal{H}_N[\hat{\omega}]-\alpha\mathcal{G}_N[\hat{\omega}]} \prod_{i=1}^{N} d\hat{\omega}_i. \tag{88}$$

This is a Gaussian probability density, well-defined if $\beta + \alpha\lambda_i > 0$ for all i. This condition leads to three possible regimes: (i) $\beta < 0, \alpha > 0$, (ii) $\beta > 0, \alpha > 0$, (iii) $\beta > 0, \alpha < 0$. In each case, Kraichnan considered the energy spectrum $\mathcal{E}_i[\hat{\omega}] = \frac{|\hat{\omega}_i|^2}{2\lambda_i}$ and computed its average value with respect to the Gibbs measure [42, 44]: $\langle \mathcal{E}_i \rangle = \frac{1}{2(\beta+\alpha\lambda_i)}$. In the negative temperature ($\beta < 0$) regime, the spectrum peaks at the gravest mode ϕ_1; there is even an *infrared divergence* when $\beta \to -\alpha\lambda_1$. This is classically interpreted as an indication that not only nonlinear interactions in 2D flows tend to transfer energy towards the large scales (the *inverse cascade*), but there is a tendency for energy to accumulate in the gravest mode to form a *condensate* [6, 21, 85]. Note that the average value of each vorticity mode vanishes by symmetry: $\langle \hat{\omega}_i \rangle = 0$, because a given vorticity field and its opposite have the same probability in the canonical ensemble. Of course, in reality, the system will spontaneously break the symmetry and choose a vorticity field, which can be computed in the limit of large N using large deviations results for the macrostates as we did above. In the energy-enstrophy ensemble, averaging over the set of equilibrium states indeed yields a vanishing mean value, thereby showing that statistical mechanics is more about most probable states than average values.

3.6.2 Large Deviations in the Microcanonical Ensemble

Using the same notations as in the previous paragraph, one may assume that the truncated vorticity field is distributed according to the microcanonical measure

$$\mu^{(N)}_{E,\Gamma_2}(d\hat{\omega}) = \frac{1}{\Omega_N(E,\Gamma_2)} \delta(\mathcal{H}_N[\hat{\omega}] - E)\delta(\mathcal{G}_N[\hat{\omega}] - \Gamma_2) \prod_{i=1}^{N} d\hat{\omega}_i, \tag{89}$$

instead of the Gibbs measure $\mu^{(N)}_{\beta,\alpha}(d\hat{\omega})$, with the structure function given by

$$\Omega_N(E,\Gamma_2) = \int \delta(\mathcal{H}_N[\hat{\omega}] - E)\delta(\mathcal{G}_N[\hat{\omega}] - \Gamma_2) \prod_{i=1}^{N} d\hat{\omega}_i. \tag{90}$$

Rather exceptionally, since both constraints involve quadratic functions, the structure function can be computed explicitly, using integral representations of the Dirac distributions [10], and thus also the entropy:

$$\Omega_N(E,\Gamma_2) = e^{NS(E,\Gamma_2)+o(N)}, \tag{91}$$

$$S(E,\Gamma_2) = \frac{1}{2}\ln(\Gamma_2 - 2\lambda_1 E). \tag{92}$$

Note that Bouchet and Corvellec [10] have also checked with explicit computations that this entropy defined as the joint large deviation rate function for

the energy and enstrophy observables (i.e. the Boltzmann formula $S(E,\Gamma_2) = \lim(1/N)\ln\Omega_N(E,\Gamma_2)$, given in (92)) coincides with the entropy defined through the variational problem for the macrostates, as expected from the contraction principle (Eq. (47)). A similar computation of the structure function was carried out by Kastner and Schnetz [40] for the mean-field spherical model defined in Sect. 2.4.2.

From the joint large deviation principle for the energy and enstrophy, we can deduce a large deviation principle for the energy spectrum observable [10]:

$$\mu^{(N)}_{E,\Gamma_2}(\mathcal{E}_i[\hat{\omega}] = E_i) = e^{N\mathscr{S}^{(i)}_{E,\Gamma_2}[E_i]+o(N)}, \tag{93}$$

with

$$\mathscr{S}^{(1)}_{E,\Gamma_2}[E_1] = \begin{cases} \frac{1}{2}\ln(\Gamma_2 - 2\lambda_2 E + 2(\lambda_2-\lambda_1)E_1) & \text{if } 0 < E_1 < E \\ -\infty & \text{otherwise} \end{cases}, \tag{94}$$

and for $i > 1$,

$$\mathscr{S}^{(i)}_{E,\Gamma_2}[E_i] = \begin{cases} \frac{1}{2}\ln(\Gamma_2 - 2\lambda_1 E - 2(\lambda_i-\lambda_1)E_i) & \text{if } 0 \le E_i \le E \\ -\infty & \text{otherwise} \end{cases}. \tag{95}$$

The large deviation rate functions are monotonous: $\mathscr{S}^{(1)}_{E,\Gamma_2}[E_1]$ is an increasing function of E_1, and $\mathscr{S}^{(i)}_{E,\Gamma_2}[E_i]$ are decreasing functions of E_i. Therefore, the most probable energy spectrum in the limit $N \to +\infty$ has all its energy in the gravest mode. This can be seen as the microcanonical counterpart of the Kraichnan argument presented in Sect. 3.6.1. It provides further theoretical evidence for the spectral condensation in 2D turbulence.

The above discussion on the vanishing of the average truncated vorticity field also applies in the microcanonical ensemble. The mean-field theory allows to compute the most probable macrostates: we find a linear mean-field equation for the coarse-grained vorticity field: $\bar{\omega} = \beta/(2\alpha)\bar{\psi}$, which is easily solved and yields $\bar{\omega} = \sqrt{2\lambda_1 E}\phi_1$, in agreement with the above prediction.

4 Conclusion

In this chapter, we have given a brief introduction to the methods of equilibrium statistical mechanics applied to models of turbulent flows, focusing on the case of two-dimensional flows. The main purpose of the course was to show, in the context of a lattice discretization of the system, how some well-chosen observables, such as the distribution of fined-grained vorticity levels, concentrate in probability around a set of equilibrium values. Such properties are conveniently expressed using the theory of large deviations. In fact, we have closely followed the principles of equilibrium

statistical mechanics formulated in the language of large deviations, as exposed for instance in [89]. A major ingredient in deriving the large deviation results is the long-range character of the interactions, because it leads to the existence of a representation function for the energy. This is a major simplification, as it allows us to compute the probability of a macrostate with respect to the uniform measure and then deduce the probability with respect to the microcanonical measure. We have emphasized this point by considering another observable, the coarse-grained vorticity field (for which there is no representation function for the vorticity distribution) and by making the analogy with a simpler system, the mean-field Ising model.

The large deviation principle leads to a variational problem characterizing the most probable macrostates. This allows to compute coarse-grained vorticity fields which should correspond in practice to the final state of the system, if ergodicity holds. This provides a statistical explanation of the spontaneous emergence of coherent structures in two-dimensional flows. The equilibrium states obtained may depend on the choice of probability measure in phase space: we have discussed the relations between the standard ensembles of statistical mechanics and given a connection with the concavity properties of the entropy.

In the simpler context of the energy-enstrophy measure, we have explained that the energy spectrum observable also satisfies a large deviation principle, which shows that the most probable state has all its energy condensed in the gravest mode. This is physically consistent with the familiar ideas of inverse cascade of energy and energy condensation for 2D flows.

References

1. Arnold VI (1989) Mathematical methods of classical mechanics, 2nd edn. Springer, New York
2. Batchelor G (1969) Computation of the energy spectrum in homogeneous two-dimensional turbulence. Phys Fluids 12(Suppl. II):233–239. doi:10.1063/1.1692443
3. Baxter RJ (1982) Exactly solved models in statistical mechanics. Academic Press, London
4. Berlin TH, Kac M (1952) The spherical model of a ferromagnet. Phys Rev 86:821. doi:10.1103/PhysRev.86.821
5. Biferale L, Musacchio S, Toschi F (2012) Inverse energy cascade in three-dimensional isotropic turbulence. Phys Rev Lett 108(16):164501. doi:10.1103/PhysRevLett.108.164501
6. Boffetta G, Ecke RE (2012) Two-dimensional turbulence. Annu Rev Fluid Mech 44:427. doi:10.1146/annurev-fluid-120710-101240
7. Boucher C, Ellis RS, Turkington B (1999) Spatializing random measures: doubly indexed processes and the large deviation principle. Ann Probab 27:297–324
8. Boucher C, Ellis RS, Turkington B (2000) Derivation of maximum entropy principles in two-dimensional turbulence via large deviations. J Stat Phys 98(5–6):1235–1278
9. Bouchet F (2008) Simpler variational problems for statistical equilibria of the 2D Euler equation and other systems with long range interactions. Physica D 237:1976–1981. doi:10.1016/j.physd.2008.02.029
10. Bouchet F, Corvellec M (2010) Invariant measures of the 2D Euler and Vlasov equations. J Stat Mech P08021. doi:10.1088/1742-5468/2010/08/P08021
11. Bouchet F, Simonnet E (2009) Random changes of flow topology in two-dimensional and geophysical turbulence. Phys Rev Lett 102:094504. doi:10.1103/PhysRevLett.102.094504

12. Bouchet F, Sommeria J (2002) Emergence of intense jets and Jupiter's Great Red Spot as maximum-entropy structures. J Fluid Mech 464:165–207. doi:10.1017/S0022112002008789
13. Bouchet F, Venaille A (2012) Statistical mechanics of two-dimensional and geophysical flows. Phys Rep 515:227–295. doi:10.1016/j.physrep.2012.02.001
14. Campa A, Dauxois T, Ruffo S (2009) Statistical mechanics and dynamics of solvable models with long-range interactions. Phys Rep 480:57–159. doi:10.1016/j.physrep.2009.07.001
15. Charney JG (1971) Geostrophic turbulence. J Atmos Sci 28:1087–1094. doi:10.1175/1520-0469(1971)028<1087:GT>2.0.CO;2
16. Chavanis PH (2003) Generalized thermodynamics and Fokker-Planck equations: applications to stellar dynamics and two-dimensional turbulence. Phys Rev E 68:036108
17. Chavanis PH (2006) Phase transitions in self-gravitating systems. Int J Mod Phys B 20:3113. doi:10.1142/S0217979206035400
18. Chavanis PH, Dubrulle B (2006) Statistical mechanics of the shallow-water system with an a priori potential vorticity distribution. C R Phys 7:422–432. doi:10.1016/j.crhy.2006.01.007
19. Chavanis PH, Sommeria J (1996) Classification of self-organized vortices in two-dimensional turbulence: the case of a bounded domain. J Fluid Mech 314:267–297. doi:10.1017/S0022112096000316
20. Chavanis PH, Sommeria J (2002) Statistical mechanics of the shallow water system. Phys Rev E 65:026302. doi:10.1103/PhysRevE.65.026302
21. Chertkov M, Connaughton C, Kolokolov I, Lebedev V (2007) Dynamics of energy condensation in two-dimensional turbulence. Phys Rev Lett 99(8):084501. doi:10.1103/PhysRevLett.99.084501
22. Cipra BA (1987) An introduction to the Ising model. Am Math Mon 94(10):937–959
23. Dauxois T, Ruffo S, Arimondo E, Wilkens M (eds) (2002) Dynamics and thermodynamics of systems with long range interactions. Lecture notes in physics, vol 602. Springer, New York. doi:10.1007/3-540-45835-2
24. DiBattista M, Majda AJ (2001) Equilibrium statistical predictions for baroclinic vortices: the role of angular momentum. Theor Comput Fluid Dyn 14(5):293–322
25. Ellis RS (1985) Entropy, large deviations, and statistical mechanics. Springer, New York
26. Ellis RS, Haven K, Turkington B (2000) Large deviation principles and complete equivalence and nonequivalence results for pure and mixed ensembles. J Stat Phys 101:999–1064. doi:10.1023/A:1026446225804
27. Ellis RS, Haven K, Turkington B (2002) Nonequivalent statistical equilibrium ensembles and refined stability theorems for most probable flows. Nonlinearity 15:239. doi:10.1088/0951-7715/15/2/302
28. Eyink G, Sreenivasan K (2006) Onsager and the theory of hydrodynamic turbulence. Rev Mod Phys 78:87–135. doi:10.1103/RevModPhys.78.87
29. Falkovich G (2011) Fluid mechanics. Cambridge University Press, Cambridge
30. Fjortoft R (1953) On the changes in the spectral distribution of kinetic energy for twodimensional, nondivergent flow. Tellus 5:225–230
31. Frisch U (1995) Turbulence, the legacy of A.N. Kolmogorov. Cambridge University Press, Cambridge
32. Herbert C (2013) Additional invariants and statistical equilibria for the 2D Euler equations on a spherical domain. J Stat Phys 152:1084–1114. doi:10.1007/s10955-013-0809-6
33. Herbert C (2014) Nonlinear energy transfers and phase diagrams for geostrophically balanced rotating-stratified flows. Phys Rev E 89:033008. doi:10.1103/PhysRevE.89.033008
34. Herbert C (2014) Restricted partition functions and inverse energy cascades in parity symmetry breaking flows. Phys Rev E 89:013010. doi:10.1103/PhysRevE.89.013010
35. Herbert C, Dubrulle B, Chavanis PH, Paillard D (2012) Phase transitions and marginal ensemble equivalence for freely evolving flows on a rotating sphere. Phys Rev E 85:056304. doi:10.1103/PhysRevE.85.056304
36. Herbert C, Dubrulle B, Chavanis PH, Paillard D (2012) Statistical mechanics of quasi-geostrophic flows on a rotating sphere. J Stat Mech P05023. doi:10.1088/1742-5468/2012/05/P05023

37. Herbert C, Pouquet A, Marino R (2014) Restricted equilibrium and the energy cascade in rotating and stratified flows. J Fluid Mech 758:374–406. doi:10.1017/jfm.2014.540
38. Ising E (1925) Beitrag zur theorie des ferromagnetismus. Z Phys 31:253–258
39. Joyce GS (1966) Spherical model with long-range ferromagnetic interactions. Phys Rev 146:349
40. Kastner M, Schnetz O (2006) On the mean-field spherical model. J Stat Phys 122:1195–1214
41. Kolmogorov AN (1941) The local structure of turbulence in incompressible viscous fluid for very large Reynolds' numbers. Dokl Akad Nauk SSSR 30:301. doi:10.1098/rspa.1991.0075
42. Kraichnan RH (1967) Inertial ranges in two-dimensional turbulence. Phys Fluids 10:1417–1423. doi:10.1063/1.1762301
43. Kraichnan RH (1973) Helical turbulence and absolute equilibrium. J Fluid Mech 59:745–752
44. Kraichnan RH, Montgomery DC (1980) Two-dimensional turbulence. Rep Prog Phys 43:547. doi:10.1088/0034-4885/43/5/001
45. Landau L, Lifchitz E (1971) Physique Théorique, Tome VI: Mécanique des fluides. Mir, Moscou
46. Lanford OE (1973) Entropy and equilibrium states in classical statistical mechanics. In: Lenard A (ed) Statistical mechanics and mathematical problems. Lecture notes in physics, vol 20. Springer, Berlin, pp 1–113
47. Lee TD (1952) On some statistical properties of hydrodynamical and magneto-hydrodynamical fields. Q Appl Math 10:69–74
48. Leith C (1968) Diffusion approximation for two-dimensional turbulence. Phys Fluids 11:671–673. doi:10.1063/1.1691968
49. Leprovost N, Dubrulle B, Chavanis PH (2006) Dynamics and thermodynamics of axisymmetric flows: theory. Phys Rev E 73:046308. doi:10.1103/PhysRevE.73.046308
50. Lilly DK (1983) Stratified turbulence and the mesoscale variability of the atmosphere. J Atmos Sci 40:749–761
51. Lim CC (2001) A long range spherical model and exact solutions of an energy enstrophy theory for two-dimensional turbulence. Phys Fluids 13:1961
52. Lim CC (2012) Phase transition to super-rotating atmospheres in a simple planetary model for a nonrotating massive planet: exact solution. Phys Rev E 88(6):066304. doi:10.1103/PhysRevE.86.066304
53. Lucarini V, Blender R, Herbert C, Pascale S, Ragone F, Wouters J (2014) Mathematical and physical ideas for climate science. Rev Geophys 52:809–859. doi:10.1002/2013RG000446
54. Majda AJ, Wang X (2006) Nonlinear dynamics and statistical theories for basic geophysical flows. Cambridge University Press, Cambridge
55. McWilliams JC (1984) The emergence of isolated coherent vortices in turbulent flow. J Fluid Mech 146:21–43. doi:10.1017/S0022112084001750
56. Merilees PE, Warn H (1975) On energy and enstrophy exchanges in two-dimensional non-divergent flow. J Fluid Mech 69(04):625–630
57. Michel J, Robert R (1994) Large deviations for Young measures and statistical mechanics of infinite dimensional dynamical systems with conservation law. Commun Math Phys 159:195–215. doi:10.1007/BF02100491
58. Michel J, Robert R (1994) Statistical mechanical theory of the great red spot of Jupiter. J Stat Phys 77:645–666. doi:10.1007/BF02179454
59. Miller J (1990) Statistical mechanics of Euler equations in two dimensions. Phys Rev Lett 65:2137–2140. doi:10.1103/PhysRevLett.65.2137
60. Miller J, Weichman PB, Cross MC (1992) Statistical mechanics, Euler's equation, and Jupiter's Red Spot. Phys Rev A 45:2328–2359. doi:10.1103/PhysRevA.45.2328
61. Naso A, Chavanis PH, Dubrulle B (2011) Statistical mechanics of Fofonoff flows in an oceanic basin. Eur Phys J B 80:493–517. doi:10.1140/epjb/e2011-10440-8
62. Naso A, Monchaux R, Chavanis PH, Dubrulle B (2010) Statistical mechanics of Beltrami flows in axisymmetric geometry: theory reexamined. Phys Rev E 81:066318. doi:10.1103/PhysRevE.81.066318
63. Nazarenko SV (2010) Wave turbulence. Lecture notes in physics, vol 825. Springer

64. Olver PJ (2000) Applications of Lie groups to differential equations. Graduate texts in mathematics. Springer
65. Onsager L (1944) Crystal statistics. I. A two-dimensional model with an order-disorder transition. Phys Rev 65:117
66. Padmanabhan T (1990) Statistical mechanics of gravitating systems. Phys Rep 188:285–362. doi:10.1016/0370-1573(90)90051-3
67. Paret J, Tabeling P (1997) Experimental observation of the two-dimensional inverse energy cascade. Phys Rev Lett 79:4162–4165
68. Penrose O, Lebowitz JL (1979) In: Montroll EW, Lebowitz JL (eds) Towards a rigorous molecular theory of metastability. Fluctuation phenomena, Chap. 5. North-Holland, Amsterdam, p 293
69. Potters M, Vaillant T, Bouchet F (2013) Sampling microcanonical measures of the 2D Euler equations through Creutz's algorithm: a phase transition from disorder to order when energy is increased. J Stat Mech P02017. doi:10.1088/1742-5468/2013/02/P02017
70. Pouquet A, Marino R (2013) Geophysical turbulence and the duality of the energy flow across scales. Phys Rev Lett 111:234,501. doi:10.1103/PhysRevLett.111.234501
71. Qi W, Marston JB (2014) Hyperviscosity and statistical equilibria of Euler turbulence on the torus and the sphere. J Stat Mech P07020. doi:10.1088/1742-5468/2014/07/P07020
72. Rhines PB (1979) Geostrophic turbulence. Annu Rev Fluid Mech 11:401–441
73. Robert R (1989) Concentration et entropie pour les mesures d'Young. C R Acad Sci Paris, Sér I 309:757
74. Robert R (1990) Etats d'équilibre statistique pour l'écoulement bidimensionnel d'un fluide parfait. C R Acad Sci Paris, Série I 311:575
75. Robert R (1991) A maximum-entropy principle for two-dimensional perfect fluid dynamics. J Stat Phys 65:531–553. doi:10.1007/BF01053743
76. Robert R (2000) On the statistical mechanics of 2D Euler equation. Commun Math Phys 212:245–256. doi:10.1007/s002200000210
77. Robert R, Sommeria J (1991) Statistical equilibrium states for two-dimensional flows. J Fluid Mech 229:291–310. doi:10.1017/S0022112091003038
78. Robert R, Sommeria J (1992) Relaxation towards a statistical equilibrium state in two-dimensional perfect fluid dynamics. Phys Rev Lett 69:2776–2779. doi:10.1103/PhysRevLett.69.2776
79. Rockafellar R (1970) Convex analysis. Princeton University Press, Princeton
80. Ruelle D (1969) Statistical mechanics: rigorous results. Benjamin, Amsterdam
81. Ruelle D (1989) Chaotic evolution and strange attractors. Lezioni Lincee, Accademia Nazionale dei Lincei
82. Rutgers MA (1998) Forced 2D turbulence: experimental evidence of simultaneous inverse energy and forward enstrophy cascades. Phys Rev Lett 81:2244–2247
83. Salmon R (1998) Lectures on geophysical fluid dynamics. Oxford University Press, New York
84. Serre D (1984) Les invariants du premier ordre de l'équation d'Euler en dimension trois. Physica D 13:105–136. doi:10.1016/0167-2789(84)90273-2
85. Smith LM, Yakhot V (1993) Bose condensation and small-scale structure generation in a random force driven 2D turbulence. Phys Rev Lett 71:352–355
86. Sommeria J (2001) Course 8: two-dimensional turbulence. In: Lesieur M, Yaglom A, David F (eds) New trends in turbulence, Les Houches theoretical physics summer school, Chap. 8. Springer
87. Tabeling P (2002) Two-dimensional turbulence: a physicist approach. Phys Rep 362:1–62
88. Thalabard S, Dubrulle B, Bouchet F (2014) Statistical mechanics of the 3D axisymmetric Euler equations in a Taylor-Couette geometry. J Stat Mech P01005
89. Touchette H (2009) The large deviation approach to statistical mechanics. Phys Rep 478:1–69. doi:10.1016/j.physrep.2009.05.002
90. Touchette H, Ellis RS, Turkington B (2004) An introduction to the thermodynamic and macrostate levels of nonequivalent ensembles. Physica A 340:138–146. doi:10.1016/j.physa.2004.03.088

91. Turkington B (1999) Statistical equilibrium measures and coherent states in two-dimensional turbulence. Comm Pure Appl Math 52:781–809. doi:10.1002/(SICI)1097-0312(199907)52:7<781:AID-CPA1>3.0.CO;2-C
92. Turkington B, Whitaker N (1996) Statistical equilibrium computations of coherent structures in turbulent shear layers. SIAM J Sci Comput 17:1414. doi:10.1137/S1064827593251708
93. Vallis GK (2006) Atmospheric and oceanic fluid dynamics: fundamentals and large-scale circulation. Cambridge University Press, Cambridge
94. Venaille A (2012) Bottom-trapped currents as statistical equilibrium states above topographic anomalies. J Fluid Mech 699:500. doi:10.1017/jfm.2012.146
95. Venaille A, Bouchet F (2011) Oceanic rings and jets as statistical equilibrium states. J Phys Oceanogr 41:1860. doi:10.1175/2011JPO4583.1
96. Venaille A, Vallis GK, Griffies SM (2012) The catalytic role of beta effect in barotropization processes. J Fluid Mech 709:490–515. doi:10.1017/jfm.2012.344

Recent Developments on the Micropolar and Magneto-Micropolar Fluid Systems: Deterministic and Stochastic Perspectives

Kazuo Yamazaki

Abstract We review recent developments on the micropolar and magneto-micropolar fluid systems in spatial dimensions two and three from both deterministic and stochastic perspectives. Under the deterministic setting, we review the global regularity result in two-dimensional space with zero angular viscosity and a regularity criterion in three-dimensional space that involves only two velocity vector field components. Under the stochastic setting, we review the existence of a weak martingale solution in three-dimensional space and the unique strong solution in two-dimensional space under a suitable condition on the noise. Throughout the paper, we compare these results with other partial differential equations related to fluid mechanics, such as the Navier-Stokes equations, magnetohydrodynamics and Boussinesq systems.

1 Introduction

We study the following micropolar fluid (MPF) system (1) and (2) as well as the magneto-micropolar fluid (MMPF) system (3)–(5) presented in a three-dimensional case:

$$\begin{aligned} &\frac{\mathrm{d}u}{\mathrm{d}t} + (u\cdot\nabla)u + \nabla\pi - (\mu+\chi)\Delta u \qquad (1)\\ &= \chi(\nabla\times w) + f_1(y,t) + g_1(y,t)\frac{\mathrm{d}W_1}{\mathrm{d}t},\\ &\delta\frac{\mathrm{d}w}{\mathrm{d}t} + \delta(u\cdot\nabla)w - \gamma\Delta w \qquad (2)\\ &= -2\chi w + (\alpha+\beta)\nabla\mathrm{div}w + \chi(\nabla\times u) + f_2(y,t) + g_2(y,t)\frac{\mathrm{d}W_2}{\mathrm{d}t}, \end{aligned}$$

K. Yamazaki (✉)
Department of Mathematics, Washington State University, Pullman, WA 99164-3113, USA
e-mail: kyamazaki@math.wsu.edu

S. Heinz and H. Bessaih (eds.), *Stochastic Equations for Complex Systems*,
Mathematical Engineering, DOI 10.1007/978-3-319-18206-3_4

$$\frac{\mathrm{d}u}{\mathrm{d}t} + (u\cdot\nabla)u - r(b\cdot\nabla)b + \nabla\pi - (\mu+\chi)\Delta u \tag{3}$$
$$= \chi(\nabla\times w) + \tilde{f}_1(\tilde{y},t) + \tilde{g}_1(\tilde{y},t)\frac{\mathrm{d}W_1}{\mathrm{d}t},$$
$$\delta\frac{\mathrm{d}w}{\mathrm{d}t} + \delta(u\cdot\nabla)w - \gamma\Delta w \tag{4}$$
$$= -2\chi w + (\alpha+\beta)\nabla\mathrm{div}w + \chi(\nabla\times u) + \tilde{f}_2(\tilde{y},t) + \tilde{g}_2(\tilde{y},t)\frac{\mathrm{d}W_2}{\mathrm{d}t},$$
$$\frac{\mathrm{d}b}{\mathrm{d}t} + (u\cdot\nabla)b - (b\cdot\nabla)u - \nu\Delta b = \tilde{f}_3(\tilde{y},t) + \tilde{g}_3(\tilde{y},t)\frac{\mathrm{d}W_3}{\mathrm{d}t} \tag{5}$$

subjected to the following divergence-free and initial conditions:

$$\nabla\cdot u = \nabla\cdot b = 0, \quad (u,w,b)(x,0) = (u_0,w_0,b_0)(x).$$

In the Eqs. (1)–(5) we denoted $y \triangleq (u,w)$, $\tilde{y} \triangleq (u,w,b)$, where u, w, b, π represent the velocity, micro-rotational velocity, the magnetic vector fields and the hydrostatic pressure scalar field respectively. Moreover, $W_i, i = 1,2,3$ are the Wiener processes in m_i-dimension respectively. We also denoted physically meaningful quantities: $r = \frac{\mathrm{M}^2}{\mathrm{ReRm}}$ where M is the Hartmann number, Re the Reynolds number, Rm the magnetic Reynolds number, χ the vortex viscosity, μ the kinematic viscosity, δ the microinertia, α, β, γ the angular viscosities, $\nu = \frac{1}{\mathrm{Rm}}$ all of which taking into account of conditions such as Calusius-Duhem inequality we assume to be positive unless specifically mentioned. Finally, the functions $f_i, g_i, \tilde{f}_i, \tilde{g}_i, i = 1,2,3$ are forcing terms.

Hereafter, for simplicity let us denote $\frac{\mathrm{d}}{\mathrm{d}t}$ by ∂_t and $\frac{\mathrm{d}}{\mathrm{d}x_i}$ by $\partial_i, i = 1,2,3$ and assume that $\delta = r = 1$. Let us use the notation $A \lesssim_{a,b} B$ to imply that there exists a non-negative constant c that depends on a, b such that $A \le cB$. We also write the Lebesgue and Sobolev spaces L^p, $W^{m,p}$, $H^m \triangleq W^{m,2}$ respectively and

$$\mathbb{L}^p \triangleq (L^p)^d, \quad \mathbb{W}^{m,p} \triangleq (W^{m,p})^d.$$

Both the MPF and the MMPF systems are generalizations of many other important partial differential equations (PDE) of fluid mechanics and hence analysis on these systems are of much interest to wide audience of mathematicians, engineers and physicists. Firstly, the MMPF system at $w \equiv b \equiv 0$ deduces the Navier-Stokes equations (NSE) which is well-known for its various applications in real world as well as the mathematically challenging problem whether given an initial data sufficiently smooth, its solution will remain smooth for all time or not. Moreover, the MMPF system at $\chi = 0, w \equiv 0$ reduces to the magnetohydrodynamics (MHD) system which describes the motion of electrically conducting fluids and has broad applications in applied sciences including astrophysics, geophysics and plasma physics. We also observe that the MMPF system (3)–(5) at $b \equiv 0$ reduces to the MPF system (1) and (2).

The micropolar fluids were formally introduced in [15] as the fluid consisting of bar-like elements, for example anisotropic fluids, such as liquid crystals made up of dumbbell molecules and animal blood. Subsequently, the MMPF system was introduced by the authors in [1] in which they studied Serrin-type stability. Both systems found much attraction for further investigation thereafter ([14, 28, 52] for the MPF system, [21, 30, 32, 51] for the MMPF system and the references found therein).

The rest of this manuscript is organized as follows. In the next section, we discuss new results in the deterministic case when $g_i, \tilde{g}_i \equiv 0$ in (1)–(5). Thereafter, we discuss new results in the stochastic case when $g_i, \tilde{g}_i$ are not necessarily identically zero. Finally, we finish with a brief conclusion.

2 Deterministic Case

2.1 Global Regularity of the 2D MMPF System with Zero Angular Viscosity

In this section, we specifically study the two-dimensional (2D) MMPF system with a spatial domain being $\mathbb{R}^2$ which takes the following form:

$$\partial_t u + (u \cdot \nabla)u - (b \cdot \nabla)b + \nabla\pi - (\mu + \chi)\Delta u = \chi(\nabla \times w), \tag{6}$$

$$\partial_t w + (u \cdot \nabla)w - \gamma\Delta w = -2\chi w + \chi(\nabla \times u), \tag{7}$$

$$\partial_t b + (u \cdot \nabla)b - (b \cdot \nabla)u - \nu\Delta b = 0. \tag{8}$$

The present form (6)–(8) is due to the fact that following the previous work (for example [14, 28]) on the 2D case, we set

$$u = (u_1, u_2, 0), \quad b = (b_1, b_2, 0), \quad w = (0, 0, w_3). \tag{9}$$

We remark that the results in this section remain valid after keeping $\tilde{f}_i, i = 1, 2, 3$ under a suitable condition. Let us set the following standard notations:

$$\Omega \triangleq \nabla \times u = \partial_1 u_2 - \partial_2 u_1, \quad j \triangleq \nabla \times b = \partial_1 b_2 - \partial_2 b_1, \quad \nabla \times w = (\partial_2 w, -\partial_1 w) \tag{10}$$

where $\nabla \times u, \nabla \times b$ represent the vorticity and current density respectively.

It is well known (for example [21, 28]) that by classical methods, the system (6)–(8) when $\mu, \chi, \gamma, \nu > 0$ admits a unique weak solution (u, w, b) globally in

time. This result may be understood as a generalization of analogous results for the 2D NSE and the 2D MHD system [34]. Let us present our result:

Theorem 1 *([46]) For every* $(u_0, w_0, b_0) \in \mathbb{H}^s(\mathbb{R}^2), s > 2$, *there exists a unique solution triple* (u, w, b) *to (6)–(8) with* $\gamma = 0$ *such that*

$$u, b \in C([0,\infty); \mathbb{H}^s(\mathbb{R}^2)) \cap L^2([0,\infty); \mathbb{H}^{s+1}(\mathbb{R}^2)), \quad w \in C([0,\infty); \mathbb{H}^s(\mathbb{R}^2)).$$

The proof of the local existence of the unique solution can be achieved in many ways, for example using mollifiers following the work on the NSE. Let us elaborate on the difficulty of extending such local existence to global as claimed in the statement of Theorem 1. Taking $\mathbb{L}^2$-inner products with (u, w, b) on (6)–(8) at $\gamma = 0$ respectively, using divergence-free property of u, b, summing and using the fact that

$$\int_{\mathbb{R}^2} (\nabla \times w) \cdot u \mathrm{d}x = \int_{\mathbb{R}^2} (\nabla \times u) w \mathrm{d}x$$

lead to

$$\begin{aligned} &\frac{1}{2}\partial_t(\|u\|_{\mathbb{L}^2}^2 + \|w\|_{\mathbb{L}^2}^2 + \|b\|_{\mathbb{L}^2}^2) + (\mu+\chi)\|\nabla u\|_{\mathbb{L}^2}^2 + 2\chi\|w\|_{\mathbb{L}^2}^2 + \nu\|\nabla b\|_{\mathbb{L}^2}^2 \\ &\quad \le 2\chi\|w\|_{\mathbb{L}^2}\|\nabla u\|_{\mathbb{L}^2} \le 2\chi\|w\|_{\mathbb{L}^2}^2 + \frac{\chi}{2}\|\nabla u\|_{\mathbb{L}^2}^2 \end{aligned} \tag{11}$$

where we used the H*ö*lder's and Young's inequalities. Therefore, after absorbing the right hand side, integrating in time we obtain

$$\sup_{t\in[0,T]} \left(\|u\|_{\mathbb{L}^2}^2 + \|w\|_{\mathbb{L}^2}^2 + \|b\|_{\mathbb{L}^2}^2\right)(t) + \int_0^T \|\nabla u\|_{\mathbb{L}^2}^2 + \|\nabla b\|_{\mathbb{L}^2}^2 \mathrm{d}\tau \lesssim_{u_0,w_0,b_0} 1. \tag{12}$$

We observe that the claim in Theorem 1 is reminiscent of the important result that although the 2D NSE is $\mathbb{L}^2$-norm critical, the 2D Euler equations, which is the NSE with $(\mu + \chi) = 0$, admits a global regularity result ([54]). The key observation in [54] was that taking a curl on the 2D Euler equations reduces the equations to a transport equation of vorticity Ω so that $\|\Omega\|_{\mathbb{L}^\infty}$ becomes bounded uniformly in time which is more helpful than $\|u\|_{\mathbb{L}^2}$-bound in the process of *a priori* estimates. Experimenting this idea and taking a curl on (6) gives

$$\partial_t \Omega - (\mu+\chi)\Delta\Omega = -(u\cdot\nabla)\Omega + (b\cdot\nabla)j - \chi\Delta w. \tag{13}$$

Due to the lack of angular viscosity, we have no obvious way to handle $-\chi\Delta w$. An immediate idea is to couple this estimate with that of w in regularity high enough to absorb $-\chi\Delta w$. However, taking $\mathbb{L}^2$-inner products on (7) at $\gamma = 0$ with $-\Delta w$ leads to

$$\frac{1}{2}\partial_t\|\nabla w\|_{\mathbb{L}^2}^2 \leq \int_{\mathbb{R}^2} \nabla u \cdot \nabla w \cdot \nabla w \mathrm{d}x - \chi \int_{\mathbb{R}^2} (\nabla \times u)\Delta w \mathrm{d}x \tag{14}$$

for which it is not clear at all how to handle the first non-linear term without angular viscosity. In fact, we can take Hölder's and Gagliardo-Nirenberg inequalities to obtain

$$\int_{\mathbb{R}^2} \nabla u \cdot \nabla w \cdot \nabla w \mathrm{d}x \leq \|\nabla u\|_{\mathbb{L}^2}\|\nabla w\|_{\mathbb{L}^4}^2 \lesssim \|\Omega\|_{\mathbb{L}^2}\|\nabla w\|_{\mathbb{L}^2}\|\Delta w\|_{\mathbb{L}^2}$$

so that clearly in the presence of the angular viscosity, this estimate may be closed to lead to the global regularity result. Therefore, the lack of angular viscosity seems to create a major obstacle in attaining the necessary *a priori* estimates.

Remark 1 We point out here the distinctive difference between the MPF or the MMPF system and the Boussinesq system which may be written with same notations as (6) and (7) as follows:

$$\partial_t u + (u \cdot \nabla)u + \nabla\pi - (\mu + \chi)\Delta u = \chi w_2, \tag{15}$$

$$\partial_t w + (u \cdot \nabla)w - \gamma\Delta w = 0. \tag{16}$$

The crucial fact here is that χw_2 in (15) is less singular than $\chi(\nabla \times w)$ of (6) and the current issue of $-\chi\Delta w$ in (13) being too singular would be much less severe in the case of the Boussinesq system. As we will discuss in subsequent sections our results in the stochastic case, we believe that this difference may bring interesting challenges in mathematical analysis so that even though the stochastic Boussinesq system has been studied intensively (for example [16]), perhaps not all the results known for the stochastic Boussinesq system may be readily generalized to the stochastic MPF or the MMPF system. At least in the deterministic case, there are many results that exist for the Boussinesq system (for example [22]) that do not seem to be easily generalized to the MPF system. Similarly, many results that are known to exist for the deterministic MHD system may not be readily generalized to the MMPF system due to same issue.

The first important idea in the proof of Theorem 1 is the following observation from [14] that by defining

$$Z \triangleq \Omega - \left(\frac{\chi}{\mu + \chi}\right) w, \tag{17}$$

we can take advantage of its evolution in time governed by the equation of

$$\partial_t Z = (\mu + \chi)\Delta Z - (u \cdot \nabla)Z - c_1 Z + c_2 w + (b \cdot \nabla) j \tag{18}$$

where we denoted

$$c_1 \triangleq \frac{\chi^2}{\mu+\chi} \geq 0, \quad c_2 \triangleq \frac{2\chi^2}{\mu+\chi} - \frac{\chi^3}{(\mu+\chi)^2}.$$

Multiplying (18) by $|Z|^{p-2}Z$, integrating in space, using the divergence-free property of u and Hölder's inequality and dividing by $\|Z\|_{\mathbb{L}^p}^{p-1}$, we obtain taking limit $p \to \infty$,

$$\partial_t \|Z\|_{\mathbb{L}^\infty} \lesssim \|w\|_{\mathbb{L}^\infty} + \|b\|_{\mathbb{L}^\infty} \|\nabla j\|_{\mathbb{L}^\infty}. \tag{19}$$

On the other hand, from (7) with $\gamma = 0$ we can estimate similarly

$$\frac{1}{p}\partial_t \|w\|_{\mathbb{L}^p}^p + 2\chi \|w\|_{\mathbb{L}^p}^p \leq \chi \|\Omega\|_{\mathbb{L}^p} \|w\|_{\mathbb{L}^p}^{p-1} \lesssim \|Z\|_{\mathbb{L}^p} \|w\|_{\mathbb{L}^p}^{p-1} + \|w\|_{\mathbb{L}^p}^p$$

due to the divergence-free property of u, Hölder's inequality and (17). Dividing by $\|w\|_{\mathbb{L}^p}^{p-1}$ and taking limit $p \to \infty$ lead to

$$\partial_t \|w\|_{\mathbb{L}^\infty} \lesssim \|Z\|_{\mathbb{L}^\infty} + \|w\|_{\mathbb{L}^\infty} \tag{20}$$

so that in sum of (19) and (20), we obtain

$$\partial_t (\|Z\|_{\mathbb{L}^\infty} + \|w\|_{\mathbb{L}^\infty}) \lesssim \|Z\|_{\mathbb{L}^\infty} + \|w\|_{\mathbb{L}^\infty} + \|b\|_{\mathbb{L}^\infty} \|\nabla j\|_{\mathbb{L}^\infty}.$$

This inequality is very similar to the key observation for the 2D generalized MHD system that led to many new results very recently (for example [8, 24, 38, 41, 42, 50, 53] and references found therein). Indeed, we may execute an iteration scheme in a way that a certain bound of j will lead to a bound of Z, which in turn leads to the bound of w and then Ω until its regularity is high enough so that via a commutator estimate using Besov space techniques, the proof of Theorem 1 can be completed.

In more detail, using (12) and taking advantage of (18), we can obtain the following bound:

$$\sup_{t\in[0,T]} (\|Z\|_{\mathbb{L}^2}^2 + \|\Omega\|_{\mathbb{L}^2}^2 + \|j\|_{\mathbb{L}^2}^2)(t) + \int_0^T \|\nabla Z\|_{\mathbb{L}^2}^2 + \|\nabla j\|_{\mathbb{L}^2}^2 d\tau \lesssim 1 \tag{21}$$

(see Proposition 3 in [46]). We can improve the bounds uniform in time furthermore; specifically $\forall \quad q \in [2, 4]$, we can obtain the following bound:

$$\sup_{t\in[0,T]} (\|Z\|_{\mathbb{L}^q} + \|\Omega\|_{\mathbb{L}^q} + \|j\|_{\mathbb{L}^q})(t) \lesssim 1 \tag{22}$$

(see Proposition 4 in [46]). Using (12), (21) and (22) we can propel the bounds up to

$$\int_0^T \|\Omega\|_{\mathbb{L}^\infty} + \|w\|_{\mathbb{L}^\infty}^2 + \|\nabla j\|_{\mathbb{L}^2} d\tau \lesssim 1. \tag{23}$$

Due to the classical results from [3], one can understand that we have a sufficient bound in terms of u from $\|\Omega\|_{\mathbb{L}^\infty}$ in (23). Moreover, due to the following Brezis-Wainger type inequality

$$\|\nabla f\|_{\mathbb{L}^\infty} \lesssim \|f\|_{\mathbb{L}^2} + \|\nabla f\|_{\mathbb{H}^1} \log_2(2 + \|f\|_{\mathbb{H}^s}) + 1$$

valid $\forall \quad f \in \mathbb{L}^2(\mathbb{R}^2) \cap \mathbb{H}^s(\mathbb{R}^2), s > 2$ (see [6, 48] for the proof of this specific inequality), we see that we have a sufficient bound in terms of b from $\|\nabla j\|_{\mathbb{L}^2}$ in (23). However, as (23) does not provide any bound on the derivative of w, it is not clear whether (23) is sufficient to imply the higher regularity of $\mathbb{H}^s, s > 2$.

The second part of the proof of Theorem 1 is to show that (23) is indeed sufficient to complete the proof of Theorem 1. In order to explain, let us briefly recall some Besov spaces settings below all of which can be found for example in [10].

We denote by $\mathcal{S}(\mathbb{R}^2)$ the Schwartz class functions, $\mathcal{S}'(\mathbb{R}^2)$ its dual and

$$\mathcal{S}_0 \triangleq \{\phi \in \mathcal{S}, \int_{\mathbb{R}^2} \phi(x) x^l dx = 0, |l| = 0, 1, 2, ...\}.$$

Its dual $\mathcal{S}_0'$ is given by $\mathcal{S}_0' = \mathcal{S}/\mathcal{S}_0^\perp = \mathcal{S}'/\mathcal{P}$ where $\mathcal{P}$ is the space of polynomials. For $k \in \mathbb{Z}$ we define

$$A_k \triangleq \{\xi \in \mathbb{R}^2 : 2^{k-1} < |\xi| < 2^{k+1}\}.$$

It is well-known that there exists a sequence $\{\Phi_k\}$ in $\mathcal{S}(\mathbb{R}^2)$ such that

$$\text{supp } \hat{\Phi}_k \subset A_k, \quad \hat{\Phi}_k(\xi) = \hat{\Phi}_0(2^{-k}\xi) \quad \text{or} \quad \Phi_k(x) = 2^{2k}\Phi_0(2^k x) \quad \text{and}$$

$$\sum_{k=-\infty}^{\infty} \hat{\Phi}_k(\xi) = \begin{cases} 1 & \text{if} \quad \xi \in \mathbb{R}^2 \setminus \{0\}, \\ 0 & \text{if} \quad \xi = 0 \end{cases}$$

where we denote the Fourier transform of f by $\hat{f}$. Consequently, for any $f \in \mathcal{S}_0'$,

$$\sum_{k=-\infty}^{\infty} \Phi_k * f = f.$$

We can let $\Psi \in C_0^\infty(\mathbb{R}^2)$ be such that

$$1 = \hat{\Psi}(\xi) + \sum_{k=0}^{\infty} \hat{\Phi}_k(\xi), \quad f = \Psi * f + \sum_{k=0}^{\infty} \Phi_k * f,$$

for any $f \in \mathcal{S}'$ and set

$$\Delta_k f \triangleq \begin{cases} 0 & \text{if } k \leq -2, \\ \Psi * f & \text{if } k = -1, \\ \Phi_k * f & \text{if } k = 0, 1, 2, ... \end{cases}$$

The following Bernstein's inequalities have proven to be one of the most useful tools in obtaining needed estimates in Besov space settings:

Lemma 1 *Let $f \in \mathbb{L}^p(\mathbb{R}^2)$ with $1 \leq p \leq q \leq \infty$ and $0 < r < R$. Then for all $s \in \mathbb{Z}^+ \cup \{0\}$, and $\lambda > 0$, there exists a constant $C_s \geq 0$ such that*

$$\sup_{|k|=s} \|\partial^k f\|_{\mathbb{L}^q} \leq C_s \lambda^{s+2(\frac{1}{p}-\frac{1}{q})} \|f\|_{\mathbb{L}^p} \qquad \text{if supp } \hat{f} \subset \{\xi : |\xi| \leq \lambda r\},$$

$$C_s^{-1} \lambda^s \|f\|_{\mathbb{L}^p} \leq sup_{|k|=s} \|\partial^k f\|_{\mathbb{L}^p} \leq C_s \lambda^s \|f\|_{\mathbb{L}^p} \quad \text{if supp } \hat{f} \subset \{\xi : \lambda r \leq |\xi| \leq \lambda R\},$$

and if we replace derivative ∂^k by the fractional derivative, the inequalities remain valid only with trivial modifications.

We also recall the Bony's paraproduct decomposition:

$$fg = T_f g + T_g f + R(f, g)$$

where

$$T_f g = \sum_k S_{k-1} f \Delta_k g, \quad R(f, g) = \sum_{k,k':|k-k'|\leq 1} \Delta_k f \Delta_{k'} g, \quad S_{k-1} = \sum_{m:m\leq k-2} \Delta_m.$$

We refer to [10] for more details on Besov spaces. Now in [14, 46], the following commutator estimates were proved:

Lemma 2 *Let $s > -1$, $f \in \mathbb{H}^s(\mathbb{R}^2) \cap \mathbb{L}^\infty(\mathbb{R}^2)$, $\nabla g \in \mathbb{H}^s(\mathbb{R}^2) \cap \mathbb{L}^\infty(\mathbb{R}^2)$, $\nabla \cdot g = 0$. Then for any $k \geq 3$,*

$$\|[\Delta_k, g^i \partial_i] f\|_{\mathbb{L}^2} \lesssim c_k 2^{-ks} (\|\nabla g\|_{\mathbb{L}^\infty} \|f\|_{\mathbb{H}^s} + \|\nabla g\|_{\mathbb{H}^s} \|f\|_{\mathbb{L}^\infty}).$$

Moreover, for $s > 0$ if additionally $\nabla f \in \mathbb{L}^\infty(\mathbb{R}^2)$, then for any $k \geq -1$,

$$\|[\Delta_k, g^i \partial_i] f\|_{\mathbb{L}^2} \lesssim c_k 2^{-ks} (\|\nabla g\|_{\mathbb{L}^\infty} \|f\|_{\mathbb{H}^s} + \|g\|_{\mathbb{H}^s} \|\nabla f\|_{\mathbb{L}^\infty})$$

where $\{c_k\} \in l^2_{k\geq -1}$.

We just mention that the proof of Lemma 2 makes use of Bernstein's inequalities in Lemma 1 and Bony's paraproduct decomposition and refer to [14, 46] for details.

Using Lemma 2, one can show that indeed (23) is sufficient to reach the higher regularity of $\mathbb{H}^s, s > 2$ (see Proposition 2 [46]). We omit further details and refer to [46].

2.2 Regularity Criterion of the 3D MMPF System in Terms of Two Velocity Components

In this section, we specifically study the three-dimensional (3D) MMPF system with a spatial domain being $\mathbb{R}^3$, although generalization to $\mathbb{T}^3$ is possible. It takes the following form:

$$\partial_t u + (u \cdot \nabla)u - (b \cdot \nabla)b + \nabla\pi - (\mu + \chi)\Delta u = \chi(\nabla \times w), \tag{24}$$

$$\partial_t w + (u \cdot \nabla)w - \gamma\Delta w = -2\chi w + (\alpha + \beta)\nabla \mathrm{div} w + \chi(\nabla \times u), \tag{25}$$

$$\partial_t b + (u \cdot \nabla)b - (b \cdot \nabla)u - \nu\Delta b = 0. \tag{26}$$

In [30, 32], the authors obtained the local existence of the unique weak solution and extended to be global under small initial data conditions. The global regularity issue of the system (24)–(26) is expected to be extremely difficult because its special case, as we discussed, is the NSE.

In the absence of global regularity results, an important direction of research is extension and improvements of conditions for regularity initiated by the pioneering work in [35]:

Theorem 2 *([35]) If u is a weak solution to the 3D NSE in $[0, T]$ and*

$$\int_0^T \|u\|_{\mathbb{L}^p}^r \mathrm{d}\tau < \infty, \quad \frac{3}{p} + \frac{2}{r} < 1, \quad p \in (3, \infty],$$

then u is smooth.

Remark 2 We remark here that as we will discuss more in subsequent sections, there is also an increasing interest in the uniqueness of a solution to the stochastic partial differential equations (SPDE), such as the stochastic NSE (for example [17]).

Moreover, in the deterministic case the result concerning the partial regularity theory for the NSE by the authors in [7] is well-known and an analogous study for the stochastic NSE with additive noise has been initiated by the authors in [20].

For a system which consists of a solution (u, w, b) as (24)–(26), it is typically expected that a certain bound on all u, w, b are required for the local strong solution to be extended globally in time. However, the author in [51] was able to show that the following condition on the velocity vector field u alone suffices:

$$\int_0^T \|u\|_{\mathbb{L}^p}^r \mathrm{d}\tau < \infty, \quad \frac{3}{p} + \frac{2}{r} \leq 1, \quad 3 < p \leq \infty \tag{27}$$

(see also [52] for the MPF system). We remark that the condition described in (27) imposes a certain bound on all three components u_1, u_2, u_3 of $u = (u_1, u_2, u_3)$. Let us present our result:

Theorem 3 *([45]) Let $u_0, w_0, b_0 \in \mathbb{H}^s(\mathbb{R}^3)$, $s \geq 3$. Suppose*

$$u, w, b \in C([0, T); \mathbb{H}^s(\mathbb{R}^3)) \cap L^2([0, T); \mathbb{H}^{s+1}(\mathbb{R}^3)), \tag{28}$$

is a solution to the MMPF system (24)–(26) and there exists a constant $C_0 \geq 0$ so that

$$\sum_{l=2}^{3} \int_0^T \|u_l\|_{\mathbb{L}^{p_l}}^{r_l} \mathrm{d}\tau \leq C_0, \quad \frac{3}{p_l} + \frac{2}{r_l} \leq \frac{1}{2}, \quad 6 < p_l \leq \infty. \tag{29}$$

Then (u, w, b) remains in the same regularity class of (28) on $[0, T']$ for some $T' > T$.

Remark 3

1. Let us emphasize that (29) imposes no condition on u_1 at all. Moreover, we note that the Theorem 3 also gives a new result for the MPF system because the MMPF system at $b \equiv 0$ reduces to the MPF system.
2. The proof of Theorem 3 is inspired by similar component reduction results on the regularity criterion for the solution to the NSE, for example [26]. However, the proof in [26] depends crucially on the divergence-free property of u of the NSE while w in (24)–(26) lacks this advantage.
3. It is an interesting open problem whether we can reduce this regularity criterion presented in (29) to one component, for example u_3. In fact, even though such a result is well-known for the NSE (for example [26]), it remains open even for the MHD system (see [43, 45]). It is also a research direction of great importance whether the upper bound of $\frac{1}{2}$ in (29) may be improved up to 1 as in (27).

The proof of Theorem 3 consists of two key steps. Firstly, the standard commutator estimates show that the $\mathbb{H}^1$-bounds of (u, w, b) imply higher regularity for the solution to the system (24)–(26). Upon the $\mathbb{H}^1$-estimates of (u, w, b) which starts by taking $\mathbb{L}^2$-inner products on (24)–(26) with $(-\Delta u, -\Delta w, -\Delta b)$ respectively, the following decomposition of the non-linear terms in (24) and (26) were crucial:

Lemma 3 *([45]) Suppose $u, b \in C^\infty(\mathbb{R}^3)$, $\nabla \cdot u = \nabla \cdot b = 0$. Then*

$$\begin{aligned} &\int_{\mathbb{R}^3} (u \cdot \nabla)u \cdot \Delta u - (b \cdot \nabla)b \cdot \Delta u + (u \cdot \nabla)b \cdot \Delta b - (b \cdot \nabla)u \cdot \Delta b \mathrm{d}x \\ &\lesssim \sum_{l=2}^{3} \int_{\mathbb{R}^3} |u_l|(|\nabla u||\nabla^2 u| + |\nabla b||\nabla^2 b|) + |b_l|(|\nabla u||\nabla^2 b| + |\nabla b||\nabla^2 u|)\mathrm{d}x \end{aligned} \tag{30}$$

(see also [43, 44]). With this decomposition, we may manipulate our estimates to shift the sufficient condition for regularity to u_2, u_3, b_2, b_3. The second key step in the proof of Theorem 2 is the following estimate:

Lemma 4 *([45]) Let (u, b) satisfy (24) and (26) in $[0, T]$ and $l \in \{1, 2, 3\}$. Then for any $t \in [0, T]$, $p \in (2, 6]$,*

$$\sup_{\tau\in[0,t]} \|b_l(\tau)\|^2_{\mathbb{L}^p} \leq \|b_l(0)\|^2_{\mathbb{L}^p} + c(p) \int_0^t \|\nabla b(\tau)\|^2_{\mathbb{L}^2} \|u_l(\tau)\|^2_{\mathbb{L}^{\frac{6p}{6-p}}} \mathrm{d}\tau \tag{31}$$

where $\frac{6p}{6-p} = \infty$ if $p = 6$

(see also [43, 44, 55]).

The message of this lemma is that one can estimate the lth component of b in terms of the same lth component of u. The proof of Lemma 4 relies on the simplicity of the equation that governs the evolution of b_l in time according to (26), namely

$$\partial_t b_l - \nu \Delta b_l = -(u \cdot \nabla) b_l + (b \cdot \nabla) u_l$$

so that upon any $\mathbb{L}^p$-estimate of b_l, the first non-linear term vanishes due to the divergence-free property of u while in the second non-linear term, u_l is already *separated*.

With these two lemmas in hand, the rest of the proof consists of careful energy estimates using anisotropic Sobolev inequalities. We refer interested readers to [45] for details.

3 Stochastic Case

3.1 Existence of Weak Martingale Solution for the 3D MPF and the MMPF Systems with Non-Lipschitz Multiplicative Noise

In this section, we study the 3D MPF system (1) and (2) and the MMPF systems (3)–(5) fully. We first remark that in case $g_i, \tilde{g}_i, i = 1, 2, 3$ do not depend on the solution y, $\tilde{y}$ respectively so that the noise is only additive rather than multiplicative, these SPDE may be solved in a way that is very similar to the deterministic case. Indeed, the author in [18] considered the stochastic NSE (see [12] in the case of the stochastic Burgers equations)

$$\mathrm{d}u(t) + [(u \cdot \nabla)u(t) + \nabla\pi(t) - (\mu + \chi)\Delta u(t)]\mathrm{d}t = f_1(t)\mathrm{d}t + g_1(t)\mathrm{d}W_1(t) \tag{32}$$

where we emphasize in particular that g_1 is independent of u. A remarkable strategy to tackle this SPDE with such an additive noise is to consider the following auxiliary Ornstein-Uhlenbeck equation

$$\mathrm{d}z_\delta(t) - [(\mu + \chi)\Delta z_\delta(t) - \delta z_\delta(t)]\mathrm{d}t = g_1(t)\mathrm{d}W_1(t), \quad \delta \in \mathbb{R}^+ \tag{33}$$

for which the solution is well understood due to the lack of nonlinearity (see [11]). Hence, one can study the equation of the difference $u - z_\delta$ for which the noise term cancels and therefore the techniques from deterministic case becomes applicable.

We mention that for the Boussinesq system (15) and (16), the authors in [9, 23] independently showed that the system admits a globally regular unique solution pair (u, w) even in cases $\mu+\chi > 0, \gamma = 0$ and $\mu+\chi = 0, \chi > 0, \gamma > 0$. Considering an appropriate Ornstein-Uhlenbeck equation and canceling the noise term, the authors in [5] extended such results to the stochastic Boussinesq system with additive noise. The stochastic MHD system with additive noise is also considered by the authors in [2, 37].

In case $g_i, \tilde{g}_i, i = 1, 2, 3$ depend on the solution $y, \tilde{y}$ respectively, the noise must be handled with more care. Let us consider the following non-slip boundary and perfectly conducting wall conditions with nonrandom initial data on the boundary of some bounded domain $D \subset \mathbb{R}^3$:

$$\begin{cases} u|_{\partial D}(t) = w|_{\partial D}(t) = 0, & \forall \quad t \in [0, T], \\ b \cdot n|_{\partial D} = 0, & \forall \quad t \in [0, T], \\ (\nabla \times b) \times n|_{\partial D} = 0, & \forall \quad t \in [0, T] \end{cases} \tag{34}$$

where n is an outward unit normal vector on ∂D. For the case of the domain being $\mathbb{R}^3$, we refer to for example [29] where the author studied the stochastic NSE in the whole space.

Let us explain further notations and define the weak martingale solution to the MPF system (1) and (2) and the MMPF system (3)–(5). We write $H_0^m = \mathrm{Ker}(\gamma_0)$ where $\gamma_0 : H^m(D) \mapsto L^2(\partial D)$ is the bounded trace operator that agrees with $v \mapsto v|_{\partial D}$ for $v \in C^1(\overline{D})$ and denote $\mathbb{H}_0^m \triangleq (H_0^m(D))^d$.

Given any separable Banach space E, we denote by $\mathcal{B}(E)$ the Borel σ-algebra on E and $L_T^p(E), 1 \le p \le \infty$ the space of functions endowed with a norm

$$\|v\|_{L_T^p(E)} \triangleq \left(\int_0^T \|v\|_E^p \mathrm{d}\tau \right)^{\frac{1}{p}}, \quad 1 \le p < \infty,$$

with a standard generalization at $p = \infty$. We further denote by

$$\begin{aligned} \mathcal{V}_1 &\triangleq \{v \in (C_c^\infty)^3 : \nabla \cdot v = 0\}, \\ V_1 &\triangleq \{v \in \mathbb{H}_0^1 : \nabla \cdot v = 0\}, \\ \mathcal{V}_2 &\triangleq \{v \in (C^\infty(\overline{D}))^3 : \nabla \cdot v = 0, v \cdot n|_{\partial D} = 0\}, \end{aligned}$$

$$V_2 \triangleq \{v \in \mathbb{H}^1 : \nabla \cdot v = 0, \quad v \cdot n|_{\partial D} = 0\},$$
$$H_1 = H_2 \triangleq \{v \in \mathbb{L}^2 : \nabla \cdot v = 0, \quad v \cdot n|_{\partial D} = 0\}.$$

We endow V_1 with the inner product

$$((u, v))_1 \triangleq \sum_{i=1}^{3} (\partial_i u, \partial_i v) \text{ where } (u, v) \triangleq \sum_{i=1}^{3} \int_D u_i(x) v_i(x) \mathrm{d}x,$$

and V_2 with the inner product

$$((u, v))_2 \triangleq (\nabla \times u, \nabla \times v).$$

We let

$$V \triangleq V_1 \times \mathbb{H}_0^1 \times V_2$$

endowed with its norm for $\Phi^i \triangleq (X^i, Y^i, Z^i) \in V, i = 1, 2,$

$$((\Phi^1, \Phi^2)) \triangleq ((X^1, X^2))_1 + ((Y^1, Y^2))_1 + ((Z^1, Z^2))_2, \quad ((\Phi^i, \Phi^i)) \triangleq \|\Phi^i\|^2.$$

In case $Z^i \equiv 0$ as in the solution for the stochastic MPF system (1) and (2), we have $((\Phi^1, \Phi^2)) \triangleq ((X^1, X^2))_1 + ((Y^1, Y^2))_1$. We also let

$$H \triangleq H_1 \times \mathbb{L}^2 \times H_2$$

endowed with its norm

$$(\Phi^1, \Phi^2) \triangleq (X^1, X^2) + (Y^1, Y^2) + (Z^1, Z^2), \quad (\Phi^i, \Phi^i) \triangleq |\Phi^i|^2,$$

for which if $Z^i \equiv 0$ as in the solution for the stochastic MPF system (1) and (2), we have $(\Phi^1, \Phi^2) = (X^1, X^2) + (Y^1, Y^2)$. We introduce the space $L^p(\Omega, \mathcal{F}, P; L^r(0, T; \mathbb{L}^s))$ endowed with a norm

$$\|u\|_{L^p(\Omega,\mathcal{F},P;L^r(0,T;\mathbb{L}^s))} \triangleq \left(E\|u(\omega, \cdot, \cdot)\|^p_{L^r(0,T;\mathbb{L}^s)}\right)^{\frac{1}{p}}.$$

We define three operators A_1, A_2, A_3 with their domains respectively by

$$< A_1 X^1, X^2 > \triangleq -(\mu + \chi)(\Delta X^1, X^2),$$
$$< A_2 Y^1, Y^2 > \triangleq < -\gamma \Delta Y^1 - (\alpha + \beta)\nabla \mathrm{div} Y^1 + 2\chi Y^1, Y^2 >,$$
$$< A_3 Z^1, Z^2 > \triangleq -\nu < \Delta Z^1, Z^2 >,$$

$$D(A_1) = \mathbb{H}^2 \cap V_1,$$
$$D(A_2) = \mathbb{H}^2 \cap \mathbb{H}_0^1,$$
$$D(A_3) = H_1 \cap \left\{ b \in \mathbb{H}^2 : (\nabla \times b) \cdot n|_{\partial D} = 0 \right\}.$$

Finally, we let

$$< A\Phi^1, \Phi^2 > \triangleq < A_1 X^1, X^2 > + < A_2 Y^1, Y^2 > + < A_3 Z^1, Z^2 > .$$

In case $b \equiv 0$ as in the solution for the stochastic MPF system (1) and (2), we have $< A\Phi^1, \Phi^2 > \triangleq < A_1 X^1, X^2 > + < A_2 Y^1, Y^2 >$.

Next, we define $B(\tilde{y}) \triangleq (B_1(\tilde{y}), B_2(\tilde{y}), B_3(\tilde{y}))$ with $\tilde{y} = (u, w, b)$ where

$$B_1(\tilde{y}) \triangleq (u \cdot \nabla)u - (b \cdot \nabla)b - \chi \nabla \times w,$$
$$B_2(\tilde{y}) \triangleq (u \cdot \nabla)w - \chi \nabla \times u, \quad B_3(\tilde{y}) \triangleq (u \cdot \nabla)b - (b \cdot \nabla)u,$$

and thus with $y = (u, w, 0)$ for the MPF system (1) and (2), $B(y) \triangleq (B_1(y), B_2(y), B_3(y))$ where

$$B_1(y) = (u \cdot \nabla)u - \chi \nabla \times w, \quad B_2(y) = (u \cdot \nabla)w - \chi \nabla \times u, \quad B_3(y) = 0.$$

We note the following property for $\tilde{y} = (u, w, b)$ obtained similarly to the computations in (11) and (12):

$$\begin{aligned} &< A\tilde{y}, \tilde{y} > + < B(\tilde{y}), \tilde{y} > \\ &\geq \mu \|\nabla u\|_{\mathbb{L}^2}^2 + \gamma \|\nabla w\|_{\mathbb{L}^2}^2 + (\alpha + \beta)\|\mathrm{div} w\|_{\mathbb{L}^2}^2 + \chi \|w\|_{\mathbb{L}^2}^2 + \nu \|\nabla b\|_{\mathbb{L}^2}^2 \geq \tilde{c}\|y\|^2 \end{aligned} \tag{35}$$

for some constant $\tilde{c} \triangleq c(\mu, \gamma, \alpha, \beta, \chi, \nu) > 0$.

Finally, we let

$$f \triangleq \begin{pmatrix} f_1 \\ f_2 \end{pmatrix}, \quad g \triangleq \begin{pmatrix} g_1 & 0 \\ 0 & g_2 \end{pmatrix}, \quad W \triangleq \begin{pmatrix} W_1 \\ W_2 \end{pmatrix},$$

$$\tilde{f} \triangleq \begin{pmatrix} \tilde{f}_1 \\ \tilde{f}_2 \\ \tilde{f}_3 \end{pmatrix}, \quad \tilde{g} \triangleq \begin{pmatrix} \tilde{g}_1 & 0 & 0 \\ 0 & \tilde{g}_2 & 0 \\ 0 & 0 & \tilde{g}_3 \end{pmatrix}, \quad \tilde{W} \triangleq \begin{pmatrix} W_1 \\ W_2 \\ W_3 \end{pmatrix}.$$

We now state the definition of a weak martingale solution and our theorem only on the MPF system for simplicity:

Definition 1 A weak martingale solution to (1) and (2) is a system $(\Omega, \mathcal{F}, \mathcal{F}_t, P, W, y)$ where

1. $(\Omega, \mathcal{F}, \mathcal{F}_t, P)$ is a filtered probability space,
2. $W(t)$ is $(m_1 + m_2)$-dimensional $\mathcal{F}_t$ measurable standard Wiener processes,

3. $y \in L^p(\Omega, \mathcal{F}, P; L^2(0,T; V_1 \times \mathbb{H}_0^1)) \cap L^p(\Omega, \mathcal{F}, P; L^\infty(0,T; H_1 \times \mathbb{L}^2)) \quad \forall$ $p \in [1, \infty)$,
4. for almost every t, $y(t)$ is $\mathcal{F}_t$-measurable,
5. for any $v \in D(A)$, almost surely $\forall \quad t \in [0,T]$

$$(y(t), v) + \int_0^t < Ay(\tau) + B(y(\tau)), v > \mathrm{d}\tau \tag{36}$$
$$= (y_0, v) + \int_0^t < f(y(\tau), \tau), v > \mathrm{d}\tau + \int_0^t (g(y(\tau), \tau) dW(\tau), v).$$

Theorem 4 *([47]) Suppose $y_0 \triangleq y(0) \in H_1 \times \mathbb{L}^2$ and $f_i, g_i, i = 1, 2$ are nonlinear mappings that are continuous in t, f continuous from $H_1 \times \mathbb{L}^2$ to $\mathbb{H}^{-1} \times \mathbb{H}^{-1}$, g_1, g_2 continuous from H_1 to $H_1^{\times m_1}$ and $\mathbb{L}^2$ to $(\mathbb{L}^2)^{\times m_2}$ respectively and*

$$\|f_1(y,t)\|_{\mathbb{H}^{-1}} \lesssim 1 + \|u\|_{H_1}, \quad \|f_2(y,t)\|_{\mathbb{H}^{-1}} \lesssim 1 + \|w\|_{\mathbb{L}^2},$$
$$\|g_1(y,t)\|_{H_1^{\times m_1}} \lesssim 1 + \|u\|_{H_1}, \quad \|g_2(y,t)\|_{(\mathbb{L}^2)^{\times m_2}} \lesssim 1 + \|w\|_{\mathbb{L}^2},$$

where $\times m_i$ denotes direct product m_i times. Then there exists a solution to (1) and (2) as in Definition 1. Moreover, there exists a unique $\pi \in L^1(\Omega, \mathcal{F}, P; W^{-1,\infty}(0,T; L^2(D)))$ such that $\int_D \pi \mathrm{d}x = 0$ in $(C_c^\infty([0,T]))'$ and (1) and (2) holds in $((C_c^\infty([0,T] \times D))')^3$.

The key ingredients in this type of proof consists of *a priori* estimates on approximating sequence using stochastic calculus such as Burkholder-Davis-Gundy inequality and applications of Prokhorov's and Skorokhod's theorems as initiated by the author in [4] for the stochastic NSE (see [33] for the case of the stochastic MHD system, [13] for the stochastic MHD-α model).

Lemma 5 *([31]) A family of probability measures on E is relatively compact if and only if it is tight.*

Lemma 6 *([36]) For arbitrary sequence of probability measures $\{P_n\}_n$ on $(E, \mathcal{B}(E))$ weakly convergent to a probability measure P, there exists a probability space $(\Omega, \mathcal{F}, P)$ and random variables $\xi, \xi_1, \ldots, \xi_n, \ldots$ with values in E such that*

1. *the probability law of ξ_n, $\mathcal{L}(\xi_n)(A) \triangleq P(\omega \in \Omega : \xi_n(\omega) \in A\} \quad \forall \quad A \in \mathcal{F}$ is P_n,*
2. *the probability law of ξ is P,*
3. *$\lim_{n\to\infty} \xi_n = \xi \quad P-$ almost surely.*

The existence of the pressure term is proven by a careful application of the following generalization of de Rham's Theorem to processes:

Lemma 7 *([27]) Let D be a bounded, connected, Lipschitz open subset of $\mathbb{R}^d$, $d = 2, 3, 4$ and $(\Omega, \mathcal{F}, P)$ a complete probability space and given $r_0, r_1 \in [1, \infty]$, $s_1 \in \mathbb{Z}$, $h \in L^{r_0}(\Omega, \mathcal{F}, P; W^{s_1,r_1}(0,T; (\mathbb{H}^{-1}(D))^d))$ be such that $\forall \quad v \in (C_c^\infty(D))^d$, $\nabla \cdot v = 0$, $P-$almost surely*

$$< h, v >_{((C_c^\infty(D))')^d \times (C_c^\infty(D))^d} = 0 \quad \text{in } (C_c^\infty)'(0,T).$$

Then there exists unique $\pi \in L^{r_0}(\Omega, \mathcal{F}, P; W^{s_1,r_1}(0,T; L^2(D)))$ *such that* P*-almost surely* $\nabla \pi = h$ *in* $((C_c^\infty([0,T] \times D))')^d$, $\int_D \pi \mathrm{d}x = 0$ *in* $(C_c^\infty([0,T]))'$.

3.2 Unique Strong Solution for the 2D MPF and the MMPF Systems with Lipschitz Multiplicative Noise

In this section, we study the 2D MPF system (1) and (2) and the MMPF systems (3)–(5) fully with appropriate modifications as done in (6)–(8), (34) along with all the notations in the previous sections (see [49] for details). Analogously to the deterministic case, it is of much interest whether the weak martingale solution discussed in the previous section may be unique or strong and if so, in what sense. Firstly, we recall the notion of a strong solution only to the stochastic MPF system for simplicity:

Definition 2 A strong solution to (1) and (2) on the given $(\Omega, \mathcal{F}, \mathcal{F}_t, P, W)$ is a process y where

1. $y \in L^p(\Omega, \mathcal{F}, P; L^2(0,T; V_1 \times \mathbb{H}_0^1)) \cap L^p(\Omega, \mathcal{F}, P; L^\infty(0,T; H_1 \times \mathbb{L}^2))$ $\forall \ p \in [1, \infty)$,
2. for almost every t, $y(t)$ is $\mathcal{F}_t$-measurable,
3. for any $v \in V$, almost surely $\forall \ t \in [0,T]$, (36) holds.

Theorem 5 *([49]) Suppose* $y_0 \in H_1 \times \mathbb{L}^2$ *and* $f_i, g_i, i = 1, 2$ *are nonlinear mappings that are continuous in* $t \in [0,T]$, $f(0,t) = 0$, $g(0,t) = 0 \ \forall \ t \in [0,T]$, *and there exist two constants* $L_f, L_g > 0$ *such that with* $y^i = (u^i, w^i, b^i)$, $i = 1, 2$,

$$
\begin{aligned}
&\|f_1(y^1,t) - f_1(y^2,t)\|_{\mathbb{H}^{-1}} \leq L_f \|u^1 - u^2\|_{H_1}, \\
&\|f_2(y^1,t) - f_2(y^2,t)\|_{\mathbb{H}^{-1}} \leq L_f \|w^1 - w^2\|_{\mathbb{L}^2}, \\
&\|g_1(y^1,t) - g_1(y^2,t)\|_{H_1^{\times m_1}} \leq L_g \|u^1 - u^2\|_{H_1}, \\
&\|g_2(y^1,t) - g_2(y^2,t)\|_{(\mathbb{L}^2)^{\times m_2}} \leq L_g \|w^1 - w^2\|_{\mathbb{L}^2},
\end{aligned}
$$

where $\times m_i$ *denotes direct product* m_i *times. Then there exists a unique strong solution to (1) and (2) in the sense of Definition 2. Moreover, there exists a unique* $\pi \in L^1(\Omega, \mathcal{F}, P; W^{-1,\infty}(0,T; L^2(D)))$ *such that* $\int_D \pi \mathrm{d}x = 0$ *in* $(C_c^\infty([0,T]))'$ *and (1) and (2) holds in* $((C_c^\infty([0,T] \times D))')^2$.

The proof relies on the classical Yamada-Watanabe theorem:

Lemma 8 *([39, 40]) Path-wise uniqueness implies uniqueness in the sense of probability law.*

A consequence of this lemma is the existence of the strong solution.

The condition of path-wise uniqueness for solutions to SPDE is just as interesting as the case of deterministic PDE. In this regard, we just mention that in [25] the authors obtained such condition that are similar to the Serrin-type $\mathbb{L}^p - L^r$ regularity criteria that we also discussed in the previous section.

4 Conclusion

As the mathematical analysis on PDE related to fluid mechanics remain a great challenge, it is of much interest whether the noise may perhaps have significant effect, possibly help the well-posedness of the PDE or not (see [19] and references found therein). In this regard, the MPF and the MMPF systems provide a good model for further study from both deterministic and stochastic perspectives, due to their distinctive features from other models such as the NSE, the MHD and Boussinesq systems.

Acknowledgments The author wishes to express his gratitude to Professor Hakima Bessaih and Professor Annie Millet for stimulating discussion in this direction of research.

References

1. Ahmadi G, Shahinpoor M (1974) Universal stability of magneto-micropolar fluid motions. Int J Eng Sci 12:657–663
2. Barbu V, Da Prato G (2007) Existence and ergodicity for the two-dimensional stochastic magneto-hydrodynamics equations. Appl Math Optim 56:145–168
3. Beale JT, Kato T, Majda A (1984) Remarks on the breakdown of smooth solutions for the 3-D Euler equations. Comm Math Phys 94:61–66
4. Bensoussan A (1995) Stochastic Navier-Stokes equations. Acta Appl Math 38:267–304
5. Boling G, Xueke P (2011) Global well-posedness of the stochastic 2D Boussinesq equations with partial viscosity. Acta Math Sci Ser B Engl Ed 31B:1968–1984
6. Brezis H, Wainger S (1980) A note on limiting cases of Sobolev embeddings and convolution inequalities. Comm Partial Differ Equ 5:773–789
7. Caffarelli L, Kohn R, Nirenberg L (1982) Partial regularity of suitable weak solutions of the Navier-Stokes equations. Comm Pure Appl Math 35:771–831
8. Cao C, Wu J, Yuan B (2014) The 2D incompressible magnetohydrodynamics equations with only magnetic diffusion. SIAM J Math Anal 46:588–602
9. Chae D (2006) Global regularity for the 2-D Boussinesq equations with partial viscous terms. Adv Math 203:497–513
10. Chemin J-Y (1998) Perfect incompressible fluids. Clarendon Press, Oxford
11. Da Prato G, Zabczyk J (1992) Stochastic equations in infinite dimensions. Cambridge University Press, Cambridge
12. Da Prato G, Debussche A, Temam R (1994) Stochastic Burgers' equation. NoDEA Nonlinear Differ Equ Appl 1:389–402
13. Deugoue G, Razafimandimby PA, Sango M (2012) On the 3-D stochastic magnetohydrodynamic-α model. Stoch Process Appl 122:2211–2248
14. Dong B-Q, Zhang Z (2010) Global regularity of the 2D micropolar fluid flows with zero angular viscosity. J Differ Equ 249:200–213
15. Eringen AC (1966) Theory of micropolar fluids. J Math Mech 16:1–18
16. Ferrario B (1997) The B*é*nard problem with random perturbations: dissipativity and invariant measures. NoDEA Nonlinear Differ Equ Appl 4:101–121
17. Ferrario B (2003) Uniqueness result for the 2D Navier-Stokes equation with additive noise. Stoch Stoch Rep 75:435–442
18. Flandoli F (1994) Dissipativity and invariant measures for stochastic Navier-Stokes equations. NoDEA Nonlinear Differ Equ Appl 1:403–423

19. Flandoli F (2008) An introduction to 3D stochastic fluid dynamics. In: SPDE in hydrodynamic: recent progress and prospects. Lecture notes in mathematics, vol 1942. Springer, Berlin, pp 51–150
20. Flandoli F, Romito M (2002) Partial regularity for the stochastic Navier-Stokes equations. Trans Am Math Soc 354:2207–2241
21. Galdi GP, Rionero S (1977) A note on the existence and uniqueness of solutions of the micropolar fluid equations. Int J Eng Sci 15:105–108
22. Hmidi T, Keraani S, Rousset R (2010) Global well-posedness for Euler-Boussinesq system with critical dissipation. Comm Partial Differ Equ 36:420–445
23. Hou T, Li C (2005) Global well-posedness of the viscous Boussinesq equations. Discret Contin Dyn Syst 12:1–12
24. Jiu Q, Zhao J (2014) Global regularity of 2D generalized MHD equations with magnetic diffusion. Z Angew Math Phys 1–11
25. Krylov NV, Röckner M (2005) Strong solutions of stochastic equations with singular time dependent drift. Probab Theory Relat Fields 131:154–196
26. Kukavica I, Ziane M (2006) One component regularity for the Navier-Stokes equations. Nonlinearity 19:453–469
27. Langa JA, Real J, Simon J (2003) Existence and regularity of the pressure for the stochastic Navier-Stokes equations. Appl Math Optim 48:195–210
28. Lukaszewicz G (1999) Micropolar fluids. Theory and applications, Birkhäuser, Boston
29. Mikulevicius R, Rozovskii BL (2004) Stochastic Navier-Stokes equations for turbulent flows. SIAM J Math Anal 35:1250–1310
30. Ortega-Torres EE, Rojas-Medar MA (1999) Magneto-micropolar fluid motion: global existence of strong solutions. Abstr Appl Anal 4:109–125
31. Prokhorov YV (1956) Convergence of random processes and limit theorems in probability theory. Theory Probab Appl 1:157–214
32. Rojas-Medar MA (1997) Magneto-micropolar fluid motion: existence and uniqueness of strong solutions. Math Nachr 188:301–319
33. Sango M (2010) Magnetohydrodynamic turbulent flows: existence results. Phys D 239: 912–923
34. Sermange M, Temam R (1983) Some mathematical questions related to the MHD equations. Comm Pure Appl Math 36:635–664
35. Serrin J (1962) On the interior regularity of weak solutions of the Navier-Stokes equations. Arch Ration Mech Anal 9:187–195
36. Skorokhod AV (1956) Limit theorems for stochastic processes. Theory Probab Appl 1:261–290
37. Sritharan SS, Sundar P (1999) The stochastic magneto-hydrodynamic system. Infin Dimens Anal Quantum Probab Relat Top 2:241–265
38. Tran CV, Yu X, Zhai Z (2013) On global regularity of 2D generalized magnetohydrodynamic equations. J Differ Equ 254:4194–4216
39. Watanabe S, Yamada T (1971) On the uniqueness of solutions of stochastic differential equations. J Math Kyoto Univ 11:155–167
40. Watanabe S, Yamada T (1971) On the uniqueness of solutions of stochastic differential equations II. J Math Kyoto Univ 11:553–563
41. Yamazaki K (2014) Remarks on the global regularity of the two-dimensional magnetohydrodynamics system with zero dissipation. Nonlinear Anal 94:194–205
42. Yamazaki K (2014) On the global regularity of two-dimensional generalized magnetohydrodynamics system. J Math Anal Appl 416:99–111
43. Yamazaki K (2014) Remarks on the regularity criteria of three-dimensional magnetohydrodynamics system in terms of two velocity field components. J Math Phys 55:031505
44. Yamazaki K (2014) Component reduction for regularity criteria of the three-dimensional magnetohydrodynamics systems. Electron J Differ Equ 2014:1–18
45. Yamazaki K (2014) $(N-1)$ velocity components condition for the generalized MHD system in N-dimension. Kinet Relat Models 7:779–792

46. Yamazaki K (2015) Global regularity of the two-dimensional magneto-micropolar fluid system with zero angular viscosity. Discret Contin Dyn Syst 35:2193–2207
47. Yamazaki K (2014) 3-D stochastic micropolar and magneto-micropolar fluid systems with non-Lipschitz multiplicative noise. Commun Stoch Anal 8:413–437
48. Yamazaki K (2015) On the global regularity of N-dimensional generalized Boussinesq system. Appl Math 60:103–133
49. Yamazaki K, Unique strong solution for the 2-D stochastic micropolar and magneto-micropolar fluid systems (submitted)
50. Ye Z, Xu X (2014) Global regularity of the two-dimensional incompressible generalized magnetohydrodynamics system. Nonlinear Anal 100:86–96
51. Yuan B (2010) Regularity of weak solutions to magneto-micropolar fluid equations. Acta Math Sci Ser B Engl Ed 30B:1469–1480
52. Yuan B (2010) On regularity criteria for weak solutions to the micropolar fluid equations in Lorentz space. Proc Am Math Soc 138:2025–2036
53. Yuan B, Bai L (2014) Remarks on global regularity of 2D generalized MHD equations. J Math Anal Appl 413:633–640
54. Yudovich V (1963) Non stationary flows of an ideal incompressible fluid. Zhurnal Vych Matematika 3:1032–1066
55. Zhang Z (2014) Remarks on the global regularity criteria for the 3D MHD equations via two components. Z Angew Math Phys 1–11

Pathwise Sensitivity Analysis in Transient Regimes

Georgios Arampatzis, Markos A. Katsoulakis and Yannis Pantazis

Abstract The instantaneous relative entropy (IRE) and the corresponding instantaneous Fisher information matrix (IFIM) for transient stochastic processes are presented in this paper. These novel tools for sensitivity analysis of stochastic models serve as an extension of the well known relative entropy rate (RER) and the corresponding Fisher information matrix (FIM) that apply to stationary processes. Three cases are studied here, discrete-time Markov chains, continuous-time Markov chains and stochastic differential equations. A biological reaction network is presented as a demonstration numerical example.

1 Introduction

Sensitivity analysis, for a general mathematical model, is defined to be the quantification of system response to parameter perturbations. Questions on the robustness, (structural) identifiability, experimental design, uncertainty quantification, estimation and control can be addressed through sensitivity analysis [1]. Moreover, it is a necessary analysis tool for the study of kinetic models such as chemical and biochemical reaction networks [1, 2]. The mathematical models considered in this paper are models that describe phenomena exhibiting stochasticity: stochastic differential equations (SDE), discrete-time and continuous-time Markov chains (DTMC and CTMC). Some of the mathematical tools for the sensitivity analysis of such systems include log-likelihood methods and Girsanov transformations [3–5], polynomial chaos [6], finite difference methods [7, 8] and pathwise sensitivity methods [9].

G. Arampatzis (✉) · M.A. Katsoulakis · Y. Pantazis
Department of Mathematics and Statistics, University of Massachusetts, Amherst, MA, USA
e-mail: arampatzis@math.umass.edu

M.A. Katsoulakis
e-mail: markos@math.umass.edu

Y. Pantazis
e-mail: pantazis@math.umass.edu

S. Heinz and H. Bessaih (eds.), *Stochastic Equations for Complex Systems*, Mathematical Engineering, DOI 10.1007/978-3-319-18206-3_5

Closely related to the log-likelihood methods are various linear-response-based approaches, for instance in the context of chemical kinetics [10], as well as in recent mathematical work for linear response in non-equilibrium systems [11, 12].

In [13], the authors propose a new methodology for the pathwise sensitivity analysis of complex stochastic stationary dynamics based on the Relative Entropy (RE) between path distributions and the Relative Entropy Rate (RER). These two quantities provide a measure of the sensitivity of the entire time-series distribution. The space of all such time-series is referred in probability theory as the "path space". RER measures the loss of information per unit time in path space after an arbitrary perturbation of parameter combinations. Moreover, RER and the corresponding Fisher Information Matrix (FIM) become computationally feasible in certain cases as they admit explicit formulas. In fact, it is been showed in [13] that the proposed pathwise sensitivity analysis has the following properties: (a) it is rigorously valid for the sensitivity of long-time, stationary dynamics, (b) it is a gradient-free sensitivity analysis method suitable for high-dimensional parameter spaces, (c) the computation of RER and FIM does not require the explicit knowledge of the equilibrium probability distribution, relying only on information for local dynamics, i.e., it is suitable for non-equilibrium systems.

In this paper we extend the RE and FIM tools, developed in [13] for stationary processes, to transient and non-stationary processes. The extension is based on the notion of instantaneous RE (IRE) and instantaneous FIM (IFIM), see for example Eqs. (10) and (12) in text. These sensitivity tools provide an instantaneous measure for the sensitivity of a system arising from information theoretic tools. Moreover, both IRE and IFIM, which are independent of observable functions, can be used as upper bounds for observable depended sensitivities, see for example the discussion in Conclusions and [14, 15].

The rest of the paper is organized as follows: In Sect. 2 a review of the RE and the FIM is given. In Sects. 3–5 the new quantities IRE and IFIM are presented for discrete-time Markov chains, continuous-time Markov chains and stochastic differential equations, respectively. In Sect. 6, a numerical example for a biological reaction network is utilized and IRE and IFIM are computed in the course of a stochastic simulation and various observations are discussed. Finally, in Sect. 7, concluding remarks and connections with existing work are discussed.

2 Time-Dependent Sensitivity Analysis

2.1 Decomposition of the Pathwise Relative Entropy

The relative entropy (or Kullback-Leibler divergence) of a probability measure P with respect to (w.r.t.) another probability measure $\bar{P}$ is defined as [16, 17]

$$\mathcal{R}\left(P \mid \bar{P}\right) := \begin{cases} \int \log \frac{dP}{d\bar{P}} dP, & P \ll \bar{P} \\ \infty\,, & \text{otherwise} \end{cases} \tag{1}$$

where $\frac{dP}{d\bar{P}}$ is a function known as the Radon-Nikodym derivative which is well-defined when P is absolutely continuous w.r.t. $\bar{P}$ (denoted as $P \ll \bar{P}$) while the integration is performed w.r.t. the probability measure P. Relative entropy has been utilized in a diverge range of scientific fields from statistical mechanics [18] to telecommunications [17] and finance [19] and possesses the following fundamental properties:

(i) $\mathcal{R}\left(P \mid \bar{P}\right) \geq 0$,
(ii) $\mathcal{R}\left(P \mid \bar{P}\right) = 0$ if and only if $P = \bar{P}$ P-almost everywhere, and,

These properties allow us to view relative entropy as a "distance" (more precisely a divergence) between two probability measures capturing the relative importance of uncertainties [20]. From an information theory perspective, relative entropy measures the *loss/change of information* when $\bar{P}$ is considered instead of P [17].

Let a stochastic process—either discrete-time or continuous-time—be denoted by X_t and let the path space $\mathcal{X}$ be the set of all trajectories $\{X_t\}_{t=0}^{T}$. We denote by $Q_{0:T}$ the path space distribution, i.e., the probability to see a particular element of path space, $\mathcal{X}$. Denote by $\bar{Q}_{0:T}$ the path space distribution of another process, $\bar{X}_t$. The pathwise relative entropy of the distribution $Q_{0:T}$ w.r.t. the distribution $\bar{Q}_{0:T}$ assuming that they are absolutely continuous w.r.t. each other is written using (1) as

$$\mathcal{R}\left(Q_{0:T} \mid \bar{Q}_{0:T}\right) = \int \log \frac{dQ_{0:T}}{d\bar{Q}_{0:T}} dQ_{0:T}\,. \tag{2}$$

A key property of pathwise relative entropy is that it is an increasing function of time which is the analog of the second thermodynamic law in statistical physics [17]. To this end, for various important Markov processes, it can be shown exploiting the Markov property, that the pathwise relative entropy can be written as an averaged quantity as

$$\mathcal{R}\left(Q_{0:T} \mid \bar{Q}_{0:T}\right) = \begin{cases} \mathcal{R}\left(\nu \mid \bar{\nu}\right) + \sum_{i=1}^{T} \mathcal{H}\left(Q_i \mid \bar{Q}_i\right)\,, & \text{if time is discrete} \\ \mathcal{R}\left(\nu \mid \bar{\nu}\right) + \int_0^T \mathcal{H}\left(Q_t \mid \bar{Q}_t\right) dt\,, & \text{if time is continuous}\,, \end{cases} \tag{3}$$

where $\mathcal{R}\left(\nu \mid \bar{\nu}\right)$ is the relative entropy of the initial distribution ν w.r.t. the perturbed initial distribution $\bar{\nu}$, while $\mathcal{H}\left(Q_\cdot \mid \bar{Q}_\cdot\right)$ denotes the instantaneous relative entropy (for explicit formulas we refer to Eqs. (10), (16) and (24)). We named the quantity $\mathcal{H}\left(Q_\cdot \mid \bar{Q}_\cdot\right)$ instantaneous relative entropy because it is also non-negative but more importantly is the time-derivative of the pathwise relative entropy and inherits the properties of the relative entropy. Notice that the notation for instantaneous relative entropy is somewhat confusing but it will become clear when specific examples will be presented in the following sections.

Moreover the relative entropy rate is defined for a broad class of stochastic processes including Markov and semi-Markov processes as [21] as the limit

$$\mathcal{H}\left(Q \mid \bar{Q}\right) = \lim_{T\to\infty} \frac{1}{T}\mathcal{R}\left(Q_{0:T} \mid \bar{Q}_{0:T}\right) . \tag{4}$$

Relative entropy rate is closely related to the instantaneous relative entropy in two fundamental ways. Firstly it is the limit of instantaneous relative entropy as time goes to infinity, whenever this limit is defined and second it holds at the stationary regime that

$$\mathcal{H}\left(Q_i \mid \bar{Q}_i\right) = \mathcal{H}\left(Q \mid \bar{Q}\right) \tag{5}$$

for the discrete-time case with $i = 1, \ldots, T$ and similarly for the continuous-time case.

2.2 Sensitivity Analysis and Fisher Information Matrix

In [13], the authors proposed the relative entropy between path distributions to perform sensitivity analysis arguing that pathwise relative entropy takes into account not only the equilibrium properties but also the complex dynamics of a stochastic process. Specifically, denote by $Q^{\theta}_{0:T}$ the path space distribution of the process X_t, parametrized by the parameter vector $\theta \in \mathbb{R}^K$. Consider also a perturbation vector, $\epsilon \in \mathbb{R}^K$, and denote by $Q^{\theta+\epsilon}_{0:T}$ the path space distribution of the perturbed process $\bar{X}_t$. The pathwise relative entropy of the distribution $Q^{\theta}_{0:T}$ w.r.t. the distribution $Q^{\theta+\epsilon}_{0:T}$ assuming that they are absolutely continuous w.r.t. each other is written using (2) as

$$\mathcal{R}\left(Q^{\theta}_{0:T} \mid Q^{\theta+\epsilon}_{0:T}\right) = \int \log \frac{dQ^{\theta}_{0:T}}{dQ^{\theta+\epsilon}_{0:T}} dQ^{\theta}_{0:T} . \tag{6}$$

An attractive approach to sensitivity analysis that is rigorously based on relative entropy calculations is the Fisher Information Matrix (FIM). Indeed, assuming smoothness in the parameter vector, it is straightforward to obtain the following expansion for (6) [17, 22],

$$\mathcal{R}\left(Q^{\theta}_{0:T} \mid Q^{\theta+\epsilon}_{0:T}\right) = \frac{1}{2}\epsilon^T \mathcal{I}(Q^{\theta}_{0:T})\epsilon + O(|\epsilon|^3) , \tag{7}$$

where the $K \times K$ pathwise FIM $\mathcal{I}\left(Q^{\theta}_{0:T}\right)$ is defined as the Hessian of the pathwise relative entropy. As (7) readily suggests, relative entropy is locally a quadratic function of the parameter vector θ. Indeed, the pathwise RE for any perturbation can be recovered up to third-order utilizing only the pathwise FIM. Moreover, similar expansions hold for the instantaneous relative entropy and the relative entropy rate. The decomposition of the pathwise FIM reads

$$\mathcal{I}\big(Q^{\theta}_{0:T}\big) = \begin{cases} \mathcal{I}\big(\nu^{\theta}\big) + \sum_{i=1}^{T} \mathcal{I}_{\mathcal{H}}\big(Q^{\theta}_{i}\big)\ , & \text{if time is discrete} \\ \mathcal{I}\big(\nu^{\theta}\big) + \int_{0}^{T} \mathcal{I}_{\mathcal{H}}\big(Q^{\theta}_{t}\big)dt\ , & \text{if time is continuous} \end{cases} \tag{8}$$

where $\mathcal{I}\big(\nu^{\theta}\big)$ is the FIM of the initial distribution ν^{θ} while $\mathcal{I}_{\mathcal{H}}\big(Q^{\theta}_{\cdot}\big)$ denotes the instantaneous FIM. In the following sections concrete examples of stochastic Markov processes are presented whose pathwise relative entropy and the associated pathwise FIM are provided.

3 Discrete-Time Markov Chains

This section presents explicit formulas of the various relative entropy quantities defined in the previous section as well as the associated FIMs for the case of discrete-time Markov chains. The analysis of the DTMC case serves (a) as a more intuitive and manageable example of stochastic processes and (b) as a intermediate step to handle the continuous-time Markov chain case.

Next, let $\{x_i\}_{i\in\mathbb{Z}^+}$ be a discrete-time time-homogeneous Markov chain with separable state space E. The transition probability kernel of the Markov chain denoted by $P^{\theta}(x, dx')$ depends on the parameter vector $\theta \in \mathbb{R}^K$. Assume that the transition kernel is absolutely continuous with respect to the Lebesgue measure and the transition probability density function $p^{\theta}(x, x')$ is always positive for all $x, x' \in E$ and for all $\theta \in \mathbb{R}^K$. Exploiting the Markov property, the path space probability density $Q^{\theta}_{0:T}$ for the path $\{x_i\}_{i=0}^{T}$ at the time horizon $0, 1, \ldots, T$ starting from the initial distribution $\nu^{\theta}(x)dx$ is given by

$$Q^{\theta}_{0:T}\big(x_0, \ldots, x_T\big) = \nu^{\theta}(x_0)\, p^{\theta}(x_0, x_1) \ldots p^{\theta}(x_{T-1}, x_T)\,.$$

We consider a perturbation vector $\epsilon \in \mathbb{R}^K$ and the Markov chain $\{\bar{x}_i\}_{i\in\mathbb{Z}^+}$ with transition probability density function, $p^{\theta+\epsilon}(x, x')$, initial density, $\nu^{\theta+\epsilon}(x)$, as well as path distribution $Q^{\theta+\epsilon}_{0:T}$. The product representation of the path distributions results in an additive representation of the relative entropy of the path distribution $Q^{\theta}_{0:T}$ w.r.t. the perturbed path distribution $Q^{\theta+\epsilon}_{0:T}$. Let $\nu^{\theta}_{i}(x)$ denote the probability density function of the Markov chain at time instant i given that the initial distribution is ν^{θ}, whose formula is provided by the Chapman-Kolmogorov equation,

$$\nu^{\theta}_{i}(x) = \int_{E} \cdots \int_{E} \nu^{\theta}(x_0)\, p^{\theta}(x_0, x_1) \ldots p^{\theta}(x_{i-1}, x) dx_0 \ldots dx_{i-1}\ .$$

The following theorem presents the decomposition of the pathwise relative entropy.

Theorem 1 *(a) The pathwise relative entropy for the above-defined discrete-time Markov chain is decomposed as*

$$\mathcal{R}\left(Q^{\theta}_{0:T} \mid Q^{\theta+\epsilon}_{0:T}\right) = \mathcal{R}\left(\nu^{\theta} \mid \nu^{\theta+\epsilon}\right) + \sum_{i=1}^{T} \mathcal{H}\left(Q^{\theta}_{i} \mid Q^{\theta+\epsilon}_{i}\right)\ , \tag{9}$$

where the instantaneous relative entropy is equal to

$$\mathcal{H}\left(Q_i^\theta \mid Q_i^{\theta+\epsilon}\right) = \mathbb{E}_{\nu_{i-1}^\theta}\Big[\int_E p^\theta(x,x')\log\frac{p^\theta(x,x')}{p^{\theta+\epsilon}(x,x')}dx'\Big]. \tag{10}$$

(b) Assuming that the transition probability function is differentialble w.r.t. the parameter vector θ, the pathwise FIM is also decomposed as

$$\mathcal{I}\big(Q_{0:T}^\theta\big) = \mathcal{I}\big(\nu^\theta\big) + \sum_{i=1}^{T}\mathcal{I}_{\mathcal{H}}\big(Q_i^\theta\big)\,, \tag{11}$$

where the instantaneous pathwise FIM is given by

$$\mathcal{I}_{\mathcal{H}}\big(Q_i^\theta\big) = \mathbb{E}_{\nu_{i-1}^\theta}\left[\int_E p^\theta(x,x')\nabla_\theta\log p^\theta(x,x')\nabla_\theta\log p^\theta(x,x')^T dx'\right]\,. \tag{12}$$

Proof (a) The proof of this part of the theorem can be found in [17, Chap. 2] under the title "Chain rule for relative entropy" but for the shake of completeness we present it here. The Radon-Nikodym derivative of the unperturbed path distribution w.r.t. the perturbed path distribution takes the form

$$\frac{dQ_{0:T}^\theta}{dQ_{0:T}^{\theta+\epsilon}}\big(\{x_i\}_{i=0}^T\big) = \frac{\nu^\theta(x_0)\prod_{i=0}^{T-1}p^\theta(x_i,x_{i+1})}{\nu^{\theta+\epsilon}(x_0)\prod_{i=0}^{T-1}p^{\theta+\epsilon}(x_i,x_{i+1})}\,,$$

which is well-defined since the transition probabilities are always positive. Then,

$$\begin{aligned}
&\mathcal{R}\left(Q_{0:T}^\theta \mid Q_{0:T}^{\theta+\epsilon}\right)\\
&= \int_E\cdots\int_E \nu^\theta(x_0)\prod_{j=1}^{T}p^\theta(x_{j-1},x_j)\log\frac{\nu^\theta(x_0)\prod_{i=1}^{T}p^\theta(x_{i-1},x_i)}{\nu^{\theta+\epsilon}(x_0)\prod_{i=1}^{T}p^{\theta+\epsilon}(x_{i-1},x_i)}dx_0\ldots dx_T\\
&= \int_E\cdots\int_E \nu^\theta(x_0)\prod_{j=1}^{T}p^\theta(x_{j-1},x_j)\log\frac{\nu^\theta(x_0)}{\nu^{\theta+\epsilon}(x_0)}dx_0\ldots dx_T\\
&\quad+\sum_{i=1}^{T}\int_E\cdots\int_E \nu^\theta(x_0)\prod_{j=1}^{T}p^\theta(x_{j-1},x_j)\log\frac{p^\theta(x_{i-1},x_i)}{p^{\theta+\epsilon}(x_{i-1},x_i)}dx_0\ldots dx_T\\
&= \mathcal{R}\left(\nu^\theta \mid \nu^{\theta+\epsilon}\right) + \sum_{i=1}^{T}\mathcal{H}\left(Q_i^\theta \mid Q_i^{\theta+\epsilon}\right)\,,
\end{aligned}$$

where $\mathcal{R}\left(\nu^\theta \mid \nu^{\theta+\epsilon}\right) = \mathbb{E}_{\nu^\theta}\Big[\log\frac{\nu^\theta(x)}{\nu^{\theta+\epsilon}(x)}\Big]$ is the relative entropy of the unperturbed initial distribution w.r.t. the perturbed one, while the instantaneous relative entropy

(of the time-varying pathwise relative entropy) is

$$\mathcal{H}\left(Q_i^\theta \mid Q_i^{\theta+\epsilon}\right) = \mathbb{E}_{\nu_{i-1}^\theta}\Big[\int_E p^\theta(x,x') \log \frac{p^\theta(x,x')}{p^{\theta+\epsilon}(x,x')} dx'\Big] .$$

(b) The proof of this part of the theorem is similar to the proof of the pathwise FIM for the relative entropy rate in [13]. We present it with minor but necessary adaptations. Let $\delta p(x,x') = p^{\theta+\epsilon}(x,x') - p^\theta(x,x')$, then the instantaneous relative entropy $\mathcal{H}\left(Q_i^\theta \mid Q_i^{\theta+\epsilon}\right)$ at the ith time instant is written as

$$\begin{aligned}\mathcal{H}\left(Q_i^\theta \mid Q_i^{\theta+\epsilon}\right) &= -\int_E\int_E \nu_{i-1}^\theta(x) p^\theta(x,x') \log\left(1+\frac{\delta p(x,x')}{p^\theta(x,x')}\right) dx dx' \\ &= -\int_E\int_E \left[\nu_{i-1}^\theta(x)\delta p(x,x') - \frac{1}{2}\nu_i^\theta(x)\frac{\delta p(x,x')^2}{p^\theta(x,x')} + O(|\delta p(x,x')|^3)\right] dx dx' .\end{aligned}$$

Moreover, for all $x \in E$, it holds that

$$\int_E \delta p(x,x')dx' = \int_E p^{\theta+\epsilon}(x,x')dx' - \int_E p^\theta(x,x')dx' = 1-1 = 0.$$

Since the transition probability function is differentiable w.r.t. the parameter vector θ, a Taylor series expansion to δp gives,

$$\delta p(x,x') = \epsilon^T \nabla_\theta p^\theta(x,x') + O(|\epsilon|^2) .$$

Thus, we finally obtain for all $i = 1,\dots,T$, that

$$\begin{aligned}\mathcal{H}\left(Q_i^\theta \mid Q_i^{\theta+\epsilon}\right) &= \frac{1}{2}\int_E\int_E \nu_{i-1}^\theta(x)\frac{(\epsilon^T\nabla_\theta p^\theta(x,x'))^2}{p^\theta(x,x')} dx dx' + O(|\epsilon|^3) \\ &= \frac{1}{2}\epsilon^T\Big(\int_E\int_E \nu_{i-1}^\theta(x) p^\theta(x,x')\nabla_\theta \log p^\theta(x,x')\nabla_\theta \log p^\theta(x,x')^T dx dx'\Big)\epsilon + O(|\epsilon|^3) \\ &= \frac{1}{2}\epsilon^T \mathcal{I}_{\mathcal{H}}(Q_i^\theta)\epsilon + O(|\epsilon|^3)\end{aligned}$$

where,

$$\mathcal{I}_{\mathcal{H}}(Q_i^\theta) = \mathbb{E}_{\nu_{i-1}^\theta}\left[\int_E p^\theta(x,x')\nabla_\theta \log p^\theta(x,x')\nabla_\theta \log p^\theta(x,x')^T d\,x'\right]$$

is the instantaneous FIM associated to the instantaneous relative entropy.

Consequently, the pathwise FIM $\mathcal{I}(Q_{0:T}^\theta)$, i.e., the Hessian of the pathwise relative entropy (9) at point θ, is given by

$$\mathcal{I}(Q_{0:T}^\theta) = \mathcal{I}(\nu^\theta) + \sum_{i=1}^T \mathcal{I}_{\mathcal{H}}(Q_i^\theta) ,$$

where $\mathcal{I}(\nu^\theta) = \mathbb{E}_{\nu^\theta}[\nabla_\theta \log \nu^\theta(x) \nabla_\theta \log \nu^\theta(x)^T]$ is the FIM of the initial distribution. □

Remark 1 Let '$\otimes$' denote the product operator of two distributions (i.e., $\nu \otimes p(A \times B) = \int_A p(x, B)\nu(x)dx$). Then, the instantaneous relative entropy can be written as a relative entropy of the probability measure $\nu_{i-1}^\theta \otimes p^\theta$ w.r.t. the probability measure $\nu_{i-1}^\theta \otimes p^{\theta+\epsilon}$. Mathematically,

$$\mathcal{H}\left(Q_i^\theta \mid Q_i^{\theta+\epsilon}\right) = \mathcal{R}\left(\nu_{i-1}^\theta \otimes p^\theta \mid \nu_{i-1}^\theta \otimes p^{\theta+\epsilon}\right) ,$$

and similarly for the associated instantaneous FIM it holds that

$$\mathcal{I}_\mathcal{H}(Q_i^\theta) = \mathcal{I}(\nu_{i-1}^\theta \otimes p^\theta) .$$

Remark 2 The instantaneous relative entropy $\mathcal{H}\left(Q_i^\theta \mid Q_i^{\theta+\epsilon}\right)$ is different from, and should not be confused with, the relative entropy of the unperturbed distribution at the ith (or the $(i-1)$th) time instant ν_i^θ (or ν_{i-1}^θ) w.r.t. the respective perturbed distribution $\nu_i^{\theta+\epsilon}$ (or $\nu_{i-1}^{\theta+\epsilon}$). Indeed, it holds that

$$\mathcal{H}\left(Q_i^\theta \mid Q_i^{\theta+\epsilon}\right) = \mathcal{R}\left(\nu_{i-1}^\theta \otimes p^\theta \mid \nu_{i-1}^\theta \otimes p^{\theta+\epsilon}\right) \neq \mathcal{R}\left(\nu_i^\theta \mid \nu_i^{\theta+\epsilon}\right) ,$$

as well as $\mathcal{H}\left(Q_i^\theta \mid Q_i^{\theta+\epsilon}\right) \neq \mathcal{R}\left(\nu_{i-1}^\theta \mid \nu_{i-1}^{\theta+\epsilon}\right)$. Moreover, an explicit formula for the probability distribution at the ith time instant ν_i^θ is generally not available making the computation of the relative entropy $\mathcal{R}\left(\nu_i^\theta \mid \nu_i^{\theta+\epsilon}\right)$ intractable. On the other hand, the instantaneous relative entropy $\mathcal{H}\left(Q_i^\theta \mid Q_i^{\theta+\epsilon}\right)$ can be computed in a straightforward manner as a statistical average since it incorporates only the transition probabilities which are known functions.

Stationary regime: In the stationary regime, the initial distribution is the stationary distribution, μ^θ. Thus, for all $i = 1, \ldots, T$ it holds that $\nu_i^\theta = \mu^\theta$ and the instantaneous relative entropy is a constant function of time that is equal to the relative entropy rate. The next corollary presents explicit formulas for the relative entropy rate and the associated FIM.

Corollary 1 *The relative entropy rate is equal to*

$$\mathcal{H}\left(Q^\theta \mid Q^{\theta+\epsilon}\right) = \mathbb{E}_{\mu^\theta}\Big[\int_E p^\theta(x, x') \log \frac{p^\theta(x, x')}{p^{\theta+\epsilon}(x, x')} dx'\Big] . \tag{13}$$

Similarly, the FIM associated to the RER is given by

$$\mathcal{I}_\mathcal{H}(Q^\theta) = \mathbb{E}_{\mu^\theta}\left[\int_E p^\theta(x, x) \nabla_\theta \log p^\theta(x, x') \nabla_\theta \log p^\theta(x, x')^T d\, x'\right] . \tag{14}$$

Proof Both formulas are obtained by substituting the stationary distribution μ^θ to the place of ν^θ_{i-1} in (10) and (12). □

4 Continuous-Time Markov Chains

Let $\{X_t\}_{t\in\mathbb{R}_+}$ be a continuous-time Markov chain with countable state space E. The parameter dependent transition rates, denoted by $c^\theta(x, x')$, completely define the continuous-time Markov chain. The transition rates determine the updates (jumps or sojourn times) from a current state x to a new (random) state x' through the total rate $\lambda^\theta(x) = \sum_{x'\in E} c^\theta(x, x')$ which is the intensity of the exponential waiting time for a jump from state x. The transition probabilities for the embedded Markov chain $\{x_n\}_{n\geq 0}$ defined by $x_n := X_{t_n}$ where t_n is the instance of the nth jump are $p^\theta(x, x') = \frac{c^\theta(x,x')}{\lambda^\theta(x)}$.

Assume another jump Markov process $\{\bar{X}_t\}_{t\in\mathbb{R}_+}$, defined by perturbing the transition rates by a small vector $\epsilon \in \mathbb{R}^K$. Moreover assume that the two path probabilities $Q^\theta_{0:T}$ and $Q^{\theta+\epsilon}_{0:T}$ are absolutely continuous with respect to each other which is satisfied when $c^\theta(x, x') = 0$ if and only if $c^{\theta+\epsilon}(x, x') = 0$, $\forall x, x' \in E$. The following theorem presents the decomposition of the pathwise relative entropy for the case of continuous-time Markov chains.

Theorem 2 *(a) The pathwise relative entropy for the above-defined continuous-time Markov chain is decomposed as*

$$\mathcal{R}\left(Q^\theta_{0:T} \mid Q^{\theta+\epsilon}_{0:T}\right) = \mathcal{R}\left(\nu^\theta \mid \nu^{\theta+\epsilon}\right) + \int_0^T \mathcal{H}\left(Q^\theta_t \mid Q^{\theta+\epsilon}_t\right) dt\,, \tag{15}$$

where the instantaneous relative entropy is equal to

$$\mathcal{H}\left(Q^\theta_t \mid Q^{\theta+\epsilon}_t\right) = \mathbb{E}_{Q^\theta_{0:t}}\left[\lambda^\theta(X_{t-}) \log \frac{c^\theta(X_{t-}, X_t)}{c^{\theta+\epsilon}(X_{t-}, X_t)} - \left(\lambda^\theta(X_t) - \lambda^{\theta+\epsilon}(X_t)\right)\right]. \tag{16}$$

(b) Assuming that the transition rate function $c^\theta(\cdot,\cdot)$ is differentialble w.r.t. the parameter vector θ, the pathwise FIM is also decomposed as

$$\mathcal{I}\big(Q^\theta_{0:T}\big) = \mathcal{I}\big(\nu^\theta\big) + \int_0^T \mathcal{I}_{\mathcal{H}}\big(Q^\theta_t\big)dt\,, \tag{17}$$

where the instantaneous pathwise FIM is given by

$$\mathcal{I}_{\mathcal{H}}\big(Q^\theta_t\big) = \mathbb{E}_{Q^\theta_{0:t}}\left[\lambda^\theta(X_{t-})\nabla_\theta \log c^\theta(X_{t-}, X_t)\nabla_\theta \log c^\theta(X_{t-}, X_t)^T\right]. \tag{18}$$

Proof (a) As in the discrete-time case, the key element is an explicit formula for the Radon-Nikodym derivative. The Radon-Nikodym derivative of the path distribution $Q^{\theta}_{0:T}$ w.r.t. the perturbed path distribution $Q^{\theta+\epsilon}_{0:T}$ has an explicit formula known also as Girsanov formula [18, 23],

$$\frac{dQ^{\theta}_{0:T}}{dQ^{\theta+\epsilon}_{0:T}}(\{X_t\}_{t=0}^{T}) = \cdots$$
$$\cdots = \frac{\nu^{\theta}(X_0)}{\nu^{\theta+\epsilon}(X_0)} \exp\left\{ \int_0^T \log \frac{c^{\theta}(X_{t-}, X_t)}{c^{\theta+\epsilon}(X_{t-}, X_t)} dN_t - \int_0^T [\lambda^{\theta}(X_t) - \lambda^{\theta+\epsilon}(X_t)]\, dt \right\},$$

where ν^{θ} (resp. $\nu^{\theta+\epsilon}$) is the initial distributions of $\{X_t\}_{t\in\mathbb{R}_+}$ (resp. $\{\bar{X}_t\}_{t\in\mathbb{R}_+}$) while N_t is the counting measure, i.e., counts the number of jumps in the process up to time t. Using the Girsanov formula, the pathwise relative entropy is rewritten as

$$\begin{aligned}
&\mathcal{R}\left(Q^{\theta}_{0:T} \mid Q^{\theta+\epsilon}_{0:T}\right) \\
&= \mathbb{E}_{Q^{\theta}_{0:T}}\left[\log \frac{\nu^{\theta}(X_0)}{\nu^{\theta+\epsilon}(X_0)} + \int_0^T \log \frac{c^{\theta}(X_{t-}, X_t)}{c^{\theta+\epsilon}(X_{t-}, X_t)}\, dN_t - \int_0^T [\lambda^{\theta}(X_t) - \lambda^{\theta+\epsilon}(X_t)]\, dt \right] \\
&= \mathbb{E}_{Q^{\theta}_{0:T}}\left[\log \frac{\nu^{\theta}(X_0)}{\nu^{\theta}(X_0)} \right] + \mathbb{E}_{Q^{\theta}_{0:T}}\left[\int_0^T \log \frac{c^{\theta}(X_{t-}, X_t)}{c^{\theta+\epsilon}(X_{t-}, X_t)}\, dN_t \right] - \cdots \\
&\qquad \cdots - \mathbb{E}_{Q^{\theta}_{0:T}}\left[\int_0^T [\lambda^{\theta}(X_t) - \lambda^{\theta+\epsilon}(X_t)]\, dt \right].
\end{aligned}$$

Exploiting the fact that the process $M_T := N_T - \int_0^t \lambda^{\theta}(X_t) dt$ is a martingale, we have that

$$\mathbb{E}_{Q^{\theta}_{0:T}}\left[\int_0^T \log \frac{c^{\theta}(X_{t-}, X_t)}{ac\theta + \epsilon(X_{t-}, X_t)}\, dN_t \right] = \mathbb{E}_{Q^{\theta}_{0:T}}\left[\int_0^T \lambda^{\theta}(X_{t-}) \log \frac{c^{\theta}(X_{t-}, X_t)}{c^{\theta+\epsilon}(X_{t-}, X_t)}\, dt \right].$$

Thus, the pathwise relative entropy is rewritten as

$$\begin{aligned}
&\mathcal{R}\left(Q^{\theta}_{0:T} \mid Q^{\theta+\epsilon}_{0:T}\right) \\
&= \mathcal{R}\left(\nu^{\theta} \mid \nu^{\theta+\epsilon}\right) + \mathbb{E}_{Q^{\theta}_{0:T}}\left[\int_0^T \lambda^{\theta}(X_{t-}) \log \frac{c^{\theta}(X_{t-}, X_t)}{c^{\theta+\epsilon}(X_{t-}, X_t)} - \left(\lambda^{\theta}(X_t) - \lambda^{\theta+\epsilon}(X_t)\right) dt \right] \\
&= \mathcal{R}\left(\nu^{\theta} \mid \nu^{\theta+\epsilon}\right) + \int_0^T \mathbb{E}_{Q^{\theta}_{0:T}}\left[\lambda^{\theta}(X_{t-}) \log \frac{c^{\theta}(X_{t-}, X_t)}{c^{\theta+\epsilon}(X_{t-}, X_t)} - \left(\lambda^{\theta}(X_t) - \lambda^{\theta+\epsilon}(X_t)\right) \right] dt \\
&= \mathcal{R}\left(\nu^{\theta} \mid \nu^{\theta+\epsilon}\right) + \int_0^T \mathcal{H}\left(Q^{\theta}_t \mid Q^{\theta+\epsilon}_t\right) dt,
\end{aligned}$$

where the instantaneous relative entropy is defined as

$$\mathcal{H}\left(Q_t^\theta \mid Q_t^{\theta+\epsilon}\right) = \mathbb{E}_{Q_{0:t}^\theta}\left[\lambda^\theta(X_{t-}) \log \frac{c^\theta(X_{t-}, X_t)}{c^{\theta+\epsilon}(X_{t-}, X_t)} - \left(\lambda^\theta(X_t) - \lambda^{\theta+\epsilon}(X_t)\right)\right].$$

(b) Even though not directly evident from (16), the instantaneous relative entropy for continuous-time Markov chains is locally a quadratic function of the parameter vector θ. Indeed, defining the rate difference $\delta c(x, x') = c^{\theta+\epsilon}(x, x') - c^\theta(x, x')$, the instantaneous relative entropy can be rewritten as

$$\begin{aligned}
&\mathcal{H}\left(Q_t^\theta \mid Q_t^{\theta+\epsilon}\right) \\
&= -\mathbb{E}_{Q_{0:t}^\theta}\left[\lambda^\theta(X_{t-}) \log\left(1 + \frac{\delta c(X_{t-}, X_t)}{c^\theta(X_{t-}, X_t)}\right)\right] - \mathbb{E}_{Q_{0:t}^\theta}\left[\lambda^\theta(X_t) - \lambda^{\theta+\epsilon}(X_t)\right] \\
&= -\mathbb{E}_{Q_{0:t}^\theta}\left[\lambda^\theta(X_{t-})\left(\frac{\delta c(X_{t-}, X_t)}{c^\theta(X_{t-}, X_t)} - \frac{1}{2}\left(\frac{\delta c(X_{t-}, X_t)}{c^\theta(X_{t-}, X_t)}\right)^2 + O(|\delta c(X_{t-}, X_t)|^3)\right)\right] \\
&+ \mathbb{E}_{Q_{0:t}^\theta}\left[\lambda^{\theta+\epsilon}(X_t) - \lambda^\theta(X_t)\right] \\
&= \frac{1}{2}\mathbb{E}_{Q_{0:t}^\theta}\left[\lambda^\theta(X_{t-})\left(\frac{\delta c(X_{t-}, X_t)}{c^\theta(X_{t-}, X_t)}\right)^2\right] + O(|\delta c|^3)
\end{aligned}$$

Due to the differentiability assumption on the transition rates in a neighborhood of parameter vector θ a Taylor series expansion of $\delta c(x, x') = \epsilon^T \nabla_\theta c^\theta(x, x') + O(|\epsilon|^2)$ results in

$$\begin{aligned}
&\mathcal{H}\left(Q_t^\theta \mid Q_t^{\theta+\epsilon}\right) \\
&= \frac{1}{2}\mathbb{E}_{Q_{0:t}^\theta}\left[\lambda^\theta(X_{t-})\left(\frac{\delta c(X_{t-}, X_t)}{c^\theta(X_{t-}, X_t)}\right)^2\right] + O(|\delta c|^3) \\
&= \frac{1}{2}\epsilon^T \mathbb{E}_{Q_{0:t}^\theta}\left[\lambda^\theta(X_{t-})\frac{\nabla_\theta c^\theta(X_{t-}, X_t)\nabla_\theta c^\theta(X_{t-}, X_t)^T}{c^\theta(X_{t-}, X_t)^2}\right]\epsilon + O(|\epsilon|^3) \\
&= \frac{1}{2}\epsilon^T \mathcal{I}_\mathcal{H}\left(Q_t^\theta\right)\epsilon + O(|\epsilon|^3)
\end{aligned}$$

where

$$\mathcal{I}_\mathcal{H}\left(Q_t^\theta\right) = \mathbb{E}_{Q_{0:t}^\theta}\left[\lambda^\theta(X_{t-})\nabla_\theta \log c^\theta(X_{t-}, X_t)\nabla_\theta \log c^\theta(X_{t-}, X_t)^T\right],$$

is the instantaneous FIM. Finally, the pathwise FIM is obtained from a straightforward expansion of each element of the pathwise relative entropy in terms of ϵ. It is given by

$$\mathcal{I}\left(Q_{0:T}^\theta\right) = \mathcal{I}\left(\nu^\theta\right) + \int_0^T \mathcal{I}_\mathcal{H}\left(Q_t^\theta\right) dt\,,$$

where $\mathcal{I}(\nu^\theta)$ is the FIM of the initial distribution while $\mathcal{I}_{\mathcal{H}}(Q_t^\theta)$ is the instantaneous pathwise FIM computed above. □

Stationary regime: In the stationary regime, the instantaneous relative entropy is a constant function of time since at each time instant the distribution of the states is the—typically unknown—stationary distribution. The following corollary presents explicit formulas for the relative entropy rate and the associated FIM at the stationary regime.

Corollary 2 *The relative entropy rate is equal to the ergodic average*

$$\mathcal{H}\left(Q^\theta \mid Q^{\theta+\epsilon}\right) = \mathbb{E}_{\mu^\theta}\Big[\sum_{x'\in E} c^\theta(x,x')\log\frac{c^\theta(x,x')}{c^{\theta+\epsilon}(x,x')} - (\lambda^\theta(x) - \lambda^{\theta+\epsilon}(x))\Big], \quad (19)$$

while the FIM of the relative entropy rate, computed as its Hessian, has explicit formula given by

$$\mathcal{I}_{\mathcal{H}}(Q^\theta) = \mathbb{E}_{\mu^\theta}\left[\sum_{x'\in E} c^\theta(x,x')\nabla_\theta \log c^\theta(x,x')\nabla_\theta \log c^\theta(x,x')^T\right]. \quad (20)$$

Proof At the stationary regime, the instantaneous relative entropy is rewritten as

$$\begin{aligned}
&\mathcal{H}\left(Q_t^\theta \mid Q_t^{\theta+\epsilon}\right)\\
&= \mathbb{E}_{Q_{0:t}^\theta}\left[\lambda^\theta(X_{t-})\log\frac{c^\theta(X_{t-},X_t)}{c^{\theta+\epsilon}(X_{t-},X_t)} - \left(\lambda^\theta(X_t) - \lambda^{\theta+\epsilon}(X_t)\right)\right] \quad (21)\\
&= \mathbb{E}_{\mu^\theta}\Big[\sum_{x'\in E} c^\theta(x,x')\log\frac{c^\theta(x,x')}{c^{\theta+\epsilon}(x,x')} - (\lambda^\theta(x) - \lambda^{\theta+\epsilon}(x))\Big].
\end{aligned}$$

□

5 Stochastic Differential Equations—Markov Processes

Consider a Markov process $X_t \in \mathbb{R}^d$ satisfying a stochastic differential equation of the form

$$\begin{cases} dX_t = b^\theta(X_t)dt + \sigma(X_t)dW_t \\ X_0 \sim \nu^\theta \end{cases} \quad (22)$$

where b^θ is the drift function depending on the parameter vector θ, σ is the state-dependent diffusion matrix, W_t is a d-dimensional Brownian motion while ν^θ is the initial distribution of the process. Let $Q_{0:T}^\theta$ denote the path space distribution for a specific parameter vector θ. Consider also a perturbation vector, $\epsilon \in \mathbb{R}^K$, and

denote by $Q_{0:T}^{\theta+\epsilon}$ the path space distribution of the perturbed process $\bar{X}_t$ satisfying the stochastic differential equation (22) with perturbed drift function.

Under appropriate assumption on the components of the stochastic differential equation, the pathwise relative entropy can be decomposed as in the previous cases and an explicit formula for the instantaneous relative entropy can be estimated as the following theorem asserts.

Theorem 3 *(a) Assume that the diffusion matrix, $\sigma(x)$, is invertible for all $x \in \mathbb{R}^d$ and $\mathbb{E}_{Q_{0:T}^{\theta}}[\exp\{\int_0^T |\sigma^{-1}(X_t)(b^{\theta+\epsilon}(X_t) - b^{\theta}(X_t))|^2 \, dt\}] < \infty$ (Novikov condition). Then, the pathwise relative entropy for the above-defined Markov process is decomposed as*

$$\mathcal{R}\left(Q_{0:T}^{\theta} \mid Q_{0:T}^{\theta+\epsilon}\right) = \mathcal{R}\left(\nu^{\theta} \mid \nu^{\theta+\epsilon}\right) + \int_0^T \mathcal{H}\left(Q_t^{\theta} \mid Q_t^{\theta+\epsilon}\right) dt \,, \tag{23}$$

where the instantaneous relative entropy is equal to

$$\mathcal{H}\left(Q_t^{\theta} \mid Q_t^{\theta+\epsilon}\right) = \frac{1}{2}\mathbb{E}_{\nu_t^{\theta}}\left[\left|\sigma^{-1}(x)\left(b^{\theta+\epsilon}(x) - b^{\theta}(x)\right)\right|^2\right] . \tag{24}$$

(b) Assume further that the drift function b^{θ} is differentiable w.r.t. the parameter vector θ. Then, the pathwise FIM has a similar decomposition and the instantaneous FIM is given by

$$\mathcal{I}_{\mathcal{H}}\left(Q_t^{\theta}\right) = \mathbb{E}_{\nu_t^{\theta}}\left[\nabla_{\theta} b^{\theta}(x)^T (\sigma(x)\sigma(x)^T)^{-1} \nabla_{\theta} b^{\theta}(x)\right] . \tag{25}$$

where $\nabla_{\theta} b^{\theta}$ is a $d \times K$ matrix containing all the first-order partial derivatives of the drift vector (i.e., the Jacobian matrix).

Proof (a) The inversion of the diffusion matrix is a necessary assumption for the well-posedness of the Novikov condition which in turn suffices for the two path distributions $Q_{0:T}^{\theta}$ and $Q_{0:T}^{\theta+\epsilon}$ to be absolutely continuous w.r.t. each other [24]. Additionally, the Girsanov theorem provides an explicit formula of the Radon-Nikodym derivative [24] which is given by

$$\frac{dQ_{0:T}^{\theta}}{dQ_{0:T}^{\theta+\epsilon}}\left(\{(X_t)\}_{t=0}^T\right) = \frac{d\nu^{\theta}}{d\nu^{\theta+\epsilon}}(X_0) \exp\left\{-\int_0^T u(X_t)^T dW_t - \frac{1}{2}\int_0^T |u(X_t)|^2 dt\right\} ,$$

where $u(x) = \sigma^{-1}(x)\left(b^{\theta+\epsilon}(x) - b^{\theta}(x)\right)$. Furthermore, it holds that

$$\hat{W}_t := \int_0^t u(X_s) ds + W_t \,,$$

is a Brownian motion w.r.t. the unperturbed path distribution $Q^{\theta}_{0:T}$, meaning that, for any measurable function f, it holds $\mathbb{E}_{Q^{\theta}_{0:T}}\big[\int_0^T f(X_t)^T d\hat{W}_t\big] = 0$. Then,

$$\begin{aligned}
&\mathcal{R}\left(Q^{\theta}_{0:T} \mid Q^{\theta+\epsilon}_{0:T}\right) = \mathbb{E}_{Q^{\theta}_{0:T}}\left[\log \frac{d\nu^{\theta}}{d\nu^{\theta+\epsilon}}(X_0) - \int_0^T u(X_t)^T dW_t - \frac{1}{2}\int_0^T |u(X_t)|^2 dt\right] \\
&= \mathbb{E}_{Q^{\theta}_{0:T}}\left[\log \frac{d\nu^{\theta}}{d\nu^{\theta+\epsilon}}(X_0)\right] - \mathbb{E}_{Q^{\theta}_{0:T}}\left[\int_0^T u(X_t)^T d\hat{W}_t\right] + \frac{1}{2}\mathbb{E}_{Q^{\theta}_{0:T}}\left[\int_0^T |u(X_t)|^2 dt\right] \\
&= \mathcal{R}\left(\nu^{\theta} \mid \nu^{\theta+\epsilon}\right) + \frac{1}{2}\mathbb{E}_{Q^{\theta}_{0:T}}\left[\int_0^T |u(X_t)|^2 dt\right] \\
&= \mathcal{R}\left(\nu^{\theta} \mid \nu^{\theta+\epsilon}\right) + \int_0^T \frac{1}{2}\mathbb{E}_{Q^{\theta}_{0:T}}\left[|u(X_t)|^2\right] dt \\
&= \mathcal{R}\left(\nu^{\theta} \mid \nu^{\theta+\epsilon}\right) + \int_0^T \frac{1}{2}\mathbb{E}_{\nu^{\theta}_t}|u(X_t)|^2 dt
\end{aligned}$$

where ν^{θ}_t is the distribution of the process at time instant t. Hence the instantaneous relative entropy is explicitly given by

$$\mathcal{H}\left(Q^{\theta}_t \mid Q^{\theta+\epsilon}_t\right) = \frac{1}{2}\mathbb{E}_{\nu^{\theta}_t}\left[\left|\sigma^{-1}(x)\left(b^{\theta+\epsilon}(x) - b^{\theta}(x)\right)\right|^2\right]$$

(b) Due to the differentiability assumption, a Taylor expansion of the drift function around the point θ results in $b^{\theta+\epsilon}(x) - b^{\theta}(x) = \nabla_{\theta} b^{\theta}(x)\epsilon + O(|\epsilon|^2)$ where $\nabla_{\theta} b^{\theta}$ is a $d \times K$ matrix containing all the first-order partial derivatives of the drift vector function (i.e., the Jacobian matrix). Then, it is straightforward to obtain from (24) that

$$\mathcal{I}_{\mathcal{H}}\big(Q^{\theta}_t\big) = \mathbb{E}_{\nu^{\theta}_t}\left[\nabla_{\theta} b^{\theta}(x)^T (\sigma(x)\sigma(x)^T)^{-1} \nabla_{\theta} b^{\theta}(x)\right].$$

□

Stationary regime: In the stationary regime, the instantaneous relative entropy becomes a constant function of time since the distribution of the process is equal to the stationary distribution denoted by μ^{θ} for all times. The following corollary presents explicit formulas for the relative entropy rate and the associated FIM.

Corollary 3 *Let $X_0 \sim \mu^{\theta}$. Under the assumptions of Theorem 3 the relative entropy rate is equal to*

$$\mathcal{R}\left(Q^{\theta} \mid Q^{\theta+\epsilon}\right) = \frac{1}{2}\mathbb{E}_{\mu^{\theta}}\left[\left|\sigma^{-1}(x)\left(b^{\theta+\epsilon}(x) - b^{\theta}(x)\right)\right|^2\right], \tag{26}$$

while the FIM associated with the relative entropy rate is given by

$$\mathcal{I}_{\mathcal{H}}\big(Q^{\theta}\big) = \mathbb{E}_{\mu^{\theta}}[\nabla_{\theta} b^{\theta}(x)^T (\sigma(x)\sigma(x)^T)^{-1} \nabla_{\theta} b^{\theta}(x)]. \tag{27}$$

We finally remark that a popular method for modeling non-equilibrium systems in atomistic and mesoscopic scales is based on the Langevin equation. Langevin equation is a degenerate system of stochastic differential equations whose sensitivity analysis based on the relative entropy rate and the associated pathwise FIM was performed in [25].

6 Demonstration Example

In this section we give a numerical example of the pathwise relative entropy (6) and pathwise FIM (8) for a continuous time Markov chain model. More specific, a biological reaction network is considered and the quantities instantaneous RE (16) and instantaneous FIM (18) are presented as a function of time.

6.1 Continuous Time Markov Chains: An EGFR Model

In [26], Kholodenko et al. proposed a reaction network that describes signaling phenomena of mammalian cells [27–29]. The reaction network consists of $N = 23$ species and $M = 47$ reactions. The propensity function for the R_j reaction, $j = 1, \ldots, 47$ and $j \neq 7, 14, 29$, obeys the law of mass action [2],

$$a_j(\mathbf{x}) = k_j \binom{\mathbf{x}_{A_j}}{\alpha_j} \binom{\mathbf{x}_{B_j}}{\beta_j}, \tag{28}$$

for a reaction of the general form "$\alpha_j A_j + \beta_j B_j \xrightarrow{k_j} \ldots$", where A_j and B_j are the reactant species, α_j and β_j are the respective number of molecules needed for the reaction, k_j the reaction constant and $\mathbf{x}_{A_j}$ and $\mathbf{x}_{B_j}$ is the total number of species A_j and B_j, respectively. The binomial coefficient is defined by $\binom{n}{k} = \frac{n!}{k!(n-k)!}$. The propensity functions for reactions R_7, R_{14}, R_{29} are being described by the Michaelis-Menten kinetics, see [2],

$$a_j(\mathbf{x}) = V_j \mathbf{x}_{A_j} / \left(K_j + \mathbf{x}_{A_j}\right), \quad j = 7, 14, 29\,, \tag{29}$$

where V_j represents the maximum rate achieved by the system at maximum (saturating) substrate concentrations while K_j is the substrate concentration at which the reaction rate is half the maximum value. The parameter vector contains all the reaction constants,

$$\theta = [k_1, \ldots, k_6, k_8, \ldots, k_{13}, k_{15}, \ldots, k_{28}, k_{30}, \ldots, k_{47}, V_7, K_7, V_{14}, K_{14}, V_{29}, K_{29}]^T\,. \tag{30}$$

In this study the values of the reaction constants are the same as in [26].

For the initial data and parameters chosen in this study, the time series can be split into two regimes: (a) a transient regime that approximately corresponds to the time interval [0, 50] and (b) a stationary regime which approximately corresponds to the time interval [50, ∞).

Next, we discuss two sensitivity measures of the process $\{X_s\}_{s=0}^t$: the instantaneous RE defined in (16)

$$f\left(\{X_s\}_{s=0}^t\right) = \mathcal{H}\left(Q_t^\theta \mid Q_t^{\theta+\epsilon}\right) = \mathbb{E}_{\nu_t^\theta}\Big[\sum_{j=1}^M a_j^\theta(\mathbf{x}) \log \frac{a_j^\theta(\mathbf{x})}{a_j^{\theta+\epsilon}(\mathbf{x})} - \left(a_0^\theta(\mathbf{x}) - a_0^{\theta+\epsilon}(\mathbf{x})\right)\Big], \tag{31}$$

with $t \in [0, T]$ and the averaged RE, defined as

$$g\left(\{X_s\}_{s=0}^t\right) = \frac{1}{t}\int_0^t \mathcal{H}\left(Q_s^\theta \mid Q_s^{\theta+\epsilon}\right) ds, \quad t \in [0, T]\,. \tag{32}$$

In Fig. 1 the two sensitivity measures are presented for $T = 100$. As expected, the averaged RE is smoother than the instantaneous RE while some of the qualitative characteristics remain. On the other hand, quantitative characteristics, such as the time that two instantaneous RE are crossed, are not preserved in the averaged RE. The averaged RE in the interval $[0, t]$ should be interpreted as a measure of the information accumulated in the whole interval while the instantaneous RE is a measure of the information at the time instant t. Moreover, the second observable can be used as part of an upper bound for a different sensitivity measure, see [15] for a detailed discussion.

Let us define a different sensitivity measure as the relative difference between the kth species of two systems were the ℓth parameter of the second is perturbed by ϵ',

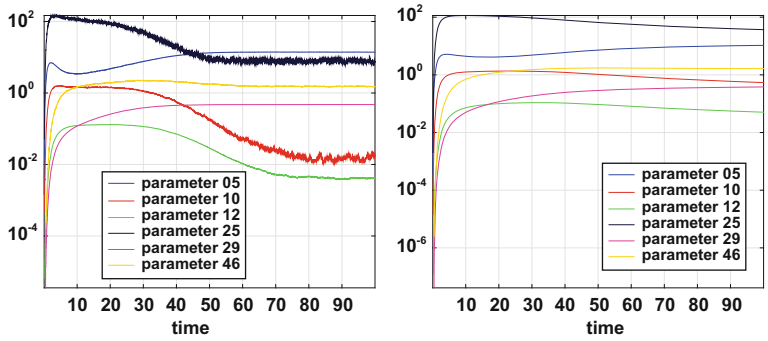

Fig. 1 The instantaneous RE, defined in (15), for the EGFR model (*left*) and the averaged RE, defined in (32) (*right*)

$$S_{k,\ell,t} := \frac{X^{\theta}_{k,t} - X^{\theta+\epsilon_\ell}_{k,t}}{X^{\theta}_{k,t}} \,. \tag{33}$$

where ϵ_ℓ is a vector with zeros everywhere and ϵ' in the ℓth position. In the following examples the value of ϵ' for a perturbation in the ℓth parameter is $\epsilon' = 0.1\theta_\ell$. By summing over all species we obtain a total sensitivity measure, which is only indexed by the parameter index and time,

$$S_{\ell,t} = \frac{1}{N}\sum_{k=1}^{N} S_{k,\ell,t} \,. \tag{34}$$

By observing the first row of Fig. 2, which shows the instantaneous RE (16) for $\ell = 10$ and $\ell = 29$, we learn that perturbations in the 10th parameter have large sensitivity for small times and as time varies the sensitivity is getting smaller. On the other hand, perturbations in the 29th parameter have small influence on the system for small times while for larger times the sensitivity becomes significant. These observations are in good agreement with the sensitivity measure (33) presented in the second and third row of Fig. 2.

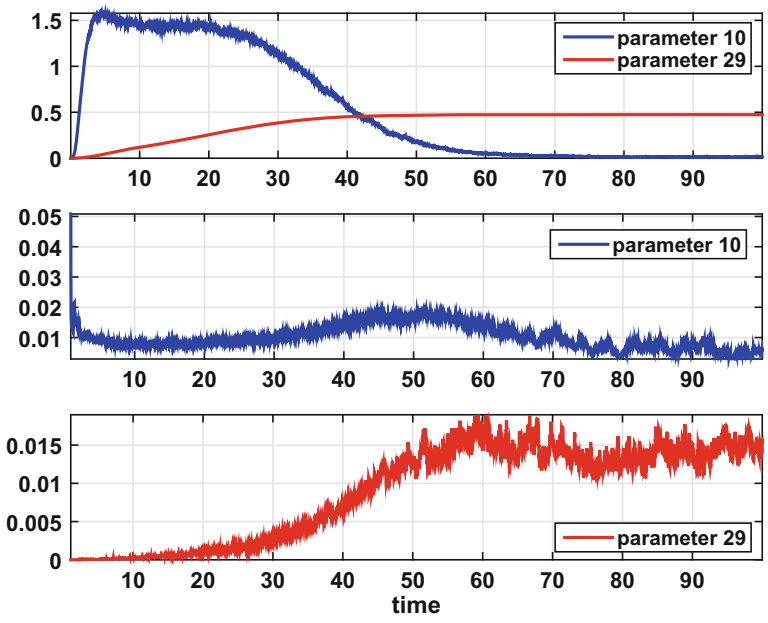

Fig. 2 Instantaneous RE (15) for the EGFR model and parameters 10 and 29 (*first row*). The total sensitivity of the system, as defined in (34), due to perturbations in the 10th parameter (*second row*) and due to the 29th parameter (*third row*)

Moreover there is a crossing in the instantaneous RE which happens around $t = 42$. After this time the sensitivity in parameter $\ell = 29$ becomes more significant than the sensitivity in parameter $\ell = 10$. This is again in agreement with the behavior of the sensitivity measure (33). This observation shows that the transient regime is more sensitive in perturbations in the 10th parameter while the equilibrium is more sensitive in perturbations in the 29th parameter.

7 Conclusions

In this paper we presented two pathwise sensitivity measures for the analysis of stochastic systems; the instantaneous relative entropy and its approximation, the instantaneous Fisher information matrix. These sensitivity tools serve as an extension to transient processes of the sensitivity tools presented in [13]. Three examples, discrete-time Markov chains, continuous-time Markov Chains and stochastic differential equations, were presented as an application of the new sensitivity measures. In Sect. 6 we demonstrated, in a biological reaction network, how the proposed pathwise sensitivity measure can be applied to transient, as well as in steady state regimes.

Finally, the pathwise sensitivity method is directly connected to a different sensitivity measure that depends on specific observables. More specifically, if we define the sensitivity index (SI) of the ℓth observable to the kth parameter as

$$S_{k,\ell} = \frac{\partial}{\partial \theta_k} \mathbb{E}\left[f_\ell \left(\{X_s\}_{s=0}^T \right) \right] , \tag{35}$$

then IFIM (18) serves as un upper bound of $S_{k,\ell}$ through the inequality,

$$|S_{k,\ell}| \leq \sqrt{\mathrm{Var}_{Q^\theta_{0:T}}(f_\ell)} \sqrt{\mathcal{I}\left(Q^\theta_{0:T}\right)_{k,k}} , \tag{36}$$

where $F = (f_1, \ldots, f_L)$ is a vector of observable functions. This inequality follows by rearranging the generalized Cramer-Rao bound for a biased estimator [30, 31]. Due to low variance of the estimator of IFIM compared to the variance of a finite difference estimator of $S_{k,\ell}$, the estimation of the right hand side of (36) is faster than that of the left hand side of (36). In [15] the authors used this inequality to efficiently screen out and exclude low sensitivity indices under a pre-specified value and then performed a coupling finite difference algorithm [8] to accurately estimate the remaining sensitivity indices $S_{k,\ell}$. In Fig. 3 the estimated SIs for the EGFR model discussed in Sect. 6 are ordered in the parameter direction using only the IFIM (18). Notice that the SIs are then grouped into four distinct regions. For a detailed presentation of this methodology we refer to [15].

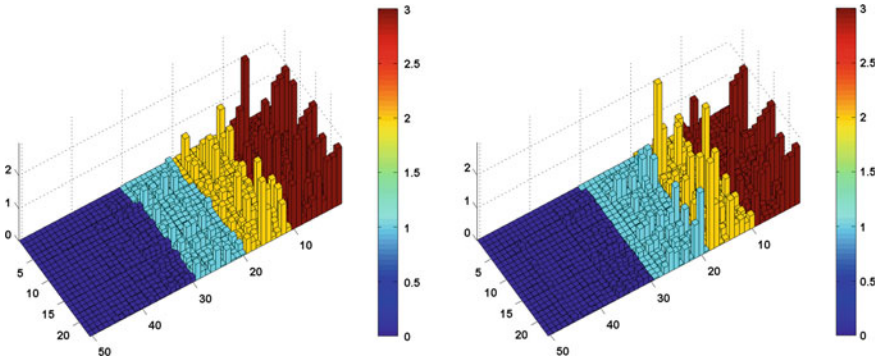

Fig. 3 Ordering of the sensitivity index (35) in the time interval [0, 50] (*left*) and [0, 100] (*right*) utilizing the averaged IRE (32). In this case $f_\ell\left(\{X_s\}_{s=0}^T\right) = \frac{1}{T}\int_0^T X_{\ell,s}ds$, which is the mean concentration of the ℓth species in time interval $[0, T]$

Acknowledgments The work of the authors was supported by the Office of Advanced Scientific Computing Research, U.S. Department of Energy, under Contract No. DE-SC0010723 and by the European Union (European Social Fund) and Greece (National Strategic Reference Framework), under the THALES Program, grant AMOSICSS.

References

1. Saltelli A, Ratto M, Andres T, Campolongo F, Cariboni J, Gatelli D, Saisana M, Tarantola S (2008) Global sensitivity analysis. The primer. Wiley, New York
2. DiStefano III J (2013) Dynamic systems biology modeling and simulation. Elsevier, New York
3. Glynn PW (1990) Likelihood ratio gradient estimation for stochastic systems. Commun ACM 33(10):75–84
4. Nakayama M, Goyal A, Glynn PW (1994) Likelihood ratio sensitivity analysis for Markovian models of highly dependable systems. Stoch Models 10:701–717
5. Plyasunov S, Arkin AP (2007) Efficient stochastic sensitivity analysis of discrete event systems. J Comput Phys 221:724–738
6. Kim D, Debusschere BJ, Najm HN (2007) Spectral methods for parametric sensitivity in stochastic dynamical systems. Biophys J 92:379–393
7. Rathinam M, Sheppard PW, Khammash M (2010) Efficient computation of parameter sensitivities of discrete stochastic chemical reaction networks. J Chem Phys 132(1–13):034103
8. Anderson David F (2012) An efficient finite difference method for parameter sensitivities of continuous-time Markov chains. SIAM J Numer Anal 50(5):2237–2258
9. Sheppard PW, Rathinam M, Khammash M (2012) A pathwise derivative approach to the computation of parameter sensitivities in discrete stochastic chemical systems. J Chem Phys 136(3):034115
10. Meskine H, Matera S, Scheffler M, Reuter K, Metiu H (2009) Examination of the concept of degree of rate control by first-principles kinetic Monte Carlo simulations. Surf Sci 603(10–12):1724–1730
11. Baiesi M, Maes C, Wynants B (2009) Nonequilibrium linear response for Markov dynamics I: jump processes and overdamped diffusions. J Stat Phys 137:1094
12. Baiesi M, Maes C, Boksenbojm E, Wynants B (2010) Nonequilibrium linear response for markov dynamics, II: Inertial dynamics. J Stat Phys 139:492

13. Pantazis Y, Katsoulakis M (2013) A relative entropy rate method for path space sensitivity analysis of stationary complex stochastic dynamics. J Chem Phys 138(5):054115
14. Dupuis P, Katsoulakis MA, Pantazis Y, Plecháč P Sesnitivity bounds and error estimates for stochastic models (in Preparation)
15. Arampatzis G, Pantazis Y, Katsoulakis MA Accelerated sensitivity analysis in high-dimensional stochastic reaction networks. Submitted to PLoS ONE
16. Kullback S (1959) Information theory and statistics. Wiley, New York
17. Cover T, Thomas J (1991) Elements of information theory. Wiley, New York
18. Kipnis C, Landim C (1999) Scaling limits of interacting particle systems. Springer, Berlin
19. Avellaneda M, Friedman CA, Holmes R, Samperi DJ (1997) Calibrating volatility surfaces via relative-entropy minimization. Soc Sci Res Netw
20. Liu HB, Chen W, Sudjianto A (2006) Relative entropy based method for probabilistic sensitivity analysis in engineering design. J Mech Des 128:326–336
21. Limnios N, Oprisan G (2001) Semi-Markov processes and reliability. Springer, Berlin
22. Abramov RV, Grote MJ, Majda AJ (2005) Information theory and stochastics for multiscale nonlinear systems., CRM monograph series. American Mathematical Society, Providence
23. Liptser RS, Shiryaev AN (1977) Statistics of random processes: I & II. Springer, New York
24. Oksendal B (2000) Stochastic differential equations: an introduction with applications. Springer, New York
25. Tsourtis A, Pantazis Y, Harmandaris V, Katsoulakis MA Parametric sensitivity analysis for stochastic molecular systems using information theoretic metrics. Submitted to J Chem Phys
26. Kholodenko BN, Demin OV, Moehren G, Hoek J (1999) Quantification of short term signaling by the epidermal growth factor receptor. J Biol Chem 274(42):30169–30181
27. Moghal N, Sternberg PW (1999) Multiple positive and negative regulators of signaling by the EGF receptor. Curr Opin Cell Biol 11:190–196
28. Hackel PO, Zwick E, Prenzel N, Ullrich A (1999) Epidermal growth factor receptors: critical mediators of multiple receptor pathways. Curr Opin Cell Biol 11:184–189
29. Schoeberl B, Eichler-Jonsson C, Gilles ED, Muller G (2002) Computational modeling of the dynamics of the MAP kinase cascade activated by surface and internalized EGF receptors. Nat Biotechnol 20:370–375
30. Casella G, Berger RL (2002) Statistical inference. Duxbury advanced series in statistics and decision sciencesThomson Learning, London
31. Kay SM (1993) Fundamentals of statistical signal processing: estimation theory. Prentice-Hall, Englewood Cliffs

The Langevin Approach: A Simple Stochastic Method for Complex Phenomena

N. Reinke, A. Fuchs, W. Medjroubi, P.G. Lind, M. Wächter and J. Peinke

Abstract We describe a simple stochastic method, so-called Langevin approach, which enables one to extract evolution equations of stochastic variables from a set of measurements. Our method is parameter free and it is based on the nonlinear Langevin equation. Moreover, it can be applied not only to processes in time, but also to processes in scale, given that the data available shows ergodicity. This chapter introduces the mathematical foundations of this Langevin approach and describes how to implement it numerically. In addition, we present an application of the method to a turbulent velocity field measured in laboratory, retrieving the corresponding energy cascade and comparing with the results from a computer fluid dynamics (CFD) simulation of that experiment. Finally, we describe extensions of the method for time series reconstruction and applications to other fields such as finance, medicine, geophysics and renewable energies.

1 Introduction

"The present state of the universe is an effect of its past states and causes its future one". Such a claim is a fundamental assumption in every physical approach to our surrounding nature and was mathematically defended for the first time two centuries ago, in 1814, by Simon Laplace. Laplace had a dream [1], one where "an intellect at a certain moment would know all forces that set nature in motion, and all positions of all items of which nature is composed, […] vast enough to submit these data to analysis […], to embrace in a single formula [all movements of the universe]". Why was this a dream? Because there are strong arguments against it, such as thermodynamic irreversibility, quantic indeterminacy and nonlinear sensitivity to initial states. But there is also a practical reason: such a high-dimensional problem, due to its huge number of variables, would only be computable if one would take as model of reality the reality itself, an approach which is pointless. To model reality one needs

N. Reinke (✉) · A. Fuchs · W. Medjroubi · P.G. Lind · M. Wächter · J. Peinke
ForWind - Center for Wind Energy Research, Institute of Physics, Carl von Ossietzky University of Oldenburg, 26111 Oldenburg, Germany
e-mail: nico.reinke@uni-oldenburg.de

S. Heinz and H. Bessaih (eds.), *Stochastic Equations for Complex Systems*,
Mathematical Engineering, DOI 10.1007/978-3-319-18206-3_6

simplifications and stochastic methods enables one to simplify reality in several adequate ways. In this chapter we describe one of such ways, which, in the last 15 years, has been successfully applied in several fields [2].

As an illustration we address the problem of turbulence, one of the central open problems in physics [3]. A turbulent fluid is governed by the so-called Navier-Stokes equations which cannot be approached analytically in all their detail. Therefore one handles Navier-Stokes equations numerically, developing discretization schemes which yield the solution of one specific problem. Such discretization in space and time corresponds in general to high-dimensional problems which, in the limit of infinitely small discrete elements, leads to infinite many degrees of freedom. Such numerical approaches to the equations governing turbulence enabled rather successful insight and modeling approaches for fundamental physics and engineering applications [3].

However, the Navier-Stokes equations, which are purely deterministic, could be substituted by a stochastic approach, using only a few—the essential—variables, say X_i $(i = 1, \ldots, N)$ and incorporating the rest of the degrees of freedom in a "stochastic bag". In this way one arrives to evolution equations of the type:

$$\frac{dX_i}{dt} = F_i(X_1, \ldots, X_N, t) + G_i(X_1, \ldots, X_N, \Gamma_1, \ldots, \Gamma_M, t) \tag{1}$$

where function $F_i(X_1, \ldots, X_N)$ is a deterministic function depending on each variable X_i and function $G_i(X_1, \ldots, X_N, \Gamma_1, \ldots, \Gamma_M)$ depends not only on variables X_i but also on stochastic forces Γ_j $(j = 1, \ldots, M)$. For $G_i \equiv 0$, Eq. (1) reduces to a deterministic dynamical system and for $G_i \sim 0$ one can take it as a deterministic dynamical system subjected to small noise of constant amplitude [4].

In general however, not only function G cannot be neglected but it possesses a much more complicated (nonlinear) dependence on the accounted variables. Such functional dependence of G is important, for instance when one intends to describe physical features of a process underlying a set of data or when aiming at predicting or reconstructing a set of observations.

Having properly defined an equation such as Eq. (1), it should be possible to reconstruct series of values of one variable, say $X \equiv X_i$ in a statistical sense, i.e. it should be possible to derive the conditional probability:

$$p(X(t + \Delta t)|X(t), X(t - \Delta t), \ldots, X(t_0)) \tag{2}$$

for each set of values $X(k)$ with $k = t_0, \ldots, t$. See sketch in Fig. 1.

In this chapter we will describe in detail how to derive an evolution equation such as Eq. (1) from a set of measurements. Our method, so-called Langevin approach, is fully introduced in Sect. 2. In Sect. 3 the Langevin approach is applied to turbulence by using the data gained from an experimental study in Sect. 3.1. Furthermore, the Langevin approach is applied to a numerical simulation of the experimental study in

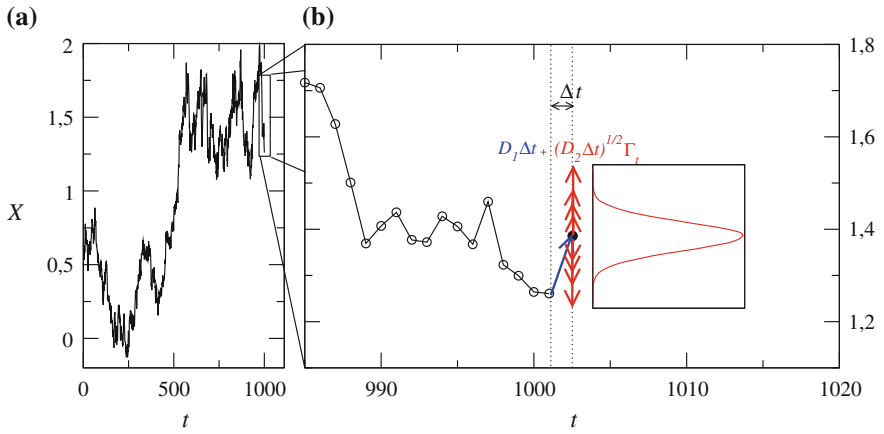

Fig. 1 Illustration of F and G in Eq. (1). The deterministic contribution, $F = D^{(1)}$, which drives the system according to $X \to X + F\Delta t$ and a stochastic contribution $G = \sqrt{D^{(2)}}\Gamma_t$ that is added to it, according to some probability distribution. Both functions $D^{(1)}$ and $D^{(2)}$ have a well-defined meaning and can be extracted from sets of measurements. See Sect. 2

Sect. 3.2. A comparative analysis, discussing the results obtained in the experiments and simulations is given in Sect. 3.3. Section 4 concludes this chapter, discussing briefly recent trends in the Langevin approach and other possible fields and topics where it can be successfully applied.

2 The Langevin Approach

To introduce the Langevin approach, we first explain in Sect. 2.1 what processes in scale[1] are and relate them with the usual processes in time. In Sect. 2.2, the necessary conditions under which the Langevin approach is applied are given together with a brief description of how to verify these conditions in empirical and simulated data. Section 2.3 describes the derivation of the deterministic and stochastic contributions with a given set of measurements taken from a process in scale. Finally, in Sect. 2.4 we derive the stochastic evolution equation describing a process in scale. A particular example is described, namely the "Brownian motion" in scale, using the Galton box as an illustration, which complements the usual Brownian motion described by Einstein [5] and Langevin [6].

[1] In statistics such processes are also known as branching processes.

2.1 Processes in Scale

There is a famous poem by Richardson [3] about turbulence which summarizes his important paper from 1920 [7]: "a turbulent fluid is composed by a few big eddies that decay into smaller eddies, these ones into even smaller eddies, and so on to viscosity". The energy that feeds the turbulent fluid enters the system on large scales—through the largest eddies—and travels towards smaller and smaller scales up to a minimum scale where it leaves the system by means of dissipation. In each of these steps the energy of the larger eddy is randomly distributed between the smaller "child" eddies. Such a pictorial view of turbulent energy traveling through a hierarchical succession of length scales leads to the concept of the turbulent energy cascade evolving in the spatial length scale as the independent variable.

One may ask if it would be possible to extract such energy cascade from empirical data, e.g. from a set of velocity measurements at one specific point of the fluid. In the following we show that indeed it is possible [2, 8, 9]. Describing how a property behaves across an ordered series of different spatial scales is analogous to the more common description of the evolution of a property in time, with the important difference that instead of the time-propagator in Eq. (2) one has now a "scale-propagator".

Assuming that one has a non-negligible stochastic contribution, the aim is to derive an equation analogous to Eq. (1) where the spatial scale r plays the role of time t. Since the independent variable r accounts for the size of some structure, like an eddy, we choose for the dependent variable the difference of an observable X at two distinct positions, separated by r, namely the *increment*

$$\Delta X_r(x) = X(x + r) - X(x) \tag{3}$$

with x being a specific location in the system. Thus, the scale-propagator describes how this increment—or difference—changes when the distance increases or decreases as follows:

$$p(\Delta X_{r+\Delta r} | \Delta X_r, \Delta X_{r-\Delta r}, \ldots, \Delta X_{r_0}). \tag{4}$$

Four important remarks are due here. First, the scale increment Δr in Eq. (4) can in general be positive or negative. In fact, as we will see in the next sections, the energy in turbulence flows from the largest scales, of the size of the system itself, toward the smallest scale at which dissipation takes place. Therefore, in turbulence one considers a scale-propagator as in (4) with $\Delta r < 0$.

Second, one should define a proper metric for the scale r. Is the spatial distance the best choice? Or is there a more appropriate functional of spatial distances? A process in time evolves according to an iteration from t to $t + dt$. The same should occur for processes in scale. However, when "iterating" from one scale to the "next", one iterates in a multiplicative way, i.e., from one scale to the next one multiplies the previous scale by some constant a, yielding a succession of scales $r_n = a^n \rightarrow r_{n+1} = a^{n+1} = ar_n$. A suitable choice of an additive scale, similar to the additive

time iteration, is the logarithmic scale $\log r$, since in this case one has $\log r_n = n \log a \rightarrow \log r_{n+1} = (n+1) \log a = \log r_n + \log a$. This logarithm scale is of importance to understand the concept of self-similarity, which is closely related to processes in scale. Self-similarity is the property that a phenomenon may manifest, by showing invariance under multiplicative changes of scale, as observed in turbulent flows. Indeed, following Richardson's poem, eddies are self-similar objects, since multiplying or dividing their size by a proper *scaling factor* we obtain an eddy again. With the logarithmic scale we "convert" the multiplicative changes into additive ones.

Third, when analyzing processes in scale, ideally one would consider a field of measurements taken simultaneously within a spatially extended region. What one typically has, contrastingly, is a set of measurements *in time* taken at a particular location. To extract processes in scale from single time series, one requires the property being measured to be ergodic: the system should display the same behaviour averaged either over time or over the space of all the system's states. In the particular case of a turbulent fluid, ergodicity reduces to the so-called Taylor hypothesis [3].

Fourth, while the derivation of a propagator in scale may be helpful for uncovering phenomena such as the energy cascade in turbulence, one may also aim to bridge from the derived propagator in scale to a propagator in time which would enable time-series reconstruction. As shown in previous works [10], our Langevin approach enables such bridging from scale to time.

Henceforth, we will consider a process in scale, i.e. a succession of increments ΔX_s of a measurable property X, with:

$$s = \log\left(\frac{R_{max}}{r}\right) \tag{5}$$

taking values from $s_0 = 0$ (largest scale $r = R_{max}$) to $s_L = \log\left(R_{max}/R_{min}\right)$ at the smallest scale $r = R_{min}$. Notice that, $ds = -dr/r$ and therefore, for $dr < 0$ one arrives again at a positive scale increment.

2.2 Necessary Conditions: Stationarity and the Markov Property

To apply our method, two important features must be met. First, the set of measures from which one extracts the succession of increments in scale must be a stationary process. Second, the process in scale must be Markovian.

For the process X_t to be stationary, the corresponding conditional probability in Eq. (2) should be invariant under a translation in time, $t \rightarrow t + T$, $\forall T$. Numerically such property cannot be tested in sets of measurements. As an alternative, one usually divides the set of measurements in n subsets of $N/n \gg 1$ data points and computes

the first four centred moments. In case the centred moments do not vary significantly from one subset to the next one, the set of measurements is taken as stationary.

The Markov condition of the scale process reads [11]:

$$p(\Delta X_{s+\Delta s}|\Delta X_s, \Delta X_{s-\Delta s}, \ldots, \Delta X_{s_0}) = p(\Delta X_{s+\Delta s}|\Delta X_s). \tag{6}$$

Notice that, an important consequence of the Markov condition is that any n-point statistics on X can be extracted from the two-point statistics [12] on the increments, $p(\Delta X_{s+\Delta s}, \Delta X_s)$, i.e. three-point statistics on X. The two-point joint distribution of the increments contains all the information of the scale process.

Equation (6) tells us that, any conditional probability distribution from the process conditioned to an arbitrarily large number of previous observations equals the condition probability conditioned to the single previous observation solely. Again, such condition is not possible to ascertain in all its mathematical detail. A weaker version of Eq. (6) suitable for numerical implementation is:

$$p(\Delta X_{s+\Delta s}|\Delta X_s, \Delta X_{s-\Delta s}) = p(\Delta X_{s+\Delta s}|\Delta X_s). \tag{7}$$

Both conditions in Eqs. (6) and (7) are equivalent under the physically reasonable assumption that the dependency of the future state on previous states decreases monotonically with the time-lag. The equality in Eq. (7) can be qualitatively verified by plotting contour plots in the range of observed values for $\Delta X_{s+\Delta s}$ and ΔX_s, and fixing $\Delta X_{s-\Delta s} = \tilde{X}$. It can also be quantitatively tested through the Wilcoxon test [13], χ^2-test, or by computing a Kullback-Leibler distance between both conditional distributions [14].

2.3 The Fokker-Planck Equation for Increments

Once the stationarity of our measures as well as the Markov condition for their increments are fulfilled, we are able to determine multipoint statistics for our increments. Since the process is Markovian in scale, it can be easily proven that for any integer N one has:

$$p(\Delta X_s, \Delta X_{s-\Delta s}, \Delta X_{s-2\Delta s}, \ldots, \Delta X_{s-N\Delta s}) =$$

$$\left[\prod_{k=1}^{N} \frac{p(\Delta X_{s-(k-1)\Delta s}, \Delta X_{s-k\Delta s})}{p(\Delta X_{s-k\Delta s})}\right] p(\Delta X_{s-N\Delta s}) \quad , \tag{8}$$

and

$$p(\Delta X_{s-k\Delta s}) = \int_{-\infty}^{\infty} p(\Delta X_{s-(k-1)\Delta s}, \Delta X_{s-k\Delta s}) d\Delta X_{s-(k-1)\Delta s}, \tag{9}$$

for all $k = 1, \ldots, N$. Thus, all information of our process is incorporated in the two-point statistics of the increments.

It is known that [12], the conditional probability distributions obeys the so-called Kramers-Moyal (KM) equation:

$$\frac{\partial}{\partial s} p(\Delta X_s | \Delta X_{s_0}) = \sum_{k=1}^{\infty} \left(-\frac{\partial}{\partial (\Delta X)} \right)^k D^{(k)}(\Delta X, s) p(\Delta X_s | \Delta X_{s_0}), \tag{10}$$

with functions $D^{(k)}$, so-called KM coefficients, being defined through conditional moments $M^{(k)}$ in the limit of small scale increments, namely:

$$D^{(k)}(\Delta X, s) = \lim_{\Delta s \to 0} \frac{M^{(k)}(\Delta X, s, \Delta s)}{k! \Delta s} \tag{11a}$$

$$M^{(k)}(\Delta X, s, \Delta s) = \int_{-\infty}^{\infty} (Y - \Delta X)^k \, p(Y | \Delta X_s) dY. \tag{11b}$$

Notice that, from Eq. (11a), one can see that mathematically each KM coefficient of order k, apart a multiplicative constant $1/k!$, is the derivative of the conditional moment of the same order k.

Numerically, there are two ways for deriving KM coefficients. One is by computing the conditional moments $M^{(k)}$ for a range of observed values of ΔX and s, which is divided in a certain number of bins, and repeating the computation for several values of Δs. In the case where the conditional moments depend linearly on Δs, at least for the lower range of values, the KM coefficients are taken as the slope of the linear interpolation of the corresponding conditional moment in that range of values. In case such linear dependency is not observed, a second procedure is possible: one computes at once the entire fraction within the limit in Eq. (11a) again for a range of observed values of ΔX and s, divided in a proper number of bins, but this time one takes the range of smallest values of Δs and through a linear interpolates infers the projection in the plane $\Delta s = 0$.

The error for $D^{(k)}$ are just given by the linear interpolation of the corresponding conditional moments as functions of Δs. The errors of each value $M^{(k)}(\Delta X, s)$, necessary for computing the errors of the linear interpolation, are given by [15]:

$$\sigma^2_{M^{(k)}}(\Delta X, \Delta s) = M^{(2k)}(\Delta X, \Delta s) - \left[M^{(k)}(\Delta X, \Delta s) \right]^2. \tag{12}$$

The KM equation (10) also holds for the single probability distribution, since multiplying both sides by $p(\Delta X_{s_0})$ and integrating in ΔX_{s_0} yields the same equation for $p(\Delta X_s)$.

An important simplification in Eq. (10) follows if the fourth KM coefficient vanishes or is sufficiently small compared to the first two KM coefficients. Such simplification is based on Pawula's Theorem which states that if $D^{(4)} \equiv 0$ then all

coefficients in Eq. (10) are identically zero except the first two. Consequently the Kramers-Moyal equation reduces to the so-called Fokker-Planck equation:

$$\frac{\partial}{\partial s} p(\Delta X_s|\Delta X_{s_0}) = \left(-\frac{\partial}{\partial(\Delta X)} D^{(1)}(\Delta X, s) + \frac{\partial^2}{\partial(\Delta X)^2} D^{(2)}(\Delta X, s)\right) p(\Delta X_s|\Delta X_{s_0}). \tag{13}$$

For such differential equation of the single probability function one can derive differential equations for the structure functions of the increments [9]. Uncertainties in Eq. (11a) can be overcome, namely when estimating the limit, by considering a subsequent optimization of $D^{(1)}$ and $D^{(2)}$. This optimization procedure is based in a cost function derived from the conditional probability density functions, which are deduced from both the experimental data and from Kramers-Moyal coefficients directly [16, 17].

2.4 Langevin Processes in Scale

The Fokker-Planck equation (13) above describes the evolution of the conditional probability density function $p(\Delta X_s|\Delta X_{s_0})$ for a process in scale which can be generated by a Langevin equation of the form:

$$\frac{d}{ds}(\Delta X) = D^{(1)}(\Delta X, s) + \sqrt{D^{(2)}(\Delta X, s)}\Gamma_s, \tag{14}$$

where Γ_s is a δ-correlated noise (in scale s) with $\langle \Gamma_s \rangle = 0$ and $\langle \Gamma_s \Gamma_{s'} \rangle = \delta(s - s')$.

To illustrate the Langevin process in scale described by Eq. (14), we consider the particular case of $D^{(1)} \propto -\Delta X$ and constant $D^{(2)}$, reducing the general Langevin equation to the particular case of Brownian motion "in scale".

What is the Brownian motion *in scale*? Though more abstract than the usual Brownian motion [6], Brownian motion in scale can be illustrated by a Galton Box [18], as sketched in Fig. 2. The Galton box is an apparatus consisting of a vertical board with interleaved rows of pins, typically with a constant distance between neighbouring pins. Balls are dropped from the top, and each time they hit a pin, they bounce, left or right, downwards. At the bottom, balls are collected in several columns separated from each other.

In a Galton box, the horizontal rows of pins represent the succession of scales, $s_1, s_2, \ldots$, with a constant distance between adjacent rows, representing the scale increment Δs. From one scale s_k to the next one s_{k+1} the possible ways a ball can bounce doubles. Since s is in fact a logarithmic scale of 2^n, $s_n = n \log 2$, and therefore s scales linearly with the vertical distance to the starting point.

As for the horizontal distance from the centred vertical line, it represents the increments ΔX. We recall that for processes in scale one has a scale s playing

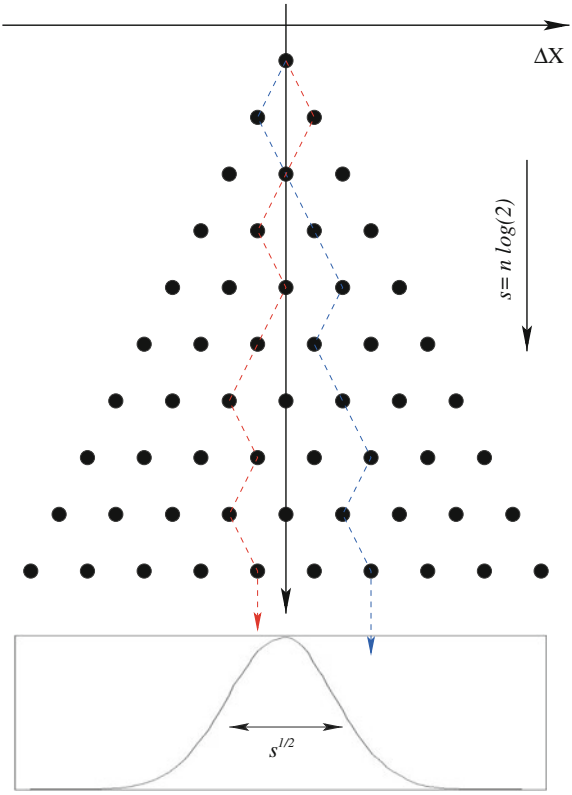

Fig. 2 The *Galton box* as an illustration of Brownian motion in scale. Note that the converging distribution for the increments is proportional to $\exp[-2(\Delta X)^2/s]$, a Gaussian distribution with standard deviation proportional to $\sqrt{s}$

the role of time and one has increments instead of single values of the observable X. Thus, similarly to the solution of the original Langevin equation for Brownian motion, in this case one also obtains a Gaussian distribution of increment values centred at $\langle \Delta X \rangle = 0$ and with a variance proportional to Δs. Note that the normal approximation of this binomial distribution is $N(0, s/4)$.

Such illustration of a process in scale is a very simple one. To properly imagine a picture of general scale processes in turbulence two important differences must be considered. First, the energy (i.e. velocity increments) flow from the largest to the smallest scales, which is opposite to the illustration with the Galton box. Second, the KM coefficients for the Galton box are those of the simplest situation that we named as Brownian motion in scale, due to its straightforward parallel with usual Brownian motion. Here the KM coefficients do not depend on scale s. In turbulence, as we will see, not only the dependency on the increments is more complicated, but there is an important dependence on the scale s.

3 Applying the Langevin Approach to Turbulence

3.1 The Langevin Approach in Laboratory Turbulence

The experiments were conducted in a closed loop wind tunnel with test section dimensions of 200 cm × 25 cm × 25 cm (length × width × height) at the University of Oldenburg. The wind tunnel has a background turbulence intensity of approximately 2 % for $U_\infty \leq 10$ m/s. The inlet velocity was set to 10 m/s, which corresponds to a Reynolds number related to the biggest grid bar length L_0 of about $Re_{L_0} = U_\infty L_0/\nu = 83800$, where ν is the kinematic viscosity. Constant temperature anemometry measurements of the velocity were performed using (*Dantec 55P01* platinum-plated tungsten wire) single-hot-wire with a wire sensing length of about $l_w = 2.0 \pm 0.1$ mm and a diameter of $d_w = 5\,\mu$m which corresponds to a length-to-diameter ratio of $l_w/d_w \approx 400$. A *StreamLine* measurement system by *Dantec* in combination with CTA Modules 90C10 and the *StreamWare* version 3.50.0.9 was used for the measurements. The hot-wire was calibrated with *Dantec Dynamics Hot-Wire Calibrator*. The overheat ratio was set to 0.8. In the streamwise direction, measurements were performed on the centerline in the range between 5 cm $\leq x \leq$ 176 cm distance to the grid. The data was sampled with $f_s = 60$ kHz with a *NI PXI 1042* AD-converter and 3.6 million samples were collected per measurement point, representing 60 s of measurements data. To satisfy the Nyquist condition, the data were low-pass filtered at frequency $f_l = 30$ kHz.

For the present work, a fractal grid was placed at the inlet of the wind tunnel, see Fig. 3. In general, fractal grids are constructed from a multiscale collection of obstacles which are based on a single pattern which is repeated in increasingly

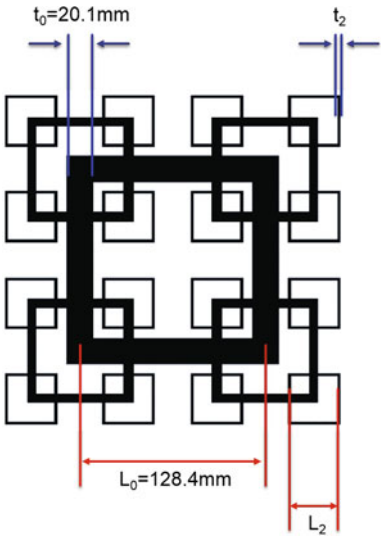

Fig. 3 Illustration of the space-filling square fractal grid (SFG) geometry, placed at the inlet of the test section for the experiments, and considered when implementing the corresponding numerical simulations

Table 1 Geometrical properties of the utilized fractal grid

N	$\sigma/\%$	L_0/mm	t_0/mm	R_L	R_t	L_r	t_r	M_{eff}/mm	T/mm
3	36.4	128.4	20.1	0.54	0.36	3.5	7.7	24.6	250

σ is the blockage ratio and T the cross section of the wind tunnel (and also of the simulation domain)

numerous copies with different scales. The pattern our fractal grid is based on is a square shape with $N = 3$ fractal iterations. The fractal iterations parameter is the number the square shape is repeated at different scales. At each iteration ($j = 0, \ldots, N-1$), the number of squares is four times higher than in the iteration $j-1$. Each scale iteration j is defined by a length L_j and a thickness t_j of the squares bars constituting the grid. The thickness of the square bars in the streamwise direction is constant. The dimensions of the square patterns are related by the ratio of the length of subsequent iterations $R_L = \frac{L_j}{L_{j-1}}$ and by the ratio of the thickness of subsequent iterations $R_t = \frac{t_j}{t_{j-1}}$; respectively. The geometry of the fractal grid we used (also called the space filling fractal grid [19]) is completely characterized by two further parameters namely the ratio of the length of the first iteration to the last one $L_r = \frac{L_0}{L_{N-1}}$ and the ratio of the thickness of the first iteration to the last one $t_r = \frac{t_0}{t_{N-1}}$.

Contrary to classical grids, fractal grids do not have a well-defined mesh size M_{eff}. However, an equivalent effective mesh size was defined in [19]. A complete quantitative description of the N3 fractal grid we used in this study is reported in Table 1.

3.2 The Langevin Approach in Simulated Turbulence

The flow over a fractal grid is described by the three dimensional, incompressible Navier-Stokes equations. The equations are discretized and solved using a turbulence model. In this investigation, the Delayed Detached Eddy Simulation (DDES) [20] with a Spalart-Allmaras background turbulence model [21], commonly referred to as SA-DDES is used. DDES is a hybrid method stemming from the Detached Eddy Simulation method (DES) [20], which involves the use of Reynolds Averaged Navier-Stokes Simulation (RANS) at the wall and Large Eddy Simulation (LES) away from it. This method combines the simplicity of the RANS formulation and the accuracy of LES, with the advantage of being less expensive, in terms of computational time, when compared with pure LES. DDES is an improvement of the original DES formulation, where the so called "modelled stress depletion" (or MSD), is treated [22, 23].

The numerical simulation was set up analogous to the experiments in order to compare the results in a consistent manner. The open source code OpenFOAM [24] was used to solve the incompressible Navier-Stokes equations. OpenFOAM is based

on the finite volume method, and it consists of a collection of libraries written in C++, which can be used to simulate a large class of flow problems. For more information about the available solvers and turbulence models, refer to the official documentation [24]. The solver used in this investigation is the transient solver pimpleFoam, which is a merging between the PISO (Pressure implicit with splitting of operator) and SIMPLE (Semi-Implicit Method for Pressure Linked Equation) algorithms. A second order central-differencing scheme is used for spatial discretization, and a backward, second-order time advancing schemes was used. The solver is parallelized using the Message-Passing Interface (MPI), which is necessary for problems of this size.

The numerical mesh was generated using the built-in OpenFOAM meshing tools blockMesh and snappyHexMesh [24]. As a result, an unstructured mesh of 24 million cells is obtained, where regions of interest in the wake are refined, as shown in Fig. 4. The fractal grid is simulated in a domain with similar dimensions as the real wind tunnel. The domain begins 2 m upstream of the fractal grid and covers a distance of 2 m downstream (see Fig. 5). The flow-parallel boundaries are treated as frictionless walls, where the slip boundary condition was applied for all flow variables. At the inflow boundary, Neumann boundary condition was used for the pressure, and Dirichlet condition for the velocity. At the outflow boundary, the pressure was set to be equal to the static pressure and a Neumann boundary condition was used for the velocity. On the fractal grid, a wall function is used for the modified viscosity $\tilde{\nu}$, with the size of the first cell of the mesh in terms of the dimensionless wall distance is $y^+ \sim 200$ [25]. For each simulation, 480 processors were used, and for each time step 4.5 GB of data was collected for post-processing. The data sampling frequency was 60 kHz, chosen to match the experimental one. It took approximatively 72 h to simulate one second of data and a total of 20 s of numerical data were collected. The data was collected in the same positions as for the experimental study. The numerical simulations were conducted on the computer cluster of the ForWind Group [26].

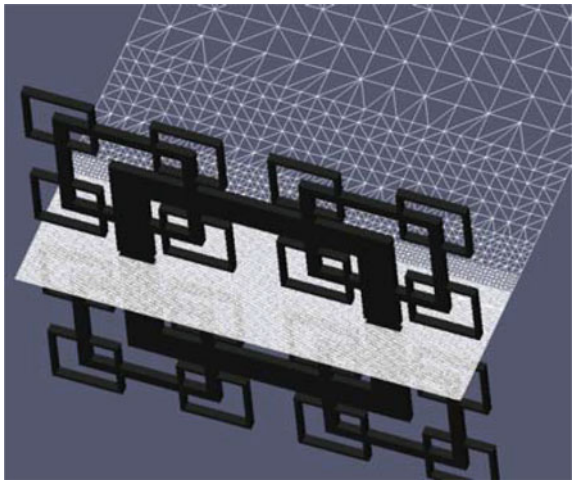

Fig. 4 Details of the computational mesh used in the computational simulations of the N3 fractal grid

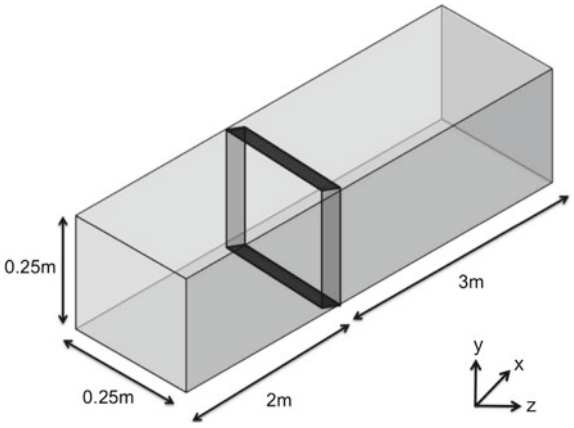

Fig. 5 Schematic representation of the numerical domain considered and the system of coordinates. The fractal grid is positioned where the *dark* block is drawn

3.3 Comparative Analysis

We estimate the Kramers-Moyal coefficients $D^{(1,2)}$ for the experimental and simulated data. The coefficients are commonly parametrized as follows:

$$D^{(1)}(u, r, x) = d_{11}(r, x) \cdot u, \tag{15}$$

$$D^{(2)}(u, r, x) = d_{22}(r, x) \cdot u^2 + d_{20}(r, x), \tag{16}$$

$$d_{ii}(r, x) = a_{ii}(x) \left(\frac{r}{\lambda}\right)^3 + b_{ii}(x) \left(\frac{r}{\lambda}\right)^2 + c_{ii}(x) \frac{r}{\lambda} + d_{ii}(x). \tag{17}$$

The results of $D^{(1,2)}$ in terms of a, b, c and d are shown in Table 2, for the downstream position $x = 0.76$ m. Note that the coefficients strongly depend on the downstream position x. We present and discuss all scales in units of Taylors microscale λ.

Table 2 Coefficients a, b, c and d of the drift and diffusion terms for experimental (Exp.) and simulated (Sim.) data, for downstream position $x = 0.76$ m

KM coeff.	Data	a	b	c	d
d_{11}	exp.	-2.7×10^{-5}	5.6×10^{-4}	-0.075	-1.0
	Sim.	6.7×10^{-7}	-7.4×10^{-4}	-0.070	-0.89
d_{22}	Exp.	-2.1×10^{-6}	2.0×10^{-4}	-0.0037	0.059
	Sim.	-6.6×10^{-6}	4.1×10^{-4}	-5.5×10^{-4}	0.072
d_{20}	Exp.	0	0	0.10	0.18
	Sim.	0	0	0.10	0.21

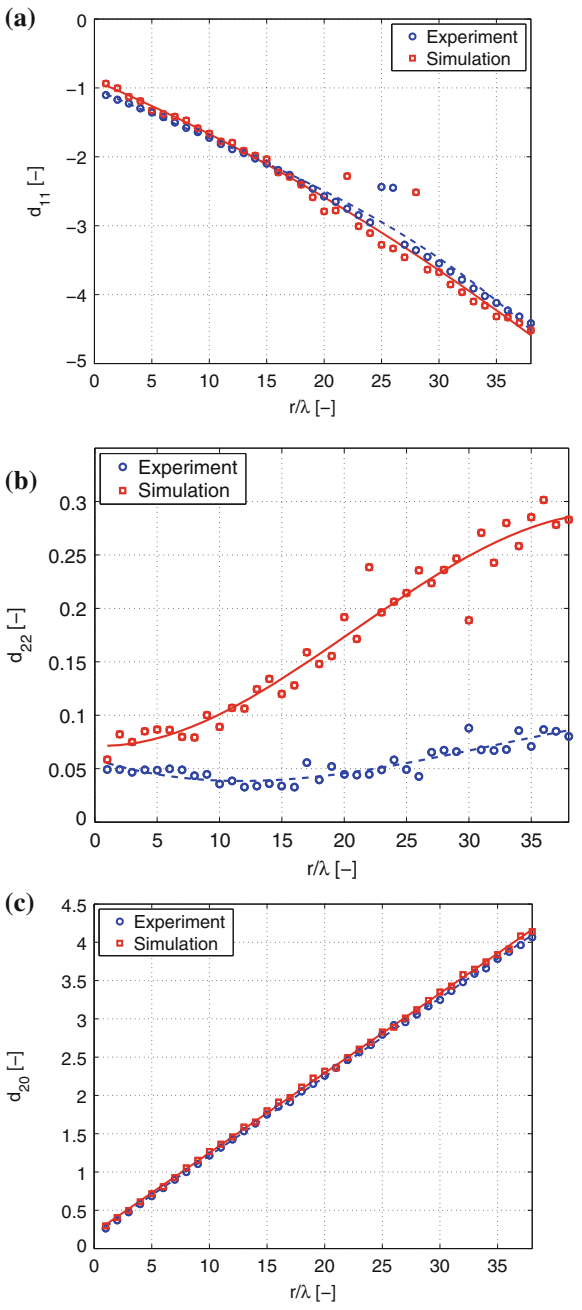

Fig. 6 Kramers-Moyal coefficients in terms of d_{11}, d_{20} and d_{22} along the inertial range, $1 \leq \frac{r}{\lambda} \leq L$

Figure 6 presents Kramers-Moyal coefficients in terms of d_{11}, d_{20} and d_{22} versus the scale r/λ. The coefficient are calculated within the inertial range. We chose this range, because the DDES simulations treat flow structures of this size as universal and simplify the turbulent flow properties by means of a sub-grid model, which is in this case the Spalart-Allmaras model. Therefore, a validation with the experimental data within the inertial range is of particular interest. Common limits of this region are $\lambda \approx 3\,\text{mm}$ (small scale) and the integral length scale $L \approx 12\,\text{cm}$ (large scale).

The development of the drift term within the inertial range is shown in Fig. 6a. Comparing the experimental and the simulated data no significant differences can be observed. Both curves indicate a stronger drift term with increasing scale, as usual for turbulent flows. The four outliers are most likely due to the optimization procedure. Rarely, local minimum are found instate of the global.

The development of the diffusion term within the inertial range is shown in Fig. 6b, c. Figure 6b shows the curvature of the diffusion term d_{22}, a very small and sensitive term. Here the experimental and the simulated data differ in their development. At large scales the curvature differ significantly ($d_{22,sim} \approx 3 \cdot d_{22,exp}$). At small scales the developments draw near, but do not converge. The magnitude of $d_{22,exp}$ is common, and shows why some studies neglect d_{22}. Figure 6c presents the diffusion term offset d_{20} within the inertial range. Such as the drift term, no essential differences between the experimental and the simulated data can be observed. The linear increasing of the offset is typical for the inertial range, it indicates the growth of the increments (velocity difference) or vortices, respectively, with scale, cf. Eq. (14).

4 Discussion and Conclusions

In this chapter we described the so-called Langevin approach, a stochastic method that enables deriving evolution equations of stochastic observables, providing important physical insight about the underlying system.

The method was applied to the problem of turbulence, addressed experimentally and by means of simulations by extracting the velocity increment time series, one recorded in a wind tunnel experiment and one simulated by a delayed detached large eddy simulation (DDES). For each case we extracted the functions defining the stochastic evolution equation, the so-called Kramers-Moyal coefficients, and parametrized them through polynomials of the scale.

The results show on the one hand good consistency in the two dominating terms, namely the linear term d_{11} of the first KM coefficient (drift) and the independent term d_{20} of the second KM coefficient (diffusion). Other terms, such as the quadratic term d_{22} for the diffusion, may present deviations that appeal for further investigation, which will carried out for a forthcoming study focusing on this specific experiment.

Concerning the Langevin approach as a stochastic method on its own, three points are worth of mention. First, the method can also be applied to the usual processes in time [2]. For that, one should simply interchange scale s and increments ΔX in Eqs. (10) and (14) by time t and observable values X respectively.

Second, while the method implies the fulfilment of two important conditions, namely stationarity and markovianity (see Sect. 2.2), the method can still be adapted to a more general situation where one or both this conditions are dropped. In case the data series is not stationary, the Langevin approach can be applied to time-windows within which the series can be taken as stationary [27]. As a result, one derives a set of KM coefficients as function of time, one for each time-window. In the case the data series is not Markovian, for instance due to measurement (additive) noise an extension is still possible [15, 28].

Finally, the Langevin approach can be applied to a broad panoply of different situations in topics ranging technical applications to biological, geophysical and financial systems, e.g. electric circuits, wind energy converters, traffic flow, cosmic microwave background radiation, granular flows, porous media, heart rhythms, brain diseases such as Parkinson and epilepsy, meteorological data, seismic time series, nanocrystalline thin films and biological macromolecules. For a review on these topics see Ref. [2].

Acknowledgments We gratefully acknowledge the computer time provided by the Facility for Large-Scale Computations in Wind Energy Research (FLOW) of the university of Oldenburg. WM thanks the German Bundesministerium für Umwelt, Naturschutz und Reaktorsicherheit (BMU), which financed this project. PGL thanks German Federal Ministry of Economic Affairs and Energy (BMWi) as part of the research project "OWEA Loads" under grant number 0325577B.

References

1. Laplace P (1814, 1951) A philosophical essay on probabilities. Dover Publications, New York
2. Friedrich R, Peinke J, Sahimi M, Tabar M (2011) Approaching complexity by stochastic methods: from biological systems to turbulence. Phys Rep 506:87
3. Pope S (2000) Turbulence flows. Cambridge University Press, Cambridge
4. Schreiber T, Kantz H (1999) Nonlinear time-series analysis. Cambridge University Press, Cambridge
5. Einstein A (1905) Über die von der molekularkinetischen theorie der wärme geforderte bewegung von in ruhenden flüssigkeiten suspendierten teilchen. Annalen der Physik 17:549–560
6. Langevin P (1908) On the theory of Brownian motion. C R Acad Sci 146:530–533
7. Richardson LF (1920) The supply of energy from and to atmospheric eddies. Proc R Soc Lond A 97:354–376
8. Friedrich R, Peinke J (1997) Description of a turbulent cascade by a Fokker-planck equation. Phys Rev Lett 78:863
9. Renner C, Peinke J, Friedrich R (2001) Experimental indications for Markov properties of small-scale turbulence. J Fluid Mech 433:383–409
10. Nawroth AP, Friedrich R, Peinke P (2010) Multi-scale description and prediction of financial time series. New J Phys 12:021–083
11. van Kampen N (1999) Stochastic processes in physics and chemistry. North-Holland, Amsterdam
12. Risken H (1984) The Fokker-Planck equation. Springer, Heidelberg
13. Wilcoxon F (1945) Individual comparisons by ranking methods. Biom Bull 1:80–83
14. Lowry R (2011) Concepts and applications of inferential statistics. http://vassarstats.net/textbook/

15. Lind P, Haase M, Boettcher F, Peinke J, Kleinhans D, Friedrich R (2010) Extracting strong measurement noise from stochastic series: applications to empirical data. Phys Rev E 81:041125
16. Kleinhans D, Friedrich R, Nawroth AP, Peinke J (2005) An iterative procedure for the estimation of drift and diffusion coefficients of Langevin processes. Phys Lett A 346:42–46
17. Nawroth AP, Peinke J, Kleinhans D, Friedrich R (2007) Improved estimation of Fokker-Planck equations through optimisation. Phys Rev E 76:056–102
18. Galton F (1894) Natural inheritance. Macmillan, New York
19. Hurst D, Vassilicos JC (2007) Scalings and decay of fractal-generated turbulence. Phys Fluids 19:035–103
20. Spalart PR, Strelets M, Allmara SR (1997) Comments on the feasibility of LES for wings, and on a hybrid RANS/LES approach. Adv DES/LES 1:137–147
21. Spalart PR, Allmara SR (1994) A one-equation turbulence model for aerodynamic flows. La Recherche Aerospatiale 1:5–21
22. Menter FR, Kuntz M (2004) The aerodynamics of heavy vehicles: trucks, buses, and trains. Lecture notes in applied and computational mechanics, vol 19
23. Spalart P, Deck S, Shur M, Squires K, Strelets M, Travin A (2006) A new version of detached-eddy simulation, resistant to ambiguous grid densities. Theor Comput Fluid Dyn 20(3):181–195
24. OpenFOAM (2013) The open source computational fluid dynamics toolbox. http://www.openfoam.com/
25. White F (1998) Fluid mechanics. McGraw-Hill Higher Education, New York
26. Flow01 (2013) Facility for large-scale computations in wind energy research. http://www.fk5.uni-oldenburg.de/57249.html
27. Camargo S, Queirós S, Anteneodo C (2006) Nonparametric segmentation of nonstationary time series. Phys Rev E 84:046–702
28. Boettcher F, Peinke J, Kleinhans D, Friedrich R, Lind PG, Haase M (2006) Reconstruction of complex dynamical systems affected by strong measurement noise. Phys Rev Lett 97:090603

Monte Carlo Simulations of Turbulent Non-premixed Combustion using a Velocity Conditioned Mixing Model

Michael Stoellinger, Denis Efimov and Dirk Roekaerts

Abstract Non-premixed turbulent combustion in a laboratory scale flame (Delft III flame) is studied using a statistical description at the one-point one-time joint velocity—scalar composition probability density function (PDF) level. The PDF evolution equation is solved using a stochastic Lagrangian Monte Carlo method. The PDF equation requires a so called micro-mixing model for closure and the performance of two micro-mixing models is investigated. The Interaction by Exchange with the Mean (IEM) micro mixing model is the most commonly adopted model. The IEM model was developed for the scalar PDF method and does not depend on velocity statistics. A physically more sound extension of the IEM is the Interaction by Exchange with the Conditional Mean (IECM) which involves mixing of the scalars towards mean values conditional on the velocity. Both models are applied in this work and it is shown that the IECM model does perform significantly better than the simple IEM model.

1 Introduction

Combustion processes are characterized by a series of fast exothermic chemical reactions between a fuel and an oxidizer accompanied by the release of heat. For large scale applications safety is of major concern and thus these devices are operated in non-premixed combustion mode. In non-premixed combustion, fuel and oxidizer

M. Stoellinger (✉)
Department of Mechanical Engineering, University of Wyoming,
Laramie, USA
e-mail: mstoell@uwyo.edu

D. Efimov
Department of Mechanical Engineering, Eindhoven University of Technology,
Eindhoven, The Netherlands
e-mail: D.V.Efimov@tue.nl

D. Roekaerts
Process & Energy, Delft University of Technology, Delft, The Netherlands
e-mail: D.J.E.M.Roekaerts@tudelft.nl

S. Heinz and H. Bessaih (eds.), *Stochastic Equations for Complex Systems*,
Mathematical Engineering, DOI 10.1007/978-3-319-18206-3_7

enter the combustion chamber in separate streams and mixing has to occur before the reactions take place. In this work we will focus on the modeling of non-premixed turbulent combustion of gaseous fuels. In non-premixed combustion the interactions between chemical and physical phenomena are of great importance. The turbulent flow field gives rise to large instantaneous fluctuations in the thermochemical quantities (such as temperature and gas composition). Molecular and turbulent diffusion greatly affect the intensity of chemical reactions. Further, the chemical reactions modify the flow field by changing the density and the viscosity of the gas mixture. The coupling of the complex interactions between the turbulent flow and chemical reactions over a large range of time and length scales poses the main difficulty for modeling turbulent combustion.

Solving numerically the exact transport equations describing turbulent combustion for all time and length scales is not suitable for engineering applications. Such simulations, called direct numerical simulation (DNS), can be performed for simple cases and due to the high computational cost their applications are limited to low Reynolds number canonical flames. The computational cost can be reduced by solving only for the mean velocity and modeling the effects of turbulent fluctuations as is done in the Reynolds Averaged Navier-Stokes (RANS) method. However, the conventional RANS method is less suitable for modeling of turbulent reacting flows as the mean chemical source term appears as unknown in the transport equations for the mean scalar composition variables (the mean chemical species concentrations and the mean enthalpy). Because the chemical source term is a highly non-linear function of the scalar composition variables it cannot be closed utilizing only the mean values of these variables, but the knowledge of the full joint statistics of the scalar composition variables is required. The exact transport equation for the one-point, one-time joint probability density function (PDF) of the scalar composition variables (SPDF) can be derived from the Navier-Stokes equations [1, 2] but is unclosed (i.e. it involves multi-point statistical information). The unclosed terms in the PDF equation are the turbulent transport and the molecular mixing of scalar variables on the smallest scales (further referred to as the micro-mixing term) and both terms need to be modeled. The main advantage of the PDF method is given by the exact treatment of the chemical reaction source term. The modeling of the micro-mixing remains the biggest challenge in the PDF approach and a variety of models have been proposed in the past [3].

In the composition PDF approach the effect of turbulent transport has to be modeled in addition to micro-mixing. A more general statistical description is based on the joint velocity-scalar PDF (VSPDF) approach which is considered in this work. The turbulent transport (i.e. correlations between scalars and velocity) does not require modeling in the VSPDF method since the velocity is included in the statistical formulation. The modeled equation for the VSPDF is solved with a stochastic Lagrangian Monte Carlo method. In the VSPDF method the micro-mixing term in the PDF transport equation appears in a form conditioned on both the velocity and the scalar composition. Most micro-mixing models are developed for the SPDF approach [3] where velocity conditioning is irrelevant and are then simply adopted in the VSPDF approach by making the assumption that the scalar mixing is independent

of the underlying velocity statistics. The hypothesis tested in this work is that the effects of velocity conditioning for micro-mixing models, used in the context of the joint velocity-scalar probability density function approach, are not negligible and should be accounted for. This work compares the performance of the Interaction by Exchange with the Mean (IEM) micro-mixing model [4] with that of its velocity conditioned version the Interaction by Exchange with the Conditional Mean (IECM) model [5].

The IEM and IECM models are both used in simulations [6] of the Delft III flame that has been studied experimentally at the Heat Transfer Section of Delft University of Technology [7, 8]. The Delft III flame is a laboratory scale piloted non-premixed co-flow flame burner with natural gas as the main fuel. Detailed measurements of the turbulent flow fields and the thermochemical quantities in the Delft III flame are available, permitting the assessment of the adopted modeling techniques.

2 Stochastic Modeling of Turbulent Non-premixed Combustion

This section outlines the development of a stochastic model for turbulent reacting flows. First, the deterministic governing equations are presented and a simplified treatment of the chemical reactions is introduced. Then, the exact but unclosed transport equation of the joint velocity-scalar PDF is presented and closure models are introduced. Finally, an efficient numerical solution method of the VSPDF equations based on a stochastic Lagrangian Monte Carlo method is briefly described.

2.1 Deterministic Conservation Equations

The description of turbulent reacting flows is based on the conservation of mass, momentum, energy and chemical species. The continuity equation describing mass conservation is given by

$$\frac{\partial \rho}{\partial t} + \frac{\partial \rho U_i}{\partial x_i} = 0 \tag{1}$$

where ρ is the density, U_i the velocity and x_i the Cartesian spatial coordinates with $i = 1, 2, 3$. Throughout this work, Einstein summation convention is adopted for repeated roman letters but not for repeated greek letters. The conservation equation for momentum can be written as

$$\frac{\partial}{\partial t}\rho U_i + \frac{\partial}{\partial x_j}\rho U_j U_i = -\frac{\partial p}{\partial x_i} - \frac{\partial}{\partial x_j}\tau_{ij} \tag{2}$$

where p is the pressure and τ_{ij} the viscous stress tensor given by

$$\tau_{ij} = -\mu \left(\frac{\partial U_i}{\partial x_j} + \frac{\partial U_j}{\partial x_i} \right) + \frac{2}{3} \mu \frac{\partial U_k}{\partial x_k} \delta_{ij}, \tag{3}$$

where μ is the viscosity of the gas mixture. The Ideal gas assumption relates the pressure to the density and temperature of the gas mixture:

$$p = \rho R_0 T \sum_{\alpha=1}^{n_s} \frac{Y_\alpha}{M_\alpha}, \tag{4}$$

where R_0 the universal gas constant, T the temperature of the mixture, n_s the total number of species, Y_α the mass fraction and M_α the molar mass of species α. Throughout this work the low Mach number approximation is adopted which implies that in the thermodynamic equation of state the pressure is assumed to be the constant ambient pressure p_0.

The conservation equation for the total specific enthalpy is given by

$$\frac{\partial}{\partial t} \rho h + \frac{\partial}{\partial x_j} \rho U_j h = -\frac{\partial}{\partial x_j} J_j^h + \rho S_h, \tag{5}$$

where J_j^h represents the molecular enthalpy flux and S_h is a source term. In this work the effects of radiative heat transfer, viscous dissipation and transient pressure are neglected and hence $S_h = 0$. The temperature dependency of the enthalpy for each of the species is given by the caloric equation of state

$$h = \sum_{\alpha=1}^{n_s} Y_\alpha \left(h_\alpha^{ref} + \int_{T_{ref}}^{T} c_{p,\alpha} \left(T' \right) dT' \right). \tag{6}$$

Here T_{ref} is the reference temperature, h_α^{ref} is the enthalpy of the species α at the reference temperature and $c_{p,\alpha}$ is the specific heat of the species α.

The conservation equations for species mass fractions Y_α read

$$\frac{\partial}{\partial t} \rho Y_\alpha + \frac{\partial}{\partial x_j} \rho U_j Y_\alpha = -\frac{\partial}{\partial x_j} J_j^\alpha + \rho S_\alpha, \tag{7}$$

where J_j^α denotes the diffusion flux and S_α is the chemical reaction source term. Neglecting effects of thermal diffusion and external body forces and assuming Fickian diffusion with equal diffusivity $\mathbb{D}$ for all species and enthalpy, the flux terms are given by

$$J_j^\alpha = -\rho \mathbb{D} \frac{\partial Y_\alpha}{\partial x_j}, \quad J_j^h = -\rho \mathbb{D} \frac{\partial h}{\partial x_j}. \tag{8}$$

2.2 Simplified Chemical Description

The overall reaction of oxidation of methane, the prevailing component of natural gas, is simply

$$CH_4 + 2O_2 \rightarrow CO_2 + 2H_2O.$$

However, in real methane combustion the conversion is a multi-step process and a high number of intermediate species and elementary reactions should be considered. As an example the Gri-Mech 3.0 reaction mechanism [9], which is reported to show good performance for laminar test cases, contains 53 species and 325 elementary reactions. Adopting such a mechanism directly means that the thermo-chemistry requires the solution of 54 coupled PDE's and that would render the problem numerically intractable in particular for turbulent flames. A viable method to drastically reduce the chemical complexity of combustion is the flamelet tabulation method. The flamelet tabulation method describes a turbulent flame as an ensemble of simple 1-d laminar flame structures that are called flamelets. The simulations of such 1-d flamelets are done prior to the main turbulent flame simulation, generating a lookup table to be used during the main simulation. In this process the whole thermochemistry is stored as a function of a few controlling scalar variables, reducing the computational costs during the main simulation.

The Flamelet Generated Manifolds (FGM) method [10] is employed in this work. The FGM for non-premixed flames is a flamelet model with tabulation based on two controlling variables: the mixture fraction ξ and the progress variable $\mathcal{Y}$. The mixture fraction ξ is a conserved scalar representing the degree of mixedness. The second controlling scalar is the reaction progress variable $\mathcal{Y}$ which is defined as a linear combination of the main combustion products [10]

$$\mathcal{Y} = \frac{Y_{CO_2}}{M_{CO_2}} + \frac{Y_{H_2O}}{M_{H_2O}} + \frac{Y_{H_2}}{M_{H_2}}. \tag{9}$$

The FGM database is generated by solving counterflow diffusion flamelets numerically. The flamelet equations are a 1-D set of partial differential equations [10]. The chemical mechanism adopted, is the aforementioned Gri-Mech 3.0 with $n_s = 53$ species and 325 elementary reactions. The main parameter in the flamelet equations is the strain rate a. The strain rate can be related to the velocity difference between the opposing fuel and oxidizer streams and the distance between the two streams. The higher the strain rate the more "strained" the flames are and the closer they get to extinction. Steady flamelets are solved for different strain rates a:

$$\begin{aligned} a = (&1, 2, 5, 7, 10, 20, 30, 40, 50, 60, 70, 80, 90, 100, \\ &200, 300, 400, 500, 550, 600, 650, 700, 720)\ [1/s] \end{aligned}$$

Then, in order for the flamelet database to account for the process of extinction, a time dependent solution of the flamelet equations has been found. This is achieved by using the most strained steady flamelet ($a = 720[1/s]$) as an initial condition and increasing the strain rate to the extinction value $a = 730[1/s]$. The time dependent simulation is continued until the pure mixing limit is reached, providing a series of additional states. Each counterflow diffusion flamelet is solved on a non-uniform grid with 150 points using grid refinement (at the locations of higher gradients more cells are automatically added to the grid), and the FGM database contains 23 steady and 12 unsteady flamelets. The flamelet equations are solved using the Chem1D software developed at the Eindhoven University of Technology [11]. A typical solution for the temperature in a flamelet with $a = 100\,\mathrm{s}^{-1}$ is shown in Fig. 1. The figure shows a plot of the temperature as a function of the mixture fraction (left) and the source term of the reaction progress variable as a function of the mixture fraction. Both figures show a strong dependence on the mixture fraction and that both the temperature and the source term of the progress variable peak around the stoichiometric mixture fraction $\xi_{st} \approx 0.07$.

The tabulation is done by interpolating the flamelet solutions on a $\xi - \mathcal{Y}$ grid, which is equidistant in both directions (150 ξ-points $\times$ 150 $\mathcal{Y}$-points). The tabulated variables are the density ρ, the temperature T and the source term of the reaction progress variable $S_{\mathcal{Y}}(\xi, \mathcal{Y})$. For an adiabatic flame such as the one considered in this work the thermo-chemistry can thus be reduced to solving two scalar equations one for the mixture fraction and one for the progress variable. To simplify the notation we introduce the composition vector $\boldsymbol{\phi}$ with components

$$\phi_\alpha = (\xi, \mathcal{Y}) \tag{10}$$

The conservation equation for the mixture fraction and for the reaction progress variable can now be combined to one equation for the composition vector

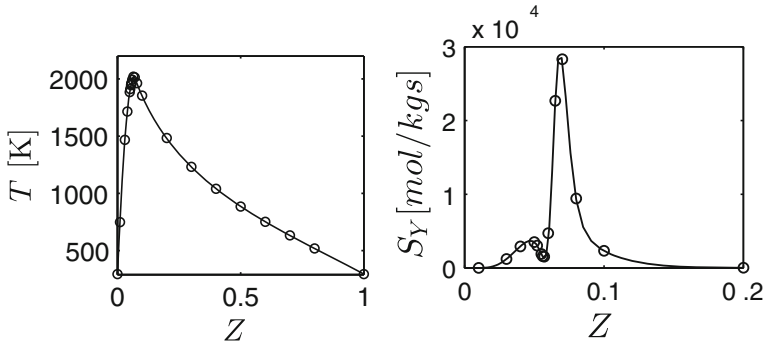

Fig. 1 Temperature as a mixture fraction (*left*) and reaction progress variable source term (*right*) for a Flamelet solution for $a = 100\,\mathrm{s}^{-1}$

$$\frac{\partial}{\partial t}\rho\phi_\alpha + \frac{\partial}{\partial x_j}\rho U_j\phi_\alpha = -\frac{\partial}{\partial x_j}J_j^\alpha + \rho S_\alpha\left(\boldsymbol{\phi}\right), \tag{11}$$

with $S_1 = 0$ since the mixture fraction is a conserved scalar and $S_2 = S_{\mathcal{Y}}(\xi, \mathcal{Y})$.

2.3 Statistical Description

The large range of time and length scales in turbulent flows make the direct solution of the deterministic equations presented in the preceding section computationally intractable for flows of practical interest. A computationally more feasible approach is to seek a statistical description. The set of random flow variables considered in this work are the velocity vector $\boldsymbol{U}$ and the composition vector $\boldsymbol{\phi} = (\xi, \mathcal{Y})$ with the corresponding sample space variables $\boldsymbol{V}$ and $\boldsymbol{\psi}$, respectively. The statistical description is based on the one-point, one-time joint velocity-composition mass density function (MDF) $\mathcal{F}_{\boldsymbol{U\phi}}\left(\boldsymbol{V}, \boldsymbol{\psi}; \boldsymbol{x}, t\right)$ [1–3]. The joint velocity-composition MDF is related to the joint velocity-composition PDF through

$$\mathcal{F}_{\boldsymbol{U\phi}}\left(\boldsymbol{V}, \boldsymbol{\psi}; \boldsymbol{x}, t\right) = \rho\left(\boldsymbol{\psi}\right) f_{\boldsymbol{U\phi}}\left(\boldsymbol{V}, \boldsymbol{\psi}; \boldsymbol{x}, t\right) \tag{12}$$

The main motivation to work with the joint velocity-composition MDF rather than with the PDF is that in turbulence modeling of flows with variable density it is customary to use density-weighted averages (Favre-averaging) to avoid terms involving density fluctuations. The Favre average of any variable Q is defined by

$$\widetilde{Q} = \frac{\langle \rho Q \rangle}{\langle \rho \rangle}. \tag{13}$$

The Favre-average of a function $Q\left(\boldsymbol{U}, \boldsymbol{\phi}\right)$ can thus be expressed simply in terms of the velocity-composition mass density function (MDF)

$$\langle \rho \rangle \widetilde{Q}\left(\boldsymbol{U}, \boldsymbol{\phi}\right) = \int_{\boldsymbol{\psi}}\int_{\boldsymbol{V}} Q\left(\boldsymbol{V}, \boldsymbol{\psi}\right) \mathcal{F}_{\boldsymbol{U\phi}}\left(\boldsymbol{V}, \boldsymbol{\psi}\right) d\boldsymbol{V} d\boldsymbol{\psi}. \tag{14}$$

In the case that a quantity Q is not a function of U and ϕ only but is a well defined property of the flow (for example containing a gradient of ϕ) then Eq. (14) is generalized to

$$\langle \rho \rangle \widetilde{Q}\left(\boldsymbol{U}, \boldsymbol{\phi}\right) = \int_{\boldsymbol{\psi}}\int_{\boldsymbol{V}} \langle Q | \boldsymbol{V}, \boldsymbol{\psi} \rangle \mathcal{F}_{\boldsymbol{U\phi}}\left(\boldsymbol{V}, \boldsymbol{\psi}\right) d\boldsymbol{V} d\boldsymbol{\psi} \tag{15}$$

The transport equation for the one-point one-time joint velocity-scalar MDF $\mathcal{F}_{\boldsymbol{U\phi}}\left(\boldsymbol{V}, \boldsymbol{\psi}; \boldsymbol{x}, t\right)$ can be derived [1–3] from the conservation Eqs. (1), (2) and (11) and reads

$$\frac{\partial}{\partial t}\mathcal{F}+\frac{\partial}{\partial x_i}V_i\mathcal{F}=-\frac{\partial}{\partial V_i}\left[\frac{1}{\rho\left(\boldsymbol{\psi}\right)}\left(-\frac{\partial\left\langle p\right\rangle}{\partial x_i}-\frac{\partial\left\langle\tau_{ij}\right\rangle}{\partial x_j}\right)\mathcal{F}\right] \tag{16a}$$

$$-\frac{\partial}{\partial V_i}\left[\frac{1}{\rho\left(\boldsymbol{\psi}\right)}\left\langle-\frac{\partial p'}{\partial x_i}-\frac{\partial\tau'_{ij}}{\partial x_j}\middle|\boldsymbol{U}=\boldsymbol{V},\boldsymbol{\phi}=\boldsymbol{\psi}\right\rangle\mathcal{F}\right] \tag{16b}$$

$$-\frac{\partial}{\partial\psi_\alpha}\left[\left(-\frac{1}{\rho\left(\boldsymbol{\psi}\right)}\frac{\partial\left\langle J_i^\alpha\right\rangle}{\partial x_i}+S_\alpha\left(\boldsymbol{\psi}\right)\right)\mathcal{F}\right] \tag{16c}$$

$$-\frac{\partial}{\partial\psi_\alpha}\left[\frac{1}{\rho\left(\boldsymbol{\psi}\right)}\left\langle-\frac{\partial J_i^{\alpha\prime}}{\partial x_i}\middle|\boldsymbol{U}=\boldsymbol{V},\boldsymbol{\phi}=\boldsymbol{\psi}\right\rangle\mathcal{F}\right]. \tag{16d}$$

The first two terms on the RHS of this Eq. (16a) and (16b) represent the evolution in velocity space and the last two terms (16c) and (16d) account for the evolution in scalar space. Terms (16a) and (16c) are closed and the terms (16b) and (16d), containing conditional expectation values, are unclosed and require to be modeled. The closed velocity evolution term (16a) contains the mean pressure gradient and mean viscous stress tensor. Unclosed velocity evolution terms describe the effects of the fluctuating pressure gradient and the fluctuating viscous stress tensor, conditional on the velocity and scalars. Both terms include gradients of fluctuating quantities that cannot be expressed in terms of the one-point PDF (since gradient statistics would require at least two-point statistical information). A typical model for this term is the so called simplified Langevin model (SLM) which is given by [1–3]

$$\begin{aligned}\frac{1}{\rho\left(\boldsymbol{\psi}\right)}\left\langle-\frac{\partial p'}{\partial x_i}-\frac{\partial\tau'_{ij}}{\partial x_j}\middle|\boldsymbol{U}=\boldsymbol{V},\boldsymbol{\phi}=\boldsymbol{\psi}\right\rangle&=\frac{1}{\rho\left(\boldsymbol{\psi}\right)}\left\langle a_i|\boldsymbol{U}=\boldsymbol{V},\boldsymbol{\phi}=\boldsymbol{\psi}\right\rangle\\&\approx a_i^M\left(\boldsymbol{V},\boldsymbol{\psi}\right)\\&=\left(\frac{1}{2}+\frac{3}{4}C_0\right)\frac{\varepsilon}{k}\left(V_i-\widetilde{U}_i\right)\\&\quad-\frac{C_0\varepsilon}{2\mathcal{F}}\frac{\partial\mathcal{F}}{\partial V_i},\end{aligned} \tag{17}$$

where $C_0=2.1$ is a model coefficient, $k=0.5\widetilde{u_i''u_i''}$ is the turbulent kinetic energy (tke) and ε the dissipation rate of the tke which has to be provided by a separate model (see below). The ratio k/ε provides a time scale for the dissipation process of the large turbulence scales and thus $\omega=\varepsilon/k$ gives a characteristic turbulence frequency.

The closed term describing the evolution in scalar space consists of the mean molecular diffusion flux and the mean reaction source term. The reaction source term is closed since the source terms only depend on the composition vector and are thus statistically fully described by the joint MDF $\mathcal{F}_{\boldsymbol{U\phi}}\left(\boldsymbol{V},\boldsymbol{\psi};\boldsymbol{x},t\right)$. This is the main advantage of working with a transport equation for the joint velocity-scalar MDF in reacting flows. If only a small number of statistical moments of the MDF are solved for (such as in conventional RANS modeling), the effects of the nonlinear chemical source terms would have to be modeled.

The unclosed scalar evolution term represents the effects of molecular mixing or micro-mixing. This term can have a drastic influence on the turbulent flame evolution. The main topic of this work is to investigate the performance of two different closure models for the micro-mixing term. As an example, the simplest closure model is the Interaction by Exchange with the Mean (IEM) model [4]

$$\begin{aligned}\frac{1}{\rho\left(\boldsymbol{\psi}\right)}\left\langle -\frac{\partial J_i^{\alpha\prime}}{\partial x_i}\middle|\boldsymbol{U}=\boldsymbol{V},\boldsymbol{\phi}=\boldsymbol{\psi}\right\rangle &= \langle\theta_\alpha|\boldsymbol{U}=\boldsymbol{V},\boldsymbol{\phi}=\boldsymbol{\psi}\rangle \\ &\approx \theta_{\alpha,mix}(\boldsymbol{V},\boldsymbol{\phi}) \\ &= -\frac{C_\phi}{2}\frac{\varepsilon}{k}\left(\psi_\alpha-\widetilde{\phi_\alpha}\right),\end{aligned} \tag{18}$$

where C_ϕ is the so called mixing parameter.

By adopting the SLM (17) and the IEM model (18) a closed evolution equation for the joint velocity-scalar MDF is obtained. Even for a steady state problem in two spatial dimensions ($dim(\boldsymbol{x}) = 2$, $dim(\boldsymbol{U}) = 2$) and using the simplified chemistry model ($dim(\boldsymbol{\psi}) = 2$) the MDF equation has derivatives in six dimensions. This makes the use of standard computational techniques, such as finite-differencing, inappropriate for this problem as the computational cost grows exponentially with the dimensions ([12]). Moreover, the MDF has to remain positive and has to satisfy the consistency property

$$\int \mathcal{F}_{\boldsymbol{U\phi}}\left(\boldsymbol{V},\boldsymbol{\psi};\boldsymbol{x},t\right)d\boldsymbol{V}d\boldsymbol{\psi}=\langle\rho\rangle, \tag{19}$$

which would be very difficult to ensure numerically using FD type discretizations. Using a stochastic Lagrangian Monte Carlo particle method the computational cost only increases linearly with the dimensionality of the equation and it is a simple matter to ensure the constraints on $\mathcal{F}$ numerically [2, 3]. The Monte Carlo method is based on a stochastic Lagrangian representation of the joint velocity-scalar MDF and is described in the next section.

2.4 Monte Carlo Method

The joint velocity-scalar MDF is represented in terms of the properties of a large number (N) of stochastic Lagrangian "fluid" particles [13]. The set of properties assigned to each particle consists of a numerical weight, the position, the velocity and the scalar composition. The particles can be viewed as different realizations of a turbulent reactive flow experiment. An estimate of the MDF $\mathcal{F}_{\boldsymbol{U\phi}}$ can then be obtained as a simple ensemble average over N particles:

$$\mathcal{F}_{\boldsymbol{U\phi},N}\left(\boldsymbol{V},\boldsymbol{\psi};\boldsymbol{x},t\right)=\Delta m\sum_{i=1}^{N}\delta\left(\boldsymbol{V}-\boldsymbol{U}^{(i)}\right)\delta\left(\boldsymbol{\psi}-\boldsymbol{\phi}^{(i)}\right)\delta\left(\boldsymbol{x}-\boldsymbol{X}^{(i)}\right) \tag{20}$$

where $\boldsymbol{U}^{(i)}$, $\boldsymbol{\phi}^{(i)}$ and $\boldsymbol{X}^{(i)}$ are respectively the velocity, the composition and the position of the ith particle, $\Delta m = M/N$ is the amount of mass each particle is representing. As $N \to \infty$, the expected value of the MDF $\left\langle \mathcal{F}_{\boldsymbol{U}\boldsymbol{\phi}N} \right\rangle$ approaches the exact one $\mathcal{F}_{\boldsymbol{U}\boldsymbol{\phi}}$. Within the Monte Carlo method, if all particles have the same numerical weight, the average of an arbitrary function of composition $Q(\boldsymbol{\phi})$ can be obtained from an ensemble of N particles as:

$$\langle Q(\phi) \rangle = \frac{1}{N} \sum_{i=1}^{N} Q\left(\phi^{(i)}\right). \tag{21}$$

The statistical error ϵ_{QN} is defined by the following equation:

$$\epsilon_{QN} = \langle Q \rangle_N - \langle Q \rangle_{N \to \infty} \tag{22}$$

and the standard deviation of the statistical error $\sigma_{\epsilon_{QN}}$ expressed in terms of the standard deviation σ_Q of Q reads:

$$\sigma_{\epsilon_{QN}} = \frac{1}{\sqrt{N}} \sigma_Q. \tag{23}$$

For more information on the numerical and statistical errors the interested reader is referred to [2].

The evolution of the Monte Carlo particles in the velocity-composition-physical space $(\boldsymbol{U}, \boldsymbol{\phi}, \boldsymbol{X})$ starting at the initial value $(\boldsymbol{U}_0, \boldsymbol{\phi}_0, \boldsymbol{x}_0)$ at the reference time t_0 are governed by the stochastic differential equations (using the SLM (17))

$$dX_i^* = U_i^* dt \tag{24}$$

$$dU_i^* = \left(\frac{1}{\rho} \frac{\partial \langle p \rangle}{\partial x_i} - \frac{\partial \left\langle \tau_{ij} \right\rangle}{\partial x_j} \right) dt + \left(\frac{1}{2} + \frac{3}{4} C_0 \right) \frac{\varepsilon}{k} \left(U_i^* - \widetilde{U}_i \right) dt + (C_0 \epsilon)^{1/2} dW_i \tag{25}$$

$$d\phi_\alpha = \theta_{\alpha,mix} dt + S_\alpha(\boldsymbol{\phi})\, dt + \frac{\partial}{\partial x_k} \left(\frac{\langle \nu \rangle}{Sc} \frac{\partial \widetilde{\phi_\alpha}}{\partial x_k} \right) dt, \tag{26}$$

where $\theta_{\alpha,mix}$ is the mixing model and $\boldsymbol{W}(t)$ is an isotropic Wiener process with the properties:

$$\langle d\boldsymbol{W}(t) \rangle = 0, \quad \left\langle dW_i(t)\, dW_j(t) \right\rangle = dt \delta_{ij}. \tag{27}$$

For the stochastic particle representation the IEM micro-mixing model is given by (using $\omega = \varepsilon/k$ for brevity)

$$\theta_{\alpha,mix}^{IEM} = -\frac{1}{2} C_\phi \omega \left(\phi_\alpha^* - \widetilde{\phi_\alpha} \right) \tag{28}$$

In the IEM method, micro-mixing is achieved by the decay of scalar variance which is modeled by the deterministic drift of individual particles' scalar values towards the local Favre-mean value. More details on the different micro-mixing models considered in this work will be given in Sect. 3.

2.5 Hybrid Solution Algorithm

A hybrid finite-volume/Monte Carlo solution algorithm ([14]) is used in this work. In the hybrid solution approach, the equations for the mean velocity $\widetilde{U}_i$ and the velocity covariance $\widetilde{u_i'' u_j''}$ (the Reynolds stress tensor) that are implied by the adopted stochastic model are solved by a conventional FV method. The hybrid method drastically reduces the bias error [2, 14] that arises from the fact that the drift term in the stochastic velocity evolution involves the local mean which is estimated by a rather small sample (about 50–200 particles per cell). The chemical composition of the flow is described completely by the stochastic particle ensemble and hence the mean density $\langle \rho \rangle$ required in the mean continuity and momentum equations is calculated from the stochastic Lagrangian solver. The domain is discretized into non-overlapping finite volumes which are used to solve for $\widetilde{U}_i$, $\widetilde{u_i'' u_j''}$, $\langle p \rangle$ and ε using a FV method and also to compute mean values from the stochastic particles such as $\langle \rho \rangle = \sum_{i \in cell} \rho^{(i)} / \sum_{i \in cell}$. The FV solver and the Monte Carlo solver are loosely coupled which means that several FV iterations (about 500) are performed and then several Monte Carlo steps (about 10) are performed forming one hybrid iteration. Figure 2 shows a sketch of the hybrid algorithm. The hybrid iterations are repeated until a converged solution is reached. Convergence is usually judged based on monitoring the mean temperature (coming from the Monte Carlo solver) at certain positions within the domain.

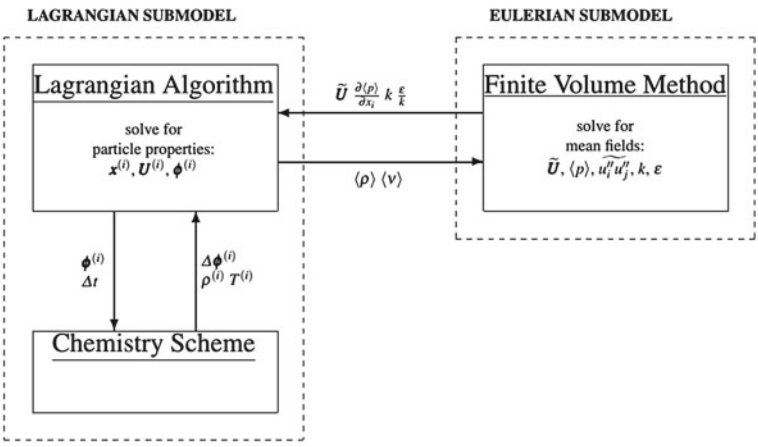

Fig. 2 Sketch of hybrid Monte Carlo solution method [12]

3 Micro Mixing Models

Modeling of the micro-mixing effects remains the biggest challenge in the PDF-approach. Its importance stems from the fact that the chemical reaction can occur only after the scalars are mixed at the smallest scales [12]. The evolution of the joint velocity-scalar MDF $\mathcal{F}_{\boldsymbol{U\phi}}(\boldsymbol{V}, \boldsymbol{\psi}; \boldsymbol{x}, t)$ by the scalar micro-mixing is described by:

$$\frac{\partial}{\partial t}\mathcal{F} = -\frac{\partial}{\partial \psi_\alpha}\left[\underbrace{\frac{1}{\rho(\boldsymbol{\psi})}\left\langle -\frac{\partial J_i^{\alpha\prime}}{\partial x_i}\middle| \boldsymbol{U}=\boldsymbol{V}, \boldsymbol{\phi}=\boldsymbol{\psi}\right\rangle}_{\theta_{\alpha,mix}}\mathcal{F}\right]. \tag{29}$$

The main topic of this work is to investigate and compare the performance of two micro-mixing models, namely the Interaction by Exchange with the Mean (IEM) model [4] and the Interaction by Exchange with the Conditional Mean (IECM) model [5].

3.1 Description of IEM and IECM Models

For a scalar composition variable $\phi_\alpha^{(n)}$ of a stochastic Lagrangian fluid particle (n) the IEM and the IECM models can be written as:

$$d\phi_\alpha^{(n)} = \theta_{\alpha,mix}^{(n)} dt$$

$$= -\frac{1}{2} C_\phi \omega \left(\phi_\alpha^{(n)} - \widetilde{\phi_\alpha}\right) dt \qquad \text{(IEM)} \tag{30}$$

$$= -\frac{1}{2} C_\phi \omega \left(\phi_\alpha^{(n)} - \widetilde{\phi_\alpha|\boldsymbol{U}}\right) dt \qquad \text{(IECM)} \tag{31}$$

where C_ϕ is a model constant with standard value 2, ω the turbulence frequency given by ϵ/k, $\widetilde{\phi_\alpha}$ is the Favre-mean of the scalar ϕ_α of all particles residing in the grid cell and $\widetilde{\phi_\alpha|\boldsymbol{U}}$ is the Favre-mean of the scalar ϕ_α conditioned on the velocity. In practice an approximation for the velocity conditioned mean of ϕ_α based on the finite particle ensemble of a grid cell has to be found. In both models, micro-mixing is achieved by the decay of scalar variance which is modeled by a deterministic drift of individual particles' scalar values towards the Favre-mean in case of the IEM and the velocity conditioned Favre-mean in case of the IECM. The scalar variance decay rate in Eqs. (30) and (31) is taken to be proportional to the turbulence frequency ω.

3.2 The Correct Local Scalar Isotropy

Closure models for micro-mixing should satisfy a number of conditions. This topic is explained in more detail in [3, 12] (and further references therein). One of these properties is the correct local scalar isotropy. This property represents the fact that scalar mixing can be dependent on the statistics of the velocity field, which is the case for inhomogeneous scalar fields with a mean scalar gradient ([5]). From the two micro-mixing models studied here, clearly, only the IECM model is designed to take this property into account. The IEM model has been originally developed for the joint composition PDF approach, where it is used to close the scalar mixing term of the PDF equation conditioned only on the scalar composition:

$$\theta_{\alpha,mix}^{IEM} = \frac{1}{\rho\left(\boldsymbol{\psi}\right)} \left\langle -\frac{\partial J_i^{\alpha\prime}}{\partial x_i} \middle| \boldsymbol{\phi} = \boldsymbol{\psi} \right\rangle. \tag{32}$$

When the IEM model is used in the joint velocity-scalar PDF approach the assumption is made that the scalar mixing term in the PDF Eq. (16) is independent of the velocity field

$$\left\langle -\frac{\partial J_i^{\alpha\prime}}{\partial x_i} \middle| \boldsymbol{U} = \boldsymbol{V}, \boldsymbol{\phi} = \boldsymbol{\psi} \right\rangle = \left\langle -\frac{\partial J_i^{\alpha\prime}}{\partial x_i} \middle| \boldsymbol{\phi} = \boldsymbol{\psi} \right\rangle, \tag{33}$$

while the IECM model accounts for such dependencies. The important consequence of this, at first sight, small modeling difference is discussed next. Without loss of generality we restrict the discussion to the mixture fraction ξ which is a conserved scalar (there is no source term due to chemical reactions). We also neglect the effects of mean molecular diffusion for simplicity since we are mostly interested in high Reynolds number flows. The transport equation for the joint velocity-mixture fraction MDF $\mathcal{F}_{\boldsymbol{U}\xi}\left(\boldsymbol{V}, \zeta; \boldsymbol{x}, t\right)$ [15] is the starting point:

$$\begin{aligned} \frac{\partial \mathcal{F}_{\boldsymbol{U}\xi}}{\partial t} + V_j \frac{\partial \mathcal{F}_{\boldsymbol{U}\xi}}{\partial x_j} &= -\frac{\partial}{\partial V_i}\left[\left\langle a_i \middle| \boldsymbol{U} = \boldsymbol{V}, \xi = \zeta \right\rangle \mathcal{F}_{\boldsymbol{U}\xi}\right] \\ &\quad - \frac{\partial}{\partial \zeta}\left[\left\langle \theta_{\xi,mix} \middle| \boldsymbol{U} = \boldsymbol{V}, \xi = \zeta \right\rangle \mathcal{F}_{\boldsymbol{U}\xi}\right], \end{aligned} \tag{34}$$

with the term $\left\langle a_i \middle| \boldsymbol{U} = \boldsymbol{V}, \xi = \zeta \right\rangle$ as defined in (17) and where $\left\langle \theta_{\xi,mix} \middle| \boldsymbol{U} = \boldsymbol{V}, \xi = \zeta \right\rangle$ represents one of the two considered micro-mixing models. Now transport equations for the mean mixture fraction $\widetilde{\xi}$ and the scalar flux $\widetilde{u_i'' \xi''}$ can be derived from the Eq. (34) by multiplying it respectively by ζ or $V_i \zeta$ and integrating over the phase space $(\boldsymbol{V}, \zeta)$, resulting in:

$$\frac{\partial \left\langle \rho \right\rangle \widetilde{\xi}}{\partial t} + \frac{\partial \left\langle \rho \right\rangle \widetilde{U_j} \widetilde{\xi}}{\partial x_j} = -\frac{\partial \left\langle \rho \right\rangle \widetilde{u_j'' \xi''}}{\partial x_j}, \tag{35}$$

and

$$\frac{\partial \langle\rho\rangle \widetilde{u_i''\xi''}}{\partial t} + \frac{\partial \langle\rho\rangle \widetilde{u_i''\xi''}\widetilde{U_j}}{\partial x_j} = -\langle\rho\rangle \widetilde{u_j''\xi''}\frac{\partial \widetilde{U}_i}{\partial x_j} - \langle\rho\rangle \widetilde{u_i''u_j''}\frac{\partial \widetilde{\xi}}{\partial x_j} + \langle\rho\rangle \widetilde{\overline{u_i''\theta_{\xi,mix}}} + \langle\rho\rangle \widetilde{a_i\xi''} - \frac{\partial \left\langle \rho u_i'' u_j'' \xi'' \right\rangle}{\partial x_j}. \tag{36}$$

In Eq. (36) the symbol $\widetilde{\overline{\quad}}$ denotes the Favre-averaging of a long expression. The micro-mixing model should not affect the mean of a scalar (it only reduces the scalar variance). Therefore, the scalar flux $\widetilde{u_i''\xi''}$ appearing in the equation for the mean mixture fraction (35) should be independent of the micro-mixing model and hence the term $\widetilde{\overline{u_i''\theta_{\xi,mix}}}$ in the equation for the scalar flux (36) should vanish [16]. Expanding this term, by substituting the Eqs. (30) and (31) for $\theta_{\xi,mix}$ for the IEM and the IECM models, gives respectively:

$$\widetilde{\overline{u_i''\theta^{IEM}_{\xi,mix}}} = -\frac{1}{2}C_\phi\omega\left[\widetilde{\overline{u_i''\left(\xi-\widetilde{\xi}\right)}}\right] = -\frac{1}{2}C_\phi\omega\left[\widetilde{u_i''\xi''}\right] \neq 0 \tag{37a}$$

$$\widetilde{\overline{u_i''\theta^{IECM}_{\xi,mix}}} = -\frac{1}{2}C_\phi\omega\left[\widetilde{\overline{u_i''\left(\xi-\widetilde{\xi|\boldsymbol{U}}\right)}}\right] = -\frac{1}{2}C_\phi\omega\left[\widetilde{u_i''\xi} - \widetilde{u_i''\xi}\right] = 0. \tag{37b}$$

Therefore, the IEM model introduces an extra term in the scalar flux equation, which influences the turbulent flux and can affect the mean scalar field. In contrast, if the IECM mixing model is applied, this term vanishes, resulting in correct representation of the local scalar isotropy. Physically this issue can be explained as the fact that fluid elements with similar velocity values (originally at the same location) will probably remain together for a longer time and due to that their conditional scalar mean will be different from the unconditional one [5]. This can be seen as mixing of the fluid elements residing in one turbulent eddy, having thus a higher chance to mix among each other.

3.3 Implementation of the IECM Micro-Mixing Model

The main difficulty of the implementation of the IECM model is finding the required velocity-conditioned averages of the scalars participating in the mixing: $\widetilde{\phi_\alpha|\boldsymbol{U}=\boldsymbol{V}}$. In this work it is achieved using an algorithm found in [17], where the particles residing in a finite volume cell are divided into subgroups according to their velocities

called "conditioning bins". The average of a particular scalar (mixture fraction or progress variable) conditional on the velocity value representative of the conditioning bin is then obtained by computing the average of this scalar from the particle scalar values that belong to the bin. Arranging the particles into the conditioning bins is done as follows, reminding that due to the $2D$ geometry the velocity space is two dimensional $\boldsymbol{U} = (U_1, U_2)$:

1. The particles in the element are sorted according to their first velocity component.
2. The sorted list is divided into N_1 parts with an approximately equal number of particles and each of these is consequently sorted in the second velocity component.
3. Again dividing each of the found lists into N_2 parts with an approximately equal number of particles results in obtaining $N_c = N_1 \times N_2$ conditioning bins, each containing particles with comparable velocity values.

An illustration of the result of this procedure is given in Fig. 3. This is shown for a cell containing $N_{p/e} = 350$ particles which are subdivided in $N_c = 12$ conditioning bins. The particles belonging to the same bin have the same symbol in the plot. The amount of particles in each conditioning bin is thus $np = 29$. The configuration of subdivision in the U_1 and U_2 velocity range for this particular example is chosen to be $N_1 = 4$ and $N_2 = 3$ respectively.

The calculation of velocity conditioned scalar Favre-mean value is considered next. Figure 4 shows the scatter plot of the same set of Monte Carlo particles as given in Fig. 3, but now plotted as a function of scalar variables ξ and $\mathcal{Y}$. The blue rectangles are drawn through the minimum and the maximum of both scalar variables in every conditioning bin, in this way a rectangle corresponding to a conditioning

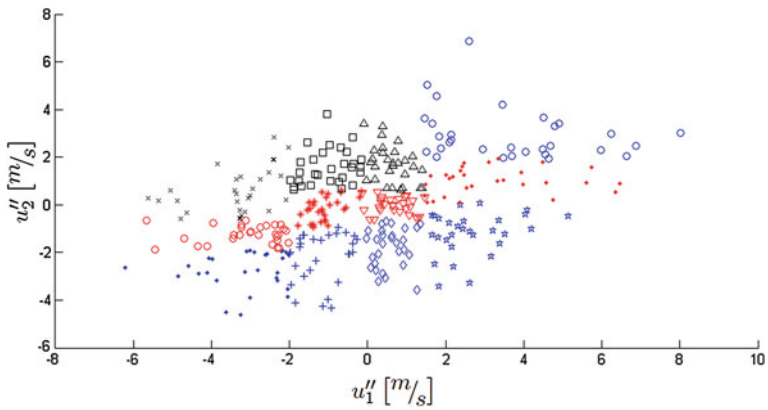

Fig. 3 Scatter plot (for one cell) of the distribution of the particles among $N_c = 12$ conditioning bins as a function of velocity fluctuations u_i''. Particles residing in one bin are assigned the same symbol

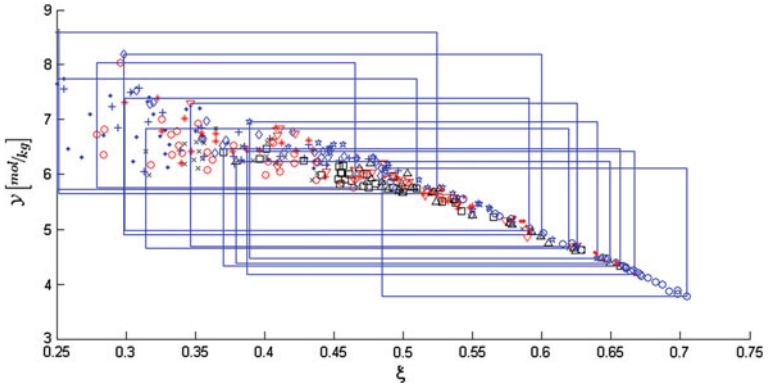

Fig. 4 Scatter plot of the Monte Carlo particles from one cell as a function of the scalar composition, particles belonging to one conditioning bin are assigned the same symbol with the range of the scalar values indicated for each conditioning bin by a *blue rectangle*

bin illustrates the range of scalars in this bin. The velocity conditioned scalar Favre-average in a conditioning bin containing np particles is estimated using:

$$\langle \phi_\alpha \,|\boldsymbol{U} = \boldsymbol{V}\rangle \approx \langle \phi_\alpha \,|\boldsymbol{U} = \boldsymbol{V}\rangle_{(np)} = \frac{1}{W^{(np)}} \sum_{i=1}^{np} w^{(i)} \phi_\alpha^{(i)}, \tag{38}$$

with $W^{(np)}$ the total numerical weight of the particles in the bin, given by:

$$W^{(np)} = \sum_{i=1}^{np} w^{(i)}. \tag{39}$$

For the mixing step, the particles of a given conditioning bin are mixed according to the Eq. (31), with the velocity conditioned scalar mean given by Eq. (38).

An idealized test case is studied to assess the quality of the method used to determine the velocity conditioned scalar mean. This test case applies the conditioning binning method, explained in this section, to a set of N_p random particles generated as a bi-variate normal distribution with the mean vector and the covariance matrix given by:

$$\boldsymbol{\mu} = \begin{pmatrix} 0.5 \\ 12 \end{pmatrix} \qquad \Sigma = \begin{pmatrix} 0.01 & 0.32 \\ 0.32 & 16 \end{pmatrix} \tag{40}$$

The first variable can be thought of as a scalar ϕ and the second as a velocity component U. The set is subdivided into $N_c = 12$ equally large bins, each containing np particles with comparable velocity U. Then the velocity conditioned mean of the scalar $\langle \phi \,|U\rangle_{(np)}$ can be estimated for each bin. The fact that the set of particles is generated as a bi-variate normal distribution with known mean and covariance values allows to calculate the exact U-conditioned mean of ϕ:

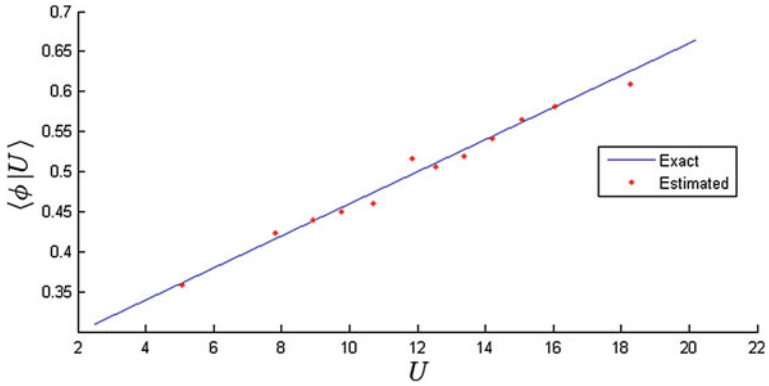

Fig. 5 Test case. Comparison of the estimated and the exact values of $\langle \phi \,|U\, \rangle$

$$\langle \phi \,|U\, \rangle = \mu_\phi + \rho \frac{\sigma_\phi}{\sigma_U} \left(U - \mu_U\right). \tag{41}$$

Now the estimated and the exact values of the velocity conditioned scalar mean can be compared. This comparison is shown in Fig. 5 for $N_p = 300$ particles (resulting in the size of each bin $np = 25$). In Fig. 5 the "estimated point" for each of the 12 conditioning bins is located at the coordinate $\left(\langle U \rangle_{(np)}, \langle \phi \,|U\, \rangle_{(np)}\right)$. In this way it is assumed that the bin-estimated U-conditioned mean of ϕ corresponds to the mean U-value in this bin $\left\langle \phi \,\middle|\, U = \langle U \rangle_{(np)} \right\rangle_{(np)}$. Therefore, the estimated conditional mean is most representative for the particles with the U value close to the bin average. For particles (contained in the same bin) with the U-value slightly deviating from the mean $\langle U \rangle_{(np)}$ the bin-estimate of the conditional mean will be slightly less representative.

This test case is performed varying the number of particles per bin np from 25 to 500, to assess the bin size dependence of the expected relative statistical error $\epsilon_{(np)}$. This is done for multiple times to perform an ensemble averaging to reduce the stochastic error. Figure 6 shows the plot of the expected relative statistical error $\epsilon_{(np)}$ as a function of the conditioning bin size np, calculated by:

$$\epsilon_{(np)} = \left\langle \left| \frac{\langle \phi |\, U \rangle_{(np)} - \langle \phi |\, U \rangle}{\langle \phi |\, U \rangle} \right| \right\rangle_{EA} \tag{42}$$

The plot shows also a regression, performed on this data set in order to fit the following equation:

$$\epsilon_{(np)}^{\text{regress}} = \sqrt{\frac{c_1}{(np)}} \quad , \tag{43}$$

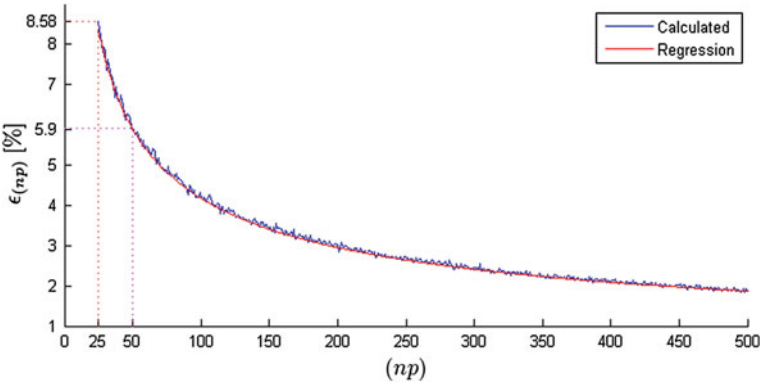

Fig. 6 Expected relative statistical error $\epsilon_{(np)}$ as a function of bin size (np)

resulting in $c_1 = 0.17$. The conducted test case shows that the statistical error of the method used to estimate the velocity conditioned scalar mean is inversely proportional to the square root of the bin size.

The actual number of particles per cell $N_{p/e}$ is varying between different cells and Monte Carlo iterations. In the PDFD code this number is controlled by the simulation input parameter "*nominal* number of particles per cell" $N_{p/e}^{nom}$. The actual number of particles per cell in a simulation lies mostly between 80 and 95 % of the $N_{p/e}^{nom}$ rarely occurring below these values. Assuming that the result of the test case, showing $\epsilon_{(np)} \propto {}^{1}/_{\sqrt{(np)}}$, can be qualitatively applied to the real joint velocity-scalar composition PDF Monte Carlo simulation, the choice of the bin size in the implemented IECM subroutine is made prescribing the minimal allowed number of particles per bin $(np)_{min}$. This is done to keep the error of the velocity conditioned scalar mean estimation as homogeneous as possible throughout the domain. Table 1 shows examples of the configurations of subdivision in the U_1 and U_2 velocity components (N_1 and N_2) for different number of particles per cell $N_{p/e}$ with the $(np)_{min} = 25$ prescribed.

One of the simulations performed has an input $N_{p/e}^{nom} = 360$ and $(np)_{min} = 25$, which implies that for most of the cells (as long as $300 < N_{p/e} < 375$) the conditioning bins configuration $N_c = 12$ ($N_1 = 4$ and $N_2 = 3$) is automatically chosen by the IECM subroutine. In practice employing the implemented IECM mixing

Table 1 Binning configuration for different number of particles in a cell $N_{p/e}$ as a result of prescribed minimal size of a conditioning bin equal $(np)_{min} = 25$

$N_{p/e}$	<50	<100	<150	<200	<225	<250	<300	<375	<400	<450	<500
$N_1 \times N_2$	1×1 (IEM)	2×1	2×2	3×2	4×2	3×3	5×2	4×3	5×3	4×4	6×3

model and taking the minimal number of particles per bin to be lower than 25 (e.g. in the order of 10) caused the resulting profiles to be heavily oscillating and discontinuous. Most probably the reason of the non-smooth profiles is the high statistical error of the conditional mean estimation. So the simulations performed in this study are done with $(np)_{min} = 25$ or $(np)_{min} = 50$.

4 Test Case and Numerical Details

4.1 Delft III Flame

To investigate the performance of the two different micro-mixing models IEM and IECM the experimental data of the Delft III flame is used. The Delft III flame is generated by a piloted non-premixed co-flow flame burner as shown in Fig. 7. The Delft III burner was designed to produce an axisymmetric turbulent diffusion flame. The burner is 1 m long and consists of the central fuel pipe surrounded by two concentric pipes providing a primary and a secondary air co-flows. The fuel is Dutch natural gas with the volumetric composition approximately given by: 81 % CH_4, 3 % C_2H_6, 15 % N_2 ([18]). Initially the fuel pipe diameter is 8 mm, at the position 16 mm upstream of the nozzle exit this diameter is decreased to 6 mm to allow a placement of 12 pilot flames, which have the purpose to stabilize the flame. The pilot flames emerge from 0.5 mm diameter holes and form a ring with a diameter of 7 mm. The pilots are premixed hydrogen/acetylene/air flames, with C to H ratio equal to that of natural gas. The outer diameter of the primary air annulus is 45 mm. A schematic of the flame burner is shown in Fig. 7 (left) together with a photograph of the burner head with the pilot flames (right). The flame is placed in a octagonal glass flame chamber with dimensions 57 cm from side to side and height 0.90 m. Also a

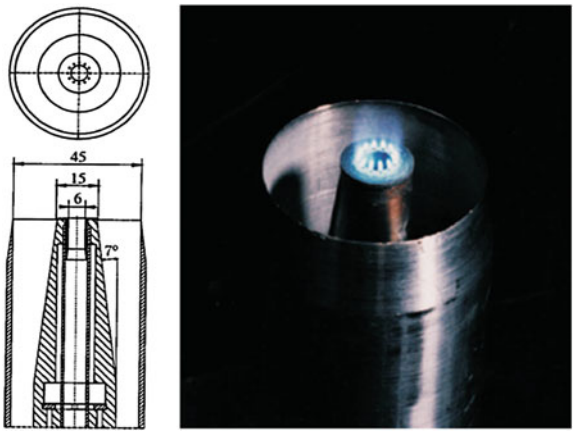

Fig. 7 Schematic of the burner (*left*, all dimensions in mm) and photograph of burner head with pilot flames (*right*)

Table 2 Flow conditions of Delft III flame [7]

Stream	U (m/s)	T (K)	Re
Fuel	21.9	295	9700
Primary air	4.4	295	8800
Secondary air	0.3	288	12,000

ventilated throat is operating, providing a secondary air co-flow which prevents an occurrence of a large-scale recirculation in the burning chamber. The conditions of the inlet streams of the fuel jet, the primary air co-flow and the secondary air co-flow of the Delft III flame can be found in Table 2.

The pilot flames stabilize the flame at the burner rim. The pilot-jets exit velocity is 13.3 m/s, and the composition of pilot mixture is: $Y_{H_2} = 0.01631$, $Y_{C_2H_2} = 0.07392$, $Y_{N_2} = 0.6983$, $Y_{O_2} = 0.211496$ and $T = 295$ K. The heat release of the 12 pilot flames forms about 1 % of the total thermal power of Delft III flame. Numerical studies of Delft III flame using PDF methods were done by [19, 20]. Both studies present results of two dimensional simulations of this flame using transported joint composition PDF methods. In two dimensional simulations of the Delft III flame the 12 separated pilot flames can not be represented exactly due to the lack of axisymmetry. The pilot flame model adopted in this work is discussed in the next section.

4.2 Numerical Setup

The stabilizing effect of the small pilot flames is crucial to prevent global extinction in simulations of the Delft III flame. In this work, the cross section of the twelve pilot flame holes is distributed into an axisymmetric ring and the velocity of the pilot flame inlet is calculated such that the experimental mass flow rate is obtained. The composition of the pilot flame is simply assumed to be a DNG-air mixture. The inlet temperature of the pilot stream is $T = 295$ K. To ensure that the pilot flames ignite the main diffusion flame we enforce the mixed is burnt condition in the region where the pilot flame is expected to be. This is done by setting the progress variable $\mathcal{Y}$ to its maximum value for all Monte Carlo particles in the region $1\,\text{mm} < x < 30\,\text{mm}$ and $3\,\text{mm} < r < 7\,\text{mm}$. The maximum value of the progress variable of a Monte Carlo particle $\mathcal{Y}^*_{max}$ is found in the FGM tables as a function of the particle's mixture fraction ξ^*. As a second measure to ensure the numerical ignition of the flame we have increased the value of the mixing parameter C_ϕ. The flame was found to be numerically ignited using $C_\phi = 11$ in the near nozzle region (up to $x = 75\,\text{mm}$) and $C_\phi = 3$ in the rest of the domain. Such large values for C_ϕ are plausible as discussed in [21] where it was reported that higher C_ϕ values (of order 10–20) can be required in PDF simulations to prevent numerical extinction.

The size of the computational domain of the simulations is given by $L_x = 1015\,\text{mm}$ and $L_r = 300\,\text{mm}$ and the domain is discretized by a 162×93 non-uniform rectangular grid (smaller cell size near axis and in the upstream region). All terms in the finite volume method are discretized with second order accurate schemes. In the hybrid finite-volume/Monte Carlo solution algorithm the joint velocity-scalar PDF Monte Carlo submodel requires the second moment closure finite-volume submodel (the Reynolds-stresses model). First an attempt has been made to start a numerical simulation of the Delft III flame using the Reynolds-stress as the finite-volume submodel and the joint velocity-scalar PDF as the Monte Carlo submodel. This resulted in the divergence of the implicit iterations of the Reynolds-stress model, making this procedure impossible. The divergence appeared in a zone with strong recirculation in a small upstream region (near the pilot) of the domain. The divergence problem was solved with a two-step approach: first, a sub-domain ($0\,\text{mm} < x < 50\,\text{mm}$) has been calculated employing a hybrid k-ϵ composition MDF (CMDF) Monte Carlo solution algorithm (see [6] for more details). The turbulent flow field and scalar composition profiles at $x = 15\,\text{mm}$ resulting from this simulation have then been used as the inflow boundary condition for the Reynolds-stress/joint velocity-scalar PDF Monte Carlo simulations presented in this work. To avoid confusion, in this paper the comparison of the simulations with the experiment is presented in the laboratory system of coordinates. In the final procedure converged solutions are obtained after 2000 hybrid iterations each consisting of 500 FV iterations followed by 10 Monte Carlo subiterations.

Within this work five different simulations have been performed, using different settings for the micro-mixing model. These are listed in the Table 3. The simulations are carried out to show the difference in performance between the IEM and the IECM models. Also an assessment is made of the dependence of the IECM model results on the number of bins and the number of particles per bin. The number of conditioning bins N_c for the IECM simulations is given in the table as the expected value. The actual number of conditioning bins for some cells can become lower if the cell does not contain enough particles to satisfy the minimum particles per bin $(np)_{min}$ requirement. Also the higher N_c configurations (see Table 1) can occur if the number of particles in a cell is high enough. The approximate distribution of the conditioning bins configurations in the simulation I is $N_c = 12$ in case of 45 % of the cells, three configurations $N_c = 10$, 15 and 16 together cover another 45 % of the

Table 3 The micro-mixing model settings for different simulations

Case	Mixing model	$N_{p/e}^{nom}$	$(np)_{min}$	$\langle N_c \rangle$
I	IECM	360	25	12
II	IECM	360	50	6
III	IECM	180	25	6
IV	IEM	360		
V	IEM	180		

cells, the remaining 10 % of the cells are distributed among other configurations. In the simulations II and III 60 % of the cells attain the $N_c = 6$ configuration and 30–35 % are subdivided between $N_c = 4$ and 8. The results of the fifth simulation IEM $N_{p/e}^{nom} = 180$ are found to be nearly identical to the results of the fourth simulation IEM $N_{p/e}^{nom} = 360$ and are not reported. The presented results of the simulations are all obtained using the same numerical settings differing only in the micro-mixing models used.

5 Results and Discussion

5.1 Velocity Statistics

This section presents results for the velocity statistics from the simulations I–IV (see Table 3) compared to the experimental LDA data. Overall, the flow fields obtained with different settings for the micro-mixing model are nearly the same, but the IEM results differ slightly from the IECM results. Figure 8 shows the radial profiles of the mean axial velocity $\widetilde{U}$ as a function of r at different axial positions x. At axial locations $x = 50\,\text{mm}$ and $x = 100\,\text{mm}$ the agreement with the experimental results is excellent. This good agreement validates the two step simulation approach discussed in Sect. 4.2 since incorrect inflow conditions would be most noticeable at $x = 50\,\text{mm}$. Further downstream the quality of the predictions is still good although the spreading rate of the jet is somewhat under predicted: the peak velocity at the center-line is too high but the profile is not wide enough (due to mass conservation in each plane). This means that the high momentum fluid from the fuel nozzle does not mix fast enough with low momentum air flow for locations $x > 150\,\text{mm}$. The results for the RMS of the axial velocity U_{RMS} (shown in Fig. 9) display an underestimation of the maximal values at the upstream locations $x = 50\,\text{mm}$ and $x = 100\,\text{mm}$. Further downstream at $x = 200\,\text{mm}$ and $x = 250\,\text{mm}$ the peak values are predicted quite well but the under-predicted spreading rate of the jet is noticeable (the U_{RMS} profiles are not wide enough).

The profiles of the turbulence kinetic energy (tke) $k = 0.5*(U_{RMS}^2+V_{RMS}^2+W_{RMS}^2)$ are shown in Fig. 10. The tke provides a measure of the overall level of turbulent fluctuations in the velocity. Very good agreement with the experimental values can be observed at locations $x = 50\,\text{mm}$ and $x = 100\,\text{mm}$ indicating the validity of the two-step solution procedure. Further downstream at $x = 150\,\text{mm}$, $x = 200\,\text{mm}$ and $x = 250\,\text{mm}$ the simulations predict slightly too large peak values and also show the under prediction of the jet spreading rate.

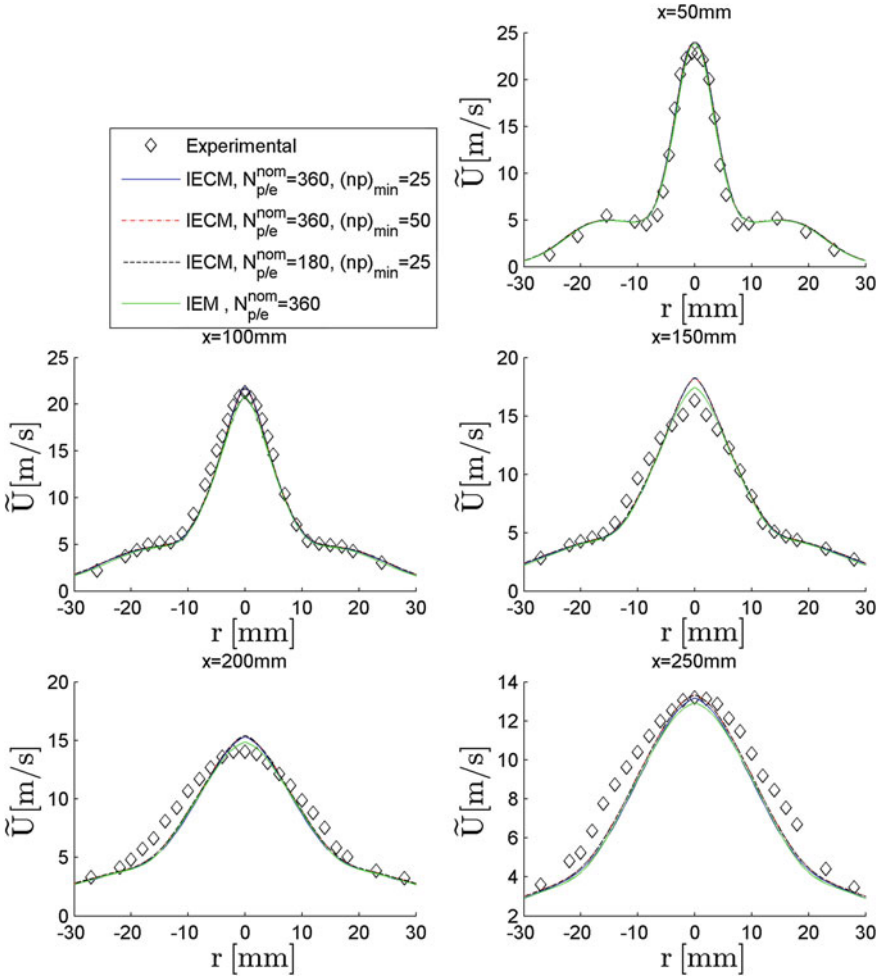

Fig. 8 Radial profiles of the mean axial velocity $\widetilde{U}$ as a function of r at different axial locations x

5.2 Results for the Mixture Fraction Fields

This section presents the results of the conserved scalar (the mixture fraction) statistics of the simulations I to IV (see Table 3) compared to the experimental data. As expected, for the scalar fields clear differences are observed between different micro-mixing models. Figure 11 shows radial profiles of the mean mixture fraction $\widetilde{\xi}$. At the axial location $x = 50\,\text{mm}$ the agreement with the experimental results is excellent and again justifies the two-step solution procedure. From the analysis of the velocity statistics it was found that the spreading rate of the jet is under predicted for the far downstream locations due to insufficient turbulent mixing of momentum.

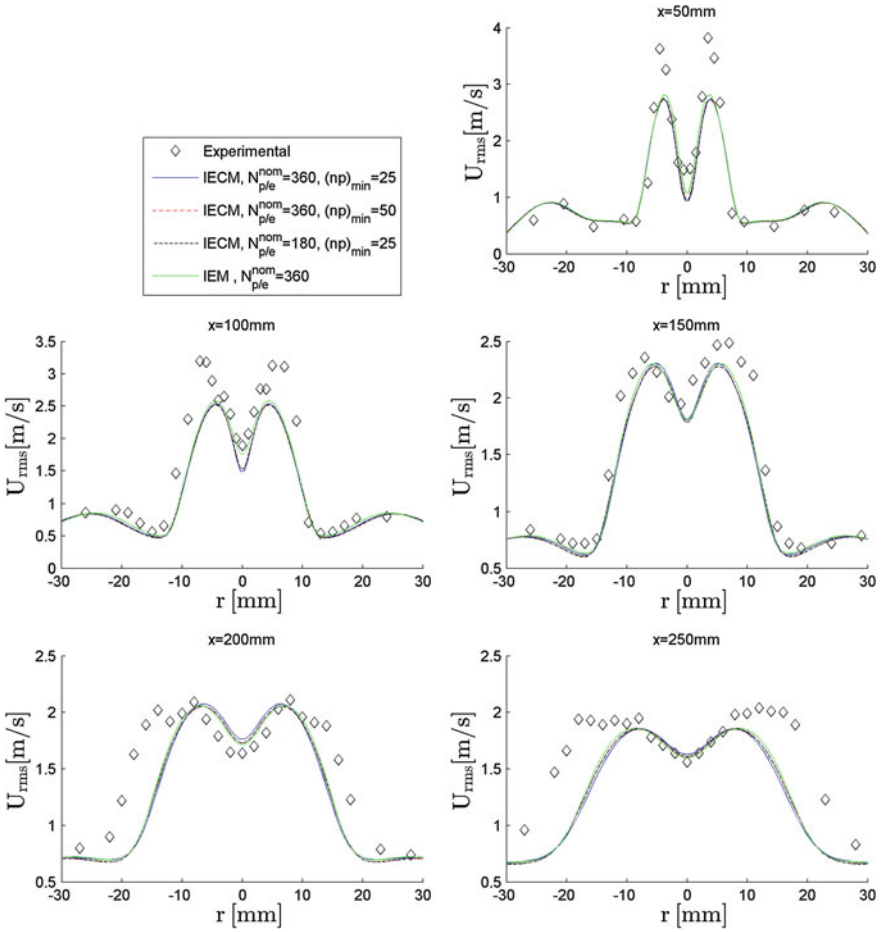

Fig. 9 Radial profiles of the root mean square of the axial velocity U_{rms} as a function of r at different axial locations x

The same mechanism of turbulent mixing is responsible for the mixing of the "conserved" scalar mixture fraction and hence we expect to see that the $\widetilde{\xi}$ profiles spread too slowly. This is indeed observed for all simulations at the downstream locations $x > 50\,\text{mm}$ but the error is much larger in the IEM results (green line) than in IECM results with the statistically best resolved IECM simulation (blue line) showing the smallest disagreement. The reason for the large error in the IEM results is directly related to the incorrect additional source term (37a) $\widetilde{\overline{u_i'' \theta^{IEM}_{\xi,mix}}} = -\frac{1}{2} C_\phi \omega \left[\widetilde{u_i'' \xi''}\right]$ in the scalar flux Eq. (36). It should be noted that the flux in radial direction $\widetilde{v'' \xi''}$ is the dominant contribution in the equation for the mean mixture fraction (35). This can be most easily seen from the commonly adopted gradient-diffusion approximation [1–3]

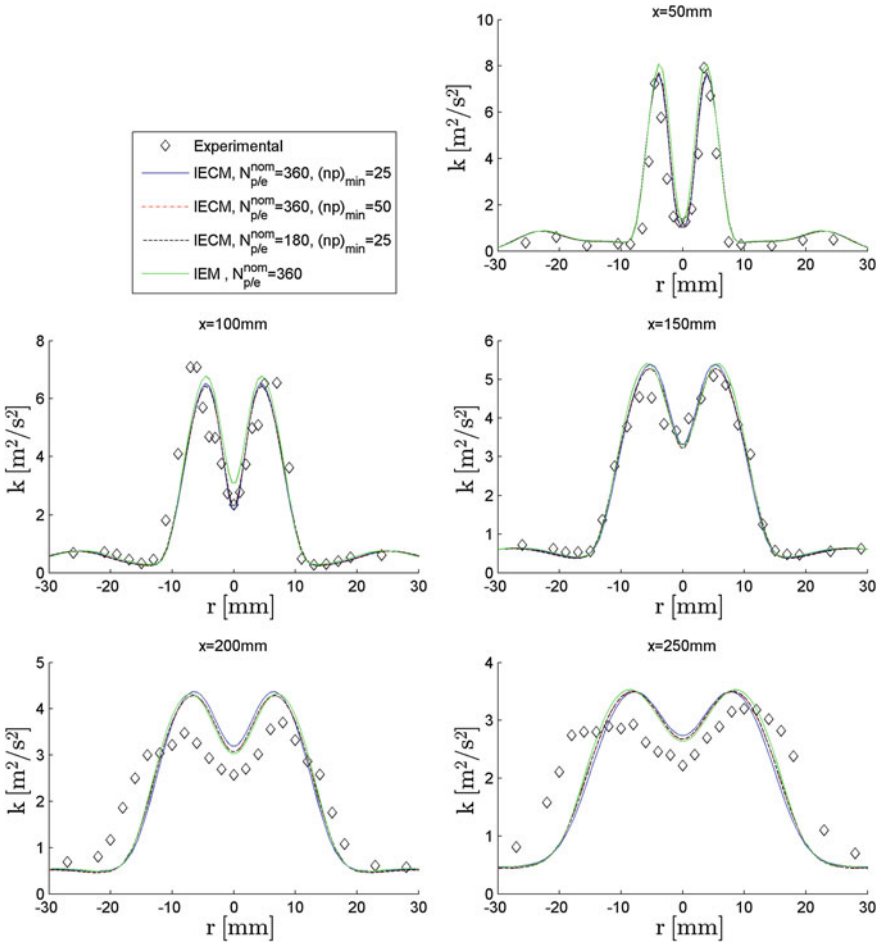

Fig. 10 Radial profiles of the turbulent kinetic energy k as a function of r at different axial locations x

$$\widetilde{u_i''\xi} \approx -\Gamma_t \frac{\partial \widetilde{\xi}}{\partial x_i}, \tag{44}$$

where Γ_T is a turbulent diffusivity. Since the radial derivative $\partial\widetilde{\xi}/\partial r$ is much larger than the axial variation in the jet flame the radial flux $\widetilde{v''\xi''}$ is much larger than the axial flux and it is positive for $r > 0$. In the equation for the radial flux component (37a) this means that the term $\widetilde{v''\theta^{IEM}_{\xi,mix}} = -\frac{1}{2}C_\phi\omega\left[\widetilde{v''\xi''}\right] < 0$ is a sink term and thus reduces the radial flux $\widetilde{v''\xi''}$. The reduced radial flux component $\widetilde{v''\xi''}$ in turn causes the insufficient mixing of the mean mixture fraction (i.e. the over prediction of the peak

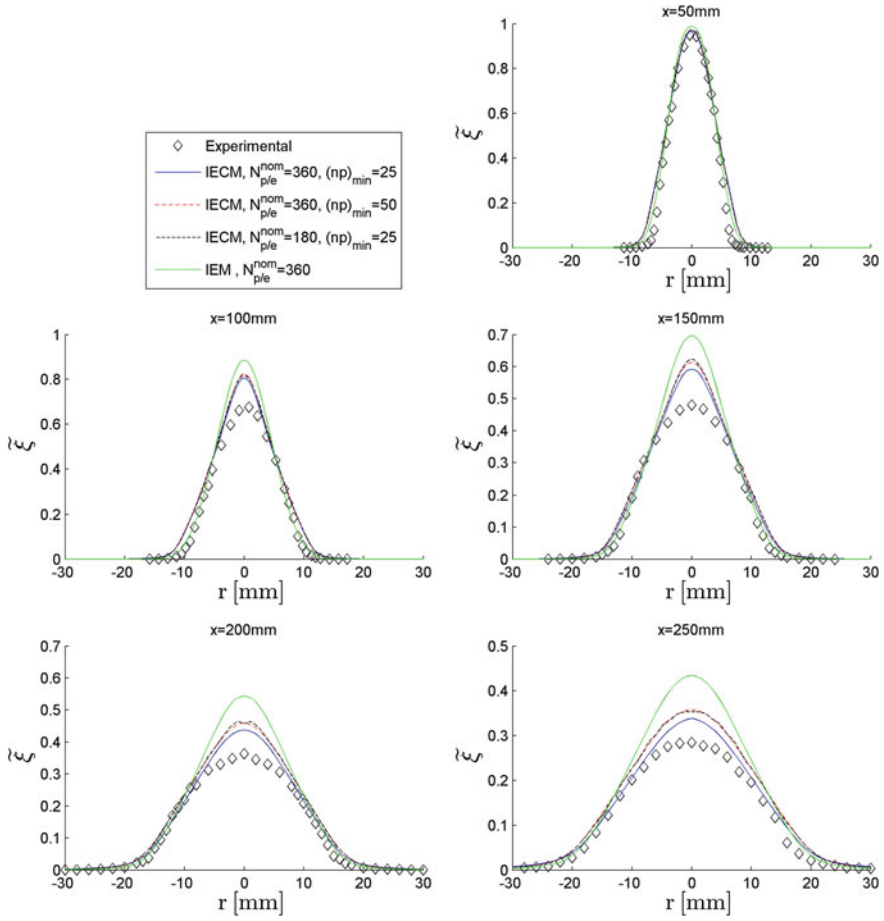

Fig. 11 Radial profiles of the mean mixture fraction $\widetilde{\xi}$ as a function of r at different axial locations x

values) for $x > 50$ in the IEM results. Since the term $\widetilde{u_i'' \theta_{\xi,mix}^{IEM}} = -\frac{1}{2} C_\phi \omega \left[\widetilde{u_i'' \xi''}\right]$ is directly proportional to the mixing constant C_ϕ and since this flame requires high C_ϕ values the effect of the erroneous sink term is so dramatic in the Delft III flame.

The radial profiles of the RMS of mixture fraction ξ_{rms} are shown in Fig. 12. Again, the results for the three IECM simulations are in much closer agreement with the experimental results than the IEM simulation results. The evolution equation for the variance $\widetilde{\xi''^2} = \xi_{rms}^2$ contains the turbulent transport term $\partial \widetilde{u_i'' \xi''^2} / \partial x_i$ and the evolution equation for $\widetilde{u_i'' \xi''^2}$ contains a similar erroneous sink for the IEM mixing model as the $\widetilde{u_i'' \theta_{\xi,mix}^{IEM}}$ term that appeared in the scalar flux equation. This erroneous

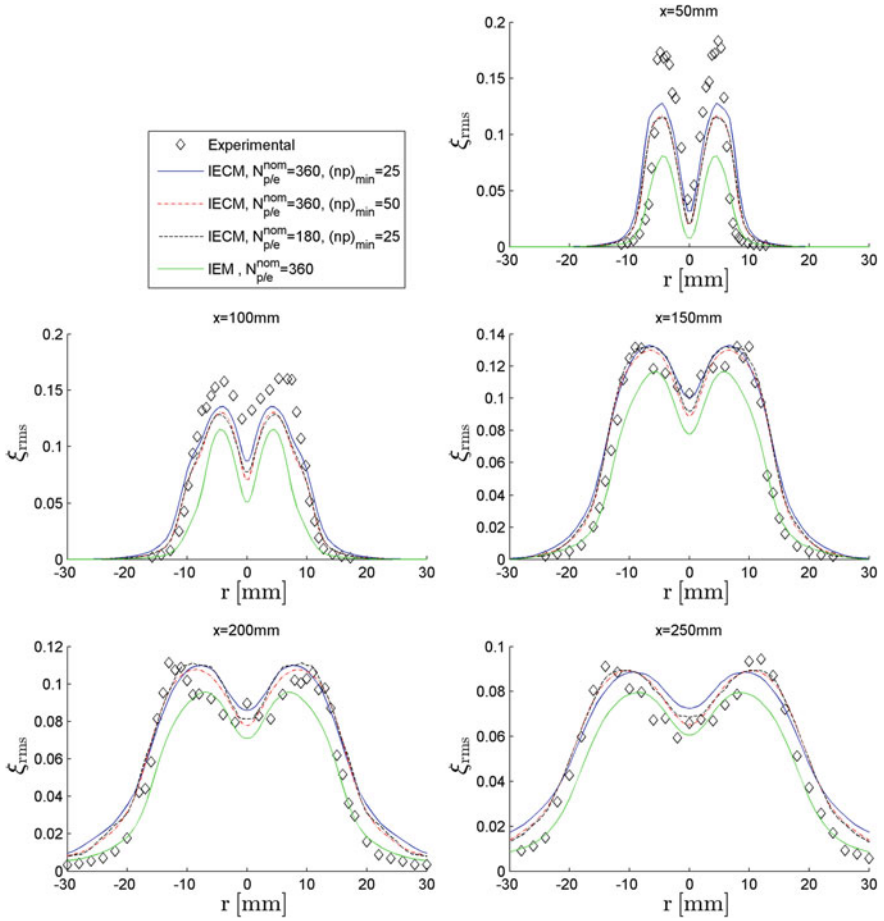

Fig. 12 Radial profiles of the root mean square of the mixture fraction ξ_{rms} as a function of r at different axial locations x

sink causes the observed under prediction of mixture fraction RMS ξ_{rms} in the IEM simulation.

5.3 Results for the Temperature

This section presents statistical results for the temperature. The temperature (and the progress variable) are strongly dependent on the mixture fraction as was shown in Sect. 2.2. Therefore, it can be expected that the observed differences between the IEM and IECM simulation results that are discussed in the previous Sect. 5.2 have a

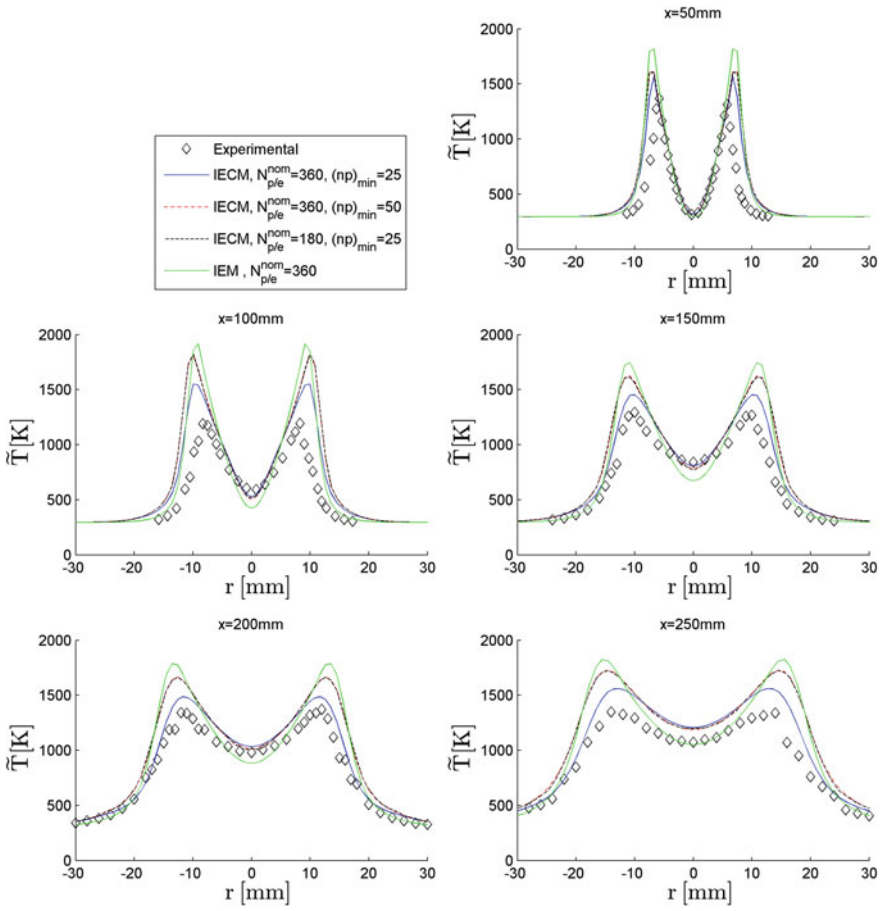

Fig. 13 Radial profiles of the mean temperature $\widetilde{T}$ as a function of r at different axial locations x

profound effect on the results for the temperature. Figure 13 shows the results for the mean temperature obtained from the four different simulations. The results obtained with the IECM micro-mixing model with the best numerical settings $N_{p/e}^{nom} = 360$, $(np)_{min} = 25$ (blue line, simulation I) shows overall the best agreement with the experimental results. At axial locations $x = 50\,\text{mm}$ and $x = 100\,\text{mm}$ the peak value of the mean temperature is over predicted but further downstream (at the axial positions $x = 150\,\text{mm}$, $x = 200\,\text{mm}$ and $x = 250\,\text{mm}$) the results for the mean temperature $\widetilde{T}$ agree quite well with the experimental results although the temperature remains slightly over predicted. The over prediction could be due to the adopted flame stabilization method. Up to $x = 75\,\text{mm}$ the value of the mixing constant is set to $C_\phi = 11$ which could cause too little local extinction and hence explain the higher than experimentally observed temperatures. A physically more sound model for C_ϕ variations will be investigated in a future study. The results of the simulation using

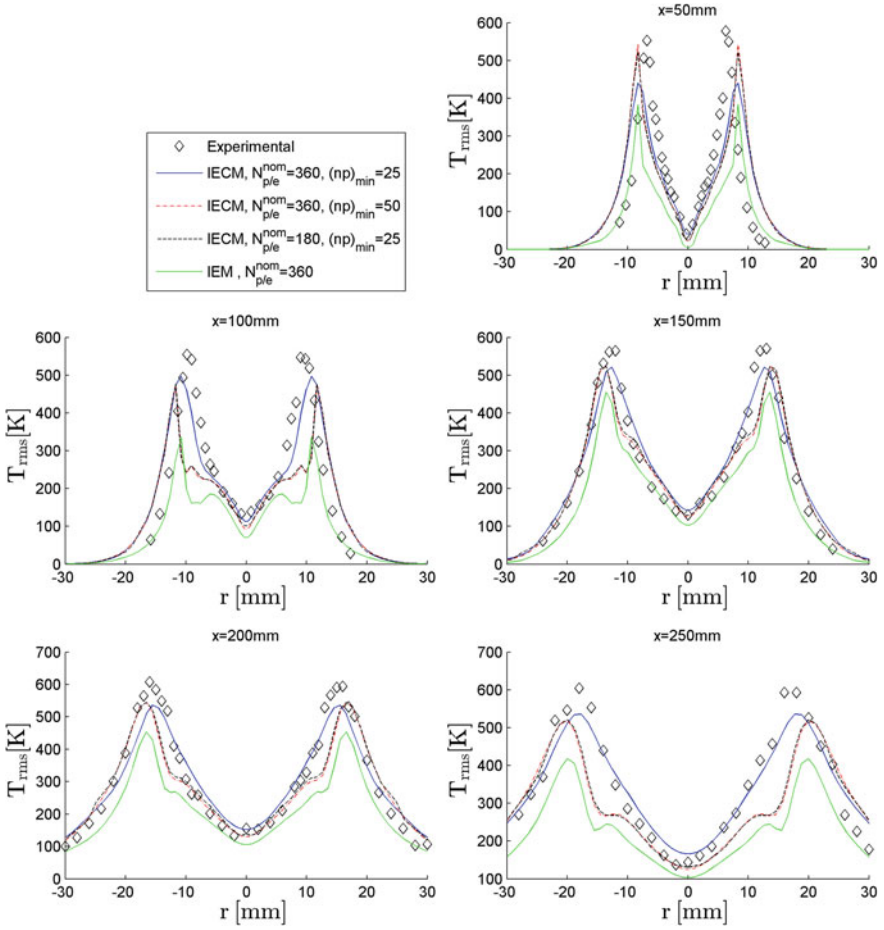

Fig. 14 Radial profiles of the root mean square of the temperature T_{rms} as a function of r at different axial locations x

the IEM micro-mixing model (green line, simulation IV) yield radial profiles of the mean temperature $\widetilde{T}$ with values which are overestimated two to three times stronger than the results with the IECM model $N_{p/e}^{nom} = 360$, $(np)_{min} = 25$. The other IECM model results (simulations II and III) fall between the IECM results of simulation I and the IEM results. The results for the mean reaction progress variable follow similar trends as for the temperature and are not shown.

The radial profiles of the RMS of temperature T_{rms} (Fig. 14) found with the IECM model are in reasonable agreement with the experimental results, however there is a moderate underestimation of the peak values. The simulation performed with the IEM model resulted in strong underestimation of T_{rms}.

5.4 Discussion on Parameters of the IECM Algorithm

The IECM model cases II and III with the input configurations respectively given by $N_{p/e}^{nom} = 360$, $(np)_{min} = 50$ and $N_{p/e}^{nom} = 180$, $(np)_{min} = 25$ have both the expected value of the number of conditioning bins per cell $\langle N_c \rangle \approx 6$. The difference between these cases is the number of particles per conditioning bin (np) which is on average twice as large in the simulation II than in the simulation III. As it can be seen throughout the Figs. 13 and 14 these two cases give similar results for all reported scalar composition variables. Thus a conclusion can be made that the $(np)_{min} = 25$ minimum amount of particles per bin is satisfactory concerning the statistical error of the conditional mean estimation, and the simulation results are not getting better if the $(np)_{min}$ is increased.

Also it can be observed that the radial profiles of $\widetilde{\xi}$ and $\widetilde{T}$ obtained with the IECM cases II and III (both with the expected value of the number of conditioning bins in a cell $\langle N_c \rangle \approx 6$) yield a better agreement with the experimental data than the IEM case results and a poorer agreement than the IECM simulation with $N_{p/e}^{nom} = 360$, $(np)_{min} = 25$ (case I with the expected value of the number of the conditioning bins in a cell $\langle N_c \rangle \approx 12$). In this way it can be concluded that the IECM model yields better results if the number of the conditioning bins in a cell increases. A possible explanation of this trend is that the IEM model does not at all account for the effects of the velocity conditioned mixing and can be thought of as having only one bin in every cell (as there is no division of particles into conditioning bins). Then employing the IECM with $\langle N_c \rangle \approx 6$, the effects of the velocity conditioned micro-mixing become taken into account causing the simulation results to become better. Apparently when the number of conditioning bins is increased to $\langle N_c \rangle \approx 12$ the quality of the simulation results improves even more as the effects of the velocity conditioned micro-mixing become better accounted for.

6 Conclusions

The most important conclusion of this work is that the influence of the underlying velocity field on the scalar micro-mixing is far from negligible. This followed from the fact that the simulation results obtained with the IECM micro-mixing model compared much better to the available experimental results than the IEM model results. A more detailed validation of the role of velocity statistics in the mixing of scalars is not possible because in the experiments no simultaneous measurements of velocity and scalars have been made. The mixture fraction profiles are up to two times less overestimated at the peak values using the IECM model. The overestimation of the mean temperature obtained with the IECM simulation is, at some locations, two to three times lower than that of the IEM simulation. Similar differences between the IEM and IECM results are found for the mean profiles of the progress variable.

A number of remarks can be made concerning the numerical method used in this thesis to implement the IECM subroutine into the PDFD code. The performance of the IECM micro-mixing model improves if the number of conditioning bins in every cell becomes larger. This improvement is due to the fact that the influence of the velocity field on the micro-mixing becomes better accounted for as the number of bins increases. In regard of the statistical error of the velocity conditioned mean estimation it can be concluded that the minimum amount of particles per bin parameter $(np)_{min}$ equal to 25 is sufficient and does not need to be increased. Changing the minimum amount of particles per bin parameter $(np)_{min}$ from 25 to 50 while keeping the number of bins unaffected does not improve the quality of the results. However due to the restriction of the minimum amount of particles per bin and the need of higher numbers of bins (in every cell) implies that employing the implemented IECM model in practice will require large amounts of particles per cell, resulting in high computational costs of the simulations.

References

1. Heinz S (2003) Statistical mechanics of turbulent flows. Springer, Berlin
2. Pope SB (1985) PDF methods for turbulent reactive flows. Prog Energy Combust Sci 11:119–192
3. Fox R (2003) Computational models for turbulent reacting flows. Cambridge University Press, Cambridge
4. Dopazo C, O'Brien EE (1974) An approach to the autoignition of a turbulent mixture. Acta Astronaut 1:1239–1266
5. Fox R (1996) On velocity-conditioned scalar mixing in homogeneous turbulence. Phys Fluids 8:2678–2691
6. Efimov D (2013) Assessment of velocity conditioned micro-mixing for PDF modeling of a turbulent non-premixed natural gas jet flame. Master's thesis, Delft University of Technology
7. de Vries J (1994) Study on turbulent fluctuations in diffusion flames using laser induced fluorescence. Ph.D. thesis, Delft University of Technology
8. Stroomer P (1995) Turbulence and OH structures in flames. Ph.D. thesis, Delft University of Technology
9. Smith GP, Golden DM, Frenklach M (1999) Gri-mech 3.0
10. Ramaekers WJS, van Oijen JA, de Goey LPH (2010) A priori testing of flamelet generated manifolds for turbulent partially premixed methane/air flames. Flow Turbul Combust 84:439–458
11. Somers B (1994) The simulation of flat flames with detailed and reduced chemical models. Ph.D. thesis, Eindhoven University of Technology
12. Wouters H (1998) Lagrangian models for turbulent reacting flows. Ph.D. thesis, Delft University of Technology
13. Pope SB (2000) Turbulent flows, 8th edn. Cambridge University Press, Cambridge
14. Correa SM, Pope S (1992) Twenty-Fourth Symposium (International) on Combustion, pp 279–285
15. Naud B, Merci B, Roekaerts D (2010) Generalized Langevin model in correspondence with a chosen standard scalar-flux second-moment closure. Flow Turbul Combust 85:363–382
16. Sawford B (2004) Micro-mixing modelling of scalar fluctuations for plumes in homogeneous turbulence. Flow Turbul Combust 72:133–160
17. Bakosi J, Franzese P, Boybeyi Z (2008) A non-hybrid method for the PDF equations of turbulent flows on unstructured grids. J Comput Phys 227:5896–5935

18. Peeters TWJ, Stroomer PPJ, de Vries JE, Roekaerts DJEM, Hoogendoorn CJ (1994) Comparative experimental and numerical investigation of a piloted turbulent natural-gas diffusion flame. Proc. Combust. Inst. 25:1241–1248
19. Nooren PA (1998) Stochastic modeling of turbulent natural-gas flames. Ph.D. thesis, Delft University of Technology
20. Merci B, Roekaerts D, Naud B (2006) Study of the performance of three micromixing models in transported scalar PDF simulations of a piloted jet diffusion flame ("Delft Flame III"). Combust Flame 144:476–493
21. Stöllinger M, Heinz S (2010) Evaluation of scalar mixing and time scale models in PDF simulations of a turbulent premixed flame. Combust Flame 157:1671–1685

Massively Parallel FDF Simulation of Turbulent Reacting Flows

P.H. Pisciuneri, S.L. Yilmaz, P.A. Strakey and P. Givi

Abstract A review is presented of the evolution of a massively parallel solver for large eddy simulation (LES) of turbulent reacting flows via the filtered density function (FDF). Development of an efficient parallel implementation is particularly challenging due to the hybrid Eulerian/Lagrangian structure of typical FDF simulators. The performance of a novel parallel simulator is assessed at each of the major steps of its development. Subsequent efforts to improve scaling at each of these stages are discussed along with the prospects for further enhancements.

1 Introduction

Despite all of the dedicated efforts towards the development of alternative and/or sustainable energy resources, combustion still provides over 85 % of the energy needs in the United States; a situation that will likely remain the same within the foreseeable future. Associated with combustion is air pollution and the greenhouse effect; thus the need for the reduction of CO_2 emissions while maintaining high combustion efficiency. These concerns, along with stringent demands to reduce petroleum consumption, are putting a high priority on combustion research. In most cases, combustion is accompanied by turbulence where the latter provides the means of

P.H. Pisciuneri (✉)
Center for Simulation and Modeling, University of Pittsburgh, Pittsburgh, PA, USA
e-mail: php8@pitt.edu

S.L. Yilmaz
MathWorks Inc., Natick, MA, USA
e-mail: leventyilmaz@gmail.com

P.A. Strakey
National Energy Technology Laboratory, Morgantown, WV, USA
e-mail: peter.strakey@netl.doe.gov

P. Givi
Department of Mechanical Engineering and Materials Science, University of Pittsburgh, Pittsburgh, PA, USA
e-mail: pgivi@pitt.edu

S. Heinz and H. Bessaih (eds.), *Stochastic Equations for Complex Systems*,
Mathematical Engineering, DOI 10.1007/978-3-319-18206-3_8

enhanced fuel-air mixing. The physics of turbulent reactive flows is notoriously difficult due to the intricacies of the interactions between chemistry and turbulence. The phenomenon of mixing at both micro and macro scales and its role and capability (or lack thereof) to provide a suitable environment for combustion, and the subsequent effects of combustion on hydrodynamics, have been at the heart of turbulent combustion research for over half a century now [1–3].

Simulation, long considered as the *third* form of science [4] (in addition to theory and experimentation) has certainly come a long way within the past three decades. It has evolved from the era of scalar computing → vector → parallel → massively parallel → current petascale → upcoming *exascale* computing. This has lead to significant progress in large scale simulation of turbulent combustion [5, 6]. Specifically, large eddy simulation (LES) is quickly replacing the traditional RANS (Reynolds averaged Navier-Stokes) simulations. This is not just in basic research, but also in industrial applications. A major progress in LES is the development of the filtered density function (FDF) methodology [7]. This has proven very effective for turbulent combustion simulations due to its capability to account for the effects of subgrid scale (SGS) chemical reactions in a very accurate manner. This is the primary reason for the broad coverage of the FDF in modern text- and hand-books [2, 8–13]. This is also the motivation for implementation of various forms of the FDF closure in commercial and government combustion codes (such as FLUENT/ANSYS, VULCAN, and US3D amongst others). For recent reviews, see Refs. [3, 14–17].

For the FDF (or any LES methodology) to be practical it must be implemented in a computationally efficient manner, especially if employed for prediction of complex flows. This important issue can be the overriding constraint. Within recent years, the *irregularly portioned* methodology has proven very useful in facilitating efficient FDF simulations. This chapter provides a summary of the state of progress in such simulations. In Sect. 2, the basic FDF formulation is summarized. This is followed by a review of the state of progress in irregularly portioned FDF simulations in Sect. 3. This section covers all of the modern domain decomposition and load balancing strategies. Section 4 provides our concluding remarks along with some recommendations for future work.

2 Filtered Density Function

The primary transport variables in chemically reactive flows are the fluid density $\rho(\mathbf{x}, t)$, the velocity vector $u_i(\mathbf{x}, t)$, $i = 1, 2, 3$ along the x_i direction, the specific enthalpy $h(\mathbf{x}, t)$, the pressure $p(\mathbf{x}, t)$, and the mass fractions of N_s species, $Y_\alpha(\mathbf{x}, t)$ $(\alpha = 1, 2, \ldots, N_s)$, where $\mathbf{x} \equiv x_i (i = 1, 2, 3)$ and t denote space and time, respectively. Implementation of LES involves the use of the spatial filtering operation [18, 19]

$$\langle Q(\mathbf{x},t)\rangle = \int_{-\infty}^{+\infty} Q(\mathbf{x}',t)\mathcal{H}(\mathbf{x}',\mathbf{x})\mathrm{d}\mathbf{x}', \tag{1}$$

where $\mathcal{H}$ denotes the filter function of width $\Delta_{\mathcal{H}}$, and $\langle Q(\mathbf{x},t)\rangle$ represents the filtered value of the transport variable $Q(\mathbf{x},t)$. In reacting flows, it is convenient to consider the Favre filtered quantity, $\langle Q(\mathbf{x},t)\rangle_L = \langle \rho Q\rangle/\langle\rho\rangle$. We consider spatially invariant and localized filter functions, $\mathcal{H}(\mathbf{x}',\mathbf{x}) \equiv \mathcal{H}(\mathbf{x}'-\mathbf{x})$ with the properties [20] $\mathcal{H}(\mathbf{x}) = \mathcal{H}(-\mathbf{x})$, and $\int_{-\infty}^{\infty}\mathcal{H}(\mathbf{x})\mathrm{d}\mathbf{x} = 1$. We consider *positive* filter functions [21] for which all the moments $\int_{-\infty}^{\infty} x^m\mathcal{H}(x)\mathrm{d}x$ exist for $m \geq 0$. The transport variables satisfy the conservation equations of mass, momentum, energy and species mass fractions [22]. The filtered form of these equations are:

$$\frac{\partial\langle\rho\rangle}{\partial t} + \frac{\partial\langle\rho\rangle\langle u_i\rangle_L}{\partial x_i} = 0, \tag{2}$$

$$\frac{\partial\langle\rho\rangle\langle u_j\rangle_L}{\partial t} + \frac{\partial\langle\rho\rangle\langle u_i\rangle_L\langle u_j\rangle_L}{\partial x_i} = -\frac{\partial\langle p\rangle}{\partial x_j} + \frac{\partial\langle\tau_{ij}\rangle}{\partial x_i} - \frac{\partial T_{ij}}{\partial x_i}, \tag{3}$$

$$\frac{\partial\langle\rho\rangle\langle\phi_\alpha\rangle_L}{\partial t} + \frac{\partial\langle\rho\rangle\langle u_i\rangle_L\langle\phi_\alpha\rangle_L}{\partial x_i} = -\frac{\partial\langle J_i^\alpha\rangle}{\partial x_i} - \frac{\partial M_i^\alpha}{\partial x_i} + \langle\rho S_\alpha\rangle, \tag{4}$$

where τ_{ij} and J_i^α denote the viscous stress tensor and the scalar fluxes, respectively. In Eq. (4), S_α denotes the source term, and this equation represents transport of the species mass fractions and enthalpy in a common form with $\phi_\alpha \equiv Y_\alpha$, $\alpha = 1,2,\ldots,N_s$, $\phi_\sigma \equiv h$, $\sigma = N_s+1$. The SGS closure problem is associated with $T_{ij} = \langle\rho\rangle\left(\langle u_iu_j\rangle_L - \langle u_i\rangle_L\langle u_j\rangle_L\right)$, $M_i^\alpha = \langle\rho\rangle\left(\langle u_i\phi_\alpha\rangle_L - \langle u_i\rangle_L\langle\phi_\alpha\rangle_L\right)$, and $\langle\rho S_\alpha\rangle$. The FDF provides an effective means for this closure. For the scalars' array $\boldsymbol{\phi}(\mathbf{x},t)$ and the velocity field, $\boldsymbol{u}(\mathbf{x},t)$, the SGS statistical information is included in the joint velocity-scalar filtered mass density function (VS-FMDF), denoted by $\mathcal{F}(\boldsymbol{v},\boldsymbol{\psi},\mathbf{x},t)$, where $(\boldsymbol{v},\boldsymbol{\psi})$ denote the probability-space for the $(\boldsymbol{u},\boldsymbol{\phi})$ fields. The exact transport equation for this FDF is [23–25]:

$$\begin{aligned}\frac{\partial\mathcal{F}}{\partial t} + \frac{\partial\left(v_k\mathcal{F}\right)}{\partial x_k} &= \frac{\partial}{\partial v_k}\left[\left\langle\frac{1}{\rho}\frac{\partial p}{\partial x_k}\middle|\boldsymbol{v},\boldsymbol{\psi}\right\rangle\mathcal{F}\right] - \frac{\partial}{\partial v_k}\left[\left\langle\frac{1}{\rho}\frac{\partial\tau_{kj}}{\partial x_j}\middle|\boldsymbol{v},\boldsymbol{\psi}\right\rangle\mathcal{F}\right]\\ &+ \frac{\partial}{\partial\psi_\alpha}\left[\left\langle\frac{1}{\rho}\frac{\partial J_j^\alpha}{\partial x_j}\middle|\boldsymbol{v},\boldsymbol{\psi}\right\rangle\mathcal{F}\right] - \frac{\partial}{\partial\psi_\alpha}\left[S_\alpha(\boldsymbol{\psi})\mathcal{F}\right],\end{aligned} \tag{5}$$

where $\langle\,|\,\rangle$ denotes the conditional filtered values. As Eq. (5) shows, the effects of SGS convection and combustion are in *closed* forms. However, all of the terms involving conditional filtered values require closure. The marginal FMDF of the scalar (S-FMDF) field, $\mathcal{F}_{\boldsymbol{\phi}}(\boldsymbol{\psi},\mathbf{x},t)$, is obtained by integration of the VS-FMDF over

the velocity domain [26, 27]:

$$\frac{\partial \mathcal{F}_{\boldsymbol{\phi}}}{\partial t} + \frac{\partial \left[\langle u_i(\mathbf{x},t)|\boldsymbol{\psi}\rangle \mathcal{F}_{\boldsymbol{\phi}}\right]}{\partial x_i} = \frac{\partial}{\partial \psi_\alpha}\left[\left\langle \frac{1}{\rho}\frac{\partial J_j^\alpha}{\partial x_j}\middle|\boldsymbol{\psi}\right\rangle \mathcal{F}_{\boldsymbol{\phi}}\right] - \frac{\partial}{\partial \psi_\alpha}\left[S_\alpha(\boldsymbol{\psi})\mathcal{F}_{\boldsymbol{\phi}}\right]. \quad (6)$$

Again, the effects of chemical reaction appear in a closed form. However, in this case, the SGS convection (second term on the left-hand side) requires closure. This approach has been the most popular among other investigators using FDF [28–49].

The SGS closures have been primarily based on modeled stochastic differential equations (SDEs) for each of the transport variables. These SDEs must account for all of the physics of turbulent combustion; including scalar mixing, chemistry, exothermicity, dilatation, and dissipation. It is straightforward to realize the capability of the FDF in that it accounts for all of the processes involving direct correlations of the transported variables. For example, there is no need for additional closures for turbulent-chemistry interactions and/or velocity-scalar correlations. A system of modeled SDEs [50, 51] based on the stochastic diffusion process [52] has proven effective for the FDF closure. The coefficients in the modeled Langevin equation will be set in such a way that the resulting Fokker-Planck equation [53] defines the modeled FDF transport equation, and thus the SGS closures. In particular, the generalized Langevin model (GLM) [54–57] combined with the linear mean square estimation (LMSE) [58, 59] has proven to be effective. This is described by [24, 60–62]

$$\mathrm{d}x_i^+ = u_i^+\,\mathrm{d}t + \sqrt{\frac{2\mu}{\langle\rho\rangle}}\,\mathrm{d}W_i, \quad (7a)$$

$$\begin{aligned}\mathrm{d}u_i^+ = &-\frac{1}{\langle\rho\rangle}\frac{\partial\langle p\rangle}{\partial x_i}\mathrm{d}t + \frac{2}{\langle\rho\rangle}\frac{\partial}{\partial x_j}\left(\mu\frac{\partial\langle u_i\rangle_L}{\partial x_j}\right)\mathrm{d}t\\ &+ \frac{1}{\langle\rho\rangle}\frac{\partial}{\partial x_j}\left(\mu\frac{\partial\langle u_j\rangle_L}{\partial x_i}\right)\mathrm{d}t - \frac{2}{3}\frac{1}{\langle\rho\rangle}\frac{\partial}{\partial x_i}\left(\mu\frac{\partial\langle u_j\rangle_L}{\partial x_j}\right)\mathrm{d}t\\ &+ G_{ij}\left(u_j^+ - \langle u_j\rangle_L\right)\mathrm{d}t + \sqrt{C_0 k\,\omega}\,\mathrm{d}W_i' + \sqrt{\frac{2\mu}{\langle\rho\rangle}}\frac{\partial\langle u_i\rangle_L}{\partial x_j}\mathrm{d}W_j, \end{aligned} \quad (7b)$$

$$\mathrm{d}\phi_\alpha^+ = -C_\phi\,\omega\left(\phi_\alpha^+ - \langle\phi_\alpha\rangle_L\right)\mathrm{d}t + S_\alpha(\boldsymbol{\phi}^+)\,\mathrm{d}t, \quad (7c)$$

where x_i^+, u_i^+, ψ_α^+ are probabilistic representations of position, velocity vector and scalar variables, respectively. μ denotes the fluid dynamic viscosity. The W terms denote the Wiener-Lévy processes in the physical (without the prime) and the velocity (with prime) spaces [63]. The terms G_{ij} and $k = T_{ii}/2\langle\rho\rangle$ denote the kernel of GLM and the SGS kinetic energy, respectively. The mixing frequency ω is defined as: $\omega = C_f k^{1/2}/\Delta_{\mathcal{H}}$. The constants: C_0, C_ϕ and C_f are model parameters and are chosen as suggested in the literature [57]. The corresponding Fokker-Planck equation, or effectively the modeled VS-FMDF transport equation becomes:

$$\frac{\partial \mathcal{F}}{\partial t}+\frac{\partial v_i \mathcal{F}}{\partial x_i}=\frac{1}{\langle\rho\rangle}\frac{\partial\langle p\rangle}{\partial x_i}\frac{\partial \mathcal{F}}{\partial v_i}-\frac{2}{\langle\rho\rangle}\frac{\partial}{\partial x_j}\left(\mu\frac{\partial\langle u_i\rangle_L}{\partial x_j}\right)\frac{\partial \mathcal{F}}{\partial v_i}$$
$$-\frac{1}{\langle\rho\rangle}\frac{\partial}{\partial x_j}\left(\mu\frac{\partial\langle u_j\rangle_L}{\partial x_i}\right)\frac{\partial \mathcal{F}}{\partial v_i}+\frac{2}{3}\frac{1}{\langle\rho\rangle}\frac{\partial}{\partial x_i}\left(\mu\frac{\partial\langle u_j\rangle_L}{\partial x_j}\right)\frac{\partial \mathcal{F}}{\partial v_i}$$
$$-G_{ij}\frac{\partial\left[\left(v_j-\langle u_j\rangle_L\right)\mathcal{F}\right]}{\partial v_i}+\frac{\partial}{\partial x_j}\left(\mu\frac{\partial\left(\mathcal{F}/\langle\rho\rangle\right)}{\partial x_j}\right)$$
$$+\frac{\partial}{\partial x_j}\left(\frac{2\mu}{\langle\rho\rangle}\frac{\partial\langle u_i\rangle_L}{\partial x_j}\frac{\partial \mathcal{F}}{\partial v_i}\right)+\frac{\mu}{\langle\rho\rangle}\frac{\partial\langle u_i\rangle_L}{\partial x_k}\frac{\partial\langle u_j\rangle_L}{\partial x_k}\frac{\partial^2\mathcal{F}}{\partial v_i\partial v_j}$$
$$+\frac{1}{2}C_0 k\,\omega\frac{\partial^2\mathcal{F}}{\partial v_i\partial v_i}+C_\phi\,\omega\frac{\partial\left[\left(\psi_\alpha-\langle\phi_\alpha\rangle_L\right)\mathcal{F}\right]}{\partial\psi_\alpha}-\frac{\partial\left[S_\alpha(\boldsymbol{\psi})\mathcal{F}\right]}{\partial\psi_\alpha}. \quad (8)$$

3 Irregularly Portioned FDF Simulator

It is commonly believed that a hybrid Eulerian-Lagrangian solver provides the most convenient means of solving the transported FDF equation [64–66]. In this setting, the physical domain is discretized in an Eulerian manner via standard formats e.g. finite difference (FD), finite volume (FV), or other methods. The FDF is represented by an ensemble of Lagrangian Monte Carlo (MC) *particles*. Each of these particles carry information pertaining to the physical field and also the position vector. Figure 1 shows a typical section of the computational domain. The discrete Eulerian grid is overlaid with an ensemble of MC particles. Modern LES typically requires order of billions of grids and with an order of magnitude more MC particles. When finite-rate

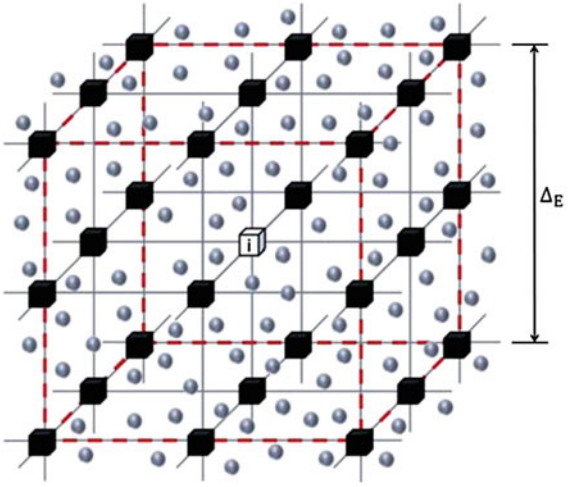

Fig. 1 A typical section of the computational domain. The *spheres* represent the Lagrangian MC particles, the *cubes* represent the Eulerian FD points and the *dashed line* represents the ensemble domain surrounding the grid point i [86]

kinetics are to be captured, the computational requirements become *monstrous*. For example, Yilmaz et al. [67] show that for even moderately sized geometries (with just 5 M grid points and 50 M particles) and a reduced kinetic mechanism (15 species) a serial, "simple" FDF simulation requires several years of CPU time!

Initially, each MC particle is given a location in physical space and stores the corresponding composition (velocity, and/or scalar) values. These particles are then transported due to convection and diffusion in physical space, and due to mixing and chemical reaction in compositional space. The filtered chemical source terms are constructed from the MC solver. For that, an ensemble domain is defined as the region surrounding an Eulerian point, and the filtered quantities are constructed via

$$\langle Q \rangle_L \approx \frac{\sum_{n \in \Delta_E} w^{(n)} Q\left(\boldsymbol{\phi}^{(n)}\right)}{\sum_{n \in \Delta_E} w^{(n)}}, \tag{9}$$

where Δ_E and $w^{(n)}$ denote the ensemble domain and particle weight, respectively. The weights are used to keep the number density approximately uniform [66]. Equation (9) becomes exact as the number of particles within the domain approaches infinity, and the size of the ensemble domain approaches zero. The SDEs governing the evolution of the MC particles require the filtered values. These are obtained via interpolation from the values at the Eulerian points.

With petascale computing a reality and exascale on the horizon, we must leverage the enormous opportunities they provide. In order to take advantage of large distributed memory systems, the Message Passing Interface (MPI) [68, 69] is used for the parallel implementation. In this approach information residing on different processors must be shared explicitly via message passing. For the hybrid solver, this results in two primary message passing tasks. The first task is sharing information at neighboring grid points. A simplified 2D example is presented in Fig. 2. Here the 9×9 grid is decomposed and distributed over 9 different ranks (MPI processes). Each rank resides on a different CPU core, delineated by the dashed lines. Evaluating derivatives at some grid point (i, j) involves a stencil operation as shown in the figure. The neighboring points used in the stencil can be local to that process or reside on neighboring processes. If the points reside on neighboring processes, the needed data must be sent from each neighbor process and received by the host process. Typically the points needed from a neighbor process are referred to as ghost or halo points. After decomposing the domain, each rank allocates extra storage for the ghost points as required by the stencil operations.

The second task is migrating particles from one cell to another as shown in Fig. 3. Here the cells surrounding each of the FD points are represented. The particles are contained in each of the cells, and the cells are distributed over 9 different ranks. Each rank is on a different CPU core, delineated by the dashed lines. Each particle evolves in physical space according to Eq. (7a). The updated particle location could be any of the neighboring cells surrounding the original host cell. Particles that migrate from one cell to a cell on a neighboring process must be message passed.

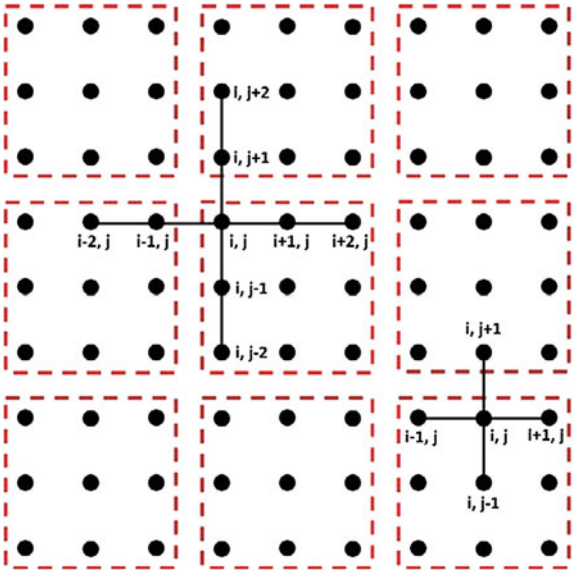

Fig. 2 A 2D grid distributed over 9 different processors. The *circles* denote the FD points and the *dash lined squares* encompass the grid points belonging to a unique rank. Shown are two different sized FD stencils

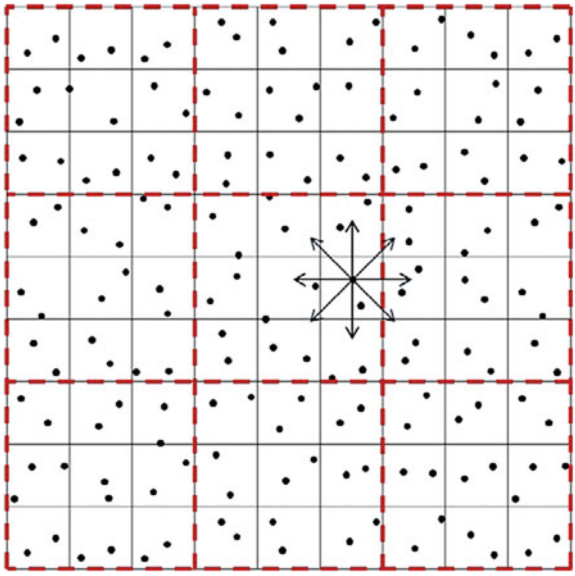

Fig. 3 A 2D grid distributed over 9 different processors. The *dots* denote the MC particles and the *dash lined squares* encompass the particles belonging to a unique rank. The *thin lines* mark the cells surrounding a FD point. The *arrows* represent potential landing spots of a particular particle after integration of Eq. (7a)

3.1 Static Block Decomposition

The first attempt at a highly scalable implementation of the hybrid FDF solver involved a simple static uniform block decomposition. In doing so, the number of grid points/cells are initially divided evenly among all of the processors. This

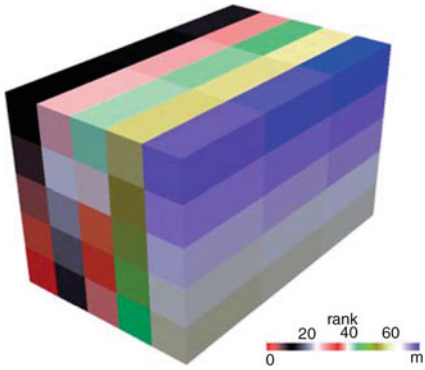

Fig. 4 A 3D block uniform decomposition. Each color corresponds to a block of grid points/cells belonging to a unique MPI process

decomposition remains unchanged throughout the entire simulation. We typically prefer partitions that are cubic in shape (in terms of an equal number of grid points/cells in all 3 directions). This is effectively the minimal edge-cut, and represents the best decomposition in terms of reducing the amount of data to be communicated. Additionally, each rank will have exactly the same communication pattern (except for ranks at the corners or edges). In terms of underlying data structures, the block partition shapes map to 3D arrays very efficiently.

The fully 3D block uniform decomposition has been implemented in an existing hybrid FDF solver [27, 31] with finite-rate kinetics calculations [70]. This solver is entirely in Fortran, using 3D arrays as the underlying data structure to store grid/cell values, which map perfectly to the block decomposition. The scheme is employed for LES of Sandia Flame D [71–73]. The domain is discretized via 120 grid points in each direction, with approximately 10M MC particles. Combustion chemistry is modeled via a reduced kinetics mechanism involving 16 species and 12 reaction steps. A sample decomposition of the domain is presented in Fig. 4. Scaling analysis is conducted of a nonreactive and a reacting flow. In the latter, S_α is evaluated for each particle via the CHEMKIN library [74], and Eq. (7c) is integrated for each particle with a stiff ODE solver [75]. The strong scaling results are presented in Fig. 5.

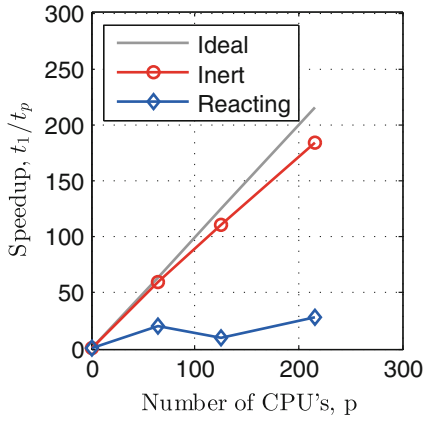

Fig. 5 Strong scaling comparisons. Results correspond to walltime for an entire iteration step

The inert case performs well, achieving approximately 85 % speedup on 216 processors. However, the reacting case shows very poor performance, merely achieving a 10 % speedup.

3.2 *Irregularly Portioned Lagrangian Monte Carlo (IPLMC)*

Poor performance of the static block decomposition methodology is due to computational "hot spots." This is shown in Fig. 6, demonstrating that simulations pertaining to regions undergoing chemical reaction are more CPU intensive. This is due to integration of Eq. (7c) for each particle within each cell (Fig. 3). In regions where $S_\alpha \neq 0$, stiff ODEs must be solved requiring multi-step integrations. In other regions, the number of substeps is significantly lower. Therefore, while distributing the number of grids/cells evenly and minimizing the communication, the block decomposition does not distribute the computational load evenly amongst the partitions. The resulting computational load imbalance is shown in Fig. 7. This is measured as the walltime needed for each rank to perform a single iteration. Many ranks spend significant chunks of time idle, while others are still busy. This idle time is the reason for poor performance due to the bulk synchronous [76] design of the flow solver.

Recognizing the computational load imbalance, Yilmaz et al. [67] proposed that each cell could be assigned a weight based on some work metric required to integrate Eq. (7c). One potential metric is the sum of the number of RHS function calls made within the ODE solver for all of the particles within a cell. An approach which has proven more effective is to merely measure the sum of the walltime spent within the ODE solver for all of the particles in a cell. The result is that each grid point/cell can be assigned a weight directly correlated to cost associated with chemical reaction. Thus

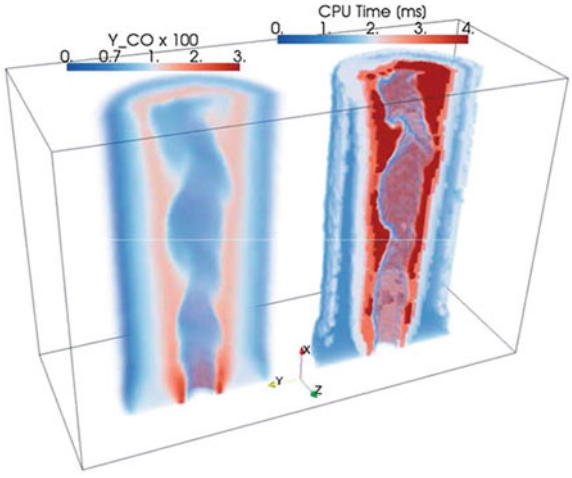

Fig. 6 Volume renderings of the mass fraction of CO (*left*), and the CPU time (*right*) [67]

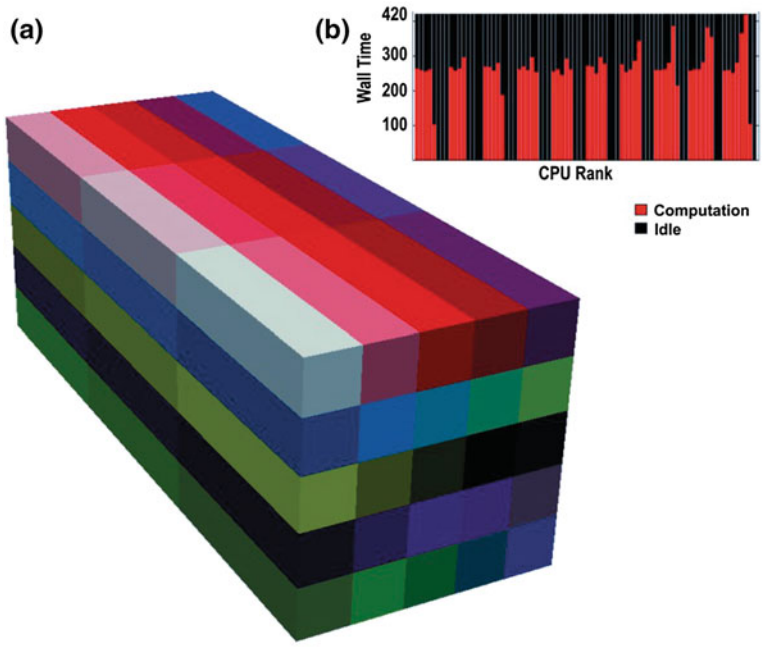

Fig. 7 **a** 3D block uniform domain decomposition. Each *colored block* represents the calculations of a unique CPU rank corresponding to a portion of the domain. **b** The walltime each CPU rank spends (*red bars*) versus the time spent idle (*black bars*)

the entire mesh can be represented as a weighted graph, and a load balanced domain decomposition can be obtained using a weighted graph partitioning algorithm [77–80]. The primary objective of the weighted graph partitioner is to evenly distribute the computational load among all the partitions. A secondary objective is to minimize the edge-cut. An example of the resulting decomposition is presented in Fig. 8. This decomposition portrays three important features. First, the computational load is distributed well over the different ranks. The amount of idle time is greatly reduced, and the duration of a given iteration is significantly reduced compared to the block uniform case. Second, the size of partitions varies. The ones containing heavier weighted cells are much smaller than those containing lighter weighted cells. Third, since the primary constraint is to balance the computational load, the edge-cut is non-optimal resulting in *irregularly* shaped partitions.

The partitions formed in this way present some significant challenges in terms of implementation. The underlying 3D arrays storing grid/cell values in the hybrid solver no longer map efficiently to each partition. Also, every stencil point must be tested for its locality, and each partition can have an arbitrarily different number of communicating neighbors. Yilmaz et al. [67] implemented the irregular decomposition only for the Lagrangian solver, and retained a simple serial implementation for the Eulerian solver. Thus, the methodology is referred to as “irregularly portioned

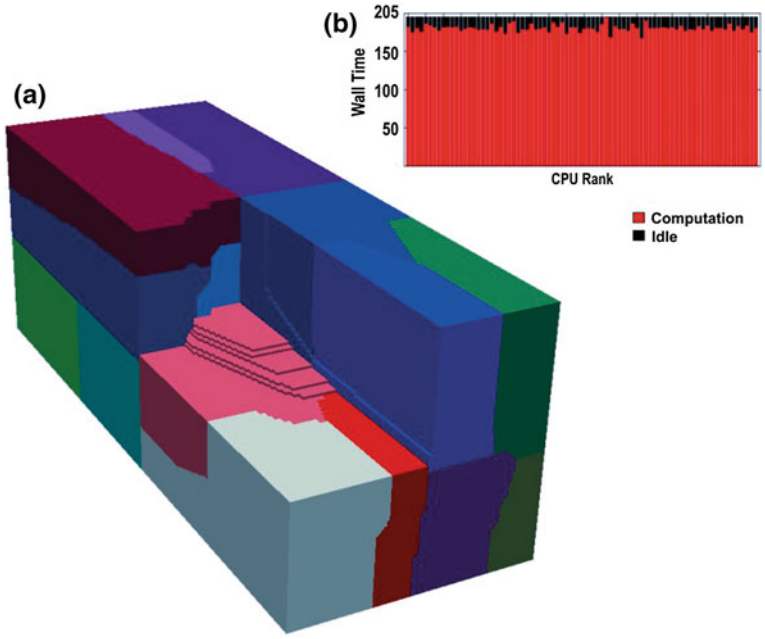

Fig. 8 **a** 3D irregular decomposition. Each *colored block* represents the calculations of a unique CPU rank corresponding to a portion of the domain. **b** The walltime each CPU rank spends (*red bars*) versus the time spent idle (*black bars*)

Lagrangian Monte Carlo" (IPLMC). The performance of the irregular decomposition can be easily assessed since the bulk of the computation time is spent inside the Lagrangian solver, while the amount of modification to the existing solver is kept to a minimum.

The performance of IPLMC is assessed via LES of a turbulent premixed Bunsen burner flame [81] using a reduced kinetics mechanism involving 9 species and 5 global reaction steps [82]. Results of the strong scaling analysis are presented in Fig. 9. The performance is nearly ideal up to 256 processors with regards to just the MC portion. The total step (including the serial Eulerian solver) shows nearly ideal scaling up to 64 processors; however, only a 47 % speedup is realized at 256 processors. This is due to Amdahl's law [83], demonstrating that the strong scaling is ultimately limited by the serial portions of the computation. Weak scaling results are presented in Fig. 10. For this analysis, work per processor is kept constant. The total step shows nearly ideal weak scaling upwards of 100 processors before beginning to tail off. At this point a communication bottleneck is exposed. The intersolver communication becomes more costly as more processors are employed. Since the Eulerian solver is serial, this one process must communicate with all of those performing the Lagrangian computation. Despite these shortcomings, the IPLMC methodology presents a significant improvement over the block uniform distribution.

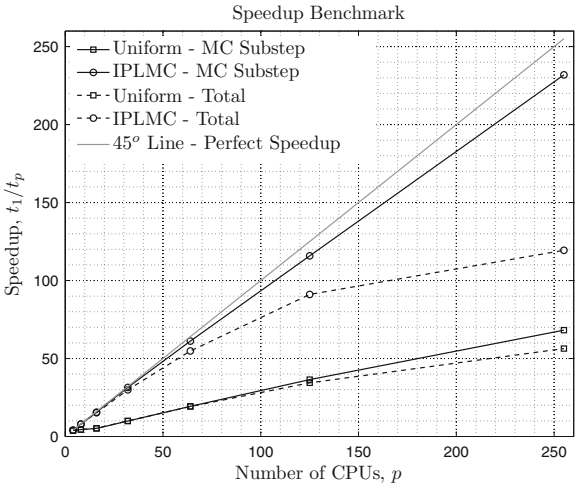

Fig. 9 Strong scaling of the IPLMC versus the block uniform decomposition. Results correspond to walltimes of a chemistry substep and an entire iteration step [67]

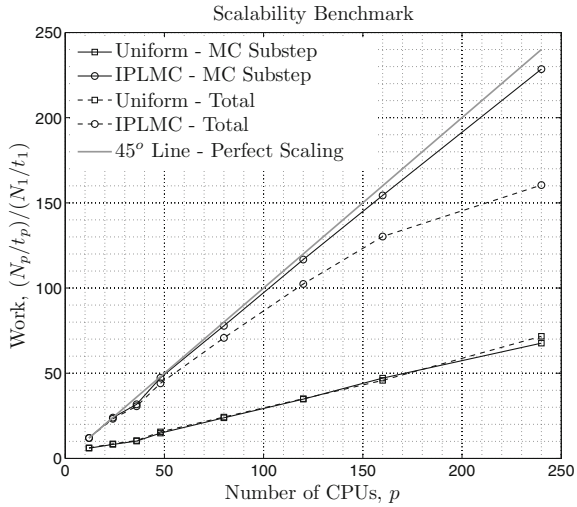

Fig. 10 Weak scaling of the IPLMC versus the block uniform decomposition. N_p denotes the total number of MC particles and increases proportional to the number of CPUs (p). Results correspond to the walltimes of a chemistry substep and an entire iteration step [67]

3.3 Irregularly Portioned Lagrangian Monte Carlo Finite Difference (IPLMCFD)

In order to overcome the shortcomings of the IPLMC, the Eulerian solver must be made parallel with the communications restricted to neighboring ranks only. To minimize the amount of intersolver communication, the partitioning of the Eulerian solver is made to match the partitioning of the Lagrangian solver from IPLMC. In an effort to more easily manage the bookkeeping, the Eulerian solver, like its Lagrangian counterpart, is developed in C++ to leverage robust data structures and algorithms in its Standard Library [84], and the Boost libraries [85]. This extended

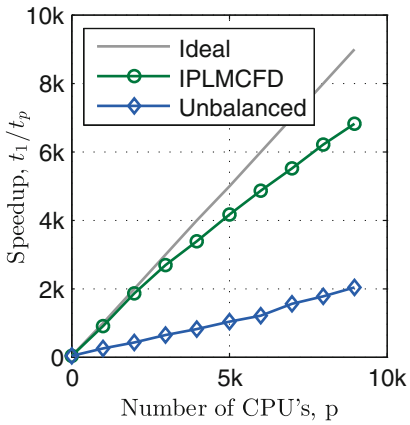

Fig. 11 Strong scaling of the IPLMCFD versus an unbalanced decomposition. Results correspond to walltime for an entire iteration step

approach is termed "irregularly portioned Lagrangian Monte Carlo finite difference" (IPLMCFD) [86]. The performance of IPLMCFD is assessed via consideration of the same case considered in the IPLMC [81].

Results of the strong scaling analysis are presented in Fig. 11. The performance of IPLMCFD is nearly ideal up to a few thousand processors. Upwards of 8,000 processors, IPLMCFD is still achieving approximately a 75 % speedup. Weak scaling results are presented in Fig. 12. Again, work per processor is kept constant. This time nearly ideal weak scaling is achieved up to 4,000 processors. It is obvious that IPLMCFD provides more than an order of magnitude improvement over IPLMC in parallel performance.

It is important to note that the scaling results as presented are for the optimal load balanced decomposition. As the flow evolves, the performance may no longer be optimal. Ideally, every iteration begins with an optimal decomposition. In

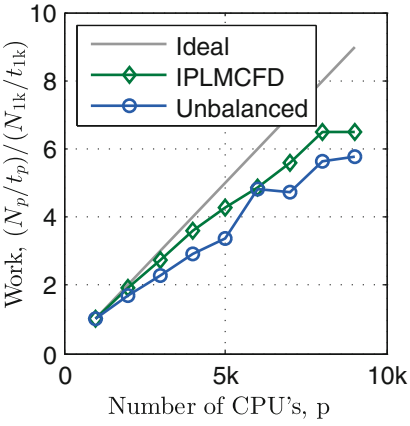

Fig. 12 Weak scaling of the IPLMCFD methodology versus an unbalanced decomposition. N_p denotes the total number of MC particles and increases proportional to the number of CPUs (p). Results correspond to walltime for an entire iteration step

practice, a decomposition performs well for some amount of time before another one is considered [67, 86].

4 Concluding Remarks

The evolution of massively parallel large eddy simulation (LES) of turbulent reactive flows via the filtered density function (FDF) has been very successful. It is demonstrated that the hybrid Eulerian/Lagrangian FDF solver and the tight coupling between its two components can be efficiently parallelized via weighted graph partitioning for domain decomposition. The weights are determined from the local effects of chemical reaction. The entire flow solver is constructed in such a way to efficiently treat the irregularly portioned partitions. Excellent scaling is demonstrated over thousands of CPU cores. Our current work has laid a strong foundation for exploiting distributed parallelism on the largest systems. However, to make more efficient usage of existing petascale and future exascale systems, additional features should be considered. Some recommendations are provided here:

Overdecomposition: For distributed parallelism, a common approach is to map one MPI rank to each CPU core. The concept of overdecomposition is to create more than one MPI rank per core. The advantage is that the computation and communications are more easily overlapped reducing the idle CPU time [76].

MPI + X: Parallelism at the distributed level (internode) is accomplished via MPI. The "+ *X*" identifies what strategy is employed at the intranode level. IPLMCFD is a flat MPI approach, reusing MPI at this level. However, shared memory approaches, such as OpenMP [87], better suit the architecture of the hardware at this level. In Fig. 13 the strong scaling analysis for IPLMCFD is repeated for one MPI process per node, rather than per core. Excellent scaling is achieved at this level upwards of 4,000 nodes. An efficient implementation of OpenMP at the intranode level (having 8–16 cores) would push scaling to tens of thousands of processors.

Accelerators: Graphics processing units (GPUs) and coprocessors (i.e. Intel Phis) have become an integral component of existing supercomputers, e.g. Titan (GPUs) [88], and Stampede (Intel Phis) [89]. Due to power constraints, these will remain critical components of future systems. As such the MPI + OpenMP approach must be extended to include accelerators. For Intel Phi coprocessors, OpenMP 4.0 [90] will support offloading calculations to the Phi. On the other hand, CUDA [91] and OpenACC [92] are two well established approaches for computing on GPUs. Given that OpenMP and OpenACC are syntactically similar, these two approaches can be followed with the same code base to take advantage of accelerators.

Dynamic Repartitioning: A balanced computational load is vital for achieving massive parallelism on distributed systems. However, the performance of a well balanced decomposition may gradually degrade over time. This is due to the evolving regions of finite-rate kinetics, or due to conditions at the system level, such as network traffic,

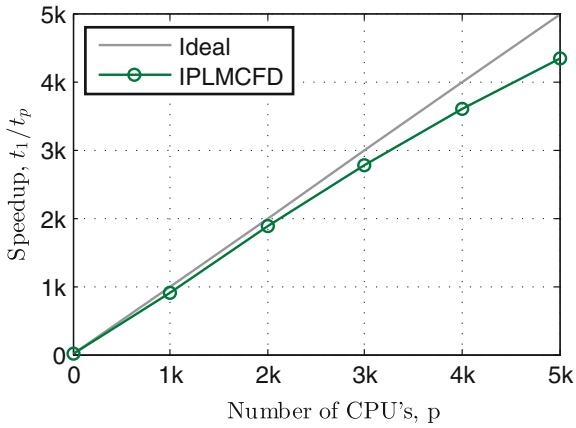

Fig. 13 Strong scaling of IPLMCFD with one MPI process per *node*. Results correspond to walltime for an entire iteration step

temperature of different CPU cores, etc. Thus, the domain decomposition should be adjusted dynamically (repartitioning). In this way, it is possible to keep the optimal load balance throughout the simulation. The issue of efficient data migration required for dynamic load balancing has been studied by many investigators; e.g. see Ref. [93]. Softwares like Zoltan [80] have been designed to treat the repartitioning and data migration. Moreover, Charm++ [94] is an entire runtime system and programming paradigm for treating the overdecomposition, load balancing, repartitioning and data migration issues.

Acknowledgments The work at the University of Pittsburgh is sponsored by AFOSR under Grant FA9550-12-1-0057, by NSF under Grant CBET-1250171, and by the NSF Extreme Science and Engineering Discovery Environment (XSEDE) under Grants TG-CTS070055N & TG-CTS120015. We are thankful to members of the Center for Simulation and Modeling at the University of Pittsburgh for their help with numerous computational issues.

References

1. Hawthorne WR, Weddell DS, Hottel HC (1948) Third Symp Combust Flame Explos Phenom 3(1):266. doi:10.1016/S1062-2896(49)80035-3
2. Kuo KK, Acharya R (2012) Fundamentals of turbulent and multiphase combustion. Wiley, Hoboken
3. Pope SB (2013) Proc Combust Inst 34(1):1. doi:10.1016/j.proci.2012.09.009
4. Holden C (1991) Science 252:1110. doi:10.1126/science.252.5009.1107
5. Chen JH (2011) Proc Combust Inst 33(1):99. doi:10.1016/j.proci.2010.09.012
6. Poinsot T, Veynante D (2011) Theoretical and numerical combustion, 3rd edn. R.T. Edwards Inc, Philadelphia
7. Givi P (2006) AIAA J 44(1):16. doi:10.2514/1.15514
8. Pope SB (2000) Turbulent flows. Cambridge University Press, Cambridge
9. Bilger RW (2000) Prog Energy Combust 26(4–6):367. doi:10.1016/S0360-1285(00)00015-0
10. Peters N (2000) Turbulent combustion. Cambridge University Press, Cambridge

11. Minkowycz WJ, Sparrow EM, Murthy JY (eds) (2006) Handbook of numerical heat transfer, 2nd edn. Wiley, New York
12. Fox RO (2003) Computational models for turbulent reacting flows. Cambridge University Press, Cambridge
13. Heinz S (2003) Flow Turbul Combust 70(1–4):115. doi:10.1023/B:APPL.0000004933.17800.46
14. Haworth DC (2010) Prog Energy Combust 36(2):168. doi:10.1016/j.pecs.2009.09.003
15. Haworth DC (2011) In: Vervisch L, Veynante D, van Beeck JPAJ (eds) Turbulent combustion. von Karman institute for fluid dynamics lecture series. Rhode-Saint-Genèse, Belgium
16. Haworth DC, Pope SB (2011) In: Echekki T, Mastorakos E (eds) Turbulent combustion modeling, fluid mechanics and its applications, vol 95. Springer, Netherlands, pp 119–142. doi:10.1007/978-94-007-0412-1_6
17. Ansari N, Jaberi FA, Sheikhi MRH, Givi P (2011) In: Maher ARS (ed) Engineering applications of computational fluid dynamics: volume 1. International energy and environment foundation, Chap 1, pp 1–22
18. Sagaut P (2010) Large eddy simulation for incompressible flows, 3rd edn. Springer, New York
19. Geurts BJ (2004) Elements of direct and large-eddy simulation. R.T. Edwards Inc, Philadelphia
20. Ghosal S, Moin P (1995) J Comput Phys 118(1):24. doi:10.1006/jcph.1995.1077
21. Vreman B, Geurts B, Kuerten H (1994) J Fluid Mech 278:351. doi:10.1017/S0022112094003745
22. Williams FA (1985) Combustion theory, 2nd edn. The Benjamin/Cummings Publishing Company, Menlo Park
23. Sheikhi MRH, Drozda TG, Givi P, Pope SB (2003) Phys Fluids 15(8):2321. doi:10.1063/1.1584678
24. Sheikhi MRH, Givi P, Pope SB (2007) Phys Fluids 19(9):095106. doi:10.1063/1.2768953
25. Sheikhi MRH, Givi P, Pope SB (2009) Phys Fluids 21(7):075102. doi:10.1063/1.3153907
26. Colucci PJ, Jaberi FA, Givi P, Pope SB (1998) Phys Fluids 10(2):499. doi:10.1063/1.869537
27. Jaberi FA, Colucci PJ, James S, Givi P, Pope SB (1999) J Fluid Mech 401:85. doi:10.1017/S0022112099006643
28. Zhou XY, Pereira JCF (2000) Flow Turbul Combust 64(4):279. doi:10.1023/A:1026595626129
29. Heinz S (2003) Flow Turbul Combust 70(1–4):153. doi:10.1023/B:APPL.0000004934.22265.74
30. Raman V, Pitsch H, Fox RO (2005) Combust Flame 143(1–2):56. doi:10.1016/j.combustflame.2005.05.002
31. Sheikhi MRH, Drozda TG, Givi P, Jaberi FA, Pope SB (2005) Proc Combust Inst 30(1):549. doi:10.1016/j.proci.2004.08.028
32. Raman V, Pitsch H (2005) Combust Flame 142(4):329. doi:10.1016/j.combustflame.2005.03.014
33. van Vliet E, Derksen JJ, van den Akker HEA (2005) AIChE J 51(3):725. doi:10.1002/aic.10365
34. Carrara MD, DesJardin PE (2006) Int J Multiph Flow 32(3):365. doi:10.1016/j.ijmultiphaseflow.2005.11.003
35. Mustata R, Valiéo L, Jiménez C, Jones W, Bondi S (2006) Combust Flame 145(1–2):88. doi:10.1016/j.combustflame.2005.12.002
36. Jones WP, Navarro-Martinez S, Röhl O (2007) Proc Combust Inst 31(2):1765. doi:10.1016/j.proci.2006.07.041
37. Jones WP, Navarro-Martinez S (2007) Combust Flame 150(3):170. doi:10.1016/j.combustflame.2007.04.003
38. James S, Zhu J, Anand MS (2007) Proc Combust Inst 31(2):1737. doi:10.1016/j.proci.2006.07.160
39. Chen JY (2007) Combust Theory Model 11(5):675. doi:10.1080/13647830601091723
40. McDermott R, Pope SB (2007) J Comput Phys 226(1):947. doi:10.1016/j.jcp.2007.05.006
41. Raman V, Pitsch H (2007) Proc Combust Inst 31(2):1711. doi:10.1016/j.proci.2006.07.152

42. Drozda TG, Sheikhi MRH, Madnia CK, Givi P (2007) Flow Turbul Combust 78(1):35. doi:10.1007/s10494-006-9052-4
43. Réveillon J, Vervisch L (1998) AIAA J 36(3):336. doi:10.2514/2.401
44. Cha CM, Trouillet P (2003) Phys Fluids 15(6):1496. doi:10.1063/1.1569920
45. Yilmaz SL, Nik MB, Givi P, Strakey PA (2010) J Propuls Power 26(1):84. doi:10.2514/1.44600
46. Ansari N, Goldin GM, Sheikhi MRH, Givi P (2011) J Comput Phys 230(19):7132. doi:10.1016/j.jcp.2011.05.015
47. Ansari N, Pisciuneri PH, Strakey PA, Givi P (2012) AIAA J 50(11):2476. doi:10.2514/1.J051671
48. Otis CC, Ferrero P, Yilmaz SL, Candler GV, Givi P (2012) In: 48th AIAA/ASME/SAE/ASEE joint propulsion conference & exhibit. AIAA, Atlanta, GA, pp 1–11. AIAA-2012-4260. doi:10.2514/6.2012-4260
49. Yilmaz SL, Ansari N, Pisciuneri PH, Nik MB, Otis CC, Givi P (2013) J Appl Fluid Mech 6(3):311
50. Gikhman II, Skorokhod AV (1972) Stochastic differential equations. Springer, New York
51. Karlin S, Taylor HM (1981) A second course in stochastic processes. Academic Press, New York
52. Stratonovich RL (1963) Introduction to the theory of random noise. Gordon and Breach, New York
53. Risken H (1989) The Fokker-Planck equation, methods of solution and applications. Springer, New York
54. Pope SB (1994) Phys Fluids 6(2):973. doi:10.1063/1.868329
55. Haworth DC, Pope SB (1986) Phys Fluids 29(2):387. doi:10.1063/1.865723
56. Dreeben TD, Pope SB (1997) Phys Fluids 9(1):154. doi:10.1063/1.869157
57. Pope SB (1994) Annu Rev Fluid Mech 26:23. doi:10.1146/annurev.fl.26.010194.000323
58. Dopazo C (1994) In: Libby PA, Williams FA (eds) Turbulent reacting flows, Chap 7, Academic Press, London, pp 375–474
59. Borghi R (1988) Prog Energy Combust 14(4):245. doi:10.1016/0360-1285(88)90015-9
60. Gicquel LYM, Givi P, Jaberi FA, Pope SB (2002) Phys Fluids 14(3):1196. doi:10.1063/1.1436496
61. Nik MB, Yilmaz SL, Givi P, Sheikhi MRH, Pope SB (2010) AIAA J 48(7):1513. doi:10.2514/1.50239
62. Nik MB, Yilmaz SL, Sheikhi MRH, Givi P (2010) Flow Turbul Combust 85(3–4):677. doi:10.1007/s10494-010-9272-5
63. Gardiner CW (1990) Handbook of stochastic methods for physics, chemistry and the natural sciences, 2nd edn. Springer, New York
64. Grigoriu M (1995) Applied non-Gaussian processes. Prentice-Hall, Englewood Cliffs
65. Kloeden PE, Platen E, Schurz H (1997) Numerical solution of stochastic differential equations through computer experiments, 2nd edn. Springer, New York
66. Madnia CK, Jaberi FA, Givi P (2006) In: Minkowycz WJ et al (eds) Handbook of numerical heat transfer, Chap 5, 2nd edn. Wiley, New York, pp 167–189. doi:10.1002/9780470172599.ch5
67. Yilmaz SL, Nik MB, Sheikhi MRH, Strakey PA, Givi P (2011) J Sci Comput 47(1):109. doi:10.1007/s10915-010-9424-8
68. Gropp W, Lusk E, Skjellum A (1999) Using MPI: portable parallel programming with the message-passing interface, 2nd edn, Scientific and engineering computation. MIT Press, Cambridge
69. Gropp W, Lusk E, Thakur R (1999) Using MPI-2: advanced features of the message-passing interface. Scientific and engineering computation. MIT Press, Cambridge
70. Pisciuneri PH (2008) Large eddy simulation of a turbulent nonpremixed jet flame using a finite-rate chemistry model. M.S. thesis, Department of Mechanical Engineering and Materials Science, University of Pittsburgh, Pittsburgh, PA
71. Barlow RS, Frank JH (1998) Proc Combust Inst 27(1):1087. doi:10.1016/S0082-0784(98)80510-9

72. Nooren PA, Versluis M, van der Meer TH, Barlow RS, Frank JH (2000) Appl Phys B 71(1):95. doi:10.1007/s003400000278
73. Sandia National Laboratories (2015) TNF workshop website, piloted jet flames. http://www.sandia.gov/TNF/pilotedjet.html
74. Kee RJ, Rupley FM, Meeks E, Miller JA (1996) CHEMKIN-III: a FORTRAN chemical kinetics package for the analysis of gas-phase chemical and plasma kinetics. Technical report. SAND96-8216, Sandia National Laboratories, Livermore, CA
75. Brown PN, Byrne GD, Hindmarsh AC (1989) SIAM J Sci Stat Comput 10(5):1038. doi:10.1137/0910062
76. Valiant LG (1990) Commun ACM 33(8):103. doi:10.1145/79173.79181
77. Karypis G, Kumar V (1998) METIS: a software package for partitioning unstructured graphs, partitioning meshes, and computing fill-reducing orderings of sparse matrices, version 4.0. University of Minnesota, Minneapolis, MN. http://glaros.dtc.umn.edu/gkhome/views/metis
78. Karypis G, Schloegel K (2013) ParMETIS: parallel graph partitioning and sparse matrix ordering library, version 4.0. University of Minnesota, Minneapolis
79. Devine K, Boman E, Heaphy R, Hendrickson B, Vaughan C (2002) Comput Sci Eng 4(2):90. doi:10.1109/5992.988653
80. Boman E, Devine K, Heaphy R, Hendrickson B, Leung V, Riesen LA, Vaughan C, Catalyurek U, Bozdag D, Mitchell W, Teresco J (2007) Zoltan 3.0: parallel partitioning, load balancing, and data-management services; user's guide. Technical report. SAND2007-4748W, Sandia National Laboratories, Albuquerque, NM. http://www.cs.sandia.gov/Zoltan/ug_html/ug.html
81. Chen YC, Peters N, Schneemann GA, Wruck N, Renz U, Mansour MS (1996) Combust Flame 107(3):223. doi:10.1016/S0010-2180(96)00070-3
82. Mallampalli HP, Fletcher TH, Chen JY (1998) J Eng Gas Turbines Power 120(4):703. doi:10.1115/1.2818457
83. Amdahl GM (1967) In: Proceedings of the April 18–20 1967, Spring joint computer conference, AFIPS'67 (Spring). ACM, New York, pp 483–485. doi:10.1145/1465482.1465560
84. Josuttis NM (1999) The C++ standard library: a tutorial and handbook. Addison-Wesley, Reading
85. Boost C++ Libraries (2015). http://www.boost.org/
86. Pisciuneri PH, Yilmaz SL, Strakey PA, Givi P (2013) SIAM J Sci Comput 35(4):C438. doi:10.1137/130911512
87. OpenMP Architecture Review Board (2015) The OpenMP API specification for parallel programming. http://www.openmp.org
88. Oak Ridge National Laboratory (2015) Titan user guide. https://www.olcf.ornl.gov/support/system-user-guides/titan-user-guide/
89. Texas Advanced Computing Center (2015) The University of Texas at Austin. Stampede user guide. https://www.tacc.utexas.edu/user-services/user-guides/stampede-user-guide
90. OpenMP Architecture Review Board (2013) OpenMP application program interface version 4.0—July 2013
91. NVIDIA Corporation (2015) NVIDIA CUDA parallel programming and computing platform. http://www.nvidia.com/object/cuda_home_new.html
92. OpenACC.org (2015) OpenACC directives for accelerators. http://www.openacc-standard.org
93. Devine KD, Boman EG, Karypis G (2006) In: Heroux M, Raghavan A, Simon H (eds) Frontiers of scientific computing, Chap 1. SIAM, Philadelphia, pp 1–29
94. Kale LV, Bhatele A (2013) In: Parallel science and engineering applications: the Charm++ approach. Series in computational physics. CRC Press, Boca Raton, Chap 1. http://www.crcpress.com/product/isbn/9781466504127